21044

NATIONAL LIBRARY
OTTAWA

BIBLIOTHÈQUE NATIONALE
OTTAWA

NAME OF AUTHOR........Johny Krahn..........

TITLE OF THESIS....Rock Slope Stability
with Emphasis on the
Frank Slide

UNIVERSITY......of Alberta..........

DEGREE FOR WHICH THESIS WAS PRESENTED......Ph.D......

YEAR THIS DEGREE GRANTED.........1974..........

Permission is hereby granted to THE NATIONAL LIBRARY OF CANADA to microfilm this thesis and to lend or sell copies of the film.

The author reserves other publication rights, and neither the thesis nor extensive extracts from it may be printed or otherwise reproduced without the author's written permission.

(Signed)....J. Krahn....

PERMANENT ADDRESS:

...Dept of Civil Eng
...University of Alberta
...Edmonton Alberta

DATED..Feb 25.....1974

NL-91 (10-68)

THE UNIVERSITY OF ALBERTA

ROCK SLOPE STABILITY
WITH EMPHASIS ON THE FRANK SLIDE

by

© JOHNY KRAHN

A THESIS
SUBMITTED TO THE FACULTY OF GRADUATE STUDIES
AND RESEARCH IN PARTIAL FULFILMENT OF THE
REQUIREMENTS FOR THE DEGREE OF
DOCTOR OF PHILOSOPHY

DEPARTMENT OF CIVIL ENGINEERING
EDMONTON, ALBERTA
SPRING, 1974

THE UNIVERSITY OF ALBERTA

FACULTY OF GRADUATE STUDIES AND RESEARCH

The undersigned certify that they have read, and recommend to the Faculty of Graduate Studies and Research for acceptance, a thesis entitled "ROCK SLOPE STABILITY WITH EMPHASIS ON THE FRANK SLIDE" submitted by Johny Krahn in partial fulfilment of the requirements for the degree of Doctor of Philosophy in Civil Engineering.

....
N. R. Morgenstern, Supervisor

....
D. M. Cruden

....
Z. Eisenstein

....
E. A. Babcock

....
B. Ladanyi, External Examiner

Date: Feb. 8/74

ABSTRACT

The disastrous results of large rock slides have resulted in the geotechnical world's increased desire to predict the degree of stability of rock slopes. The problem the engineer faces in making such predictions involves the reliability of the stability analysis. In the analysis of rock slopes, safety factors based on laboratory shear tests may, in some cases, be in error by as much as 700%. However, in a geological setting like the Frank Slide this error may only be in the order of 15%.

A relatively good correlation is obtainable between a mathematical characterization of the microscopic roughness of artifically prepared surfaces and the friction angle, ϕ. The extension of this concept to the field scale is hindered by the limited number of suitable surface exposures available for the measurement of roughness.

The frictional resistance after large shearing displacements on natural rock surfaces depends on the initial surface roughness and therefore is not a unique parameter as the residual strength is for clays. Furthermore, the shear strength on rock surfaces is

independent of sample size if the degree of roughness does not change with the area. The field shear strength of flexural-slip surfaces may not be at their ultimate value.

The geological setting of Turtle Mountain differs significantly from what has been shown in many publications. The structural form of this mountain is an anticline not a monocline.

Back-analyses of the Frank Slide indicate that the ϕ required for a safety factor of 1.0 is similar to the basic friction angle, ϕ_b. The use of peak strength parameters from flexural-slip surfaces in the back-analysis results in a safety factor of 0.86.

The mining at the base of Turtle Mountain decreased the safety factor of the sliding mass by 1% as shown by a Finite Element stress analysis.

ACKNOWLEDGEMENTS

The author of this thesis is grateful to Professor N. R. Morgenstern under whose supervision the research for this thesis was conducted. His topic suggestion and continued encouragement have been deeply appreciated.

The author is also indebted to Professor D. M. Cruden for his leadership on the Turtle Mountain geological field trips and for his helpful guidance in the interpretation of the related data.

The assistance with the work on Turtle Mountain provided by D. K. Norris is appreciated.

Appreciation is extended to R. Gitzel under whose direction the optical roughness plotter was built.

The editorial assistance rendered by W. D. Roggensack is acknowledged with appreciation.

The financial assistance provided by the National Research Council of Canada, the Department of Energy, Mines and Resources, and the University of Alberta is gratefully

acknowledged.

Finally, the author wishes to acknowledge, with many thanks, the continual encouragement, support and editorial assistance rendered by his wife, Barbara Ann, as without her, this thesis would not have been possible.

TABLE OF CONTENTS

Page

Release Form (i)

Title Page (ii)

Approval Sheet (iii)

Abstract (iv)

Acknowledgements (vi)

Table of Contents (viii)

List of Tables (xii)

List of Figures (xiii)

CHAPTER I INTRODUCTION

1.1 General 1

1.2 Purpose and scope 3

CHAPTER II THE STABILITY OF ROCK SLOPES

2.1 Introduction 6

2.2 Analytical slope stability analysis 7

2.3 Physical scale models 13

2.4 Governing parameters in slope stability analyses 13

2.5 Case histories 15

2.6 The reliability of rock slope stability analyses 17

TABLE OF CONTENTS (CONTINUED)

Page

CHAPTER III THE SHEARING RESISTANCE OF NATURAL AND ARTIFICIAL ROCK SURFACES

3.1 Introduction 27

3.2 The influence of surface irregularities on the shear strength 28

3.3 The effective i on natural rock surfaces 31

3.4 Basic friction angle of rock 33

3.5 The effect of microscopic roughness on the basic friction angle 35

3.6 Definition of roughness 36

3.7 Sample preparation 43

3.8 Shear tests and results 44

3.9 Digitization of roughness profiles 45

3.10 Digital computations 47

3.11 Amplitude distributions of asperities 49

3.12 Roughness characterization versus frictional resistance 51

3.13 Discussion of results 53

CHAPTER IV SHEAR TESTS ON NATURAL ROCK DISCONTINUITIES FROM TURTLE MOUNTAIN

4.1 Introduction 82

4.2 Sampling location 83

4.3 Sampling procedure 83

4.4 Sample preparation 86

TABLE OF CONTENTS (CONTINUED)

Page

4.5 Testing apparatus 86

4.6 Testing program 88

4.7 Results of shear tests 90

4.8 Discussion of results 92

CHAPTER V THE GEOLOGY OF TURTLE MOUNTAIN

5.1 Introduction 116

5.2 History of investigation 117

5.3 Succession of rock units within the Turtle Mountain area 120

5.4 Geology of Turtle Mountain 122

5.5 Discussion 128

CHAPTER VI THE MECHANICS OF THE FRANK SLIDE

6.1 Introduction 146

6.2 The stability analysis 147

6.3 The effect of mining on the stability of Turtle Mountain 152

6.4 Discussion 158

CHAPTER VII CONCLUDING REMARKS 169

LIST OF REFERENCES 174

APPENDIX A OPTICAL ROUGHNESS PLOTTER

A.1 Introduction 183

A.2 Theory of operation 183

A.3 Construction 184

TABLE OF CONTENTS (CONTINUED)

Page

4.5 Testing apparatus 86

4.6 Testing program 88

4.7 Results of shear tests 90

4.8 Discussion of results 92

CHAPTER V THE GEOLOGY OF TURTLE MOUNTAIN

5.1 Introduction 116

5.2 History of investigation 117

5.3 Succession of rock units within the Turtle Mountain area 120

5.4 Geology of Turtle Mountain 122

5.5 Discussion 128

CHAPTER VI THE MECHANICS OF THE FRANK SLIDE

6.1 Introduction 146

6.2 The stability analysis 147

6.3 The effect of mining on the stability of Turtle Mountain 152

6.4 Discussion 158

CHAPTER VII CONCLUDING REMARKS 169

LIST OF REFERENCES 174

APPENDIX A OPTICAL ROUGHNESS PLOTTER

A.1 Introduction 183

A.2 Theory of operation 183

A.3 Construction 184

TABLE OF CONTENTS (CONTINUED)

Page

A.4 Operating procedure 186

A.5 Results of trial tests 187

A.6 Performance 188

APPENDIX B SHEAR TEST DATA 196

APPENDIX C SPECTRAL DENSITY COMPUTER PROGRAM 230

LIST OF TABLES

Table Page

2.1 Summary of case history studies 21

3.1 Sample designation for roughness study 55

3.2 Roughness parameters for surface profiles 56

4.1 Summary of shear strength parameters 100

5.1 Width of cracks on Turtle Mountain 130

6.1 Results of stability analyses on Frank Slide 160

B.1 Shear test data 197

LIST OF FIGURES

Figure		Page
2.1	Limit equilibrium analysis of a sliding block	24
2.2	Illustration of circular arc failure surface	25
2.3	Illustration of a general failure surface	25
2.4	A three-dimensional wedge failure	26
2.5	Illustration of a potential failure surface which includes pre-existing joint sets and intact rock	26
3.1	Failure envelope for specimens with flat surfaces	57
3.2	Failure envelope for multiple inclined surfaces	58
3.3	An example of a natural discontinuity illustrating first- and second-order irregularities (after Patton, 1966)	59
3.4	An example of a time-history record x(t)	59
3.5	Casting of limestone samples	60
3.6	A typical step loaded, shear load versus deformation plot	61
3.7	Failure envelopes for rock surfaces with various roughnesses	62
3.8	An example of a surface trace from the Talysurf	63
3.9	Surface profiles for the dry sanded sample	64
3.10	Surface profiles for the diamond-saw cut surfaces	65
3.11	Surface profiles for sample lapped with #45/80 grit	66

LIST OF FIGURES (CONTINUED)

Figure Page

3.12 Surface profiles for sample lapped with #200 grit 67

3.13 Surface profiles for sample lapped with #400 grit 68

3.14 Surface profiles for sample lapped with #600 grit 69

3.15 Amplitude distributions of asperities for dry sanded sample 70

3.16 Amplitude distributions of asperities for diamond-saw cut surface 71

3.17 Amplitude distributions of asperities for surface lapped with #45/80 grit 72

3.18 Amplitude distribution of asperities for surfaces lapped with #200 grit 73

3.19 Amplitude distribution of asperities for surfaces lapped with #400 grit 74

3.20 Amplitude distribution of asperities for surfaces lapped with #600 grit 75

3.21 Centre-line-average (CLA) versus the friction angle 76

3.22 Roughness parameter, Z_2, versus the friction angle 77

3.23 Roughness parameter, Z_3, versus the friction angle 78

3.24 A typical autocorrelation plot 79

3.25 A typical spectral density plot 80

3.26 Limiting spectral criteria for roadways (after Houbolt, 1961) 81

4.1 The sample block within the slide debris 101

4.2 A flexural-slip surface within the sample block 101

4.3 Coring on the sample block 102

LIST OF FIGURES (CONTINUED)

Figure		Page
4.4	A ten-inch diameter cored sample	102
4.5	The modified shear box for the two-inch samples	103
4.6	The Wykeham-Farrance shear box	103
4.7	Natural discontinuities	104
4.8	The small roughness measuring device	105
4.9	A joint surface after shearing	105
4.10	A typical shear load versus deformation plot	106
4.11	A typical vertical deformation versus horizontal displacement plot	107
4.12	Failure envelopes for the bedding planes	108
4.13	Failure envelopes for the flexural-slip surfaces	109
4.14	Failure envelopes for the joint surfaces	110
4.15	Failure envelope for surfaces lapped with #45/80 grit	111
4.16	Failure envelope for the diamond-saw cut surfaces	112
4.17	Natural surface profiles of a bedding plane (sample B-3)	113
4.18	Natural surface profiles of a flexural-slip surface (sample S-2)	114
4.19	An idealized surface showing the effects of different sizes of specimens (after Deere, et al., 1967)	115
5.1	Location of Turtle Mountain	131
5.2	Cross-section through the north peak of Turtle Mountain (after Daly, et al., 1912)	132
5.3	Allan's cross-section through the south peak of Turtle Mountain (after Allan, 1933)	133

LIST OF FIGURES (CONTINUED)

Figure		Page
5.4	MacKay's cross-section through the south peak of Turtle Mountain (after MacKay, 1932)	134
5.5	Norris' cross-section through the south peak of Turtle Mountain (after Norris, 1955)	135
5.6	Airphoto of the Frank Slide area	136
5.7	A plan showing the general areas of the geological traverses run	137
5.8	View of north face of Hillcrest Mountain from Turtle Mountain showing the Turtle Mountain anticline in profile	138
5.9	The crest of Turtle Mountain	138
5.10	The Banff Formation in the "hoodoo" weathered area	139
5.11	Oblique aerial view of the Frank Slide from the northeast	140
5.12	Striations on bedding surfaces in an abandoned limestone quarry at the north end of Turtle Mountain	141
5.13	A rock within the slide debris showing a sheared surface	141
5.14	Geological map of Turtle Mountain area	142
5.15	Cross-section through Turtle Mountain along line A-A'	143
5.16	Cross-section through Turtle Mountain along line B-B'	144
5.17	Cross-section through Turtle Mountain along line C-C'	145
6.1	The average normal and shear stresses in relation to the failure envelopes	161
6.2	The effect of cohesion on the factor of safety for section B-B'	162
6.3	The Finite Element grid for the stresss analysis of Turtle Mountain	163

LIST OF FIGURES (CONTINUED)

Figure		Page
6.4	The initial stress distributions along the slip surface	164
6.5	The Finite Element grid around the mine area with the mine open	165
6.6	The changes in stress distributions	166
6.7	The inward movement of the mine walls	167
6.8	The style of deformation of Turtle Mountain due to the mining	168
A.1	Schematic diagram of light probe for the field roughness plotter	190
A.2	Schematic diagram of holding frame for the field roughness plotter	191
A.3	The optical roughness plotter	192
A.4	Control panel for the optical roughness plotter	192
A.5	Roughness plotter set-up in the field	193
A.6	Profile of artificial surface shown in Figure A.3	194
A.7	Roughness profiles from the field set-up shown in Figure A.5	195
B.1 - B.31	Shear load and vertical deformation versus the horizontal deformation	199
C.1	Cosine taper data window (after Bendat and Piersol, 1971)	233

CHAPTER I

INTRODUCTION

1.1 GENERAL

"VILLAGES CRUMBLE IN ITALIAN FLOOD." This was the headline of an article which appeared in the Edmonton Journal on October 10, 1963, and it related the disaster to which the villages along the Piave River, Italy, had succumbed. A gigantic rock slide just upstream from the Vaiont Dam plunged into the reservoir generating a wave of water 300 feet above the crest of the dam. The wave toppled over the dam crest flooding the Piave River valley. As the flood swept down the valley, several villages were destroyed and approximately 2,600 lives were lost (Kiersch, 1964; Muller, 1964, 1968; Mencl, 1966; Skempton, 1966; Kenney, 1967; Nonveiller, 1967).

Throughout history, similar events have occurred all over the world. To mention a few, there was the Elm Slide in Switzerland (Heim, 1932), the Tafjord Slide in Norway (Bugge, 1937), the Madison Canyon Slide in Montana (Witkind, et al., 1962) and the Frank Slide in Alberta (Daly, et al., 1912). In all these cases, numerous lives were lost which indicates the tremendous hazard to people living in potential slide areas.

As nations throughout the world are becoming more industrialized, there is an ever increasing need for more natural resources. Japan, for example, has in recent years bought coal from Alberta and British Columbia making it economically feasible to mine this product in large quantities. In some areas of the world, certain minerals have become a scarce commodity and as a result, lower quality ore bodies are becoming more economical prospects. In the case of open pit mines, the necessary removal of large quantities of material has become economically possible today with the advent of large-volume earthmoving equipment. The consequence of all these developments is that open pit mines are being planned and operated to depths and sizes that had not previously been considered (Stewart and Kennedy, 1971).

In these large open pits, one of the more important factors which must be considered in an economic analysis is the maximum slope angle at which the pit can be excavated (Steffen, et al., 1970). This is quite understandable since the minimization of the amount of waste rock, which has to be excavated in recovering an ore body, requires that the ultimate slopes be cut to the steepest possible angle. Oversteepening, on the other hand, results in slope failures which are not only dangerous to working personnel but may also cover up valuable ore in the event of a slide.

For many large pits to be profitable, the slopes must be designed at an optimum angle. Brawner (1971a) points out that on three recent projects with which he was involved, each degree of slope was associated with a potential cost or saving of from five to 15 million dollars. This demonstrates how very critical the role of the slope angle can be in the economic operation of the project.

Stewart and Kennedy (1971) have also shown that it is not only the ultimate slope angle that has an effect on the overall profitability. On the basis of cash flow they show that it is often economically more advantageous to use steep slopes during the initial stripping stages. This again points to the fact that the mine profitability is influenced by slope design considerations.

1.2 PURPOSE AND SCOPE

The above discussion indicates the need and desirability of accurately determining the degree of rock slope stability. The problem the Geotechnical Engineer is faced with in fufilling this need is whether or not it is possible, on the basis of present day analytical methods, to predict this degree of stability to the desired level of confidence.

It is the purpose of this thesis to examine this problem by firstly inspecting numerous documented records of failed slopes (Chapter 2) and secondly, by performing a detailed back-analysis of the Frank Slide which is located in southwestern Alberta.

The reliability of stablity anaylses depends to a large extent on the facility with which the operative field shear strength can be established. Various methods have been proposed for determining the shear strength; however, no one particular method has been generally accepted for routine use. These methods are reviewed in Chapter 3 and are further investigated by a study of the relationship between the microscopic surface roughness and the shearing resistance.

Obtaining a proper case history study requires an accurate knowledge of three major items, namely: (1) the geometrical and geological setting, (2) the shear strength parameters along the slip surface, and (3) the water pressures acting within the slope.

In more detail and with special reference to rock slopes, the geological setting involves establishing the lithology and stratigraphy, the attitude, geometry and spatial distribution of discontinuities and how these relate to the failure surface. The geometric setting involves ascertaining the surface profile prior to failure. Establishing the shear strength parameters requires that either field or laboratory shear tests be performed. A knowledge of the water pressures within the discontinuities is important because of its relation to the effective stress.

With these requirements in mind, the investigation of the Frank Slide is organized and presented as follows:

(1) Chapter 4 is devoted primarily to the determination of the shear strength parameters used in the back-analysis of the Frank Slide.

(2) Chapter 5 gives the geology of Turtle Mountain and the geological setting of the Frank Slide.

(3) Chapter 6 presents the analysis of the Frank Slide.

The conclusions of this thesis work are presented in Chapter 7.

CHAPTER II

THE STABILITY OF ROCK SLOPES

2.1 INTRODUCTION

In the introductory chapter the importance of establishing the degree of stability of natural rock slopes and slopes in open pit mines was discussed. To accomplish this, it is necessary to understand which factors influence the stability and then assess the stability by developing a mathematical model that represents the conditions in the slope. The two types of mathematical models that have been developed are the Limit Equilibrium Method and the Stress-Strain Analysis. Ultimately, in order to prove whether the slope conditions have been correctly modeled and for the mathematical model to have any meaning, the field evidence must confirm the theoretical predictions.

The purpose of this chapter is to briefly review the analytical methods available for the analysis of slopes and to discuss the parameters (necessary for the analysis) representing and governing the rock mass behaviour. Furthermore, it is the purpose to examine documented records of failed rock slopes and to inspect the agreement between the predicted and observed behaviour.

2.2 ANALYTICAL SLOPE STABILITY ANALYSIS

Theoretical analyses generally fall into two categories, (1) Limit Equilibrium Methods and (2) Stress-Strain Analysis.

2.2.1 THE LIMIT EQUILIBRIUM METHOD

The first step in any Limit Equilibrium Method is to assume the shape of a potential slip surface. Having done this, it is possible, using the equations of equilibrium, to determine the shearing resistance required for equilibrium to be maintained along the assumed slip surface. The required shearing resistance is then compared with the available shearing resistance which may have been determined from laboratory or field shear tests. This comparison of the available and required shearing resistance is carried out by means of the Factor of Safety. The Factor of Safety (F.S.) is defined as the value by which the shearing resistance parameters must be divided in order to bring the potential sliding mass to the point of limiting equilibrium. Finally, this procedure is repeated for many possible slip surfaces, and the most critical one is taken as the one controlling the design.

The simplest example of a limit equilibrium analysis is the case of a rigid block sliding on a planar surface as illustrated in Figure 2.1. In the absence of cohesion and pore water pressure, the activating force down the slope would be $W \cdot \sin\alpha$. The force resisting the sliding would be $W \cdot \cos\alpha \cdot \tan\phi$, where ϕ is the angle of frictional sliding resistance along the plane. The F.S. would then be the activating force divided by the resisting force. In equation form

$$\text{F.S.} = \frac{W \cdot \cos\alpha \cdot \tan\phi}{W \cdot \sin\alpha}$$

$$= \frac{\tan\phi}{\tan\alpha}$$

For a F.S. of 1.0, the point of limiting equilibrium, $\tan\phi$ would be equal to $\tan\alpha$.

In many soil slopes, the failure surface can be approximated by a circular arc. In this case, the potential sliding mass is divided into vertical sided slices (Figure 2.2), and an evaluation is made (for each slice) of the terms which express the forces driving the slices down the slope and those which resist the motion (Bishop, 1955). At the point of limiting equilibrium, the sum of the resisting forces and the sum of the driving forces must be equal. This type of analysis would also apply to rock slopes where the rock is so broken up by close irregular joints that it may be treated as a soil.

From the point of view of satisfying statics, the most advanced form of limit equilibrium analysis is the method developed by Morgenstern and Price (1965) which is capable of dealing with any shape of failure surface (Figure 2.3). This ability, of course, is highly desirable and applicable to rock slopes where the slip surface is controlled by the discontinuities within the rock mass (Piteau, 1970) and therefore may not be some simple shape like a circular arc.

With particular reference to rock slopes, Jennings (1970) has developed a method where the failure surface may follow several different joint sets (Figure 2.5). With the failure surface stepping from one joint set to another it may also pass through intact rock. Both the strength of the intact rock and the joints are taken into consideration and are viewed together as apparent strength parameters.

In rock slopes, failure may frequently occur in the shape of a wedge (Figure 2.4). The slope and the crest form two of the faces with the other being formed by discontinuities such as joints or faults intersecting the slope. This is a three-dimensional problem and therefore must be analyzed as such. This problem is complicated by the fact that numerous types of geometrical movements are possible: that is to say, the block may slide on two discontinuities at the same time, or slide on only one and break away from the other, and so forth. Goodman and Taylor (1967) treated this problem using vectors while Londe, et al. (1969, 1970) and John (1968) used stereographic projections. Hendron, et al. (1971) have also presented analytical and graphical methods to deal with these three-dimensional problems.

2.2.2 STRESS-STRAIN ANALYSIS

The most logical approach to designing a slope would be to determine the state of stress and deformations resulting from the stress change associated with the excavation. In this way with proper care, the deformations could be maintained within tolerable limits and the stresses kept to a level below failure. There are, however, several reasons why this approach in general cannot be used (Morgenstern, 1968).

In order to perform an analysis where the stresses and deformations are calculated requires not only that the equations of equilibrium be known but that the constitutive equations governing the material behavior must be discernable as well. According to Morgenstern (1968), such relationships, except for the probable general form of them, are not fully known for rock. The form of these equations would most likely be non-linear. The non-linearity together with variation in density, pore water pressure in the rock, and the variable boundary conditions presents considerable computational difficulties. Moreover, the analysis would only give the change in stress which is not sufficient unless the initial state of stress is known as well. Determination of the initial state of stress is not a simple task.

The computational difficulties have however, to a large extent, been overcome in the last decade by the Finite Element Method (Zienkiewicz and Cheung, 1967; Desai and Abel, 1972). With this method, it is possible to deal with variations in density, complex boundary conditions, anisotropy and non-linearity with relative ease (Zienkiewicz, et al., 1970; Stacey, 1970). With particular reference to rock mechanics, Goodman, et al. (1968a) have developed a special one-dimensional finite element to simulate discontinuities within the rock mass. In this way, the discontinuities can be assigned different material properties than the intact rock, making the analysis more realistic. Mahtab (1970) used this type of element in a three-dimensional study of jointed rock slopes.

To the present (1974), however, this numerical tool has been used mainly for research purposes. While the Finite Element Method has overcome the computational problems inherent in a stress-strain analysis, the material behaviour is not generally well understood which renders the analysis of limited value. For example, for the one-dimensional joint-element developed by Goodman, et al. (1968a), three parameters are needed to describe the joint behaviour: (1) the unit stiffness across the joint, (2) the unit stiffness along the joint, and (3) the shear strength along the joint. The joint stiffness concept, according to Goodman, "...is so new that no values are to be found in reports and publications about joint properties."

Duncan (1972), in commenting on the use of the finite element method for slope stability analysis, expressed the opinion that a better understanding of failure and postfailure of geotechnical material is needed before improvements can be made in stability analysis using the finite element method. He goes on to state

> "...while finite element analyses have proven useful for studying the occurrence of local failure, they have so far been less useful for studying slope stability problems. The results achieved so far in using the finite method for stability calculations have provided results which are not significantly better than those achievable using accurate equilibrium methods of slope stability analysis,..."

Undoubtedly, in the future, more research conducted in this area will result in a greater understanding of the material behaviour making this powerful numerical technique a practical design tool.

2.3 PHYSICAL SCALE MODELS

The value of scale models in the study of slope stability problems appears to be in the understanding of the rock mass behaviour as a whole. For example, Muller, et al. (1970) have shown, using scale models, how individual rock blocks within a slope can rotate and become unstable. Barton (1971a) used scale models to study the effect of different orientations of joints with respect to the slope.

While the models do aid in understanding slope behaviour, performing parametric studies using this approach would simply be too costly, too time consuming, and too unrealistic.

2.4 GOVERNING PARAMETERS IN SLOPE STABILITY ANALYSES

In examining the stability of rock slopes, the factors which generally must be considered are the geological setting, attitude, geometry and spatial distribution of discontinuities, ground water conditions and the strength parameters of the discontinuities (Piteau, 1970; Patton, et al., 1971). Of these factors, it is probable that the greatest uncertainty lies in the values adopted for the shear strength parameters.

When the shearing resistance is described by the Mohr-Coulomb failure criterion, the important shear strength parameters are C and ϕ. C is the cohesion intercept and ϕ is the angle of shearing resistance. The C value holds an unfortunate position in that the F.S. is very sensitive to a small change in C (Jaeger, 1971). For example, for a 70° slope, 100 feet high, and ϕ = 32°, the F.S. changes from 1.05 with C = 0 to 1.61 with C = 7 psi (Pentz, 1971). Moreover, this variation in C is well within the range of values obtained in shear tests (Jaeger and Rosengren, 1969).

For many rocks the shearing resistance bears a nonlinear relation to the normal pressure (Murrell, 1965; Maurer, 1966; Hobbs, 1970). The non-linear failure criterion, however, can be adequately presented as one that is piece-wise linear (Morgenstern, 1968). That is to say, a particular ϕ and C are valid only over a limited normal stress range. Therefore, even for a non-linear failure criterion, the important strength parameters can be expressed by a characteristic C and ϕ.

Establishing the ϕ and C parameters from shear tests is by no means a simple task. For laboratory testing, the problem begins with obtaining suitable samples. This sample problem is discussed further in Chapter 4 in connection with the procedures followed in obtaining samples at the Frank Slide.

Furthermore, there is the question of what size of sample constitutes a representative sample. It has generally been thought that the larger the sample, the more representative it is of the field conditions. For this reason, shear boxes have been built as large as 15 x 12 inches (Hoek and Pentz, 1968) and 15.8 x 15.8 inches (Krsmanovic, 1967). In order to test even larger samples, insitu shear tests have been performed in some cases (Krsmanovic, et al., 1966; Serafim, et al., 1968; Wallace, et al., 1969). While the larger tests may be more representative, they are also much more difficult to perform. In the case of laboratory testing, larger samples are more difficult to obtain and for the insitu tests, the cost and time involved often become prohibitive.

The effect of sample size is further considered in Chapter 4 in connection with the shear tests performed on the samples from Turtle Mountain.

2.5 CASE HISTORIES

A study was made of documented records reporting rock slope failures with the purpose of assessing the agreement between the theoretical and field behaviour. This study was also conducted in order to inspect the range of the strength parameters required for a F.S. of unity. A summary of the cases examined is presented in Table 2.1.

The ϕ and C required for a F.S. of unity for the failures examined are indeed enlightening. For all the cases examined, the ϕ is as high as 45° in only one case and the lowest ϕ required is 20°. In the majority of cases, the ϕ required is around 30°. The C required is relatively small and in many cases is zero. It is interesting to note that the ϕ required for a safety factor of unity is very similar to the basic friction angle of 30 ± 5 degrees, often assumed for rock (Ladanyi, et al., 1970; Barton, 1971b).

For the majority of cases where the shear strength parameters have been determined by some type of laboratory test, these parameters appear to compare fairly well with those obtained from the limit equilibrium analysis. The point that must be remembered, however, as was pointed out earlier, is that small changes in C can have a profound effect on the calculated factor of safety. When considering the range of C values obtained from shear tests, the correlation is not all that good and in some cases it is very poor. For example, in the Twin Buttes slide the F.S. with zero cohesion for wedge 1 is 0.73. If the C is increased to 0.52 psi, the F.S. is 1.08 and if it is increased to 1.74 psi, the F.S. is 1.93 (Seegmiller,1972). Extrapolating this trend to a C of 9 psi, the lowest value obtained from the shear tests, the F.S. is approximatly 7.0.

Although this may be an extreme example, it does reveal the magnitude by which the F.S. can be in error when calculated on the basis of shear tests.

An item which is of importance and places the majority of case histories in a position of doubtful credibility is the uncertainty surrounding the pore water pressures at the time of failure. If these assumptions are in error, it is reflected in the strength parameters required for a F.S. of unity; and, in turn, affects the comparison between the laboratory and back analysis shear strength parameters.

2.6 THE RELIABILITY OF ROCK SLOPE STABILITY ANALYSES

The strength parameters of rock, as previously noted, are difficult to determine and, furthermore, the values obtained from shear tests may not be the exact values operative in the field. The same situation applies to establishing the water pressure within the rock mass. The purpose of the factor of safety in an analysis is to compensate for these uncertainties. The numeric value used for a F.S. depends on the level of confidence which can be placed in the input parameters. This level of confidence depends, to a large extent, on the agreement observed between the predicted and actual field behaviour.

During the past several decades, in the area of soil slopes, numerous cases have been documented where a relatively good agreement has been observed between the mathematical analysis and the field observations. For example, for three first-time slides which occurred in intact clay, the computed safety factors using the peak strength parameters were within 10% of unity (Sevaldson, 1956; Skempton and Brown, 1961; Kjaernsli and Simons, 1962). This type of result has brought about an increased confidence in the limit equilibrium method of soil slope analysis. With this increased confidence, this method of analysis can now be used as a basis for the design of soil slopes.

This type of confidence has not as yet been reached in the analysis of rock slopes. In the design of open pits, the slope angle is often selected only on the basis of a consideration of the local geology and past experience. The reason for this is the general lack of agreement between the analyses and observed field behaviour. The F.S. computed on the basis of shear test results can be in error by several hundred percent. In the Twin Buttes slides, discussed in the previous section, the error is as much as 700%. This large difference, however, is not always the case. At the Frank Slide (Chapter 6), the F.S. based on the peak strength parameters from shear tests on flexural-slip surfaces differs by only 14% from a F.S. of unity. The Frank Slide analysis, however, was not as sensitive to a change in cohesion as is normally the case. Thus the F.S. can differ from unity by only a small percentage or by as much as several 100%. Since there is a possibility that the F.S. based on shear tests may be significantly in error, the reliability of analytical rock slope stability analysis has not achieved a level where it can be used as the sole basis of a slope design. A reasonable amount of judgment is still required in the selection of the shear strength parameters.

Is it possible to improve this position in rock slope analysis? Further detailed case studies may improve this position somewhat or, alternately, they will further confirm the present state of uncertainty. In the case histories listed in Table 2.1, as was noted earlier, the strength parameters required for F.S. of 1.0 are very similar to the basic friction angle as determined on flat rock samples. The same situation applies to the Frank Slide, where for a F.S. of 1.0, the average ϕ required is 37.2° which is identical with the ϕ measured on a flat sample lapped with a coarse grit (Chapter 6). Only further case histories will show whether or not this generally applies to all rock slopes. For this reason it is important to perform careful and detailed case studies. Broadly speaking, however, it is doubtful if the high level of confidence necessary to design slopes to an accuracy of within one degree will ever be reached. The material within rock slopes is simply too variable and complex to reach this position.

Since the reliability of mathematical analyses based on insitu or laboratory shear tests is not that high, the usefulness of these undertakings might be questionable. However, the situation exists that for feasibility studies, at least, only laboratory-type tests are available on which to base the design. Consequently, it is not practical to abandon the mathematical analysis unless the design is to be based solely on past experience.

Designing slopes at high factors of safety results in low angle slopes which might make an entire open pit operation uneconomical. Therefore, it is still necessary to work slopes at low factors of safety. Doing this, however, necessitates the continuous and careful monitoring of the slopes with the purpose of detecting areas of potential instability and remedying them before a catastrophe occurs.

The situation with natural slopes is somewhat more complicated. Since there is no design involved, it is a matter of stating whether the rock mass will or will not slide. This matter will be further discussed in connection with the Frank Slide.

TABLE 2.1 SUMMARY OF CASE HISTORY STUDIES

SLIDE	HEIGHT (FEET)	MATERIAL	SHEAR TEST RESULTS	STRENGTH PARAMETERS FOR F.S. = 1.0	TYPE OF ANALYSIS	COMMENTS	REFERENCE
DeBeers Mine Kimberley Area South Africa	310	Metamorphosed and normal shale	$\phi = 27^{\circ}$ $C = 0$ (wet)	Slope angle for F.S. = 1.0 is 32°	Jenning's method	Average natural slope angle in four different pits in the area is 26.5°.	Jennings, 1970
Malpasset Dam France	197	Generally fissured gneiss; along the fault, clayey breccia	$\phi = 30^{\circ}$ on fault material	30° (along fault)	Londe's 3-D method		Londe, 1973
Brilliant Cut Slide Pennsylvania	172	Clay shale and indurated clay		$\phi = 32^{\circ}$ $C = 0$ $\phi = 20^{\circ}$ $C = 16$ psi	Morgenstern-Price	Strength parameters required are similar to those obtained on soft indurated clay from another site.	Hamel, 1972
Jeffery Pit Quebec	700	Serpentinized peridotite	$\phi = 34^{\circ}$ $C = 0$ (residual results from triaxial tests)	$\phi = 34^{\circ}$ $C = 0$			Ladanyi, 1973
Vaiont Slide Italy	2000-2300	Carbonate rocks		$\phi = 20 - 28^{\circ}$ $C = 0$	2-D Limit Equilibrium method		Lo, et al., 1972 Mencl, 1966 Nonveiller, 1967 Kenney, 1967
Jersey Pit British Columbia	150	Quartz diorite	$\phi = 20 - 25^{\circ}$ $C = 2 - 5$ psi (on fault gouge)	$\phi = 34^{\circ}$ $C = 0$ or $\phi = 25^{\circ}$, $C = 1.7$ psi	2-D Limit Equilibrium method		Brawner, 1970
Number 3 Pit Natal British Columbia	200	Shales, sandstones, siltstones and coal	$\phi = 35^{\circ}$ $C = 4.5$ psi with normal load between 25 - 70 psi (for the coal)	With the measured values for the coal the parameters for the shale were $\phi = 35^{\circ}$ and $C = 8.5$ psi	2-D Limit Equilibrium method		Brawner, 1970
Harmer Pit British Columbia	140	Carbonaceous shale	Average $\phi = 32^{\circ}$ $C = ?$	$\phi = 30^{\circ}$ $C = 0$	2-D Limit Equilibrium method		Brawner, 1970
Letina Slide Czechoslovakia	88	Argillaceous shale		$\phi = 32$	Sliding block analysis	Slide mass was only three to four metres thick	Zaruba, et al., 1969

Table 2.1 Continued

SLIDE	HEIGHT (FEET)	MATERIAL	SHEAR TEST RESULTS	STRENGTH PARAMETERS FOR F.S. = 1.0	TYPE OF ANALYSIS	COMMENTS	REFERENCE
Hope Landslide British Columbia	2400	Igneous rock; slightly schistose green metavolcanic with intrusive sheets of felsite		Ø = 34° C = 0	Morgenstern-Price	Believed to have been triggered by an earthquake	Mathews and McTaggart, 1969
Gros Ventre Wyoming	1800	Interbedded calcareous sandstone and clay shale		Ø = 23° C = 0 with no pore pressure Ø = [illegible]° C = 0 with r_u = 0.4	Morgenstern-Price		Alden, 1928
Grainger County Rockslide Tennessee	46	Siltstone and shale		Ø = 30° C = 0 (with no pore pressure)	Sliding block analysis		Lawrence, 1951
Ateleya Open Pit Spain	400-820	Porphyry	Peak; Ø = 38° C = 150 psi Residual; Ø = 31° C = 0	Ø = 35° C = 15 psi	Hoek's design charts		Hoek, 1971
Filon Sur Open Pit Spain	330	Porphyry	Residual; Ø = 31° C = 0 (on prepared surfaces)	With Ø = 35°, C = 0 on planar joint surfaces, and 49° - on rough shear surfaces, the average C required = 5 psi when drained, = 35 psi with pore pressure	Barton's Limit Equilibrium method		Barton, 1971
Rocky Mountain Slopes Wyoming	Variable	Sandstone and carbonate rocks	$Ø_r$ on rough-sawn specimen sandstone; 24 - 33 carbonate; 32 - 36	For unstable slopes the bedding dipped at angles in the range of $Ø_r$ obtained on shear tests	Visual observation on the dip of sliding planes		Patton, 1966
Twin Buttes (5 slides) Arizona	1000	350' of alluvial gravels and 650' of pyrometasomatic (copper-bearing ore)	Ø = 39° C = 9-59 psi (along clay-filled joints)	Ø = 30° C = .52 psi	Wedge Analysis		Seegmiller, 1972

Table 2.1 Continued

SLIDE	HEIGHT (FEET)	MATERIAL	SHEAR TEST RESULTS	STRENGTH PARAMETERS FOR F.S. = 1.0	TYPE OF ANALYSIS	COMMENTS	REFERENCE
Steep Rock Iron Mines (9 slides) Ontario	50-215	Soft competent quartz, pyrolusite, and kaolin	ϕ = 36 - 38° C = 6 - 13 psi (triaxial tests on compacted samples)	ϕ = 37° C = 7.6 psi	Circular-arc analysis	Assumptions: 1. Water level 50% height of slope 2. Tension crack 25% height of slope	Coates, et al., 1963
Ruth Lake Mine (6 slides) Labrador	100-140	Altered slate and quartzite	ϕ = 33 - 34° C = 7 - 15 psi (triaxial tests on compacted samples)	ϕ = 34° C = 4.7 psi	Circular-arc analysis	" "	Coates, et al., 1963
Steep Rock Iron Mines (7 slides) Ontario	84-445	Altered pyroclastic containing hematite, limonite and pyrite	ϕ = 34 - 46° C = ? (triaxial tests on compacted samples)	ϕ = 40° C = 5.3 psi		" "	Coates, et al., 1963
Knob Lake Mine (15 slides) Quebec	54-145	Slate quartzite	Triaxial tests on broken material ϕ = 34° C = 3.1 - 5.2 psi	ϕ = 34° C = 4.9 psi	Slip-circle analysis		Coates, et al., 1965
Limestone Quarry, Mendip Hill England	230	Limestone with bedding separated by shales		ϕ = 25° C = 14.6 psi	Sliding block analysis		Roberts and Hoek, 1972
Open Pit Coal Mines British Columbia	150	Carbonaceous shales along shear zone	ϕ = 26 - 35° (depending on normal stress) Average = 32°	ϕ = 30 - 35° (depending on pore pressure assumptions)			Brawner, 1971b
Chuquicamata Mine Chile	600	Porphyritic grand-diorite		ϕ = 20° C = 0	Morgenstern-Price	Initiated by an earthquake	Kennedy and Niermeyer, 1970
Madison Canyon Montana	1380	Schist, gneiss and dolomite		ϕ = 36° C = 0	Morgenstern-Price		Barney, 1960
Goldau Slide Switzerland	2600	Tertiary conglomerates		ϕ = 20° C = 0 (with no pore pressure) ϕ = 14° C = 0 (with r_u = 0.4)	Sliding block analysis		Zaruba, et al., 1969

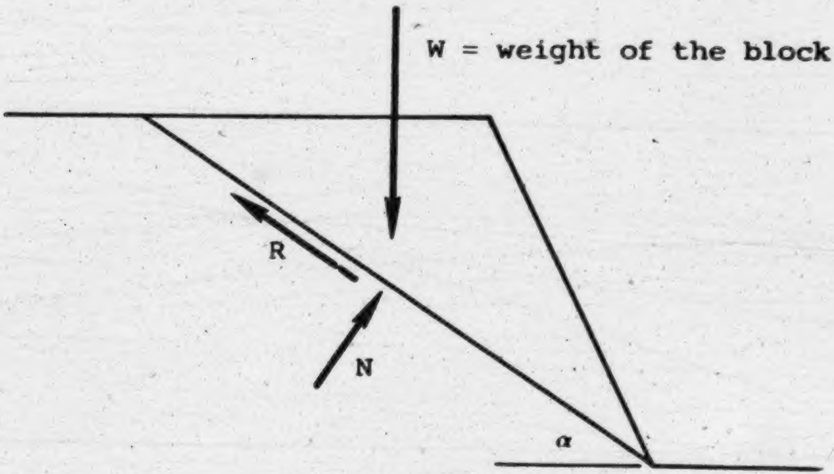

R = the resisting force

N = normal force on the failure plane

$= W \cos\alpha$

The activating force $= W \sin$

The resisting force $= N \tan \phi$

$= W \cos\alpha \ \tan \phi$

Therefore, the F.S. $= \dfrac{W \cos\alpha \ \tan \phi}{W \sin}$

$= \dfrac{\tan \phi}{\tan \alpha}$

Figure 2.1 Limit equilibrium analysis of a sliding block

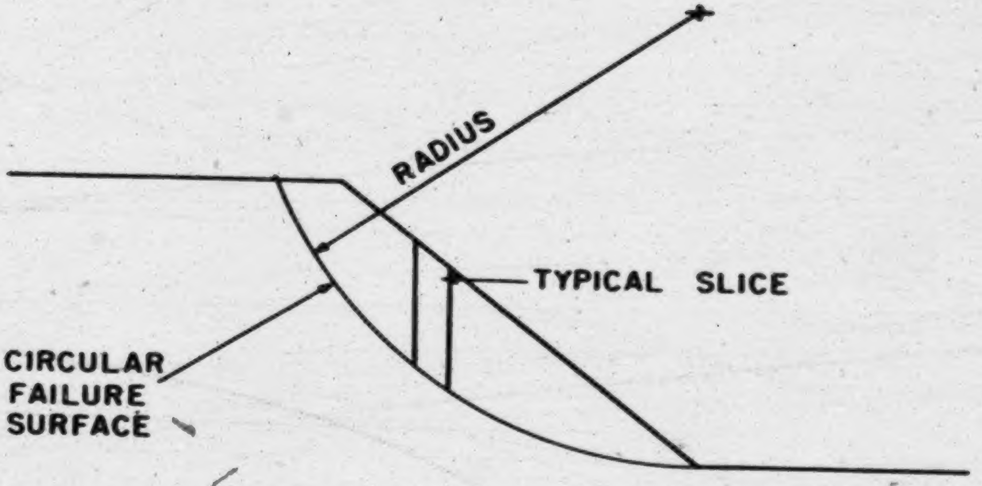
RADIUS
TYPICAL SLICE
CIRCULAR
FAILURE
SURFACE

Figure 2.2 Illustration of circular arc failure surface

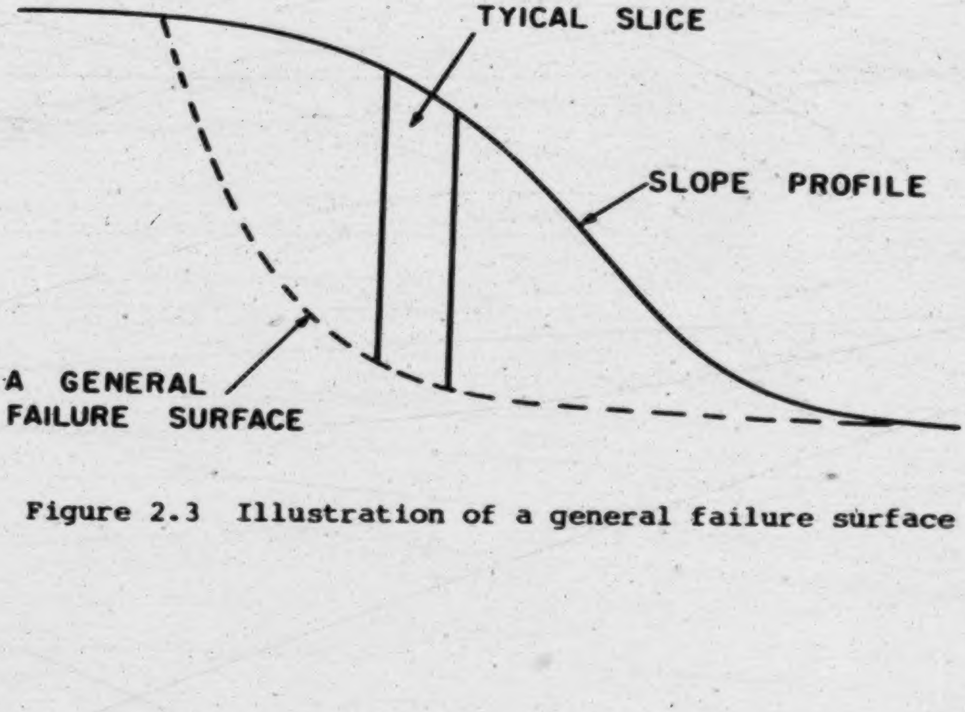
TYICAL SLICE
SLOPE PROFILE
A GENERAL
FAILURE SURFACE

Figure 2.3 Illustration of a general failure surface

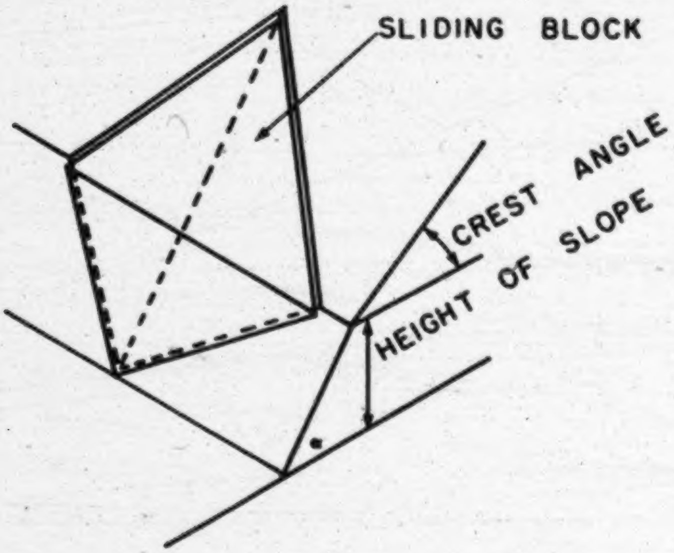
SLIDING BLOCK
CREST ANGLE
HEIGHT OF SLOPE

Figure 2.4 A three-dimensional wedge failure

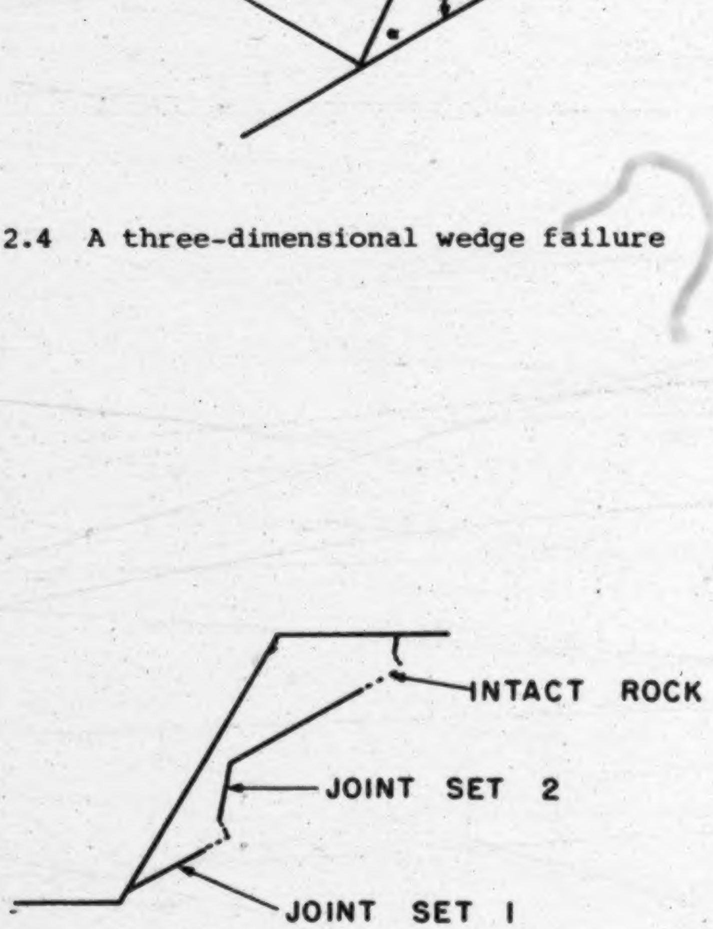
INTACT ROCK
JOINT SET 2
JOINT SET I

Figure 2.5 Illustration of a potential failure surface which includes pre-existing joint sets and intact rock

CHAPTER III

THE SHEARING RESISTANCE OF NATURAL AND ARTIFICIAL ROCK SURFACES

3.1 INTRODUCTION

In rock slope failures, movement generally occurs along structural discontinuities within the rock mass. For this reason, it is imperative that the factors controlling their shear resistance be clearly understood. Numerous shear tests have been performed on natural rock discontinuities in order to study their shearing resistance behaviour. There has generally been no consistency in the reporting of shear test data, and the data has been interpreted in a variety of ways (Jaeger, 1971).

This situation has in recent years improved somewhat in that the general trend now is to consider the shearing resistance along rock discontinuities as arising from two components: the first being the frictional resistance resulting from two flat surfaces sliding over each other and the second component arising from the resistance to sliding imposed by the geometric irregularities on the rock surface.

3.2 THE INFLUENCE OF SURFACE IRREGULARITIES ON THE SHEAR STRENGTH

The frictional component, as determined on flat surfaces, can be defined by the expression

$$S = N \tan \phi_b \text{ .... } 3.1$$

where S = shear force

N = normal force, and

ϕ_b = the basic friction angle of the material as determined on flat surfaces(Figure 3.1).

If a sample had a set of regular inclined surfaces (teeth) as illustrated in Figure 3.2, and the upper block were to slide up the slope as the shearing progressed, the sliding resistance can be defined as

$$S = N \tan (\phi_b + i) \text{ .... } 3.2$$

where "i" is the angle of inclination of the teeth upon which the sliding takes place. The validity of this relationship has been demonstrated by Newland and Allely (1957), Ripley and Lee (1961), and Patton (1966).

The riding of surface irregularities over one another can take place only if the sample dilates. When the normal stress becomes high enough to prevent dilation, the teeth will be sheared through. When this happens, the shear strength will exhibit an apparent cohesion, C, and the strength envelope can be described by

$$S = C + \tan \phi_b \quad \ldots\ldots\ldots\ldots\ldots\ldots\ldots\ldots\ldots \quad 3.3$$

Combining equations 3.2 and 3.3 to define the shear strength over the whole normal stress range results in a bilinear failure envelope as shown in Figure 3.2.

This bilinear law, as demonstrated by Patton (1966), describes very well the shear strength of idealized models with regular projections. However, for actual rock surfaces, there may be a large range of inclination angles (Figure 3.3). For this case, the simple bilinear law is somewhat unrealistic. Due to the variation in "i" values on natural rock surfaces, the change in failure mode from sliding up the slopes to shearing through them will occur over a range of normal stresses. Initially, at a very low normal stress, there will be only the sliding-up mode of failure and eventually at very high normal stresses, there will be only the shearing-through mode. In between, there could be any degree of intensity of both failure modes occurring and, as a result, the failure envelope will be curved instead of being simply bilinear. This is supported by shear test data which is often best described by a curved failure envelope (Murrell, 1965; Maurer, 1966; Hobbs, 1970).

Ladanyi and Archambault (1970) realized this and have developed a more general shear strength equation than the simple bilinear law. Their equation follows.

$$\tau = \frac{\sigma(1-a_s)(\dot{v}+f) + a_s \eta C_o \frac{m-1}{n}\left(1+n\frac{\sigma}{\eta C_o}\right)^{1/2}}{1-(1-a_s)\dot{v}f} \quad \ldots\ldots \quad 3.4$$

where σ = normal stress

τ = tangential stress

$\dot{v}$ = the dilation rate due to shearing

a_s = the shear area ratio; i.e., the fraction of the total shear surface, A, passing through solid rock

f = the average coefficient of friction for the contact surfaces of the discontinuities

η = the degree of interlocking

C = the uniaxial compression strength of the intact rock

n = the ratio between the uniaxial compressive and tensile strength of rock blocks

$m = (n+1)^{1/2}$.

This equation, while it may conceptually be correct, includes parameters like a_s, $\dot{v}$ and η which would be difficult to measure and for this reason it would be difficult to use on a routine basis.

On the basis of laboratory experiments performed on artificial material with tension discontinuities, Barton (1971a) has proposed another law for the peak strength,

$$\tau = \sigma_n \tan \left(20 \log_{10} (C_o / \sigma_n) + \phi_b\right) \text{......} \quad 3.5$$

where C_o is the uniaxial compressive strength.

The simple bilinear law, Ladanyi's equation and Barton's equation all included the ϕ_b parameter, and the rest of the terms within each equation reflect an attempt at including the shearing resistance afforded to the total shearing resistance by the surface irregularities.

3.3 THE EFFECTIVE i ON NATURAL ROCK SURFACES

Figure 3.3 presents two actual roughness profiles of natural rock discontinuities. These traces show the wide range in i values which may be present on natural rock surfaces. The problem is to determine which is the effective i. Patton (1966) was of the opinion that, generally, the irregularities could be divided into categories of first and second order irregularities. Furthermore, Patton and Deere (1971) felt that it is the first order irregularities which control the behaviour of large slopes and that past histories of tectonic loading and weathering will have reduced the interlocking effect of the small second order irregularities.

Barton (1971b) in examining this question further suggests that the ϕ + i concept is too simple because it assumes that the average angle i remains constant throughout the range of normal stresses under which dilation can take place. He suggests that the effective value of i depends on the magnitude of the normal stress. At very low normal stresses, smaller and steeper-sided projections control movement. As the normal stresses increase, these smaller projections are broken off and the more gentle undulations of the first order irregularities control the behaviour. In a series of experiments on model material which had been fractured in tension, Barton obtained an empirical relationship which can be expressed as follows,

$$i = 20 \log_{10} \left(\frac{C_o}{\sigma_n}\right) \quad \ldots\ldots\ldots\ldots\ldots\ldots\ldots \quad 3.6$$

where C is the uniaxial strength. The assumption used in deriving this relationship was that the basic friction angle for the material was 30°.

Rengers (1970) and Fecker and Rengers (1971) have shown how the effective roughness angle (i) decreases with an increase in measuring base length. This suggests that as the shear surface area increases, the effective i decreases. Therefore, the effective i is a function of the scale of the surface area.

The approach of determining the ϕ in the laboratory and then measuring the i component in the field has not been applied to practical design of rock slopes. If it has, there have been no case histories reported showing that this approach can be successfully applied. Therefore, at the present time, it is only a concept. This concept, however, has greatly aided in providing a rational basis for understanding the curvature of failure envelopes which usually occur on natural rock surfaces.

The problem with the approach of measuring the roughness in the field is the limited number of suitable rock surface exposures with a sufficient areal extent to make the measurement. This is especially true at the feasibility stage of an open pit project. Furthermore, in order to check this approach and compare it with actual failures, it would be necessary to expose the slip surface after failure to measure the roughness. To be able to examine an exposed failure surface is seldom, and more likely never, possible. This limits the applicability of this method.

3.4 BASIC FRICTION ANGLE OF ROCK

Earlier it was noted that all the recently proposed shear strength equations have a parameter included which has been referred to as the basic friction angle, ϕ_b. This is the friction angle as determined from shearing tests on flat artificially prepared surfaces (Figure 3.1).

A fair amount of study has been directed towards the problem of how the flat surfaces should be prepared for measuring ϕ_b.

Patton (1966) has suggested that the basic friction angle be determined by using rock surfaces which are rough sawn. He based his views on the fact that this value was similar to those obtained from field observations of stable, unstable and failed slopes.

Coulson (1970, 1972), in following up Patton's work, undertook an extensive investigation to further define this basic friction angle for various rock types. Generally he found that the frictional resistance depends to a large extent on the surface preparation and the surface damage which results during the shearing test. The four different processes of surface damage which occurred were (1) polishing, (2) gouging, (3) the generation of rock flour, and (4) the formation of an indurated crust. He prepared surfaces by using #80 grit, #600 grit and by sand blasting. His recommendation was that surfaces prepared with #80 grit be used to determine the basic friction angle unless the field situation warranted a polished or nearly polished surface.

According to Barton (1971b), the basic friction angle can be obtained from surfaces where the shear force displacement characteristics show no appreciable peak. The granular texture of the rock should be exposed but not to the extent that macroscopic interlocking occurs. Sand blasting appears to satisfy all these requirements.

How this basic friction angle, as determined on artificially prepared surfaces, compares with the ϕ on natural rock surfaces after large shearing displacements, still requires some clarification and will be further considered in Chapter 4.

In some of the case histories examined in Section 2.6, the ϕ required for a F.S. of 1.0 was very similar to the ϕ_b as determined on flat rough-sawn surfaces (Deere, et al., 1967). This would suggest that the proper way to determine ϕ_b would be as Patton or Barton suggested. That is to say, the flat surface should have a fairly rough texture but no large undulations.

3.5 THE EFFECT OF MICROSCOPIC ROUGHNESS ON THE BASIC FRICTION ANGLE

It was mentioned earlier that the frictional resistance on flat rock surfaces is dependent on the surface preparation. Generally the smoother the surface preparation, the lower the frictional resistance (Coulson, 1970, 1972). A question arising from this is whether or not it would be possible to obtain a correlation between the microscopic roughness and the frictional resistance. This would involve some numerical characterization of the surface. Attempts at obtaining this type of correlation have been made by Byerlee (1967) on granite and by Myers (1962) on metallic surfaces. If such a relationship could be established at the microscopic scale, it might also be possible to do the same at a larger scale. This idea was explored in some detail during the course of this thesis work for the limestone rock from Turtle Mountain. The remainder of this chapter presents the results of the roughness study.

3.6 DEFINITION OF ROUGHNESS

In order to obtain a mathematical relationship between frictional resistance and surface roughness, it is necessary to characterize a roughness profile by some numerical value.

Mechanical engineers in describing the finish on a milled surface speak of the root-mean-square value (RMS) of that surface. In the British system, a similar value is known as the centre-line-average (CLA). In fact, many apparatuses are available which will measure the CLA directly and display the result on a dial gauge.

Numerically the RMS is defined by the following equation (ASA, 1955):

$$RMS = \sqrt{\frac{1}{N}\int_{x=0}^{x=N} y^2\,dx} \quad \dots\dots\dots\dots\dots\dots\dots \quad 3.7$$

where N = the number of discrete measurements of the amplitude

y = amplitude of the roughness about a mean of zero

dx = a constant distance between the amplitude readings.

The CLA value is defined as (ASA, 1955):

$$CLA = \frac{1}{L}\int_{x=0}^{x=L} |y|\,dx \quad \dots\dots\dots\dots\dots\dots\dots \quad 3.8$$

where y = amplitude of the roughness about a mean of zero

L = the distance over which the average is taken

dx = the length between successive readings of the amplitude.

The difference between these two definitions is in magnitude only. Roughness measuring instruments calibrated for RMS will read approximately 11% higher on a given surface than those set to read CLA (ASA, 1955).

Myers (1962) has extended the RMS idea further and has given several new parameters for characterizing surface roughness. He defined his first new parameter, Z_2, as follows:

$$Z_2 = \sqrt{\frac{1}{L}\int_{x=0}^{x=L}\left(\frac{dy}{dx}\right)^2 dx} \quad \ldots\ldots\ldots\ldots\ldots\ldots\ldots \quad 3.9$$

In words, this is the RMS of the first derivative of the profile.

The second new characteristic, Z_3, is defined as the RMS of the second derivative of the surface roughness. Numerically

$$Z_3 = \sqrt{\frac{1}{L}\int_{x=0}^{x=L}\left(\frac{d^2y}{dx^2}\right)^2 dx} \quad \ldots\ldots\ldots\ldots\ldots\ldots\ldots \quad 3.10$$

The significance of the Z_3 parameter, according to Myers, is in revealing the roundness of the peaks of the roughness profile. Myers correlated these parameters with the coefficient of friction on samples of cold-rolled steel disks and found that the best relationship was obtained with the Z_2 parameter.

Another possible approach to characterizing surface roughness, especially on the microscopic scale, is to consider the profile to be the result of a stochastic process and analyze it on a statistical basis. The measurement and analysis procedure for such data has been very carefully documented by Bendat and Piersol (1971). The majority of information given here with regard to the definition of statistical terms was taken from this valuable source.

The four main statistical functions used to describe the basic properties of random data are, (1) the mean square values, (2) the probability density functions, (3) the autocorrelation functions, and (4) the spectral density function. The descriptive properties, definitions and applications of these functions are given below.

3.6.1 MEAN SQUARE VALUES

The mean square value of a sample time-history record x(t), gives a rudimentary description of the intensity of the data. It is simply equal to the average of the squared amplitudes of the sample record. In equation form, the mean value, MSV, is given by

$$MSV = \frac{1}{N} \int_{t=0}^{t=N} x^2(t)\, dt \quad \ldots\ldots\ldots\ldots\ldots\ldots\ldots\ldots \quad 3.11$$

Figure 3.4 shows a sample time-history record. The square root of the MSV is called the root mean square (RMS). When the MSV is obtained with the mean being zero, it is equal to the variance.

3.6.2 PROBABILITY DENSITY FUNCTION

The probability density function furnishes information about the properties of data in the amplitude domain. It gives the probability that the data will assume a certain value within a range x and $(x + \Delta x)$ (Figure 3.4). A special case of a probability function is the classical Gaussian function characterized by the familiar bell-shaped curve. The distribution described by the Gaussian function is commonly known as a normal distribution.

3.6.3 AUTOCORRELATION FUNCTION

In equation form the autocorrelation function (ACF) is described by

$$ACF = \frac{1}{T} \int_0^T x(t)\ x(t + \tau)\ dt \ldots\ldots\ldots\ldots\ 3.12$$

where τ is a constant time lag. This function gives an indication of the dependence of the values of the data at one time on the values at another time. The ACF will have a maximum value at zero time displacement. At this point, it will be the same as the variance.

The principal application of the ACF is to use it as a tool to detect deterministic data (e.g. a sine wave) which might be masked in a random background. For deterministic data the ACF will persist over all time displacements as opposed to random data where the ACF will diminish to zero.

3.6.4 SPECTRAL DENSITY FUNCTIONS

The power spectral density function of random data indicates the manner of the distribution of the harmonic content of the signal over the frequency range from zero to infinity. It can also be thought of as the amount of its mean square value associated with a narrow band of frequency, Δf. In equation form the spectral density function (SDF) is expressed by

$$SDF = \int_{0}^{\infty} \lim_{T \to \infty} \left[\frac{2}{T} | A_T (if) |^2 \right] df \text{ .... } 3.13$$

where $A_T(if)$ is the Fourier transform of a signal $x_T(t)$. For a detailed explanation and derivation of this equation, the reader is referred to Robson (1963).

The principal application for the SDF measurement is to establish the frequency composition of the data which in turn bears an important relationship to the characteristics of the system involved. For example, if a system has a frequency response function $H(f)$ and a random signal with a spectral density function $G(f)$ is applied to the system, the output of the system will be a random signal with a power spectral density function equal to $| H(f) |^2$ times $G(f)$.

When these statistical parameters are viewed together, they furnish similar information but in different formats. The probability density function furnishes information concerning the properties of the data in the amplitude domain while the autocorrelation function furnishes information in the time domain, and the spectral density function gives similar information in the frequency domain (Bendat, et al., 1971).

The physical significance of these parameters will become more evident with the actual digital computation of these parameters.

3.7 SAMPLE PREPARATION

The first step in exploring this concept was to prepare samples with different surface roughnesses and then determine the frictional resistance. With this in mind, samples of limestone from Turtle Mountain were prepared for direct shear testing by, first of all, using a diamond saw to cut specimens from a large rock block. The approximate size of these specimens was 1.8 x 1.8 x 3.0 inches. They were then cast in Devcon-B epoxy so that the sample would be square and fit the shear box exactly. Each half was cast separately leaving a space between the halves for the shear plane (Figure 3.5). After the casting was completed, the two halves were sawn apart using the same diamond saw which had been used for the initial trimming. This final diamond-saw cut then became the shear surface for the test. Six samples were prepared in this manner.

In order to obtain different degrees of roughness on these shear surfaces, one was left as a diamond-saw cut, while another was finished by dry sanding with a #80 grit sandpaper, and the final four were lapped with different sizes of grit. The sample designation and the corresponding surface finish of each surface are presented in Table 3.1.

3.8 SHEAR TESTS AND RESULTS

Upon completion of the sample preparation, each sample was subjected to direct shear tests using a shear box designed and built at the University of Alberta. With this apparatus, the normal load was applied with a dead weight-lever arm arrangement while the shear load was applied by a gear box-chain drive assembly powered by an electric motor (Figure 4.5). The horizontal displacement was measured with a linear variable displacement transducer (LVDT) and the shear load was measured with an 8,000-pound load cell. The shear load and displacements for these particular tests were recorded with an X-Y plotter, and the tests were run dry at a rate of deformation of 0.05 inches per minute. After having completely assembled the apparatus, with the sample in place, the horizontal deformation was started and allowed to continue until the shear load had more or less levelled off. At this point, the normal load was increased and the test continued until the shear load had once more levelled off. In this way, the sample was step loaded to the highest desired normal load. A typical shear load versus displacement graph resulting from this procedure is shown in Figure 3.6.

From these load-deformation curves, the shearing resistance was noted at each normal load and then both the shear and normal loads were divided by the initial area to convert them into stresses. The results for all the samples are shown in Figure 3.7.

The most notable feature concerning the results shown in Figure 3.7 is the wide variation in friction angle obtained from the various surfaces. From a visual inspection and by feeling the surfaces, it seemed that the rougher the surface the higher the friction angle. It was this observation which initially suggested that it might be possible to obtain a relationship between the friction angle and the surface roughness.

3.9 DIGITIZATION OF ROUGHNESS PROFILES

The first step in attempting to characterize a surface roughness was to obtain a trace of the surface profile on the microscopic scale. This was done with a Talysurf roughness measuring instrument owned by the Mechanical Engineering Department at the University of Alberta which produced a graphical output as shown in Figure 3.8. In this way, two surface profiles were obtained for each sample, one before the shear test and the other after.

Once the surface profiles were obtained, the next step was to digitize them; that is to make discrete measurements of the amplitude at regular intervals about some datum.

This was done using a digitizer available at the Computing Centre, University of Alberta. This apparatus essentially converts analog data to digital data and in one of its uses converts strip charts to digital representation. The digitizer records the X and Y co-ordinates of selected points when a cursor is run over the analog signal. The co-ordinates are recorded by the digitizer on magnetic tape making it possible to handle large quantities of data with relative ease.

For the particular problem at hand (digitizing the surface profiles) the apparatus was set to take a reading at an interval of 0.01 inches along the strip chart. This meant that 100 discrete amplitude measurements were obtained for every inch of strip chart. In this manner then, 2,048 readings were taken for each profile. The reason for this particular number is that 2^N values are required for the calculation of the spectral density function. In the present context N was chosen to be 11.

The co-ordinates of each point were initially recorded on the magnetic tape in inches with reference to the co-ordinate system of the digitizing table. Consequently, all the readings had to be converted into micro-inches and also translated to some appropriate datum relative to each profile. The datum was chosen so that the mean of all the readings for a particular profile would be zero. These manipulations were performed on the IBM-360 computer and the results stored on a 9-track magnetic tape.

Later this digital profile data was retrieved and replotted using the Calcomp Plotter at the Computing Centre. The Calcomp Plotter output for all the surface profiles obtained is shown in Figures 3.9 to 3.14. The traces in these figures are simply straight lines between the data points but the points are close enough to give the appearance of smooth curves. These computer plots were compared with the original strip charts, and there was no visible difference noted between the two. Reproducing these profiles from the digital data also aided in ensuring that there were no erroneous results in the data files.

Without the computer, the digitizer and the tape storage for information, it would not have been possible to deal with such large quantities of data.

3.10 DIGITAL COMPUTATIONS

Once the surface profiles were in digital form, it was a relatively simple matter to calculate the majority of surface characterization parameters discussed in Section 3.6. For example, to calculate the RMS, the requirement is to square all the readings, add them, divide by the number of readings and then take the square root. This is not mathematically complicated and can be easily done on the computer even though there were 2,048 readings for each profile.

The only parameter which presented some computational difficulties was the spectral density function (SDF). To determine the SDF some special techniques are required which are worth mentioning.

There are two methods available for computing SDF's. The first is the so-called "Blackman-Tukey" method (Blackman and Tukey, 1959) based on computing the autocorrelation function (ACF) initially and then calculating the Fourier transform of the ACF. The Fourier transform of the ACF is the SDF, and the ACF and SDF are known as Fourier transform pairs (Robson, 1963). A newer and more efficient way of determining the SDF is the "Cooley-Tukey" method (Cooley and Tukey, 1965) which determines the SDF via a fast Fourier transform of the original data. Bendat and Piersol (1971) give a detailed description of this method and how it is used.

Since the mathematical computations are fairly involved, several computer programs have been written to calculate the fast Fourier transform of random data. The one used during the course of this thesis was obtained from the University of Alberta Physics Department and is given in

Appendix C.

3.11 AMPLITUDE DISTRIBUTIONS OF ASPERITIES

Bowden and Tabor (1956) stated that the results from refined profilometer techniques show that the asperities on most surfaces have a Gaussian distribution. Work done by Williamson and Hunt (1968) indicated the same observation. It was felt it would be of interest to compare the distributions of the surface profiles obtained from the limestone samples with the observations of the above-mentioned authors.

From the digital data on each profile, an appropriate class interval was chosen and a count was then made of the number of readings which fell into each interval. For example, the class interval for sample 4 (before shearing) was chosen to be 20 microinches, and the number of amplitude readings on this sample which had an amplitude range of -120 to -140 was 65 (Figure 3.18). The results were plotted as bars on a frequency-versus-amplitude graph in Figures 3.15 to 3.20. The theoretical Gaussian distributions are superimposed on each of the bar graphs in order to compare the observed with the theoretical. The normal curve (Gaussian) can be easily determined by calculating the standard deviation of the digital data.

Upon examining all those distributions, it appears that generally, the actual distribution can be described fairly well by a Gaussian distribution. The best agreement was obtained for the surfaces lapped with the #200, 400 and 600 grit before the shear tests were performed (Figures 3.18, 3.19 and 3.20).

Probably one of the more interesting features that these distributions show is the change which occurs on the shear surface during the test. It is most noticeable for the samples lapped with #200 and 400 grit (Figures 3.18 and 3.19). There is a marked increase in the frequency of the amplitudes just to the right or positive side of the mean while at the same time the highest asperities have disappeared. This is quite understandable upon re-examining the corresponding surface profiles (Figures 3.12 to 3.13). From these profiles it can be seen that the positive peaks have disappeared resulting in the flat plateaus. These flat plateaus are probably the only areas of contact during the friction tests.

The only distinctive feature about the normal distribution curves, as far as characterizing them numerically, is the standard deviation which is similar to the RMS if the mean is zero.

3.12 ROUGHNESS CHARACTERIZATION VERSUS FRICTIONAL RESISTANCE

From the digital data, the CLA, RMS, Z_2 and Z_3 parameters were calculated for each surface. The results are presented in Table 3.2 together with the friction angle obtained from the direct shear tests. The friction angle, corresponding with the roughness before the test, was taken from the initial slope of the shear versus normal stress curves (Figure 3.7). The results tabulated in Table 3.2 are plotted in Figure 3.21 to 3.23. Since the CLA and RMS are similar, except for the 11% difference in numerical magnitude, only the CLA values were plotted against ϕ. The best correlation is between ϕ and the Z_2 parameter. The coefficient of correlation between ϕ and Z_2 is 0.881. In a statistical sense, the required correlation coefficient, at a significance level of 1%, should be greater than 0.708 for there to be a linear correlation. Since the correlation coefficient is higher than this, it can be stated that there is a linear correlation between Z_2 and ϕ. The same is true for Z_3 but not for the CLA parameter. The correlation coefficient between ϕ and the CLA parameter is only 0.674. This type of result is very similar to the results obtained by Myers (1962). He obtained a correlation coefficient with Z_2 of 0.84 and only 0.54 with RMS.

A typical autocorrelation function (ACF) plot is presented in Figure 3.24. Of all the ACF plots, there was really nothing distinctive about them which could be used to depict a single characterizing parameter. Therefore, this function could not be used to define a parameter with which the ϕ could be correlated. The value of ACF lies in the fact that it is a mathematical tool which can be used to determine a harmonic wave masked in the random data.

As far as establishing a single roughness parameter, the same comments apply to the spectral density functions as they do to the ACF. A typical SDF is presented in Figure 3.25. The SDF does not furnish much more information than the ACF except that the SDF is presented in the frequency domain.

Since the spectral density function has been used to study roughness profiles of airport runways and highways (Houbolt, 1961; Hutchinson, 1965), it is worthwhile to see how it has been applied in the transportation field. Figure 3.26 gives the criteria as presented by Houbolt (1961). It should be noted here that the ultimate purpose of spectral density measurements in roadways and airport runways is somewhat different than simply determining a single characterizing value for a particular roadway roughness. Their interest is more in determining which wavelengths (or frequencies) will cause excessive vertical motion to be induced when a vehicle passes over the road (Quinn, et al., 1970). The roughness spectrum indicates which wavelengths contribute to the total pavement roughness.

3.13 DISCUSSION OF RESULTS

The correlation of roughness parameters with the friction angle generally follows a linear trend with ϕ increasing as the roughness parameter increases. An increase in the roughness parameter indicates an increase in surface roughness.

The main reason for the amount of scatter obtained in the correlation data is that various types and degrees of surface damage occur during the shear test. The type of damage greatly affects the shearing resistance. Two samples with the same surface finish may exhibit a different shearing resistance because on one there may be a lot of gouging and on the other, there may be surface polishing. This is especially true for the smoother surfaces.

The correlations of roughness parameters with ϕ are good enough, especially with Z_2, that upon knowing the roughness parameters, a fairly good estimate could be made of ϕ. This approach, however, is not practical since the time and effort involved in calculating the roughness parameter is far greater than simply doing a shear test.

The advantage of performing a study like this at the microscopic scale is that it is possible to obtain a roughness profile which is representative of the type of surface. That is to say, a profile like the one shown in Figure 3.10 could have been taken anywhere on the sample and it would not have been significantly different. With the representative profile, it is possible to develop the tools necessary to define the roughness and establish what parameter is most closely correlated with ϕ. Once this has been done, there is conceptually no reason why the same principal could not be transferred to the field scale where it would be simpler to determine the roughness parameter than to perform a shear test.

The problem with testing the developed mathematical tools in the field is two-fold. Firstly, it would be necessary to have rock discontinuity exposures in the field on which a representative field roughness profile could be obtained. Three surface profiles over a five-foot distance (Figure A.7) are shown in Appendix A. Certainly these could not be considered as representative because the larger wavelengths are not complete. This means that the roughness profile would have to be obtained over a much larger distance; i.e., 100 feet. These types of exposures seldom, if ever, exist. Secondly, the associated shear tests at this scale could never be performed.

TABLE 3.1

SAMPLE DESIGNATION FOR ROUGHNESS STUDY

Sample Number	Surface Finish
1	Dry sanded
2	Diamond-saw cut
3	Lapped with 45/80 grit
4	Lapped with #200 grit
5	Lapped with #400 grit
6	Lapped with #600 grit

TABLE 3.2

ROUGHNESS PARAMETERS FOR SURFACE PROFILES

	Before Testing					After Testing				
Sample No.	Ø	CLA	RMS	Z_2	Z_3	Ø	CLA	RMS	Z_2	Z_3
1	10.5	28.3	38.5	0.075	0.026	10.5	28.0	37.4	0.093	0.028
2	27.3	93.1	121.0	0.214	0.143	15.2	80.1	101.0	0.135	0.049
3	36.0	641.0	808.0	0.338	0.253	33.0	342.0	410.0	0.236	0.142
4	31.4	72.0	88.5	0.196	0.102	22.8	67.8	84.9	0.143	0.060
5	26.0	36.8	45.8	0.150	0.059	16.3	36.9	46.8	0.109	0.032
6	24.0	27.1	34.4	0.123	0.034	19.1	22.9	28.4	0.098	0.022

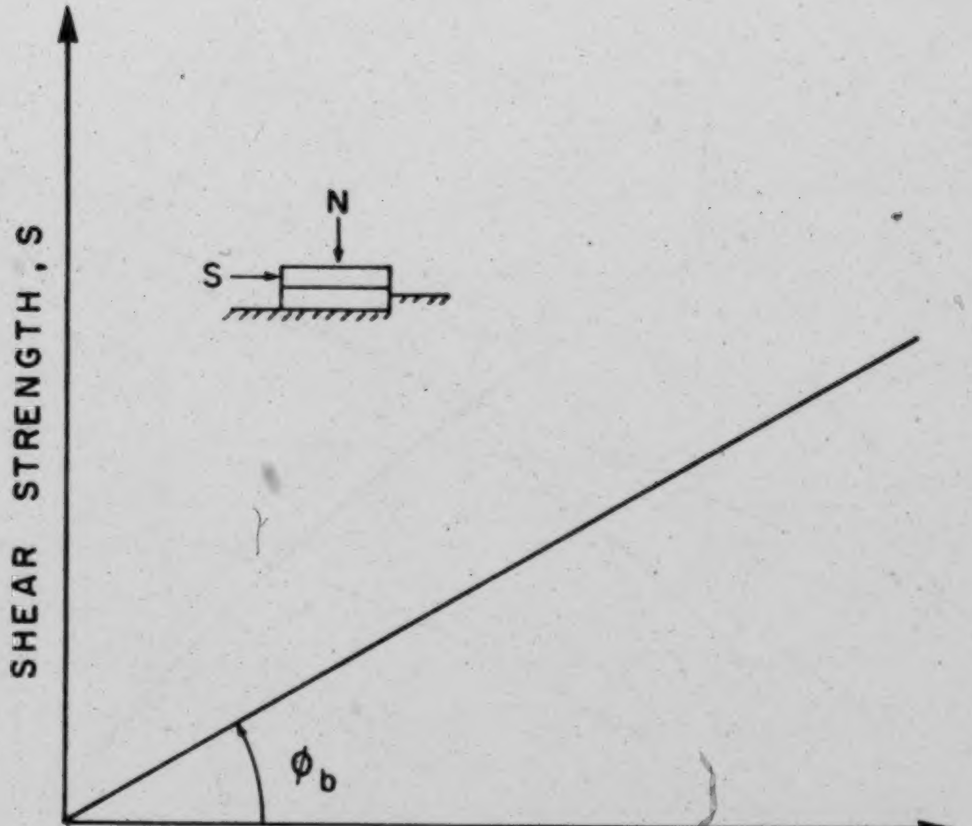
SHEAR STRENGTH, S
N
S
ϕ_b
NORMAL LOAD, N

Figure 3.1 Failure envelope for specimens with flat surfaces

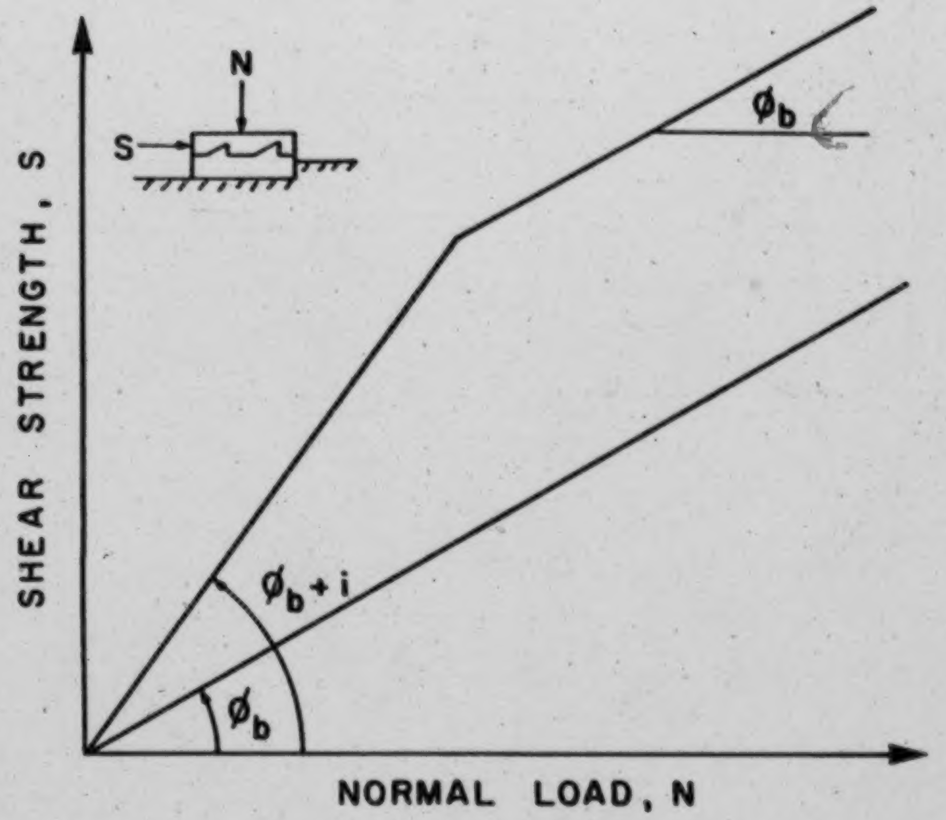

Figure 3.2 Failure envelope for multiple inclined surfaces

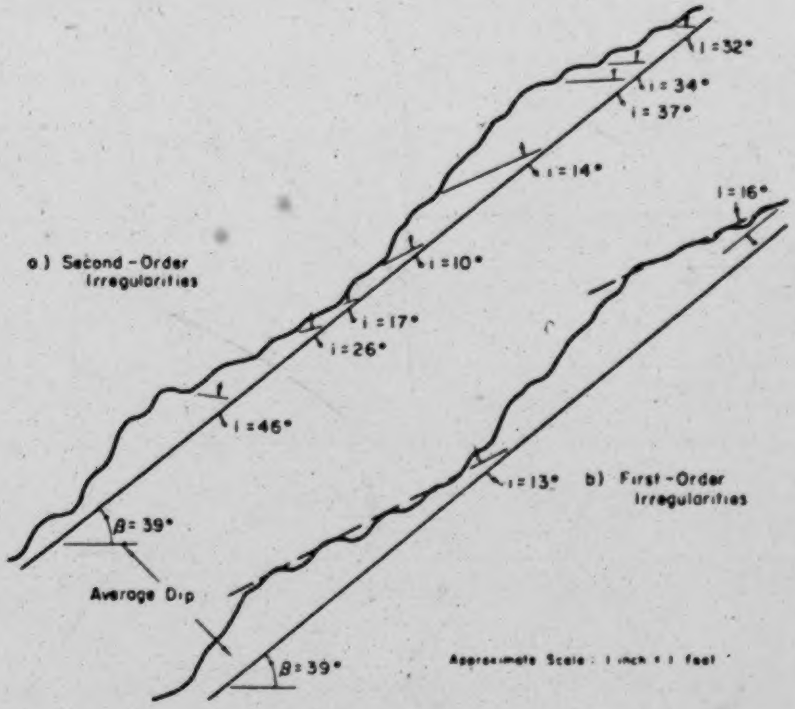
i = 32°
i = 34°
i = 37°
i = 14°
i = 16°
a) Second-Order Irregularities
i = 10°
i = 17°
i = 26°
i = 46°
i = 13°
b) First-Order Irregularities
β = 39°
Average Dip
β = 39°
Approximate Scale: 1 inch = 1 foot

Figure 3.3 An example of a natural discontinuity illustrating first- and second-order irregularities (after Patton, 1966)

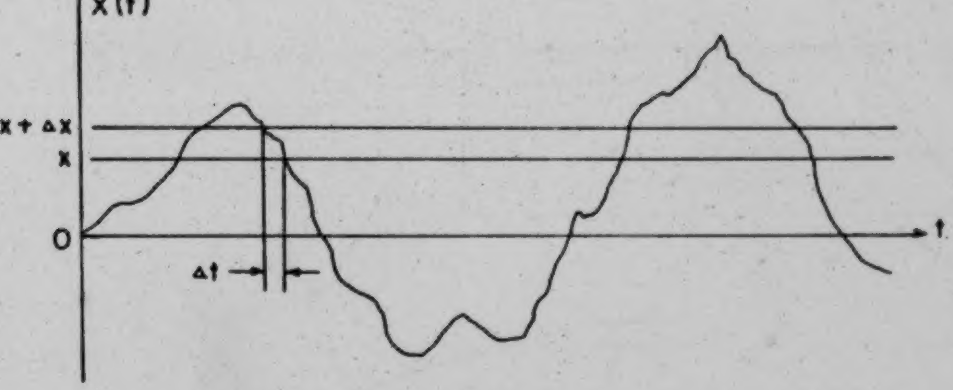

Figure 3.4 An example of a time-history record x(t)

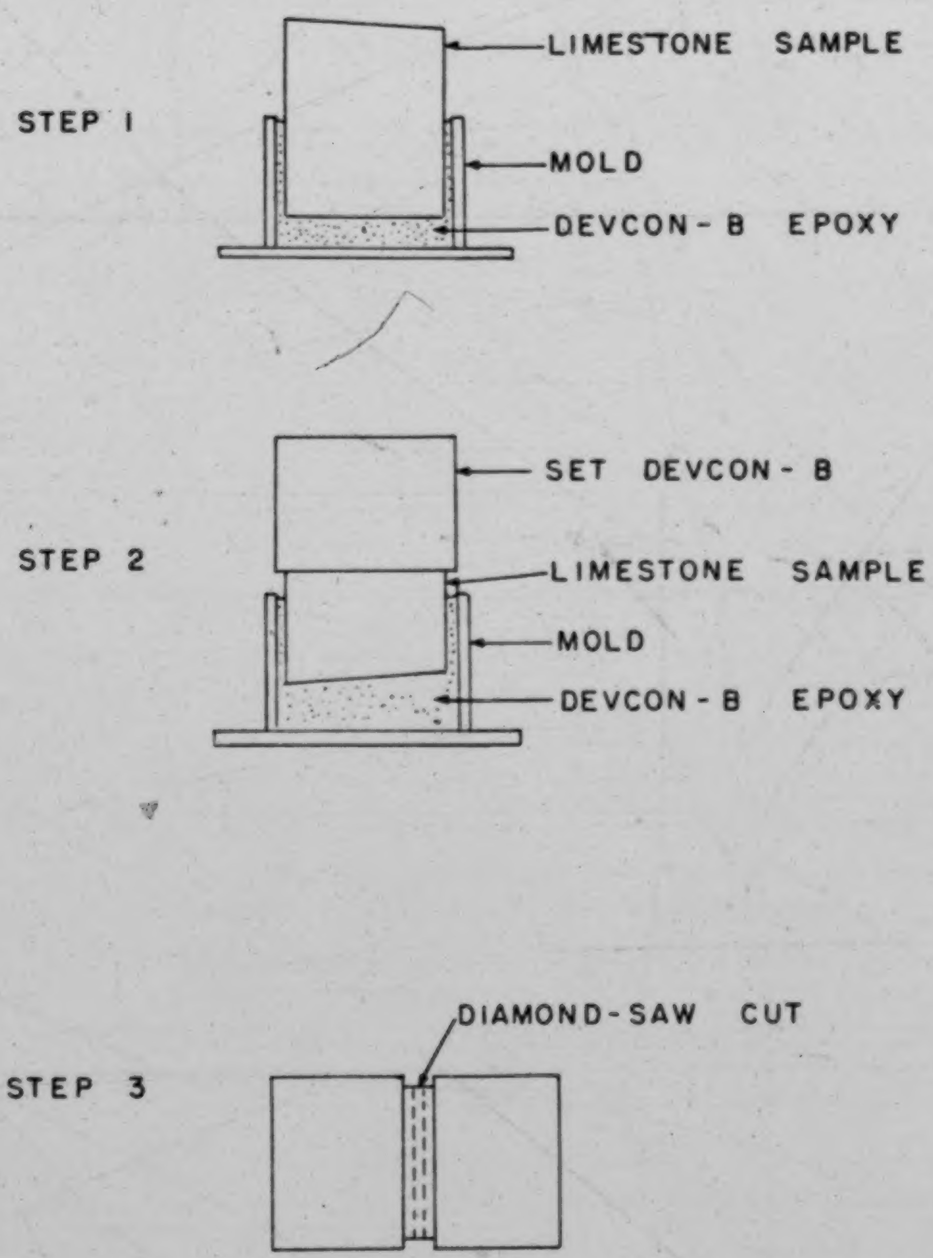
STEP I
LIMESTONE SAMPLE
MOLD
DEVCON - B EPOXY
STEP 2
SET DEVCON - B
LIMESTONE SAMPLE
MOLD
DEVCON - B EPOXY
STEP 3
DIAMOND-SAW CUT

Figure 3.5 Casting of limestone samples

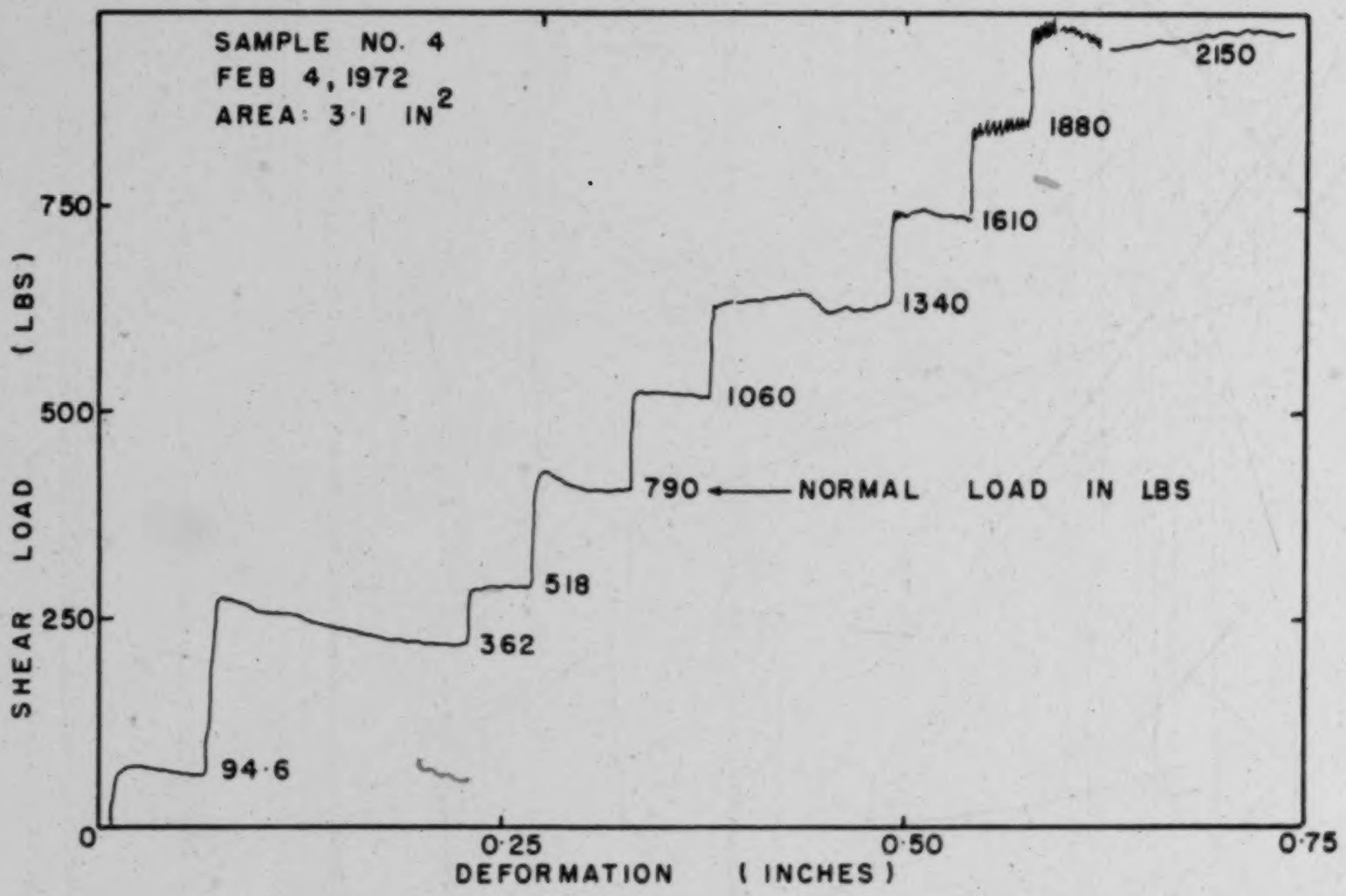

Figure 3.6 A typical step loaded, shear load versus deformation plot

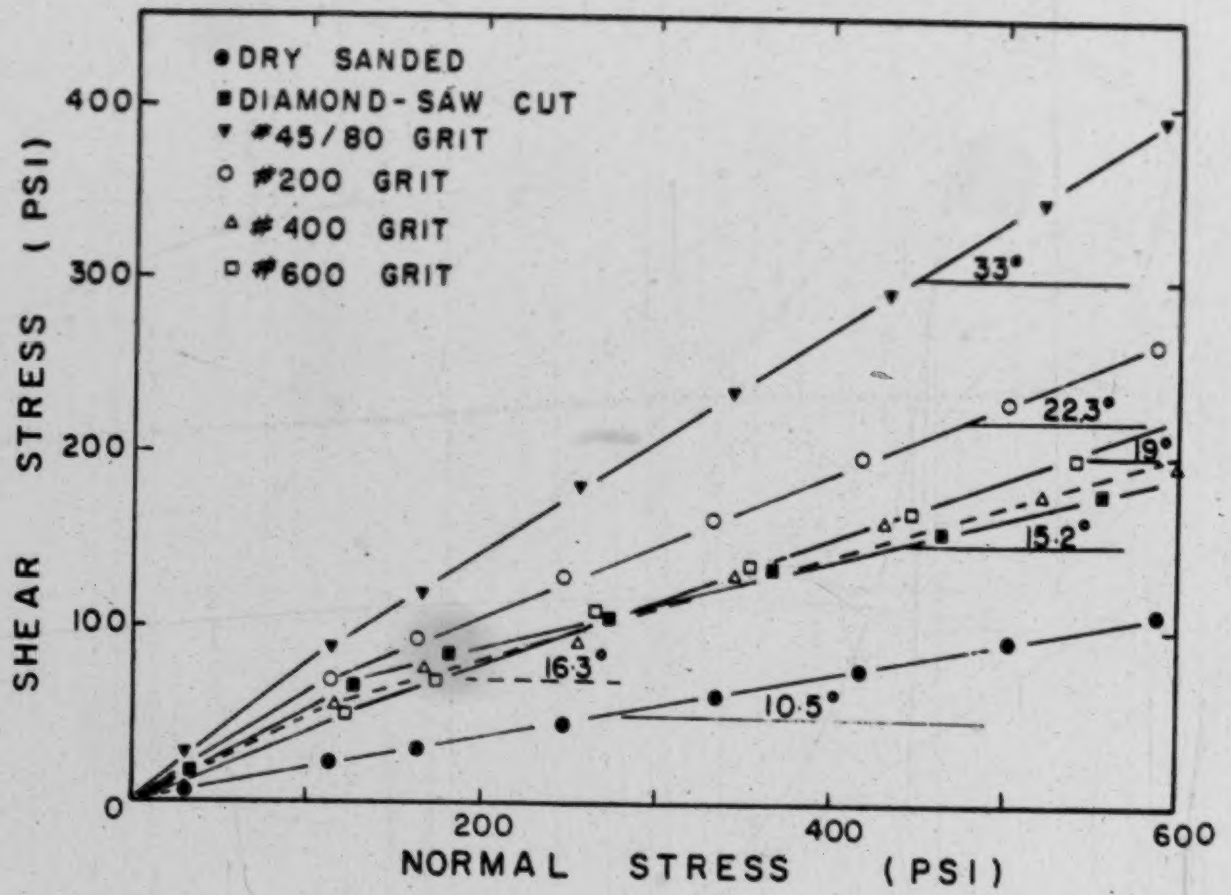

Figure 3.7 Failure envelopes for rock surfaces with various roughnesses

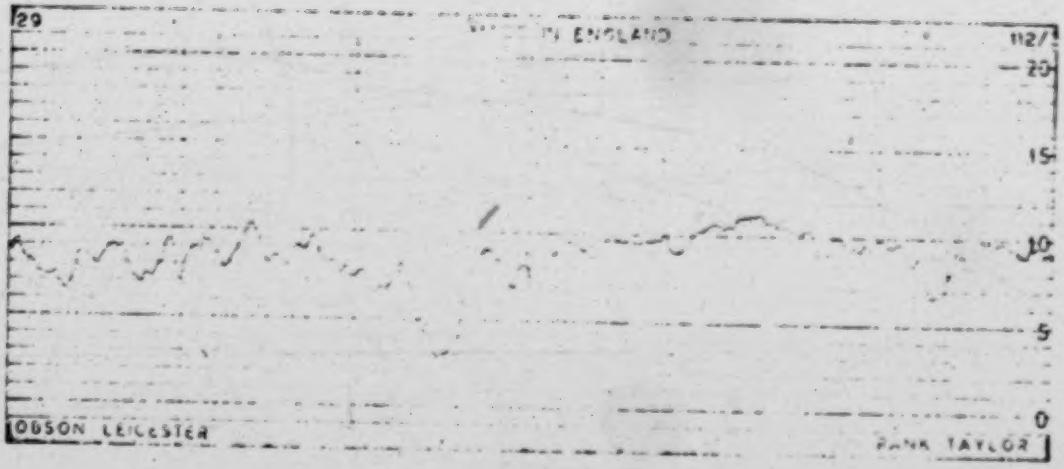

SCALE: VERTICAL 1 DIV = 100 μ"
HORIZONTAL 1 DIV = 0·002"

Figure 3.8 An example of a surface trace from the Talysurf

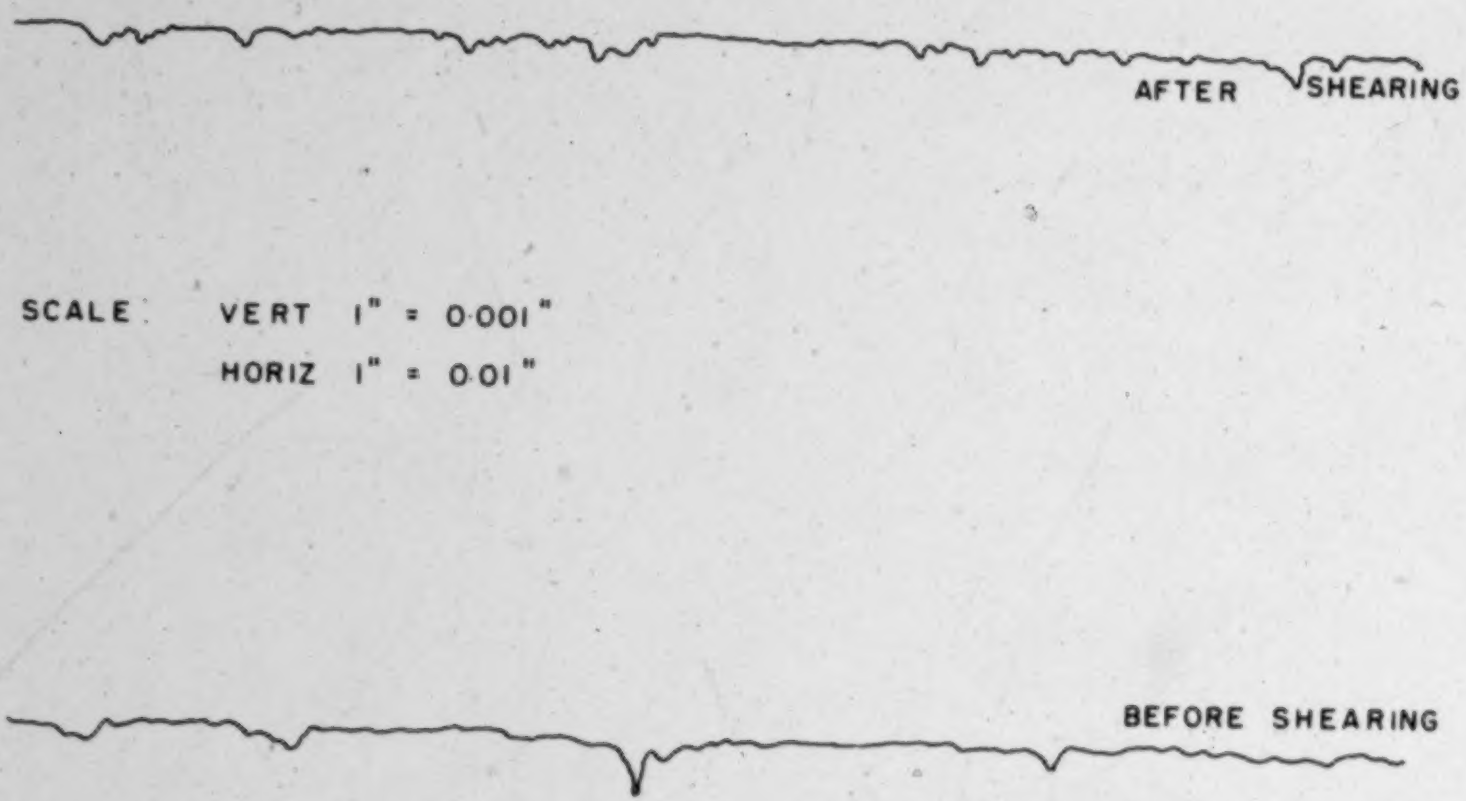

Figure 3.9 Surface profiles for the dry sanded sample

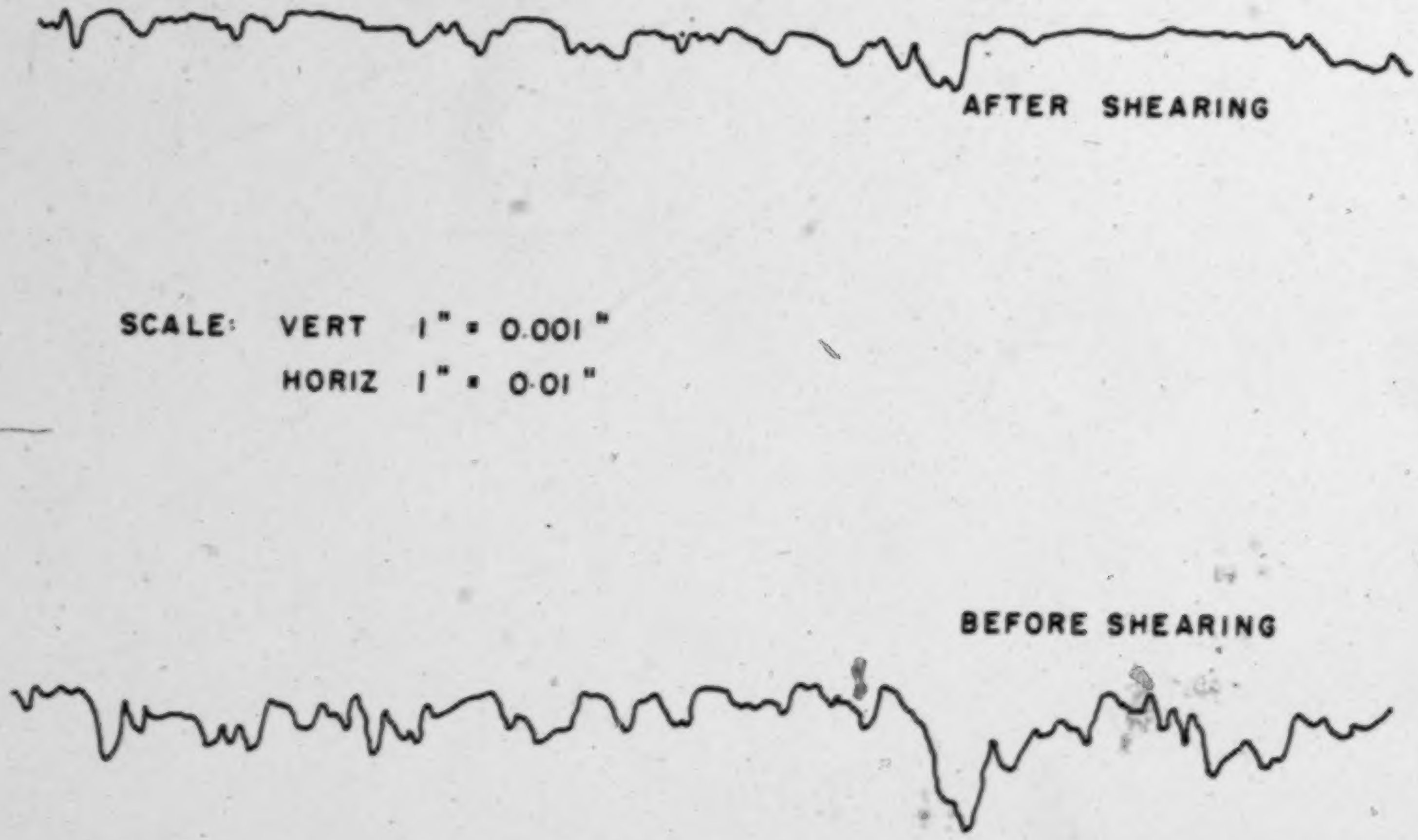

Figure 3.10 Surface profiles for the diamond-saw cut surfaces

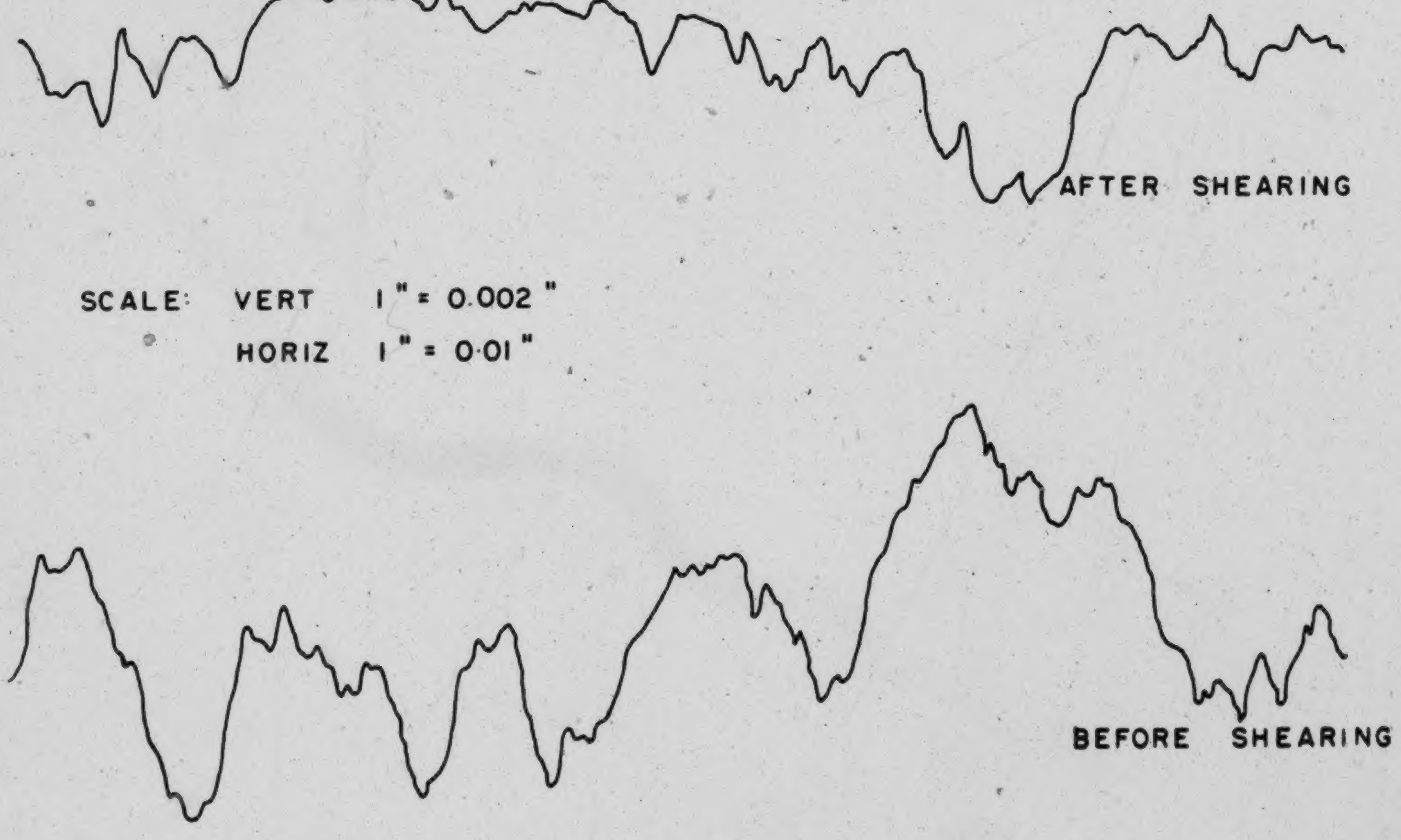

Figure 3.11 Surface profiles for sample lapped with #45/80 grit

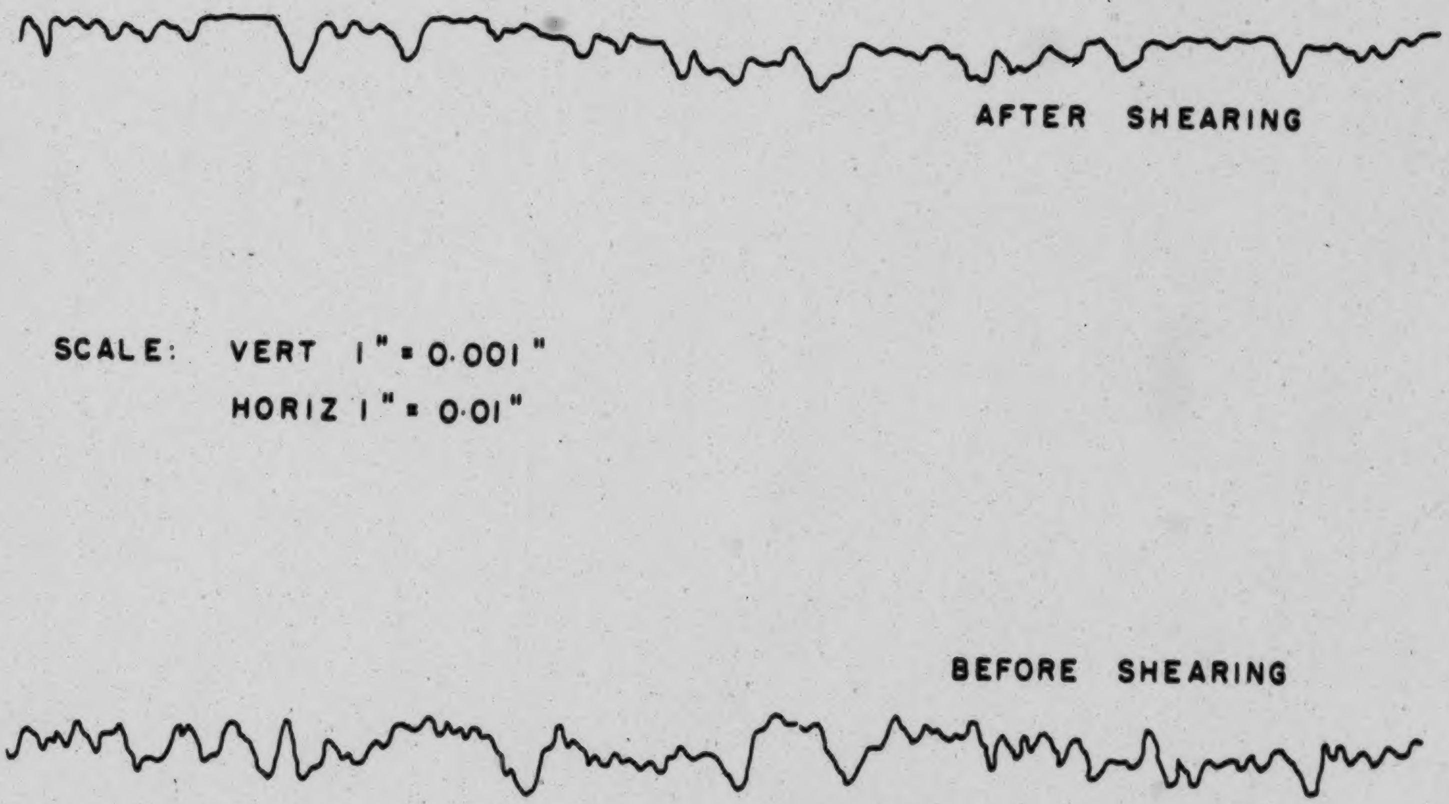

Figure 3.12 Surface profiles for sample lapped with #200 grit

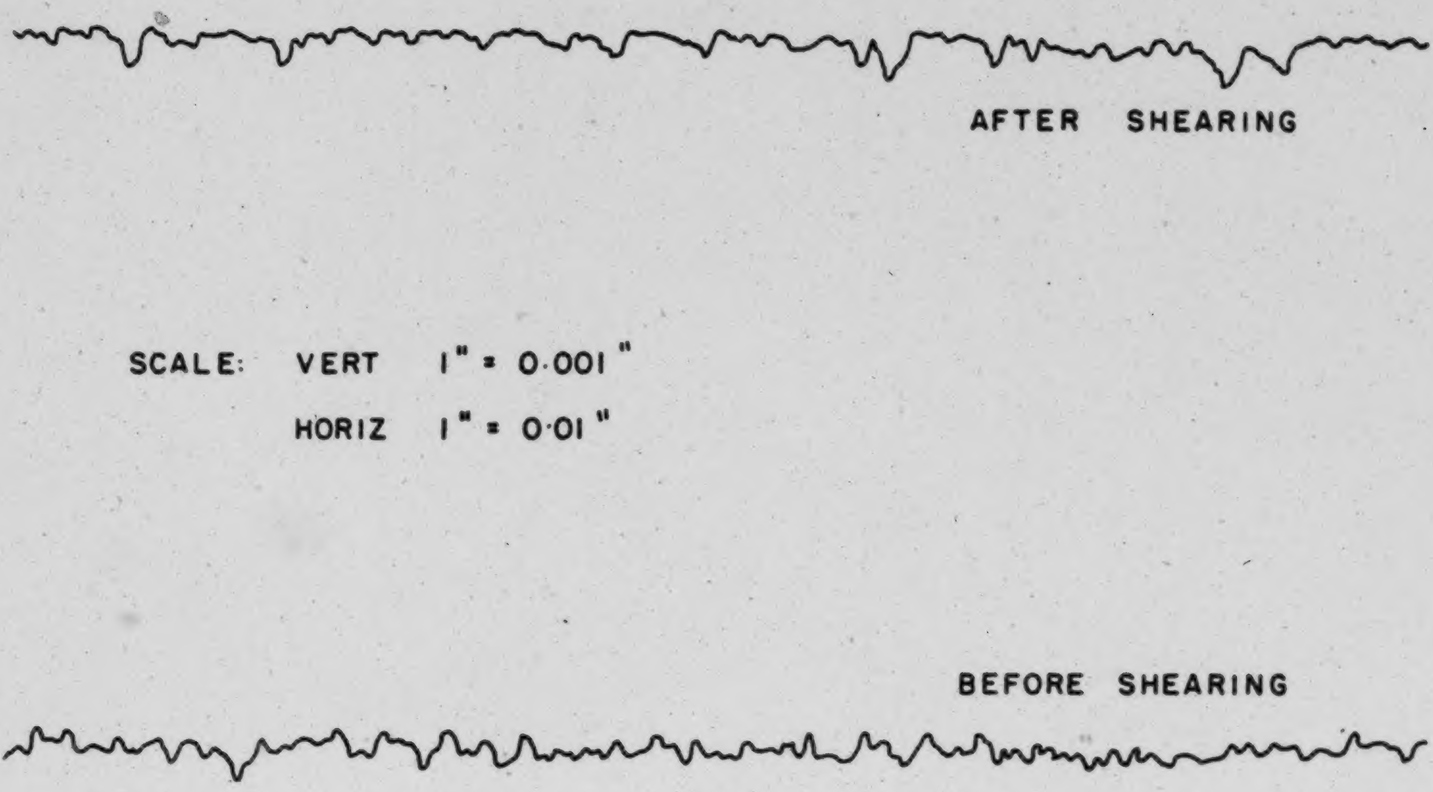

Figure 3.13 Surface profiles for sample lapped with #400 grit

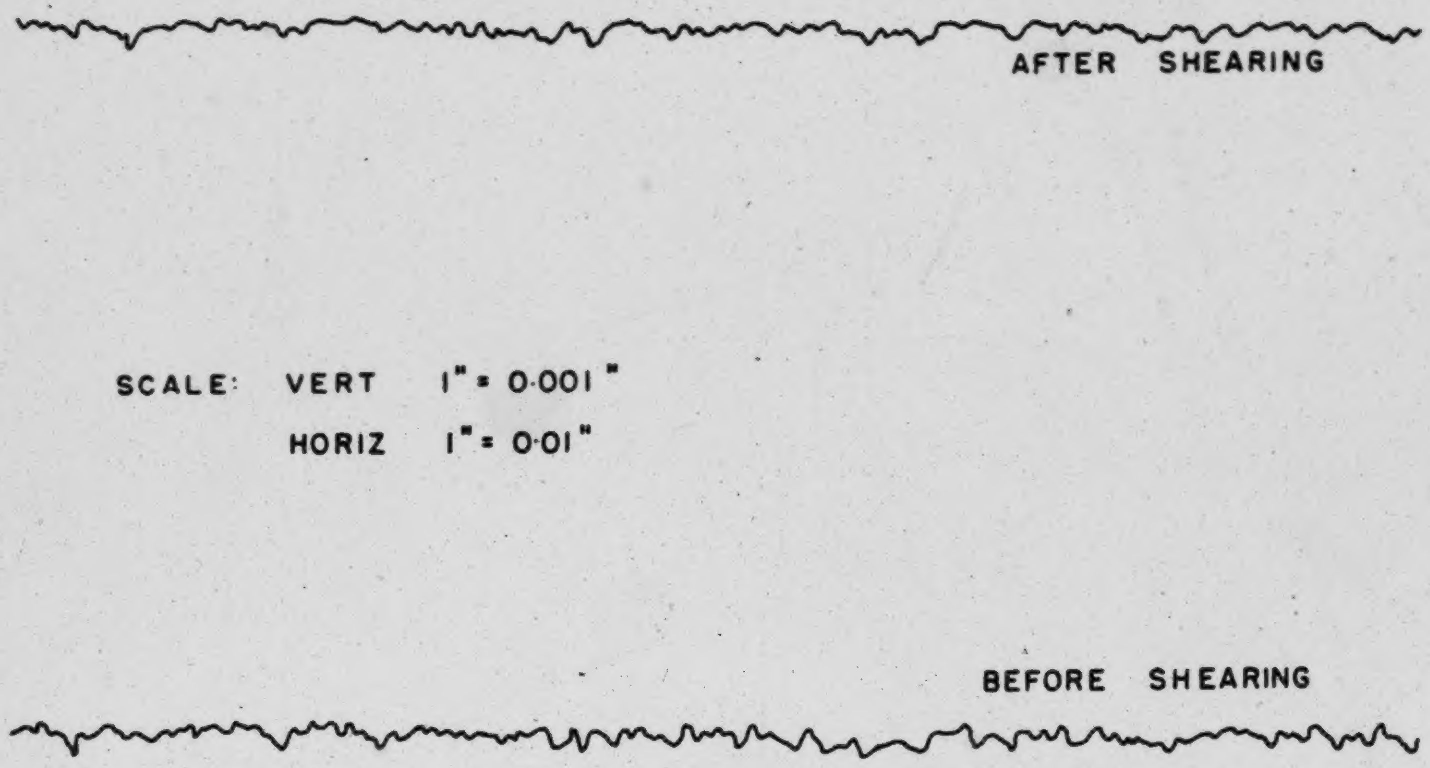

Figure 3.14 Surface profiles for sample lapped with #600 grit

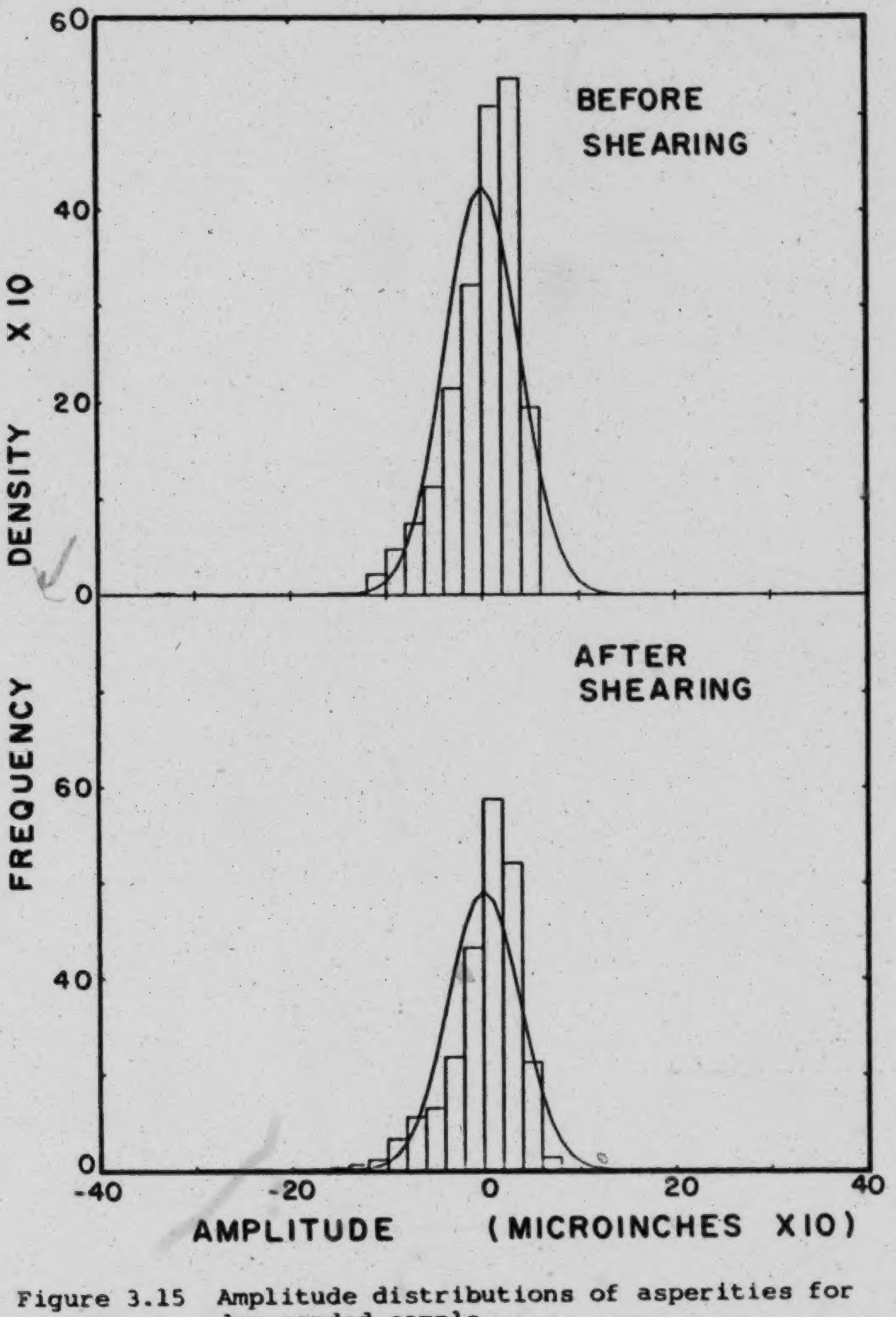

Figure 3.15 Amplitude distributions of asperities for dry sanded sample

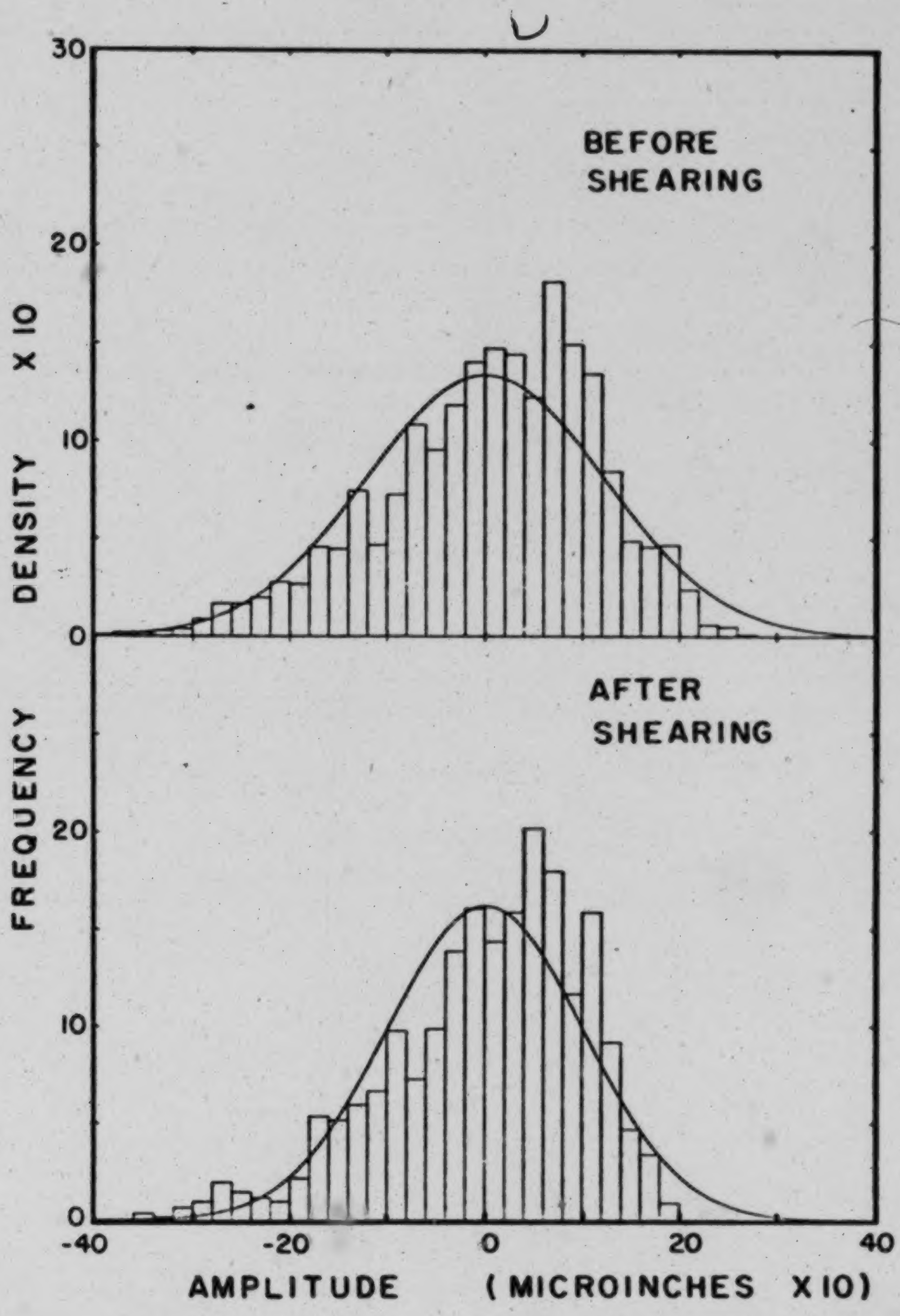

Figure 3.16 Amplitude distributions of asperities for diamond-saw cut surface

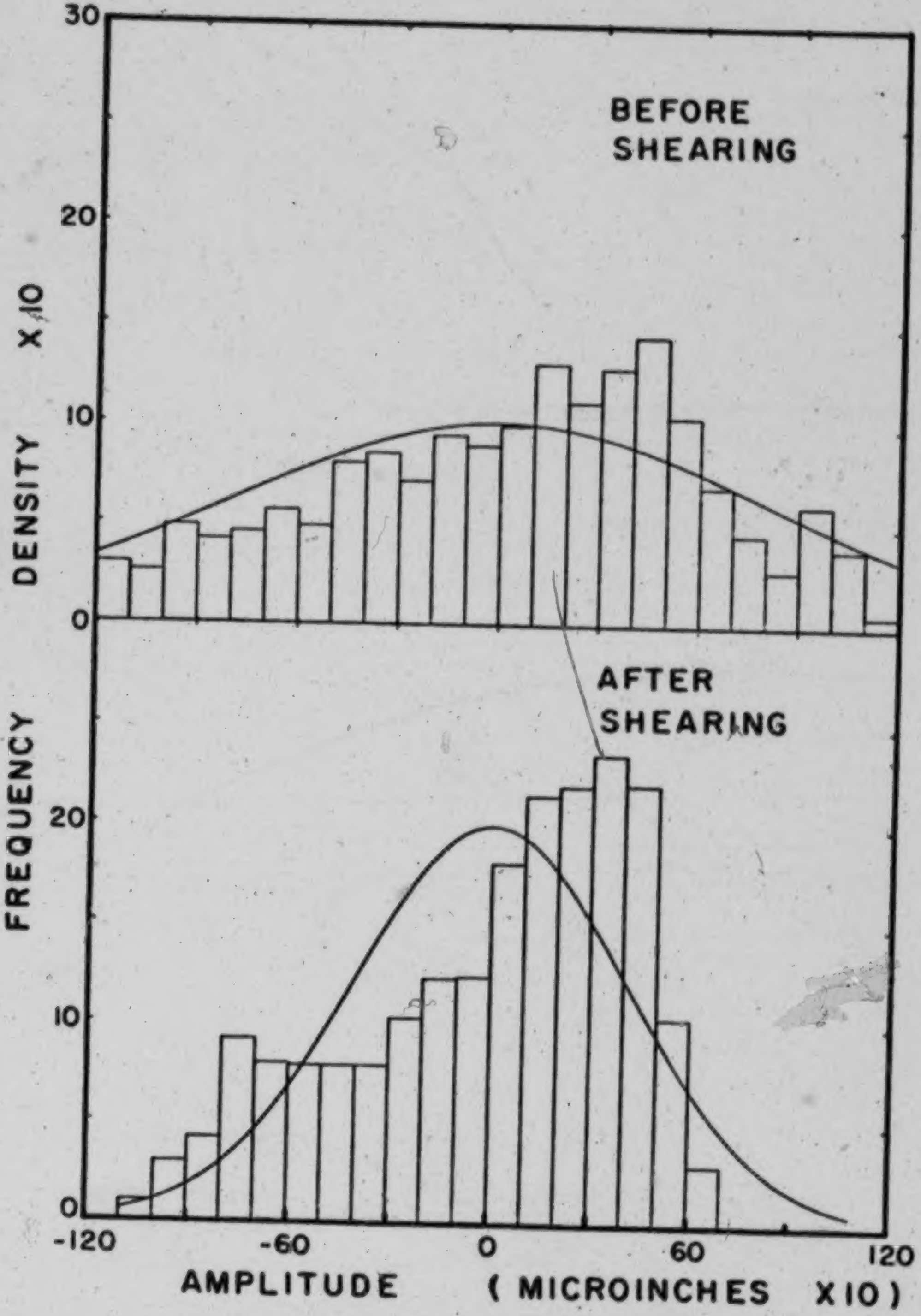

Figure 3.17 Amplitude distributions of asperities for surface lapped with #45/80 grit

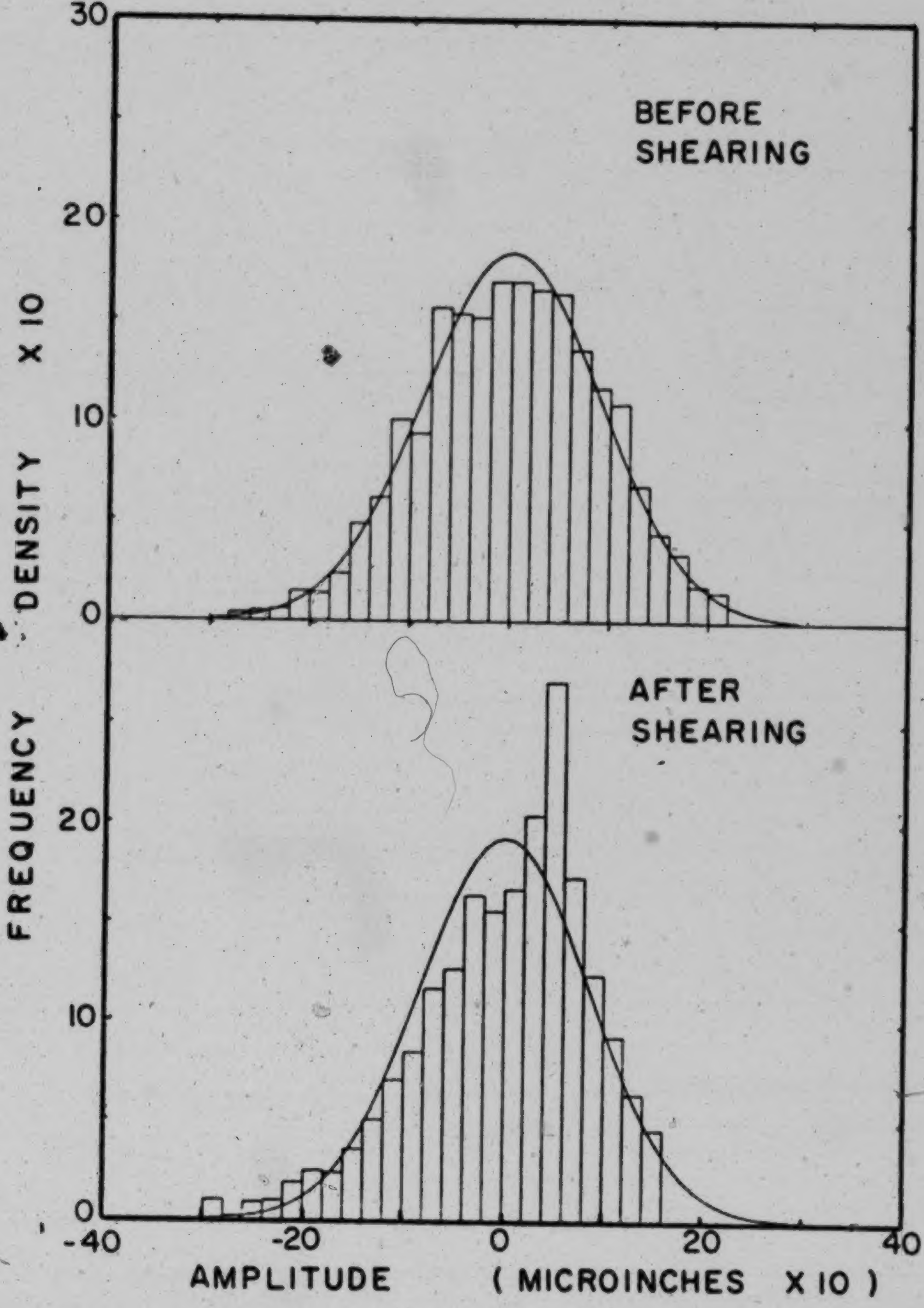

Figure 3.18 Amplitude distribution of asperities for surface lapped with #200 grit

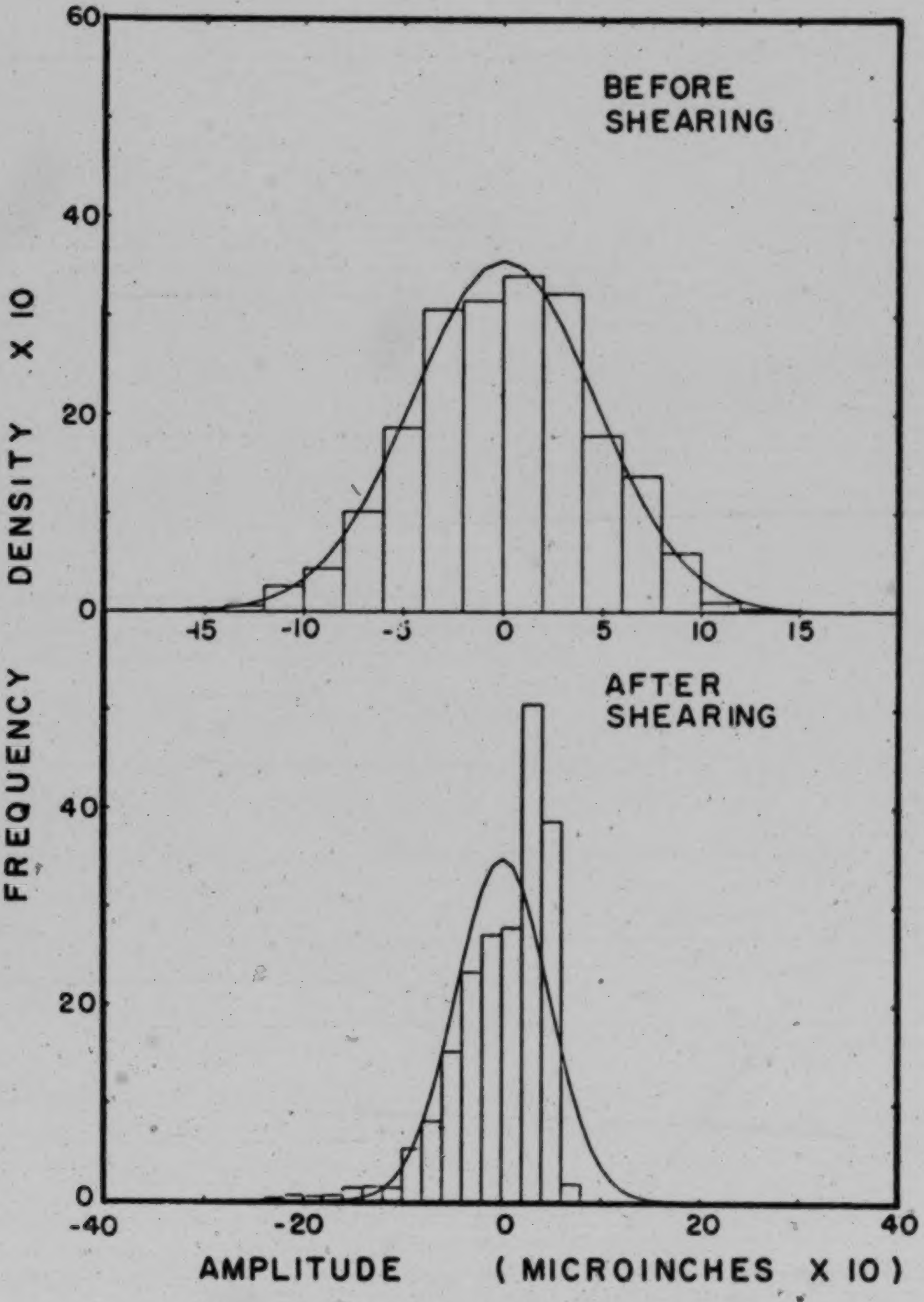

Figure 3.19 Amplitude distribution of asperities for surface lapped with #400 grit

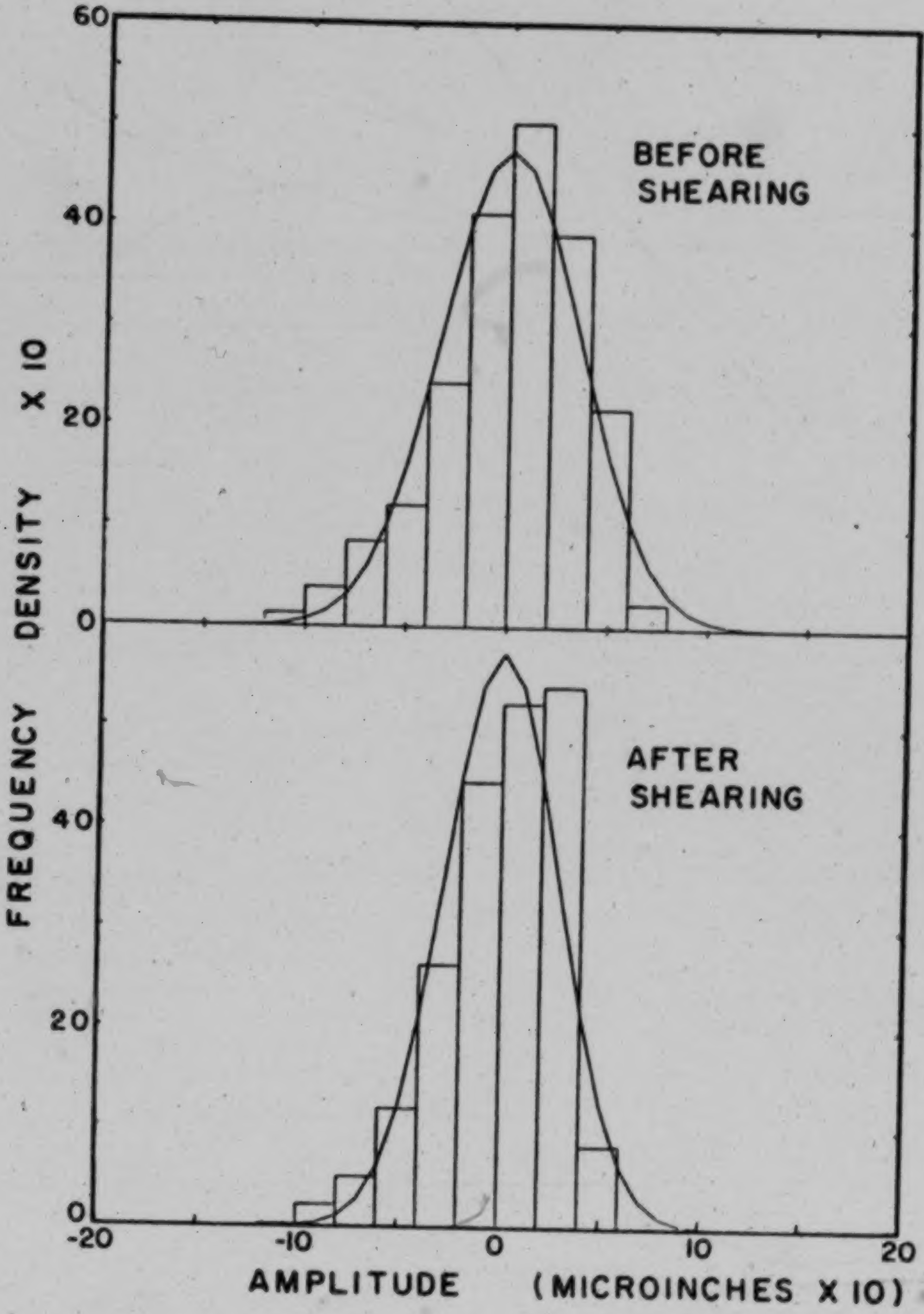

Figure 3.20 Amplitude distribution of asperities for surface lapped with #600 grit

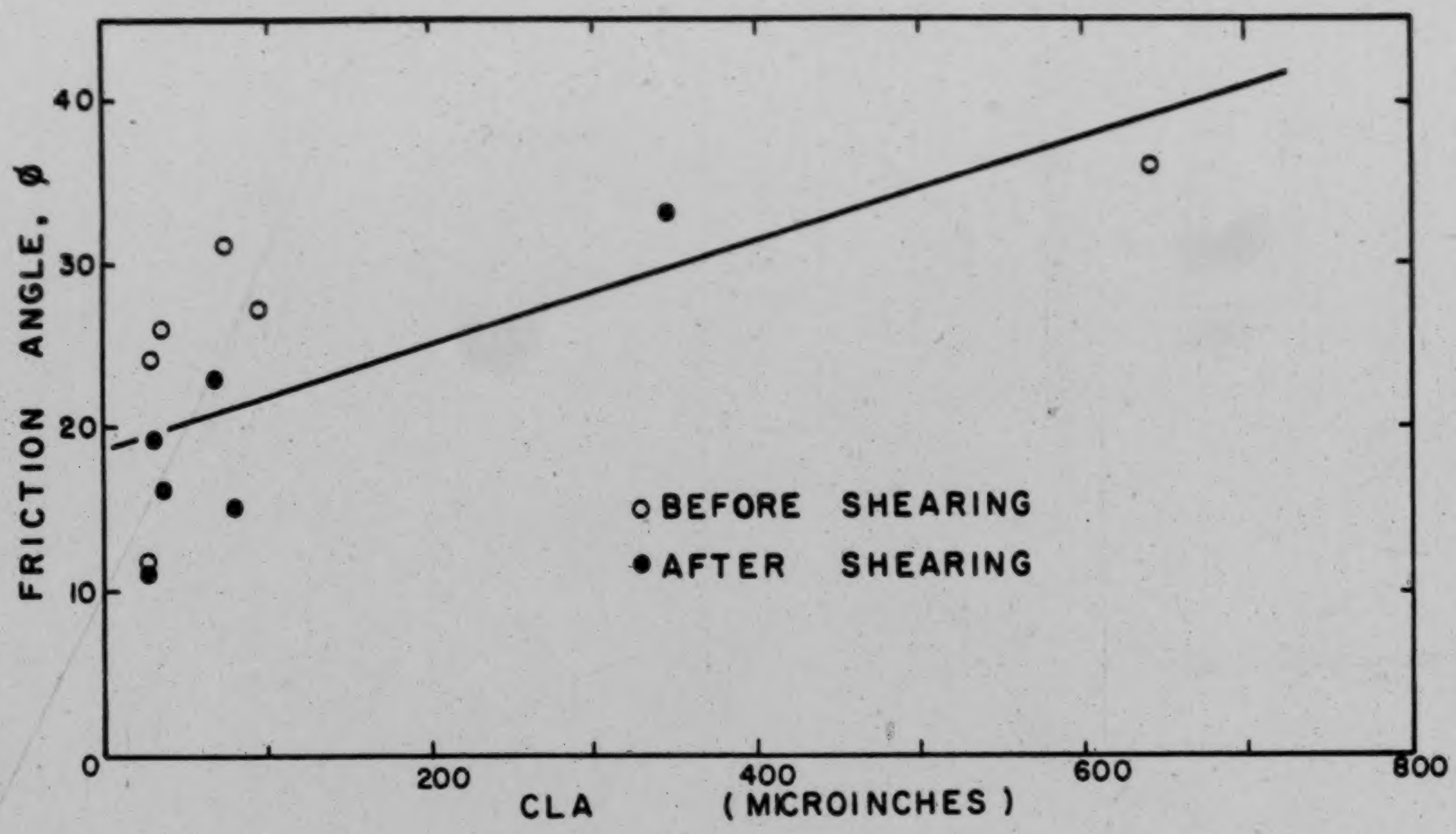

Figure 3.21 Centre-line-average (CLA) versus the friction angle

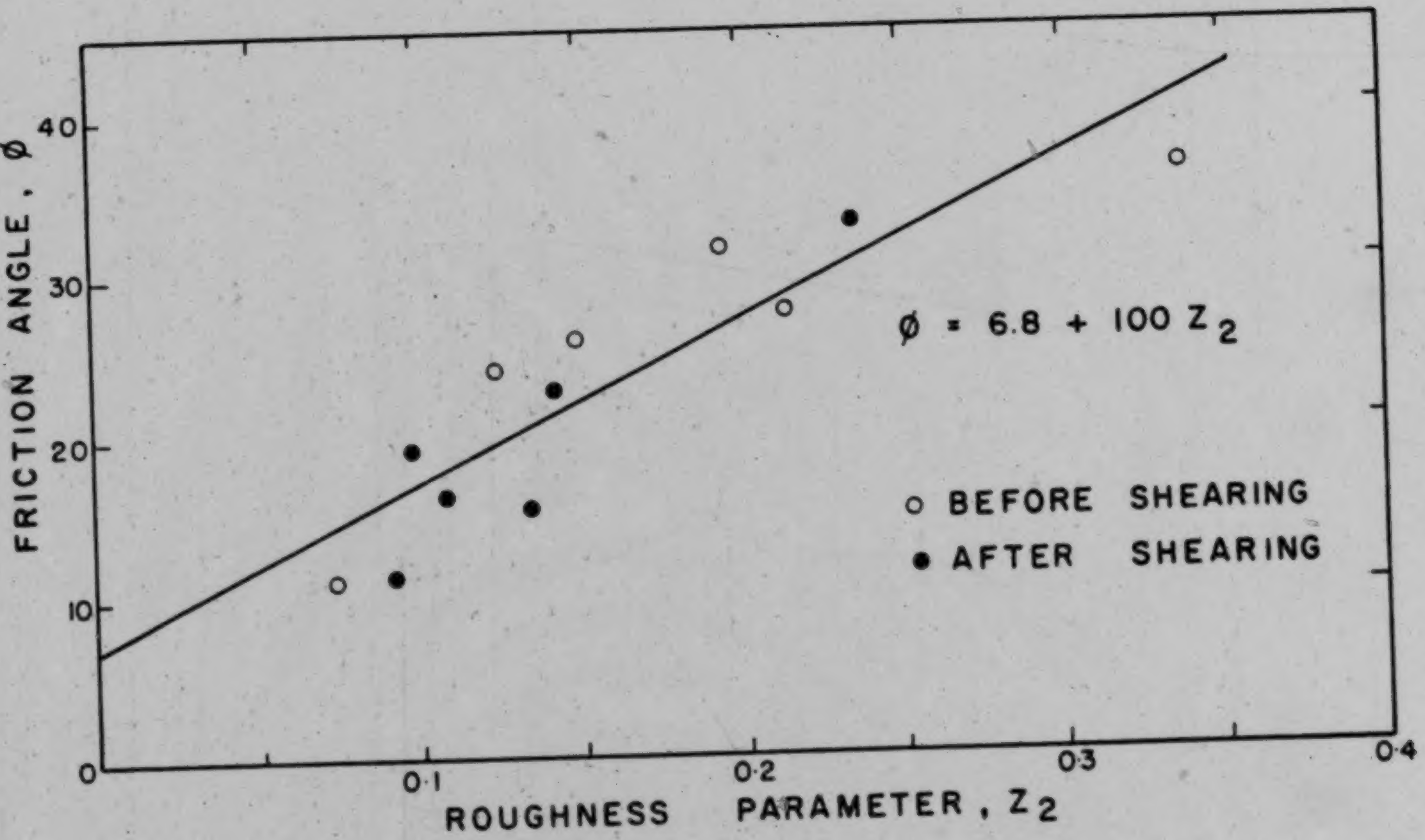

Figure 3.22 Roughness parameter, Z_2, versus the friction angle

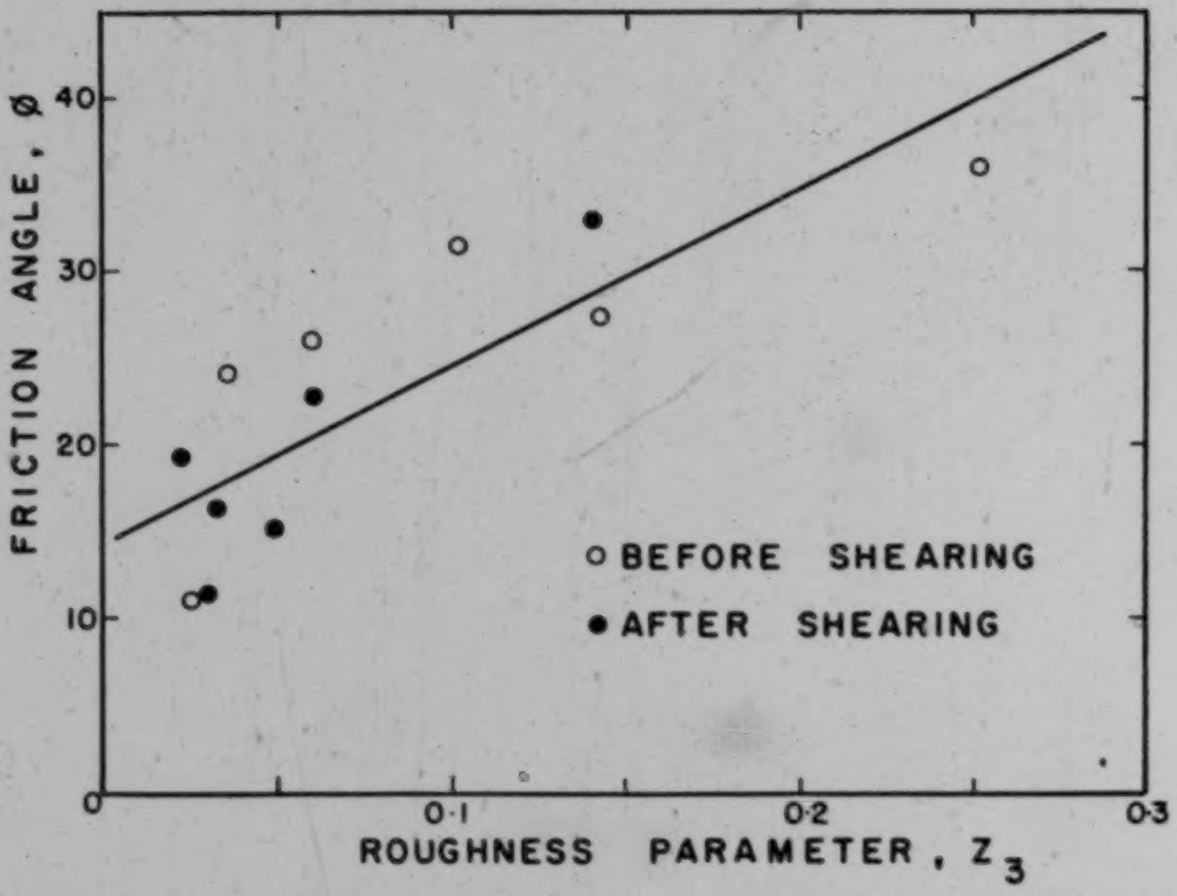

Figure 3.23 Roughness parameter, Z_3, versus the friction angle

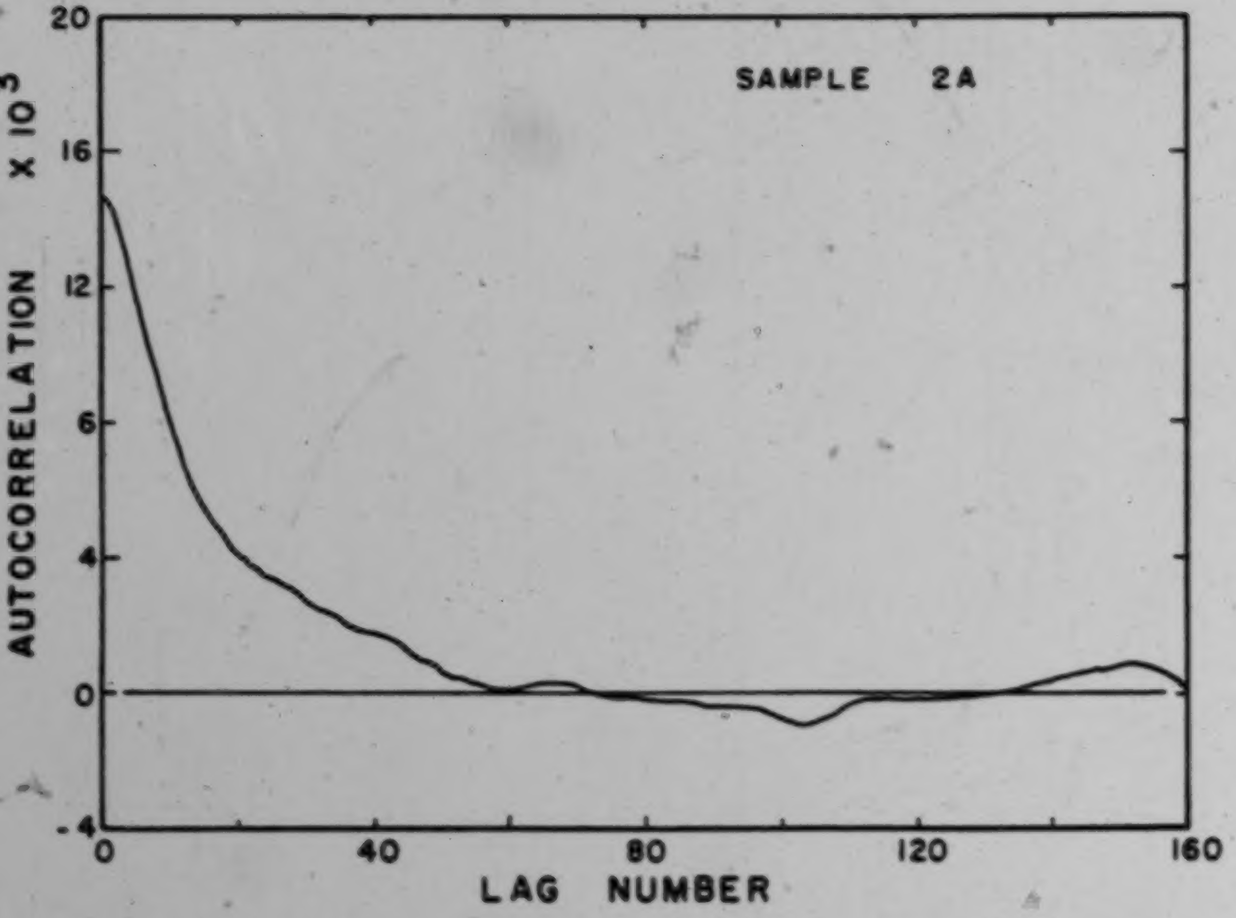

Figure 3.24 A typical autocorrelation plot

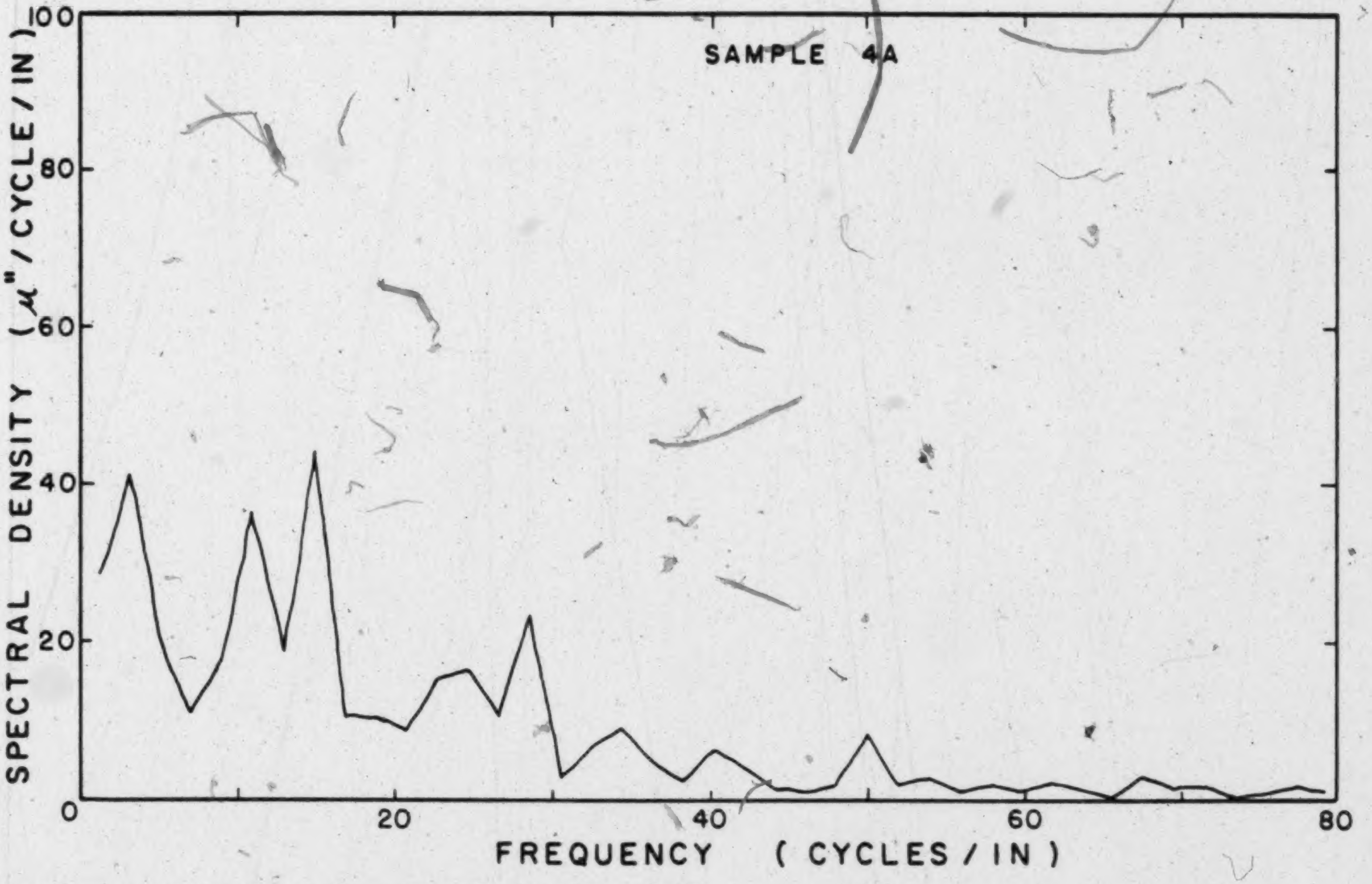

Figure 3.25 A typical spectral density plot

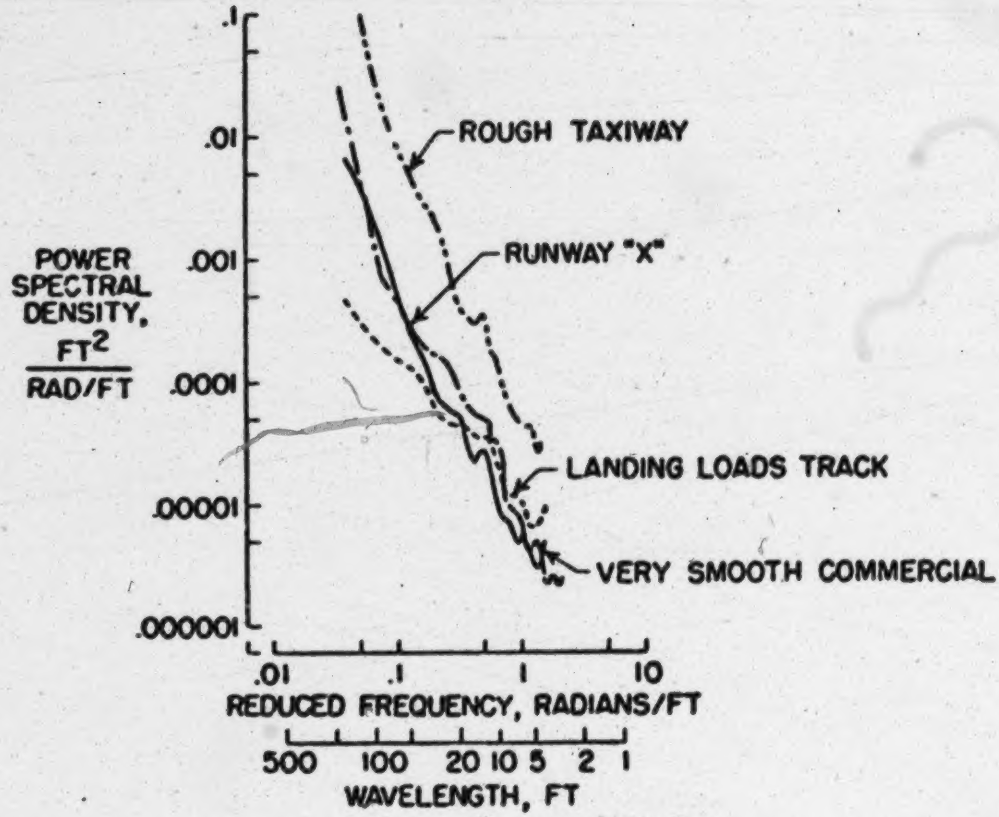

Figure 3.26 Limiting spectral criteria for roadways (after Houbolt, 1961)

CHAPTER IV

SHEAR TESTS ON NATURAL ROCK DISCONTINUITIES FROM TURTLE MOUNTAIN

4.1 INTRODUCTION

In back analyzing a slide the factor of safety is taken to be unity and in doing so, it is possible to determine the shear strength parameters required for this condition. The main purpose of the back analysis, however, is to determine how reliable the analysis is and to see if the safety factor of unity could have been predicted by determining the shear strength parameters from laboratory shear tests. Thus in the context of the Frank Slide, it was vital that the shear strength along the failure surface be determined from laboratory shear tests on samples which contained discontinuities representative of the failure surface. This chapter presents the methods used to obtain the necessary samples, how they were tested and the results obtained on the various types of discontinuities. Included as well is a discussion on the implications of the test results.

4.2 SAMPLING LOCATION

Upon exploring Turtle Mountain and the surrounding area in some detail, it was soon realized that due to the magnitude of the slide and the rough terrain, the only accessible place to obtain samples would be in the rock debris along the road. A secondary road to the west of Highway 3 passing through the rock debris was found to be the most suitable location. The major portion of the slip surface at the Frank Slide was in the Livingstone Formation as was the rock mass which slid. Therefore, the rock anywhere within the slide debris would be representative of the rock involved in the slide. A description of the Livingstone Formation is given in Chapter 5.

4.3 SAMPLING PROCEDURE

After considering the geology of Turtle Mountain, it was decided to make an attempt at sampling three different types of discontinuities; namely, joints, bedding planes and surfaces which showed signs of previous shear movement along them. The latter type will be referred to as "flexural-slip" surfaces.

The boulder chosen as the sample block is shown in

Figure 4.1. The bedding planes and joints can be very clearly seen in this Figure. Figure 4.2 shows a flexural-slip surface within the sample block.

Two methods were used to obtain samples from this boulder. One was to simply sever smaller blocks from the boulder by wedging a chisel into joints and bedding planes which were slightly open. This method worked fairly well for obtaining blocks which contained joints. However, since the bedding planes were spaced approximately two feet apart, it was impossible to obtain a single block with a bedding plane passing through it. The block would have simply been too large. Therefore, to use this method of obtaining blocks which contained bedding planes meant that each side of the bedding plane had to be worked at separately. Some bedding plane samples were obtained in this way; however, the number obtained suitable for testing was low in comparison to the number of attempts.

Generally, the problem with using only hand tools and prying away the blocks was that the size of the blocks was too large to handle so that when they were severed from the large boulder, they would fall to the ground and shatter. From the shattered rock it was possible at times to obtain small samples suitable for preparing a lab specimen.

The other method used was to core around desirable discontinuities with a masonry drill manufactured by Delro Industries Ltd., Winnipeg, Manitoba. This machine is intended for drilling large diameter holes in masonry, reinforced concrete or other hard material. The diameter of the diamond core barrel was ten inches. Figure 4.3 shows the coring machine anchored to the sample block at Turtle Mountain while Figure 4.4 shows a core obtained in this manner.

The coring method is advantageous from the point of view that the total volume of rock to be handled is more manageable and the surface area of the discontinuity is fairly large. This procedure, however, does have some severe problems associated with it which limits its uses. The biggest problem is the retrieval of the core. Sometimes, it was fortunate that a discontinuity existed at the maximum depth of coring (approximately 12 inches) and then there was no problem. However, if this was not the case, the core recovery was extremely difficult and sometimes impossible.

In most cases, whether it was a core or block sample being worked on, the specimen would fall apart into several pieces. In this case each piece was marked and the block reassembled and then wired together for transportation back to the lab.

Besides the samples which contained natural discontinuities, solid blocks of limestone were brought back to the laboratory from which the samples having artificial surfaces would be prepared.

4.4 SAMPLE PREPARATION

From the larger blocks and core samples, smaller specimens were cut to approximate size using a diamond saw. With this saw, it was impossible to get the sample exactly square and in perfect shape for the shear box. For this reason the samples were brought up to final size by casting them in Devcon-B plastic steel epoxy. It was done in a similar manner to that mentioned in Section 3.7. This casting ensured a snug fit in the shear box and also resulted in a flat horizontal surface for seating and loading the sample.

4.5 TESTING APPARATUS

Upon completing the sample preparation, each of the samples was subjected to a direct shear test. Two types of shear boxes were used for this purpose. The first, designed for 2" x 2" samples, was built at the University of Alberta and is shown in Figure 4.5. The shear load with this apparatus is applied by a gear box chain drive assembly powered by an electric motor. The normal load is applied with a dead weight lever arm arrangement. The horizontal and vertical deformations were measured with linear voltage displacement transducers (LVDT) while the shear load was measured with an 8,000-pound load cell.

The other machine used was a ten-ton Wykeham-Farrance direct shear machine shown in Figure 4.6. The shear load with this machine is applied through a variable gear arrangement powered by an electric motor. The normal load is applied through a loading yoke by a hydraulic ram. In order to maintain a more accurate control over the normal load than by simply using a dial gauge on the hydraulic pressure, a load cell was incorporated between the loading yoke and the load cap. Strain gauges on the load cell were connected to a Budd strain indicator which was then used to measure the normal load.

With the Wykeham-Farrance machine, the shear load was measured by strain gauges which had been mounted on the ten-ton proving ring. As with the small shear box, the horizontal and vertical deformations were measured with LVDT's. To measure the vertical deformation, an LVDT was mounted on each corner of the top plate. With these four LVDT's, it was possible to measure the rotation of the top half of the sample and the top loading plate. The apparatus was originally designed for 12" x 12" samples. But this was modified with spacer blocks so that 10", 8" and 6" square samples could be tested as well.

With both shear boxes, the shear load and horizontal deformation were recorded with an X-Y plotter. The vertical deformations were recorded with a Hewlett-Packard digital recorder.

In order to obtain surface profiles of the natural discontinuities, a small frame was built on which an LVDT and stylus arrangement was mounted. The vertical movement of the stylus was sensed by the LVDT and the output from the LVDT was recorded directly on an X-Y plotter. Figure 4.8 shows this apparatus. The X-Y plots were later digitized and then replotted with the Calcomp Plotter.

4.6 TESTING PROGRAM

The shear testing program was performed in two stages. To begin with, five series of 6" x 6" samples (nominal area) were prepared and tested while later, in the second stage, the 2" x 2" specimens were tested.

In the first five series of samples, three series contained natural discontinuities while the other two had artificially prepared surfaces. An example of an artificial surface would be a diamond-saw cut. The natural surface studies were composed of a series with bedding planes, a series with joints and a series with flexural-slip surfaces. The flexural-slip surfaces were prepared so that the shearing would be parallel to the striations. Figure 4.7 shows typical samples of these series. Of the two artificial series, one was lapped with a #45/80 grit and the other was made with a diamond saw. Each series contained four samples except in the case of the bedding plane series which contained only three samples.

The first series of samples was then tested in the ten-ton Wykeham-Farrance direct shear machine. The tests were run dry at a rate of deformation of 0.048 inches/minute.

The general procedure after the machine and sample had been assembled was to apply the normal load and then initialize the recording devices. When the set-up was completed, the horizontal deformation was started and continued until the total deformation was approximately 0.8 inches. At this point, the normal load was held constant and the direction of the shear displacement reversed and sheared back to its initial position.

Upon removing the samples from the shear box after the test, it was noticed that the actual area of contact had been very small. Figure 4.9 shows this remarkably well. Since the number of samples obtained in the field was limited, it was decided to make further use of these 6" x 6" samples by cutting 2" x 2" samples out of them where there had been no contact.

Thus, in the second stage, two sets of 2" x 2" samples were prepared for testing in the small shear box. These small samples were prepared only for the bedding planes and flexural-slip surfaces. Each of these two series contained four samples. After the preparation was completed, they were tested in the same way as the larger samples.

4.7 RESULTS OF SHEAR TESTS

For each of the shear tests run, a shear load versus deformation plot was obtained directly on the X-Y plotter. These X-Y plots were later digitized and replotted on the Calcomp Plotter. This was done so the curves could be plotted on a more appropriate scale and in a more presentable form. A typical result of this type of plot is shown in Figure 4.10.

The digital vertical deformation data was punched up on computer cards and then reduced on the computer and plotted on the Calcomp Plotter. Figure 4.11 shows a typical vertical deformation curve.

From each of the load-deformation curves, note was made of the peak strength and the post-peak strength in both directions. The post-peak value for shearing away from the initial position was chosen at a point after the shear resistance had essentially levelled off shown at Point "A" in Figure 4.10. The reverse post-peak value was then taken at a point when the sample had returned to the same position as it was at Point A (Figure 4.10). Since there was a fair amount of slack in the machine, this meant that the reverse post-peak value was read at Point B, to the left of Point A. This is shown in Figure 4.10.

The slack in the shear machine also showed up on the vertical deformation curves. In Figure 4.11, if the reverse portion of the curve were displaced to the right by the amount of the slack, it would fall much closer to the vertical deformation curve when shearing from the initial position.

The shear loads and corresponding normal loads were then divided by the initial area to convert them to stresses and then plotted as shown in Figures 4.12 to 4.16. The failure envelopes drawn through the data points on these figures were obtained from a linear regression analysis. The only case where the linear regression analysis was not done was on the diamond-saw cut surface. Table 4.1 gives a summary of the strength parameters obtained on each type of discontinuity.

4.8 DISCUSSION OF RESULTS

As was mentioned at the beginning of the chapter, the main purpose for performing the shear tests on the natural discontinuities was to determine strength parameters for the Frank Slide stability analysis. There are, however, some interesting observations which have emerged from the shear tests which are worth mentioning in connection with the interpretation of the data.

4.8.1 THE ULTIMATE FRICTION ANGLE

In Chapter 3 a discussion was given on the significance of the basic friction angle, ϕ_b, and the question was raised as to how it compares with the friction angle on natural rock surfaces after large shearing displacements have occurred. This friction angle on natural surfaces after large shearing displacements will be referred to as the ultimate friction angle, ϕ_u. Determining the ϕ_u on natural rock surfaces is complicated by the fact that natural surfaces are seldom, if ever, flat thereby making it difficult to isolate the resistance due to ϕ_u and that due to the geometric component. For this reason, it would be desirable to measure ϕ_u on flat artifically prepared surfaces if it could be shown that the ϕ_u on natural surfaces is the same as ϕ_b.

In order to measure ϕ_u on natural rock surfaces, it is necessary to isolate the ϕ_u term from the geometric component of the shearing resistance. This can be done by considering the post-peak shearing resistance, when shearing away from the initial position, as being $\phi_u + i$ and when shearing in the reverse direction, back to the initial position, as $\phi_u - i$. The average of the post-peak shearing resistances in both directions will be ϕ_u. To eliminate the i component in this manner requires that the i value is the same in both directions. This was considered, as discussed in Section 4.7, in selecting the post-peak values from the load-deformation curves. Furthermore, this also implies that shearing in the reverse direction should only be continued until the sample reaches its initial position. To shear past the initial position would be like starting a new test since the shearing surface would then be on the opposite side of the irregularities. In fact, by doing this, it is possible to do two tests on one sample.

The ultimate strength parameters quoted in Table 4.1 and the ultimate strength envelopes drawn in Figures 4.12 to 4.16 are based on the averages of the post-peak values in each direction.

It should be noted that even on flat surfaces like the lapped surfaces, there can be a slight difference in shearing resistance in each direction (Figure 4.15). This points out that there are other factors which can cause minor directional shearing differences. However, if there is a substantial difference in each direction, the major contributing factor would be the geometric component.

Taking an overall view of all the ϕ_u values obtained (Table 4.1), it is noted that the ϕ_u for rock surfaces is not a unique value. For the tests performed, the ϕ_u varies anywhere from 37.2° on the lapped surfaces to 14.0° on the flexural-slip surfaces. The main factor which seems to control the ϕ_u value is the type of surface damage which occurs during the tests which, in turn, depends on the condition of the shear surface before the shear test. On the flexural-slip surfaces and joints, a shiny indurated crust had formed at the points of contact which was hardly noticeable on the bedding planes. On the bedding planes there was more gouging than on the other two natural surfaces. The shiny indurated crust on the joints and flexural-slip surfaces are most likely responsible for the low ultimate strength.

The shear test results show that the ϕ_u as determined by a reversal shear test on natural rock surfaces can differ significantly from the ϕ_b as determined on flat artifically prepared surfaces. This is contrary to the assumption often made which states that they are the same. This is at least true for the limestone within the normal stress range at which the shear tests were performed in this study. At a very high normal stress, it is conceivable that the indurated crust would break and then the ultimate shearing resistance would be the same on all the surfaces. Although this may be the case, the shear behaviour at the high normal stresses is not applicable to the understanding of rock slope failures since the normal stresses along the slip surface in rock slopes are generally relatively low.

The shear strength of clays after large shearing displacements is defined as the residual strength. It is a unique value dependent only on the type of material and to some extent on the normal stress. The shear strength of rock surfaces after large shearing displacements is dependent on the same variables but it is also greatly affected by the surface roughness. Therefore within context of the the definition of the residual strength for clays, there is no residual strength for rock surfaces. For this reason the shear strength on rock surfaces after large shearing displacements will be referred to as the ultimate strength.

Whether the ϕ_u, as determined on natural surfaces from a reversal test, has any significance in the field will only become apparent from case history studies.

4.8.2 THE EFFECT OF SIZE OF SAMPLE ON THE SHEAR STRENGTH

The shear tests performed in this investigation included samples which contained the same type of discontinuity but were different in size. The larger samples had a nominal area of 6" x 6" and the smaller ones were 2" x 2". It was explained earlier how the 2" x 2" samples were obtained from the larger samples. This procedure had the added advantage of being able to investigate the size effect on the shearing resistance. When examining the results in Figures 4.12 and 4.13, it is noted that there is no significant difference between the two sizes outside of the usual scatter.

This result is probably not that surprising if an examination is made of the surface profiles of these samples. Figure 4.17 shows three typical profiles for the bedding planes and Figure 4.18 shows the profiles for the flexural-slip surfaces. These profiles were intentionally plotted at the natural scale for the most realistic comparison. From Figures 4.17 and 4.18, it can be seen that the scale of roughness on 2" x 2" samples would not be significantly different from that on 6" x 6" samples.

A similar result was observed at Imperial College where tests were performed on a 100-ton shear machine with a sample size of 15" x 12" and as well on a small ten-ton field shear machine. The two machines gave very similar results (Hoek, 1971a).

The shear tests performed in this thesis and the ones reported in the literature indicate that the shear strength is not influenced by the size of the sample as long as the scale of roughness remains constant. If the scale of roughness differs on each sample size, as shown in Figure 4.19, then the shear strength would be different on each sample because of the different geometric effects. At the scale of hundreds of feet, it would never be possible to perform a shear test. Therefore, at this large scale, it is necessary to determine the shearing resistance at a much smaller scale and then add to it the effective i as determined by field roughness measurements. The important point to remember is that the shear strength is only affected by the size of the sample if the scale of roughness changes with the size.

4.8.3 THE SHEAR STRENGTH OF BEDDING PLANES AND FLEXURAL-SLIP SURFACES

The shear strength envelopes for the bedding planes (Figure 4.12) are considerably different than those for the flexural-slip surfaces. This, at first glance, is somewhat of an anomaly since the flexural-slip surfaces are the result of shear movements along bedding planes. Therefore it would seem logical that the flexural-slip surfaces would not exhibit a peak strength and the ultimate strength would be the same as on bedding.

This, however, is not the case. The reason for this is that the mode of shear failure in the field was much different than that which is observed in the laboratory. The shearing displacements which occurred along the bedding planes during the folding of the strata occurred at very high stresses and temperatures. These conditions, together with the geologic time scale of shear movement, allowed recrystallization to take place. The recrystallization resulted in the shearing surfaces remaining in intimate contact. By subjecting a bedding plane to a shear test in the lab, the mode of shear failure and the resulting sheared surface will be much different than that which occurred during the flexural folding. Thus, although the flexural-slip surfaces are the result of flexural slipping on the bedding planes, their shear strength behaviour bears no direct relationship to the bedding planes in the realm of laboratory shear testing.

In the previous section it was pointed out that the shearing strength of natural rock surfaces is a function of the initial surface roughness and the type of surface damage which occurs during the shear tests. Both the initial surface roughness and the shearing surface damage differ on the bedding planes and the flexural-slip surfaces; therefore, it is understandable that the shear strength will be different.

TABLE 4.1

SUMMARY OF SHEAR STRENGTH PARAMETERS

	Peak		Ultimate	
Type of Sample	Ø	C (psi)	Ø	C (psi)
Bedding plane	51.7	38	32.3	8
Flexural-slip surface	28.0	32	15.6	18
Joints	32.0	25	14.0	12
Diamond-saw cut	29.0	0	29.0	0
Surface lapped with 45/80 grit	----	--	37.2	5

Figure 4.1 The sample block within the slide debris

Figure 4.2 A flexural-slip surface within the sample block

Figure 4.3 Coring on the sample block

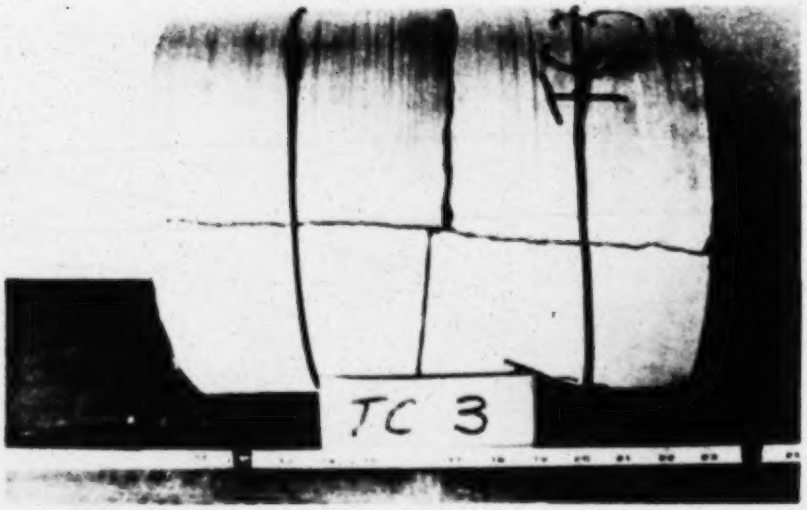

Figure 4.4 A ten-inch diameter cored sample

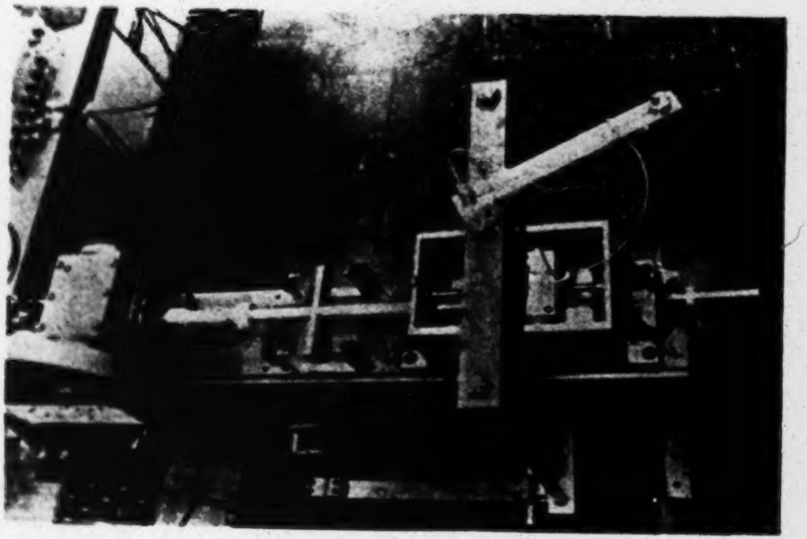

Figure 4.5 The modified shear box for the two-inch samples

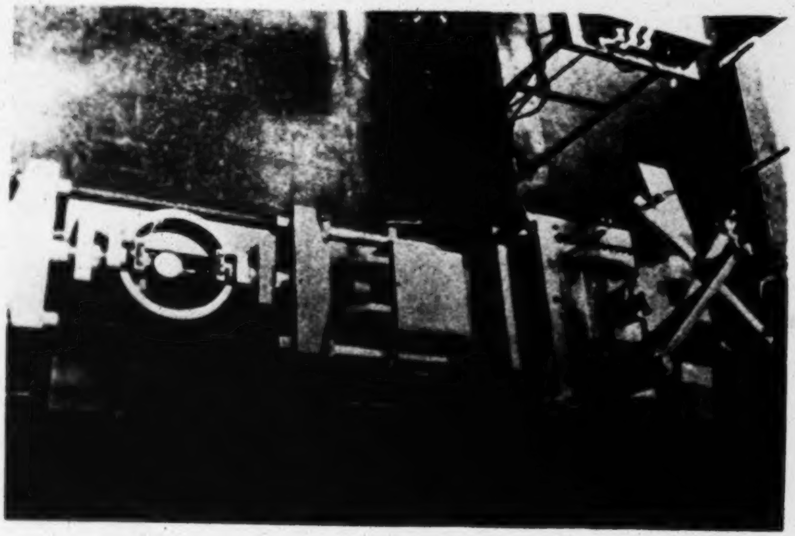

Figure 4.6 The Wykeham-Farrance shear box

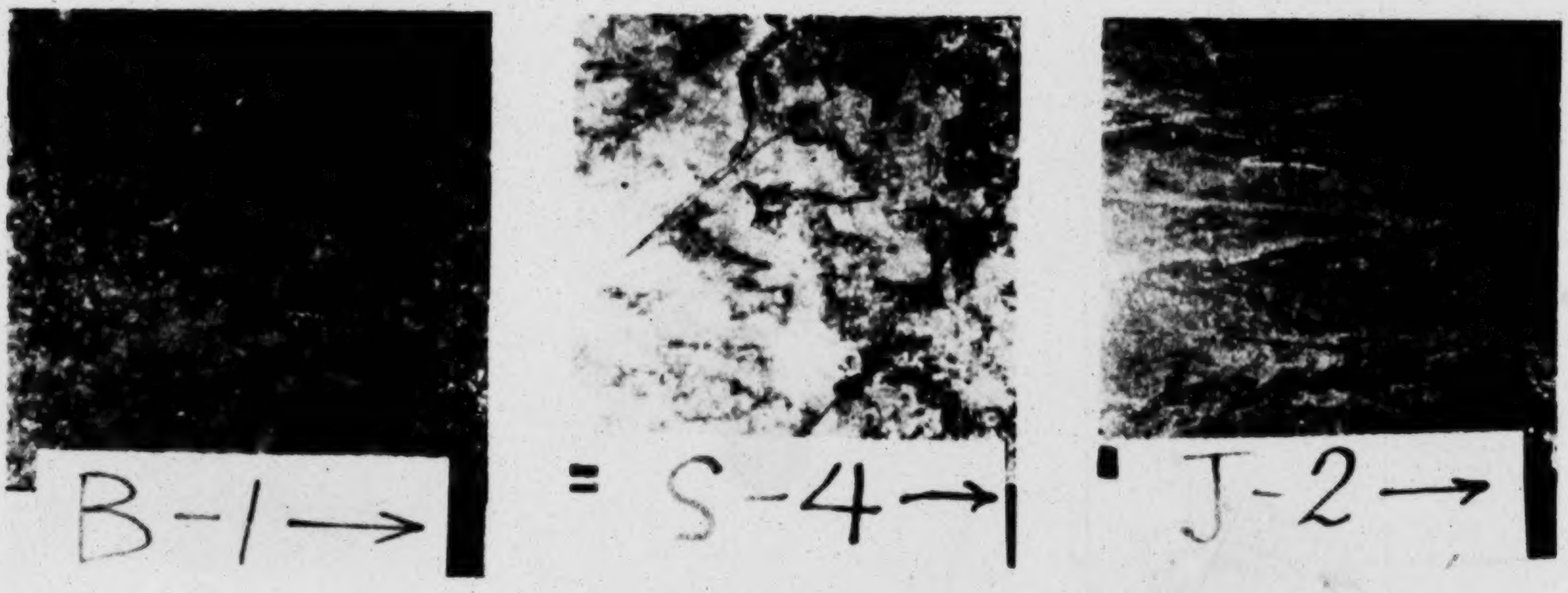

BEDDING PLANE

FLEXURAL-SLIP SURFACE

JOINT SURFACE

Figure 4.7 Natural discontinuities

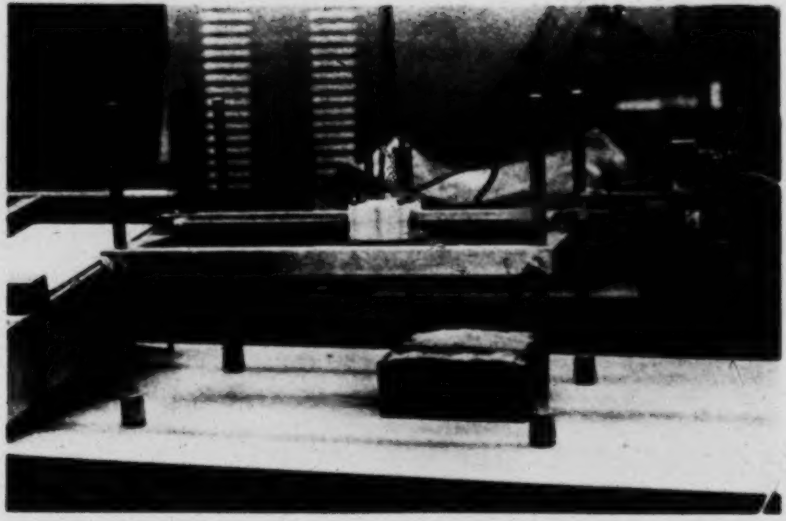

Figure 4.8 The small roughness measuring device

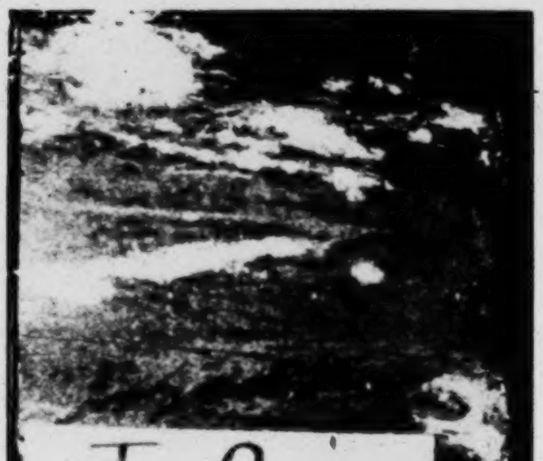

Figure 4.9 A joint surface after shearing

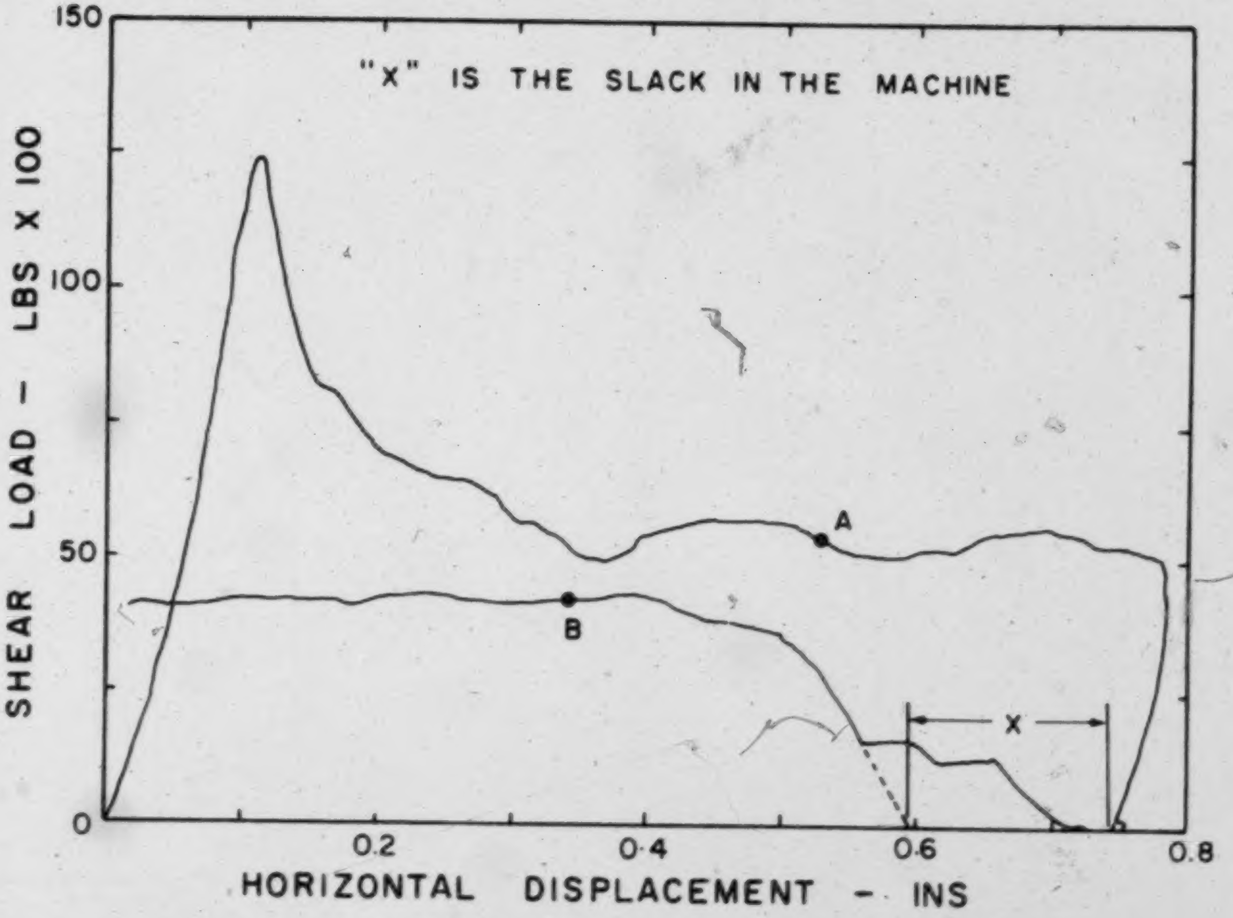

Figure 4.10 A typical shear load versus deformation plot

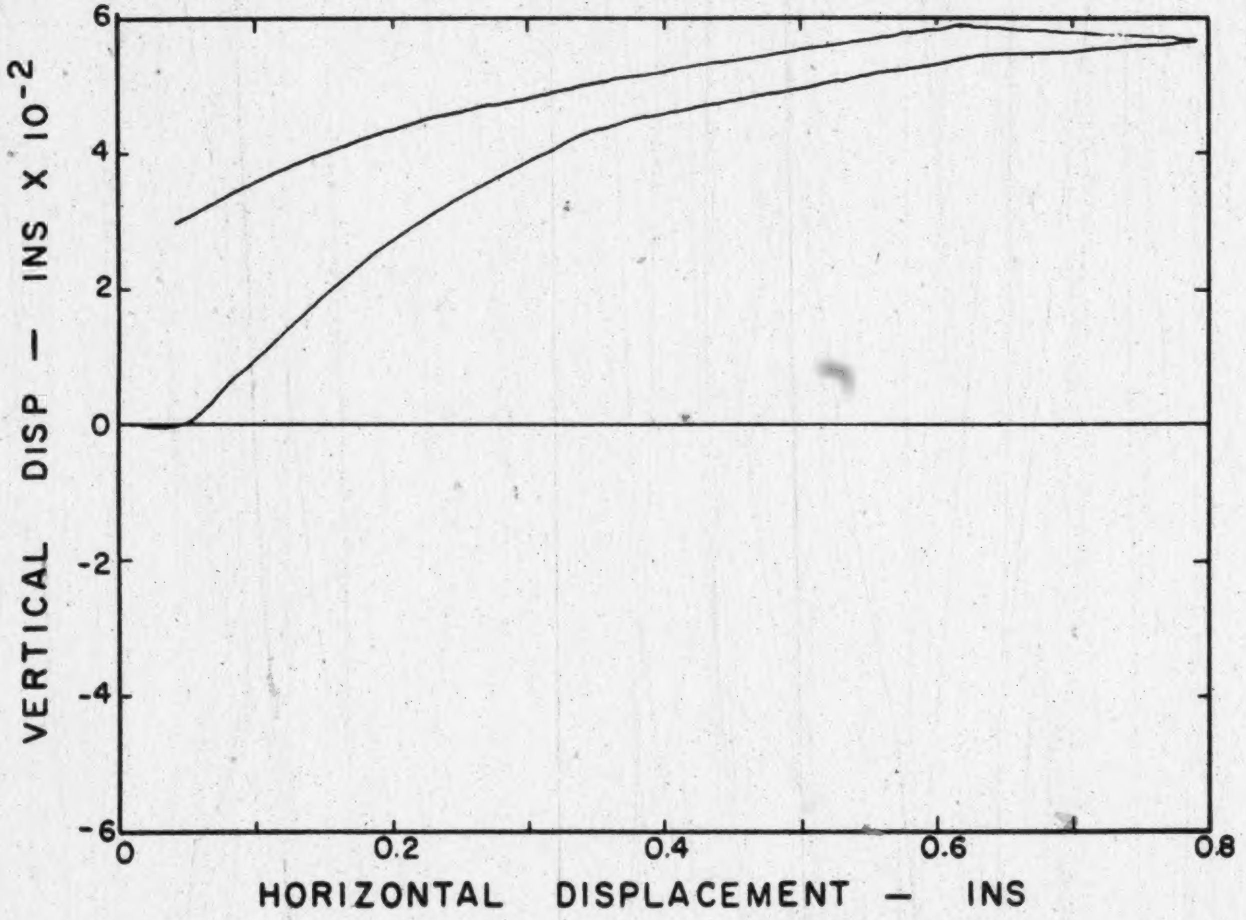

Figure 4.11 A typical vertical deformation versus horizontal displacement plot

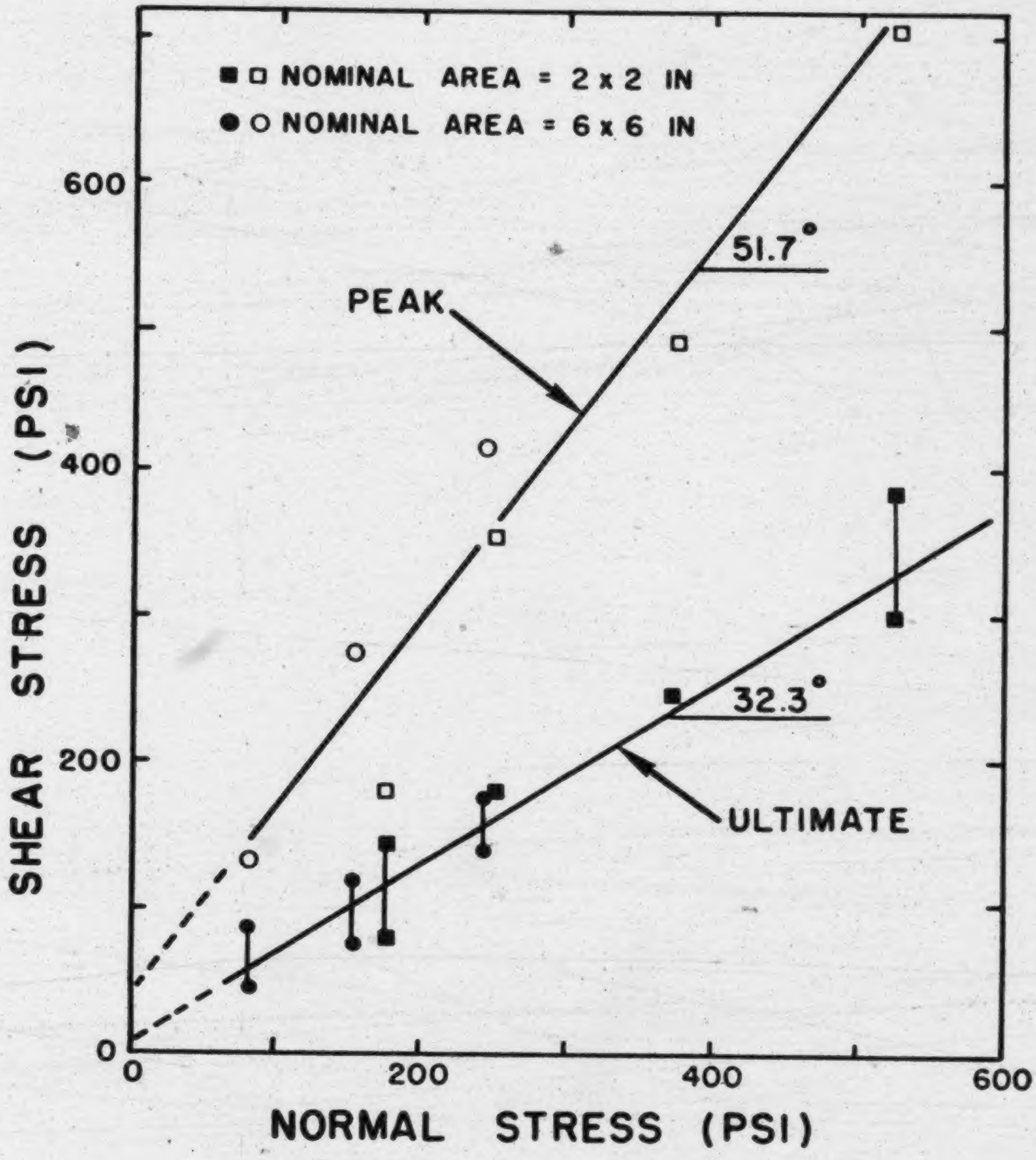

Figure 4.12 Failure envelopes for the bedding planes

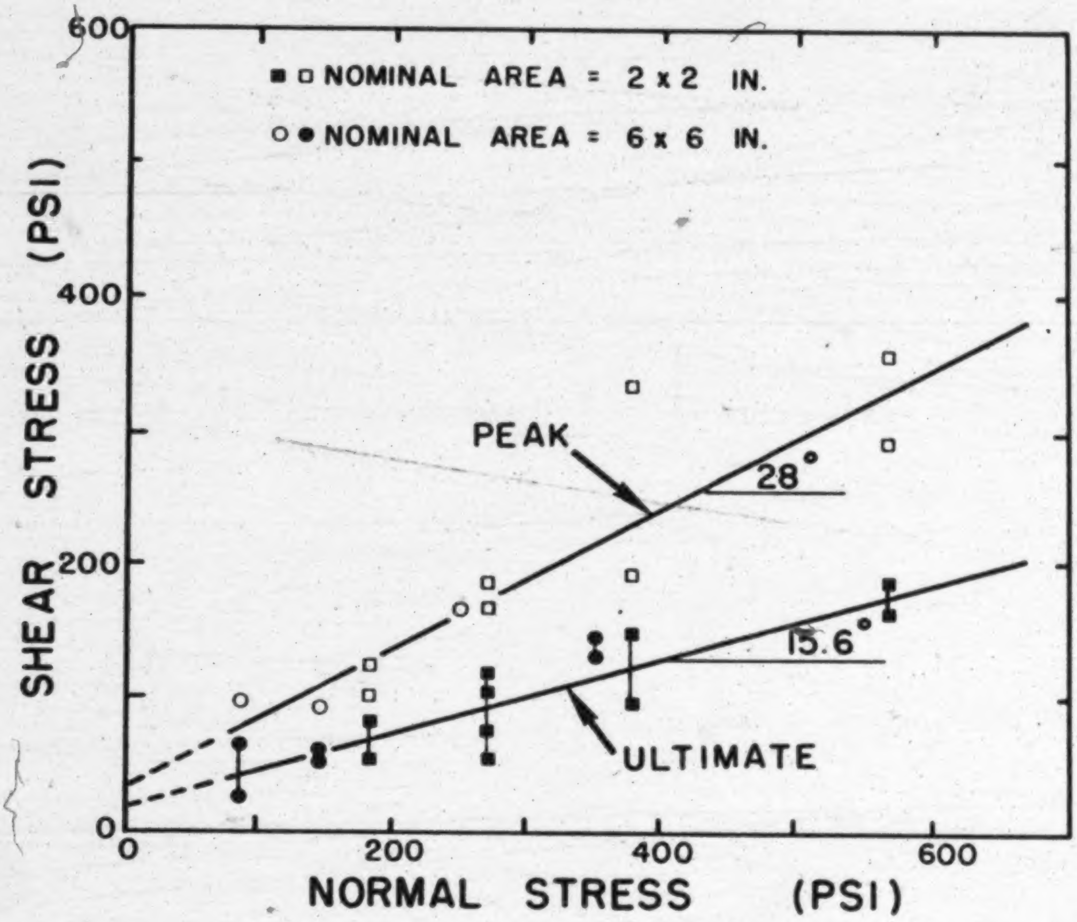

Figure 4.13 Failure envelopes for the flexural-slip surfaces

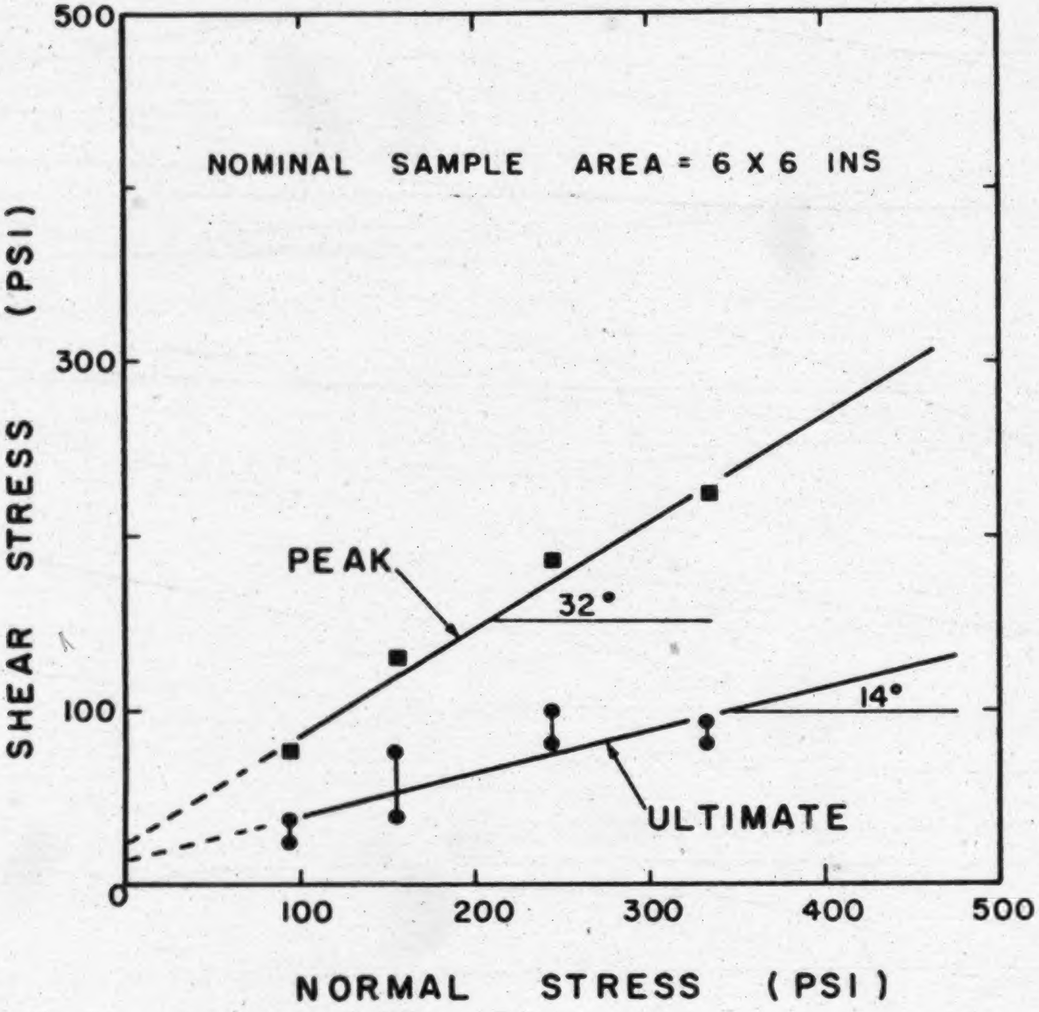

Figure 4.14 Failure envelopes for the joint surfaces

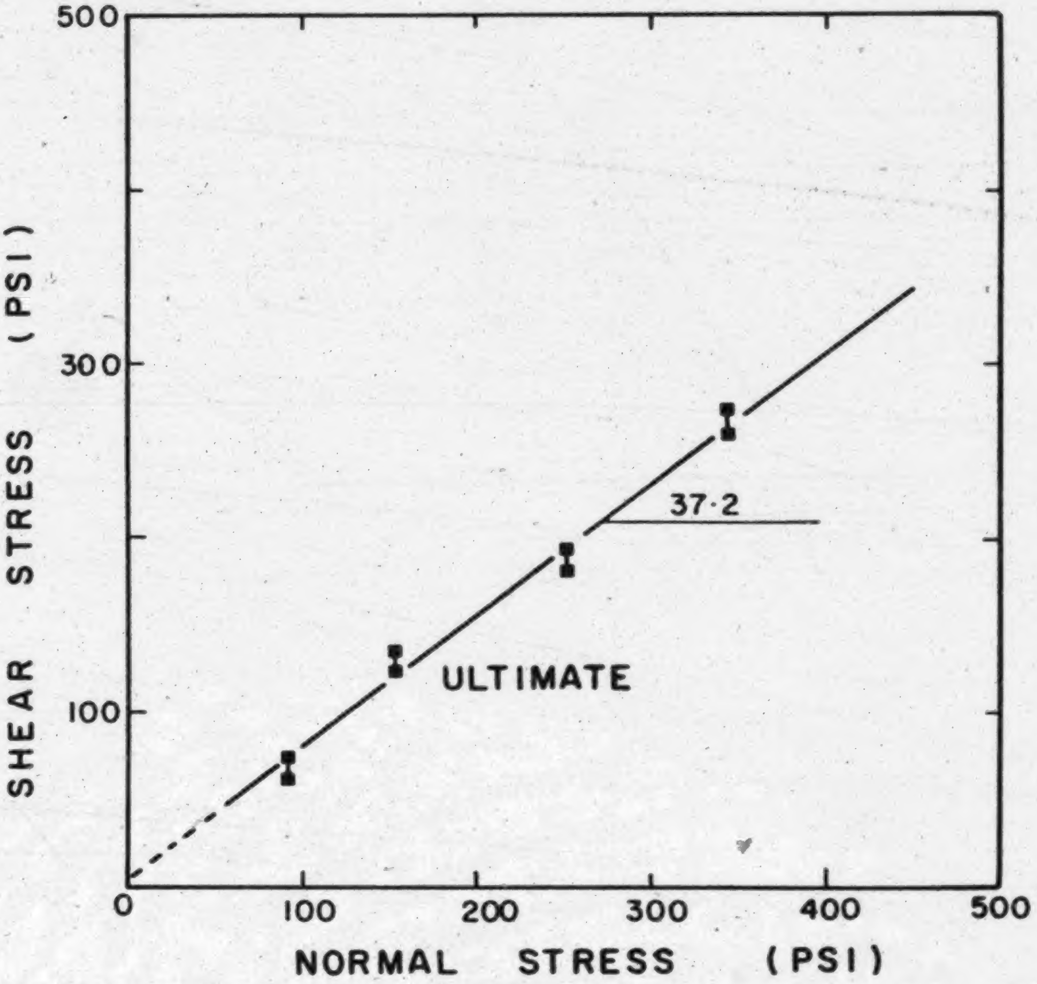

Figure 4.15 Failure envelope for surfaces lapped with #45/80 grit

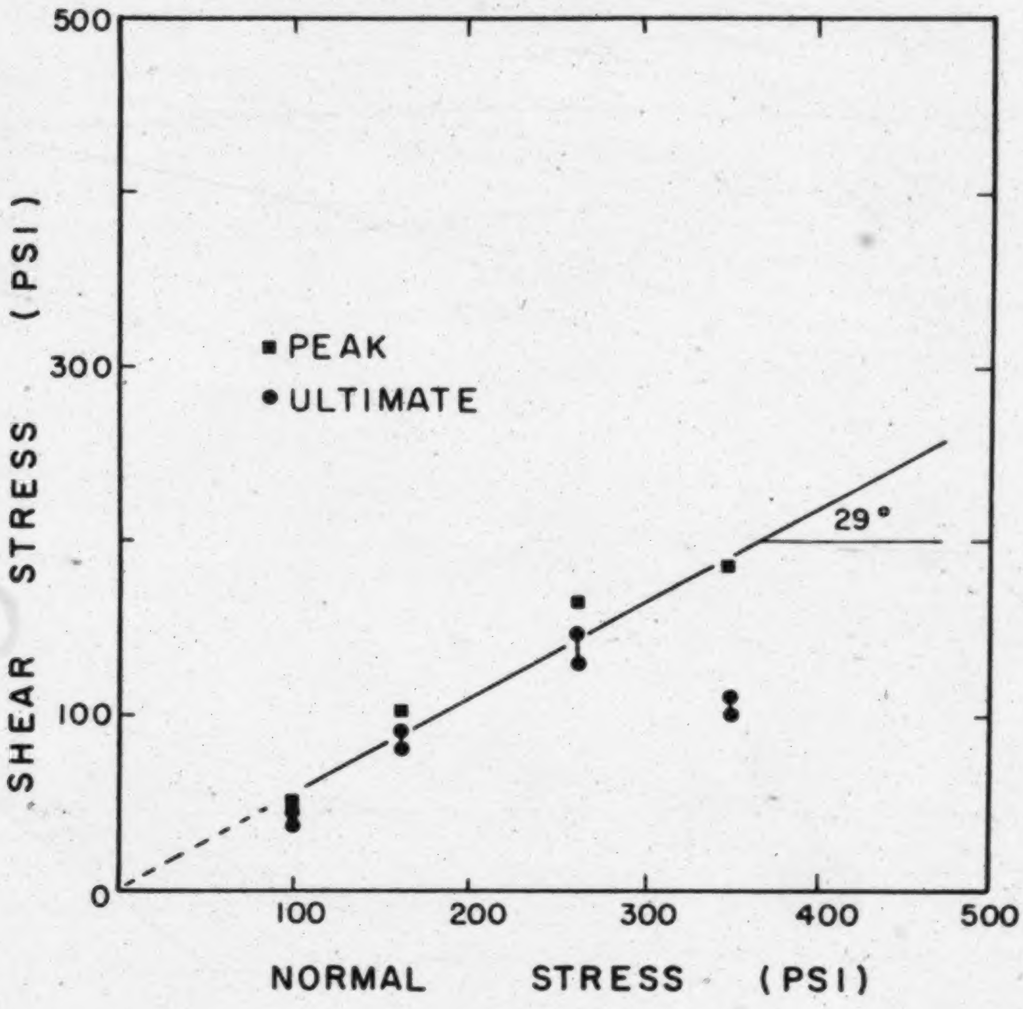

Figure 4.16 Failure envelope for the diamond-saw cut surfaces

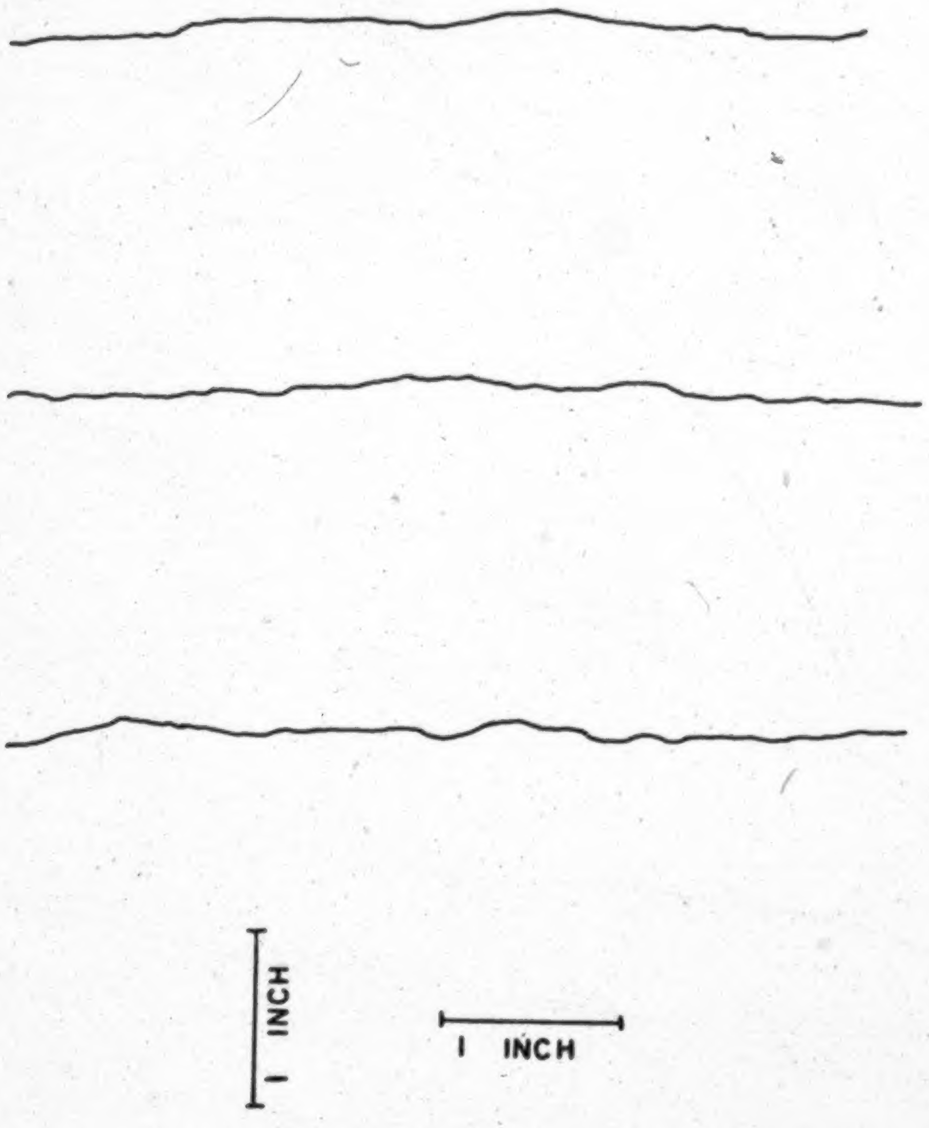
1 INCH
1 INCH

Figure 4.17 Natural surface profiles of a bedding plane (sample B-3)

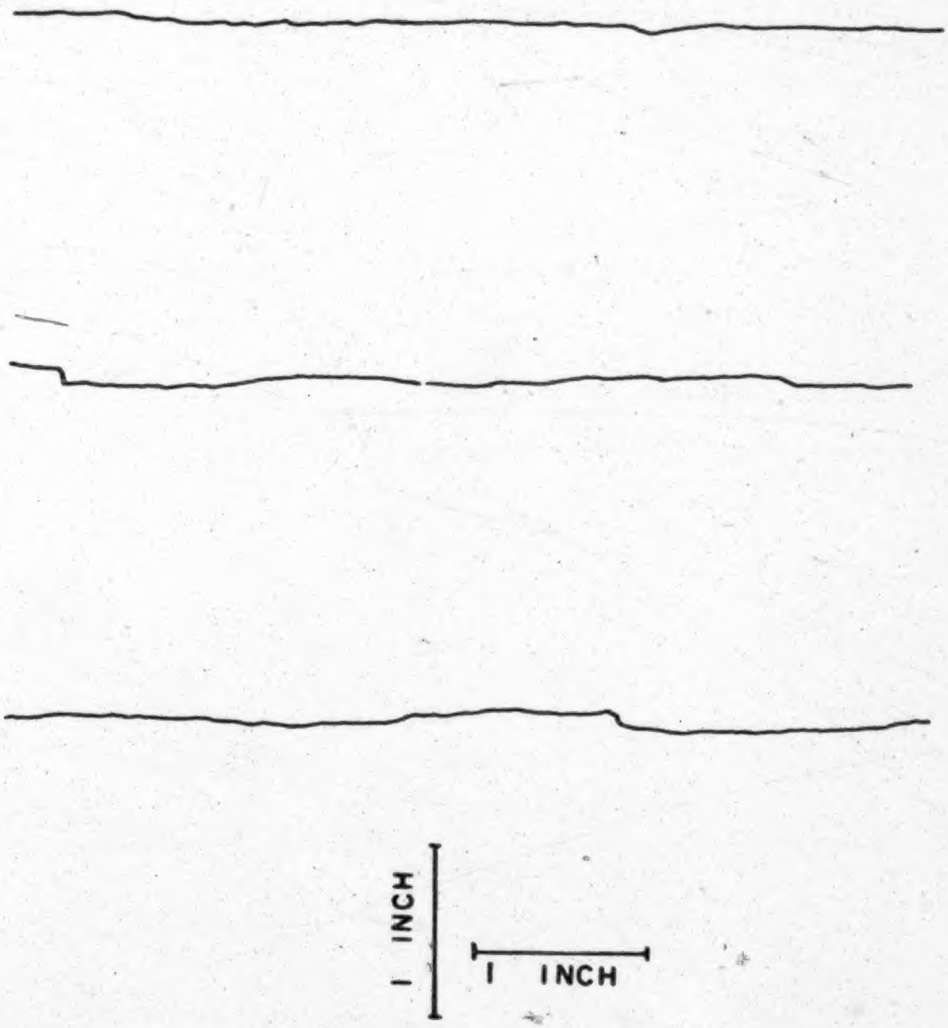

Figure 4.18 Natural surface profiles of a flexural-slip surface (sample S-2)

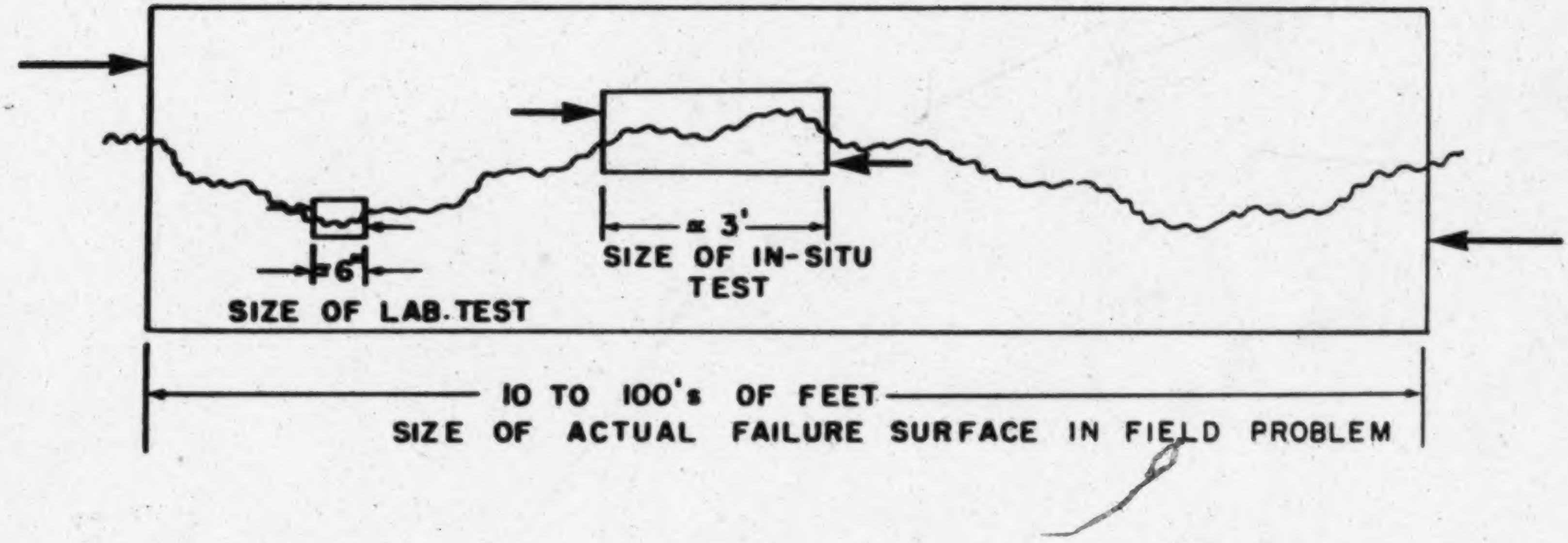
≈ 3'
SIZE OF IN-SITU TEST
6"
SIZE OF LAB.TEST
10 TO 100's OF FEET
SIZE OF ACTUAL FAILURE SURFACE IN FIELD PROBLEM

Figure 4.19 An idealized surface showing the effects of different sizes of specimens (after Deere, et al., 1967)

CHAPTER V

THE GEOLOGY OF TURTLE MOUNTAIN

5.1 INTRODUCTION

In 1903 on April 29, at 4:10 AM, a gigantic rock slide occurred on the east face of Turtle Mountain. The slide destroyed the southern end of the town of Frank, a small coal mining town in the Crowsnest Pass area of southwestern Alberta (Figure 5.1). The Canadian American Coal Company, for whom most of the inhabitants of Frank worked, was at the time mining a coal seam at the base of Turtle Mountain.

The slide debris moved down the east face of the mountain across the entrance to the Frank mine, the southern end of the Town of Frank, the main road from the east and the Canadian Pacific main line through the Crowsnest Pass. The slide then continued up the opposite side of the valley before coming to rest approximately 400 feet above the valley floor and about a mile from the base of the mountain.

Approximately 70 people lost their lives in the slide and several miners were trapped in the mine for a considerable time. The disastrous results of the slide immediately aroused the question in the survivors' minds, "will another slide occur and destroy the remainder of the town?" This fear resulted in several investigations to determine the conditions of Turtle Mountain and the possibilities of another slide.

These investigations, considered in detail below, presented conflicting reports as to the geological structure of the mountain. In order to correctly establish the geology, several trips were made to the slide and an examination made of the area. This chapter gives the geology of Turtle Mountain as envisioned from the observations made on the visits to the area and on the existing documented information.

5.2 HISTORY OF INVESTIGATION

Immediately after the slide in May, 1903, an inspection was made by R. G. McConnell and R. W. Brock of the Geological Survey of Canada. Their report, completed within a month of the disaster, gave a general survey of the geology of the mountain. They concluded that the slide occurred across, rather than along, bedding planes and believed that the primary cause for the slide was to be found in the structure of the mountain. It was their opinion that if there was any further danger of another slide, it would come from the north peak.

Brock visited Turtle Mountain again in 1909 and 1910 and became increasingly concerned about the possibility of a slide from the north peak (Brock, 1910, 1911). As a result of his report in 1910, a commission was appointed to study the conditions of Turtle Mountain.

The report of this commission (Daly, et al., 1912) again emphasized the danger of another rock slide from the north peak of Turtle Mountain. Their reasoning was that the structure of the mountain is the same along all profiles from the south side of the south peak to a point well past the north peak. They concluded that because the north peak is similar in structure to the portion which fell away, sliding was likely to occur again at the north peak. It was in this report that a cross-section (Figure 5.2) showing the geology of the north peak was published. This cross-section has appeared in many publications, notably texts by Coates (1967), Leggett (1962), Leggett (1973), Longwell, et al. (1969), Reynolds (1961), Sharpe (1938), Zaruba, et al. (1969), and in reviews by Terzaghi (1950) and Ter-Stepanian (1966).

The structure of Turtle Mountain was described as a monocline of Palaeozoic limestone dipping to the west about fifty degrees. The limestone which formed the northerly trending ridge of the Blairmore Range, of which Turtle Mountain is a part, had been thrust eastward over vertical Mesozoic sandstones, shales and coals on the Turtle Mountain Fault. The slide mass was reported to have moved eastwards down the dip of a set of strike joints perpendicular to bedding.

A geological map of the area was made in 1911 and 1912 by W. W. Leach as part of the Geological Survey's program of mapping coal deposits. It was published with a report by J. D. MacKenzie (1913) who first recognized the Turtle Mountain anticline while mapping south of the slide mass.

In 1931, J. A. Allan of the Department of Geology, University of Alberta, was commissioned by the Alberta Government to investigate the conditions of Turtle Mountain. From mapping the geology and the fissures on top of the mountain he realized that if there was any danger of another slide, it probably existed at the south peak where, on the east face of the mountain, the bedding planes dip to the east. Allan (1933) presented a cross-section of the geology of the south peak as shown in Figure 5.3. Allan's report was never published but a copy exists in the Geology Library at the University of Alberta.

R. B. MacKay (1932) of the Geological Survey of Canada mapped the coal fields in the Crowsnest area and while there considered the geology of Turtle Mountain. In his 1932 report, he gave a cross-section of the structure of the south peak (Figure 5.4). MacKay recognized the easterly dipping beds on the east face but did not recognize the anticline in the mountain.

Norris (1955) has published a map of the Blairmore area in which he also gives a general cross-section through Turtle Mountain (Figure 5.5).

5.3 SUCCESSION OF ROCK UNITS WITHIN THE TURTLE MOUNTAIN AREA

The succession of rock units within the Turtle Mountain area has been summarized by Norris (1955). The oldest rocks exposed on Turtle Mountain are Mississippian and belong to the Banff Formation. The uppermost 400 feet of this formation crop out and are medium-grained, crystalline and shaley limestones containing many dark gray and pale brown weathering chert stringers. The basal bed of the overlying Livingstone Formation, 25 feet thick, consists of coarse-grained medium to dark gray limestone with a little chert. Above this are about 300 feet of massive, gray, crystalline limestones with interbeds of argillaceous and cherty limestone, the Pekisko member. The overlying Turner Valley member is a crinoidal crystalline gray limestone. The uppermost beds of the Livingstone Formation, which is about

1,100 feet thick here, are dark gray crystalline dolomitic limestones.

The Mount Head Formation, also of Mississippian age, lies conformably on the Livingstone Formation. It is approximately 690 feet thick. The basal members consist of interbedded shaly, dark gray dolomites and limestones about 175 feet thick. There then follows 150 feet of brown-gray dolomites with interbedded argillaceous calcareous dolomite breccias, 150 feet of gray, crystalline limestone, 100 feet of limestone and dolomite, limestone and breccias and green shale, and finally 150 feet of dark gray to black fine crystalline limestone and dolomite. The Livingstone and Mount Head Formations together form the Rundle Group.

It is believed that overlying Palaeozoic strata were not involved in the slide. The strata cropping out immediately beneath the Turtle Mountain fault belong to the upper portions of the Jurassic Fernie Group; here, sandstone, siltstones and shales. The Fernie Group is overlain by the Kootenay Formation which is Lower Cretaceous in age. The basal bed of the Kootenay Formation is a dark gray, massive sandstone. Above this is a sequence of shales, sandstones, and coals containing four major coal seams. The Kootenay Formation is about 490 feet thick.

5.4 GEOLOGY OF TURTLE MOUNTAIN

From the literature on the geology of Turtle Mountain, it appeared that the cross-section of the north peak, which had been published in many textbooks, was incorrect. If a proper stability analysis was to be done, it would be necessary to establish clearly and correctly the geology of this mountain. With this in mind several field trips were conducted in the area with two main objectives. The first was to determine the geological structure of the area and the other was to establish which fabric elements of the rock mass were kinematically active during the slide. Figure 5.6 shows an airphoto of the slide area. This airphoto and the geological map shown in Figure 5.14 should be viewed in conjunction with the plan, shown in Figure 5.7, of the geological traverses run in the Turtle Mountain area.

The first traverse was run up the east face of the mountain south of the southern margin of the slide. Here are many trails cut for access to the coal workings in the Kootenay Formation. These trails were followed by vehicle as far as possible before accent on foot was begun.

In the first exposures of the Palaeozoic limestone (thrust over the Mesozoic coal-bearing formations) above the trace of the Turtle Mountain Fault, the beds dip 74 degrees eastwards. Towards the crest of the mountain there is a clear view southward along the regional strike of Hillcrest Mountain (Figure 5.8). In this figure, the easterly dipping beds which form the east limb of the Turtle Mountain anticline can be seen.

Approximately 500 feet below the mountain crest on the eastern face beyond the southern flank of the slide, the narrow hinge zone of the anticline was found. It coincided with the anticlinal crest.

Views from the crest of the mountain showed that the west face of the mountain is formed by bedding dipping at high angles to the west. Looking north from the crest towards the southern portion of the scarp of the slide shows that, at the crown, the dip of the strata is less than 30 degrees to the west. The scarp trace viewed from the south peak is concave to the east (Figure 5.9). Figure 5.9 shows the scarp to be almost vertical. It also shows the gaping cracks in the area between the peaks. These cracks are generally parallel to the strike of the beds and often gape three feet or more. There is also some relative vertical movement between large blocks outlined by this crack set and a set of cracks parallel to the dip of the beds.

Allan, in his survey in 1933, measured the width of a number of these cracks. Some of his survey stations were reoccupied but at none of them had there been perceptible movements in the 39-year interval. Table 5.1 gives the measured widths of some of Allan's stations and those obtained at the same stations in the summer of 1971.

The disturbed rock mass at the top of Turtle Mountain is not suitable for a detailed survey of the rock fabric, but the main fabric elements are evident. There are two joint sets developed perpendicular to bedding; one is parallel to the strike of the beds and the other parallel to their dip.

A second traverse was run up the northern edge of the slide debris to the area referred to as the "hoodoo" weathered area. Here a minor thrust exists above the major thrust (Turtle Mountain Fault). Overturned Livingstone Formation lies between the thrust faults.

The Banff Formation above the minor thrust is highly and complexly deformed as shown in Figure 5.10. The anticlinal hinge trace here is only 330 feet or so above the minor thrust. In this area, the east limb of the fold dips about 50 degrees to the east.

The orientation of the minor thrust plane itself is difficult to determine from the limited exposure. However, because it terminates against the Turtle Mountain Fault as this flattens up-dip, the minor thrust is probably flat lying. Beneath the minor thrust at the north margin of the slide, the Livingstone strata are thrown into open recumbent folds.

A third traverse was run up the southern margin of the slide to a point well above the major thrust fault. Here the minor thrust was not found. Above the Turtle Mountain Fault, Mount Head beds, mapped earlier as dipping westward at 30 degrees (Norris, 1955), are in fact overturned and can be traced upwards into beds dipping eastwards at high angles. These beds show a well-developed horizontal fracture cleavage that may represent the earlier stages of the minor thrust. Looking further up the slope, bedding appears to dip eastwards below the summit of the south peak but bedding planes do not daylight on the eastern slopes.

An oblique airphoto[1] of Turtle Mountain viewed from the northeast is shown in Figure 5.11. The easterly dipping beds can be distinctly seen along the southern margin of the slide. In fact, when viewing the mountain from this advantageous angle, even the crest of the Turtle Mountain Anticline is readily visible in the south peak. It can also be seen in Hillcrest Mountain beyond Turtle Mountain. This photo shows the sharp crown and westerly dipping beds on the west face.

---

[1] This photograph was obtained from Chevron Standard Ltd.

An area which is of particular interest outside the slide area is the small abandoned limestone quarry at the northerly end of Turtle Mountain. In this quarry the importance of bedding in controlling the form of the slope becomes obvious. On the west dipping limb of the anticline, there are some overhanging slopes up to 35 feet high which dip at 70 degrees. Striations can be clearly seen on the bedding surfaces (Figure 5.12). The striations parallel the dip of beds and are perpendicular to the fold axis suggesting they were formed during flexural-slip folding of the strata. Jointing in the quarry is similar to that on the mountain crest; two joint sets are perpendicular to one another and to bedding, one set is parallel to the dip of the beds, and the other is parallel to the strike. The same dominant joint sets are also evident in the large blocks found in the slide debris.

No Mesozoic rocks were found in the slide debris. From this it was concluded that the toe of the slide cropped out at or above the trace of the Turtle Mountain Fault. Many of the blocks within the slide debris have surfaces with striations similar to those on the quarry wall. This would suggest that the flexural-slip surfaces were also present within the rock mass which fell away. Figure 5.13 shows a typical block of this type.

Figure 5.14 shows a new geological map of the slide area. It is based on a map published by Norris and the additional detailed mapping done during the course of this thesis. The new map differs only in detail from the one presented by Norris. The additional mapping, however, provided information on the smaller, mesoscopic discontinuities within the slide area and allowed the identification of the kinematically active discontinuities. It also aided in placing the position of the minor thrust fault above the Turtle Mountain Fault more precisely and resulted in more information on the orientation of bedding on the east limb of the Turtle Mountain anticline.

From the new geological map and the additional information obtained from the detailed mapping, it was possible to draw new cross-sections of the slide area. These are shown in Figures 5.15 to 5.17. Their location with respect to the slide is shown in Figure 5.14.

In order to draw the general shape of the anticline, a profile was taken along a section parallel to the actual sections but just to the south of the slide margin. This is an area with a fair amount of data on the orientations of outcrops (Figure 5.14). Each one of the dip and strike readings in the vicinity of this section was projected on to the section along the strike. The dip readings were converted to the apparent dip along the section. The shape of the fold was then drawn according to Busk's method of constructing folds (Busk, 1929; Billings, 1972).

This general shape was then projected onto the sections. The positions of the folded strata were based on the traces of the formation boundaries, on the thickness of the various rock units and the position of the fold axis.

The profiles of the mountain before the slide were drawn on the basis of a photo of the mountain before the slide and the descriptions given by residents of the area familiar with the mountain before the slide (McConnell and Brock, 1904). It was reported that the portion which fell away was at a higher altitude than either the north or south peaks and that it protruded to the east farther than any part which remained. On the basis of this, a line, slightly concave to the west, was drawn from the intersection of the contours and the slide margin on one side to the corresponding point on the other side. These lines were taken to be the contours before the slide. The pre-slide profiles were then drawn with these estimated contours as a guide.

5.5 DISCUSSION

The re-examination of the geology of Turtle Mountain has established that the Frank Slide is one in which the major portion of the slip surface follows the bedding planes. It has also been shown that at the toe of the slide, the surface of rupture follows a flat-lying minor thrust fault located above the Turtle Mountain Fault. The structure to the south of the slide mass, along the trend of the Blairmore Range, is similar to the structure at the slide except that the minor thrust is not present. So it would seem that the presence of the minor thrust was a crucial factor in the stability of the slide mass. These observations are indeed in great contrast to the thinking that the slide occurred entirely across bedding which has prevailed in much of the geotechnical literature until the present.

The flexural slip folding at Turtle Mountain is a style of deformation associated with thrust folding in many areas in the Canadian Rockies (Dahlstrom, 1970). In places where this folding is associated with the critical position of a thrust fault, there is a reasonable possibility that another Frank Slide might occur. Indeed, there is evidence that other rock slides of the same magnitude have occurred already (Dishaw, 1967).

TABLE 5.1

WIDTH OF CRACKS ON TURTLE MOUNTAIN

Station	Allan's Data (Feet)	Values Measured Sept. 20, 1971 (Feet)	Elevation (Feet)
2	1.65	1.63	7173.70
3	4.10	4.20	7192.03
4	3.35	3.34	7193.63
5	4.10	4.16	7177.55
6	0.54	0.52	7156.57

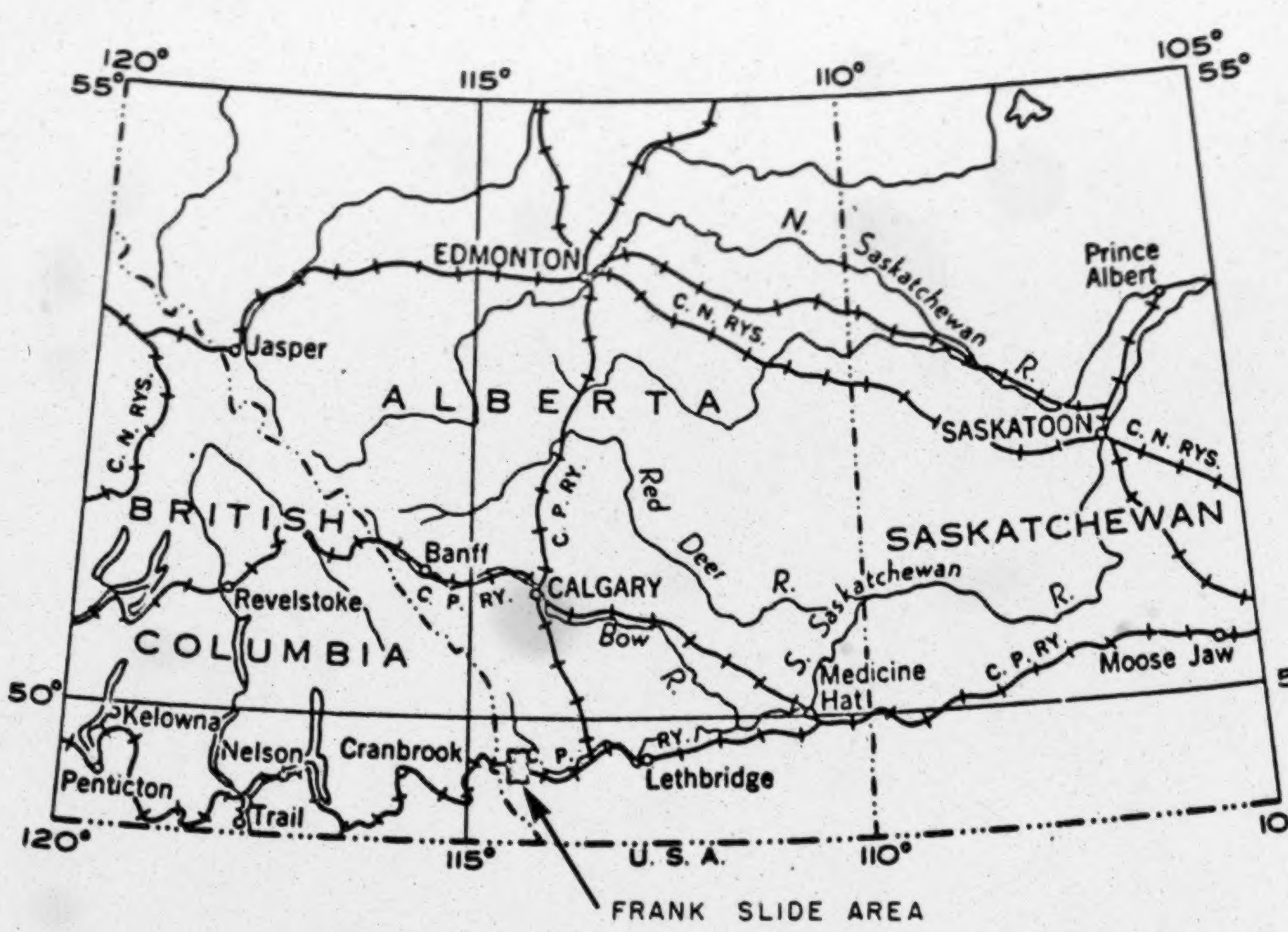
120°
55°
115°
110°
105°
55°
EDMONTON
N.
Saskatchewan
R.
Prince
Albert
C. N. RYS.
Jasper
A L B E R T A
SASKATOON
C. N. RYS.
C. N. RYS.
C. P. RY.
Red
Deer
R.
BRITISH
COLUMBIA
Banff
C. P. RY.
CALGARY
SASKATCHEWAN
Saskatchewan
R.
S.
Revelstoke
Bow
R.
Medicine
Hat
C. P. RY.
Moose Jaw
50°
50°
Kelowna
Nelson
Cranbrook
C. P.
RY.
Lethbridge
Penticton
Trail
120°
115°
U. S. A.
110°
105°
FRANK SLIDE AREA

Figure 5.1 Location of Turtle Mountain

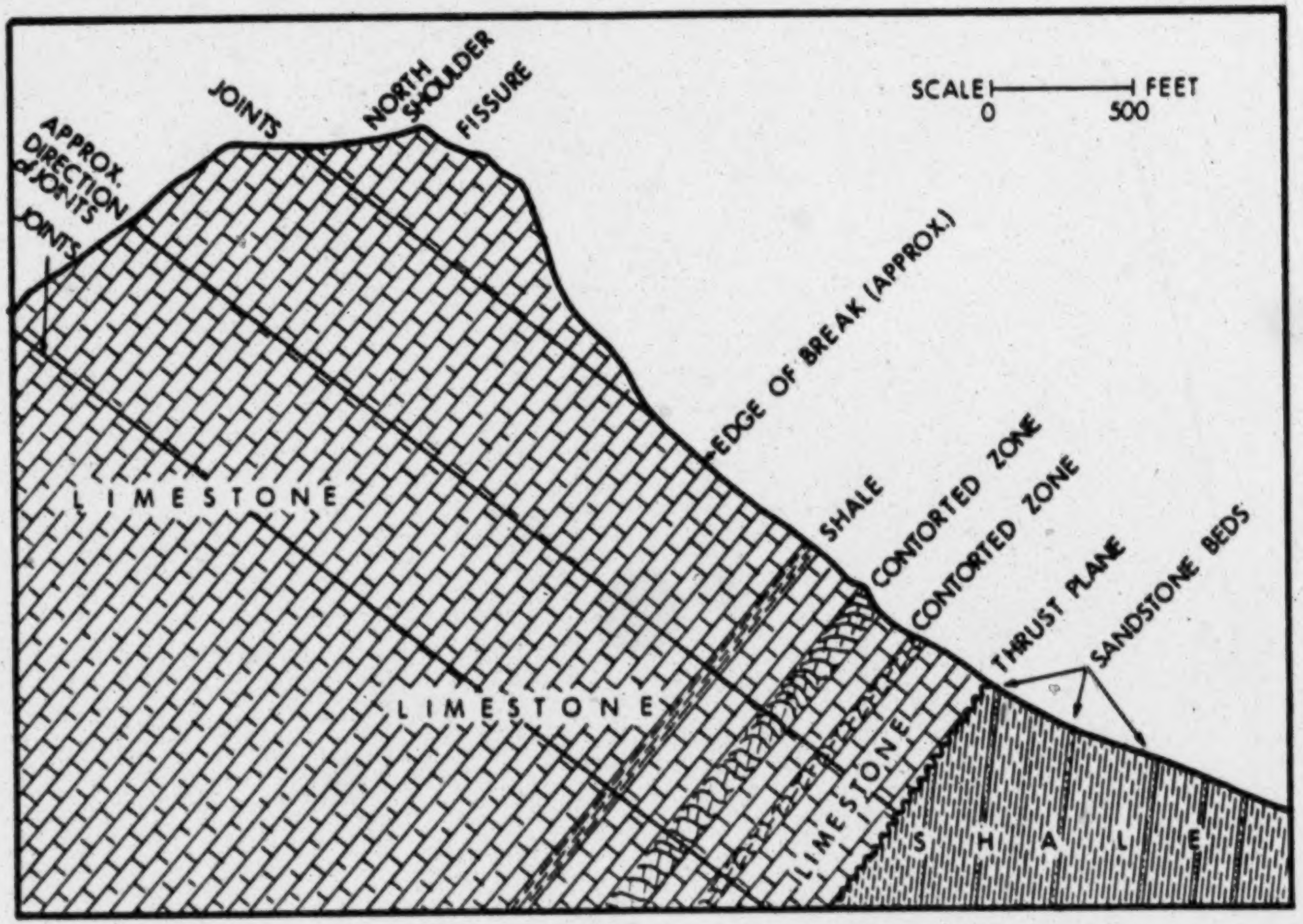
APPROX. DIRECTION of JOINTS
JOINTS
JOINTS
NORTH SHOULDER
FISSURE
SCALE 0 500 FEET
EDGE OF BREAK (APPROX.)
SHALE
CONTORTED ZONE
CONTORTED ZONE
THRUST PLANE
SANDSTONE BEDS
LIMESTONE
LIMESTONE
LIMESTONE
SHALE

Figure 5.2 Cross-section through the north peak of Turtle Mountain (after Daly, et al., 1912)

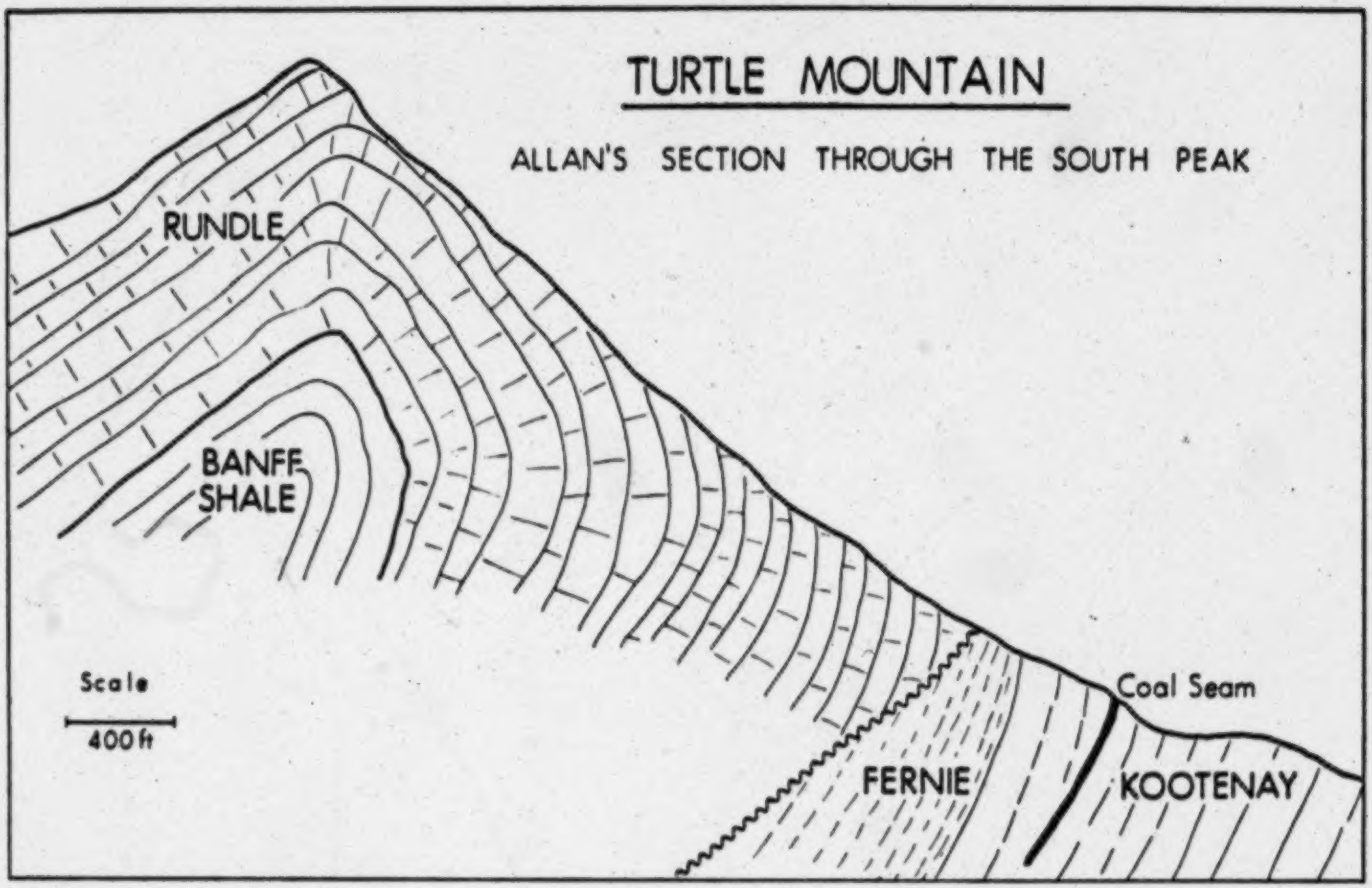
TURTLE MOUNTAIN
ALLAN'S SECTION THROUGH THE SOUTH PEAK
RUNDLE
BANFF SHALE
Scale
400 ft
FERNIE
Coal Seam
KOOTENAY

Figure 5.3 Allan's cross-section through the south peak of Turtle Mountain (after Allan, 1933)

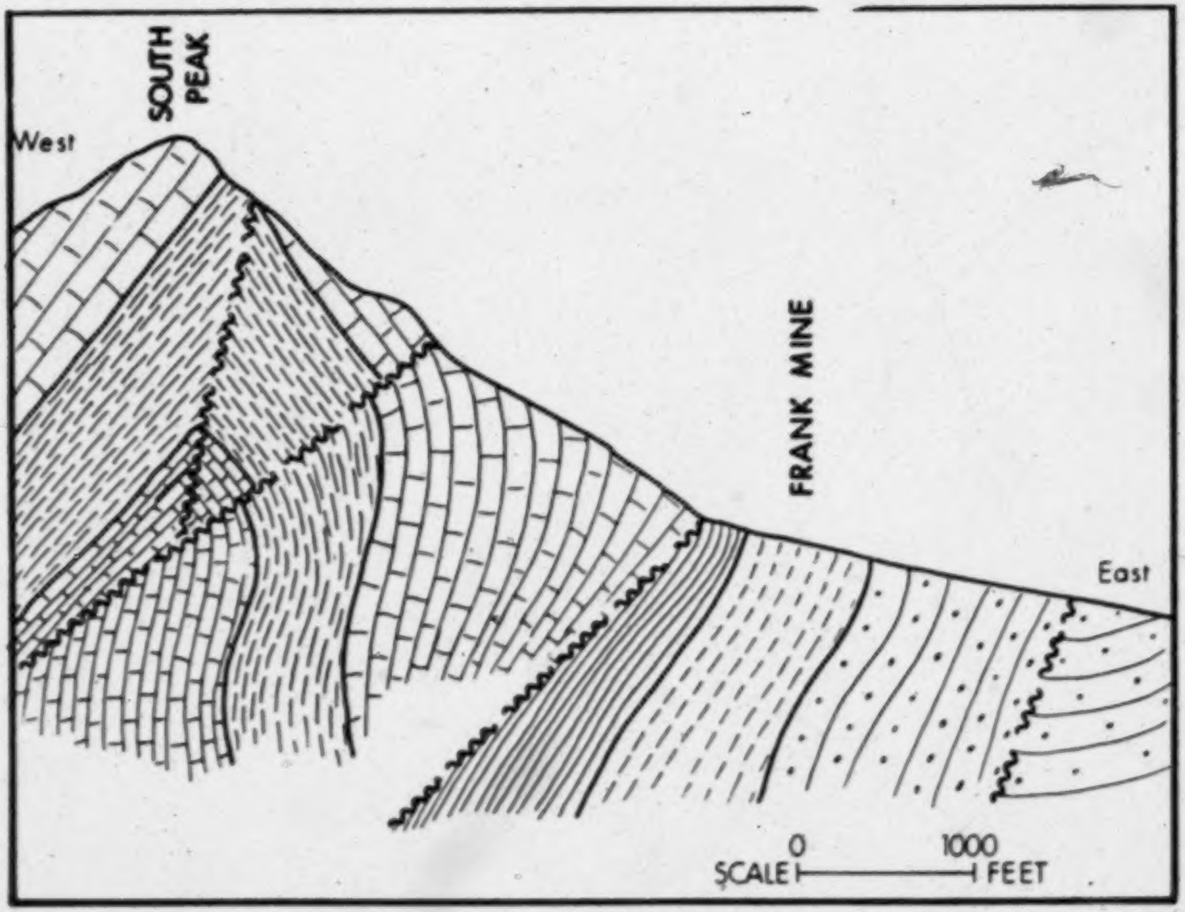
SOUTH PEAK
West
FRANK MINE
East
0
1000
SCALE
FEET

Figure 5.4 MacKay's cross-section through the south peak of Turtle Mountain (after MacKay, 1932)

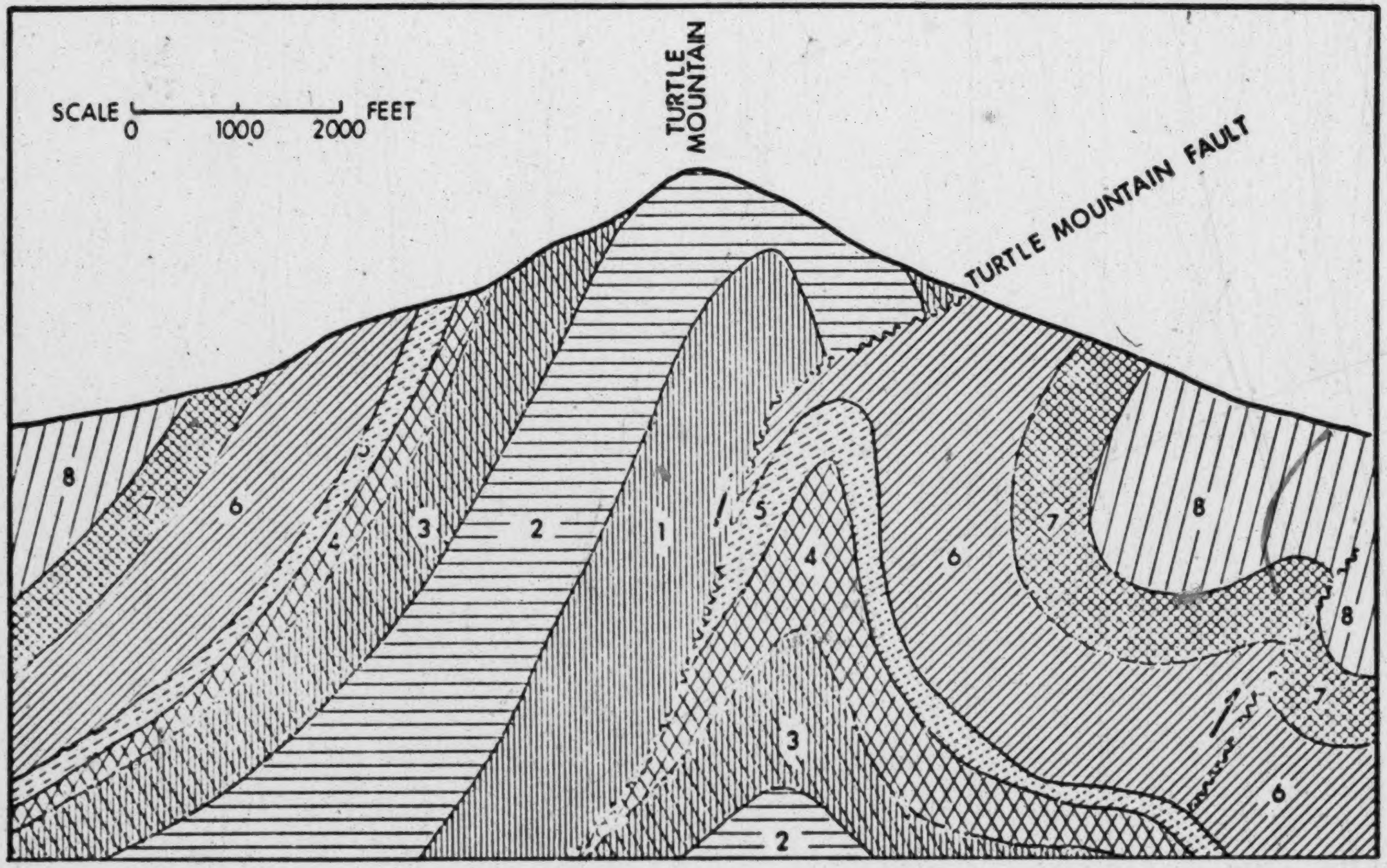
SCALE 0 1000 2000 FEET
TURTLE MOUNTAIN
TURTLE MOUNTAIN FAULT
8
7
6
4
3
2
1
5
4
3
2
6
7
8
8
7
6

Figure 5.5 Norris' cross-section through the south peak of Turtle Mountain (after Norris, 1955)

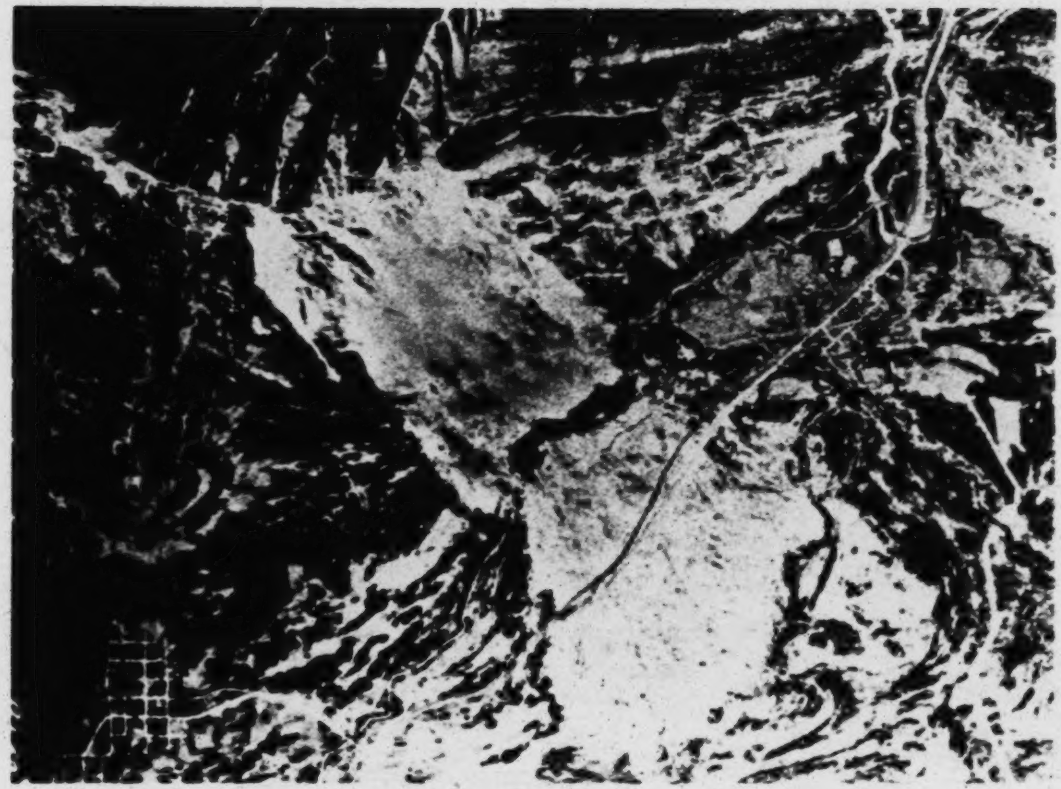

Figure 5.6 Airphoto of the Frank Slide area

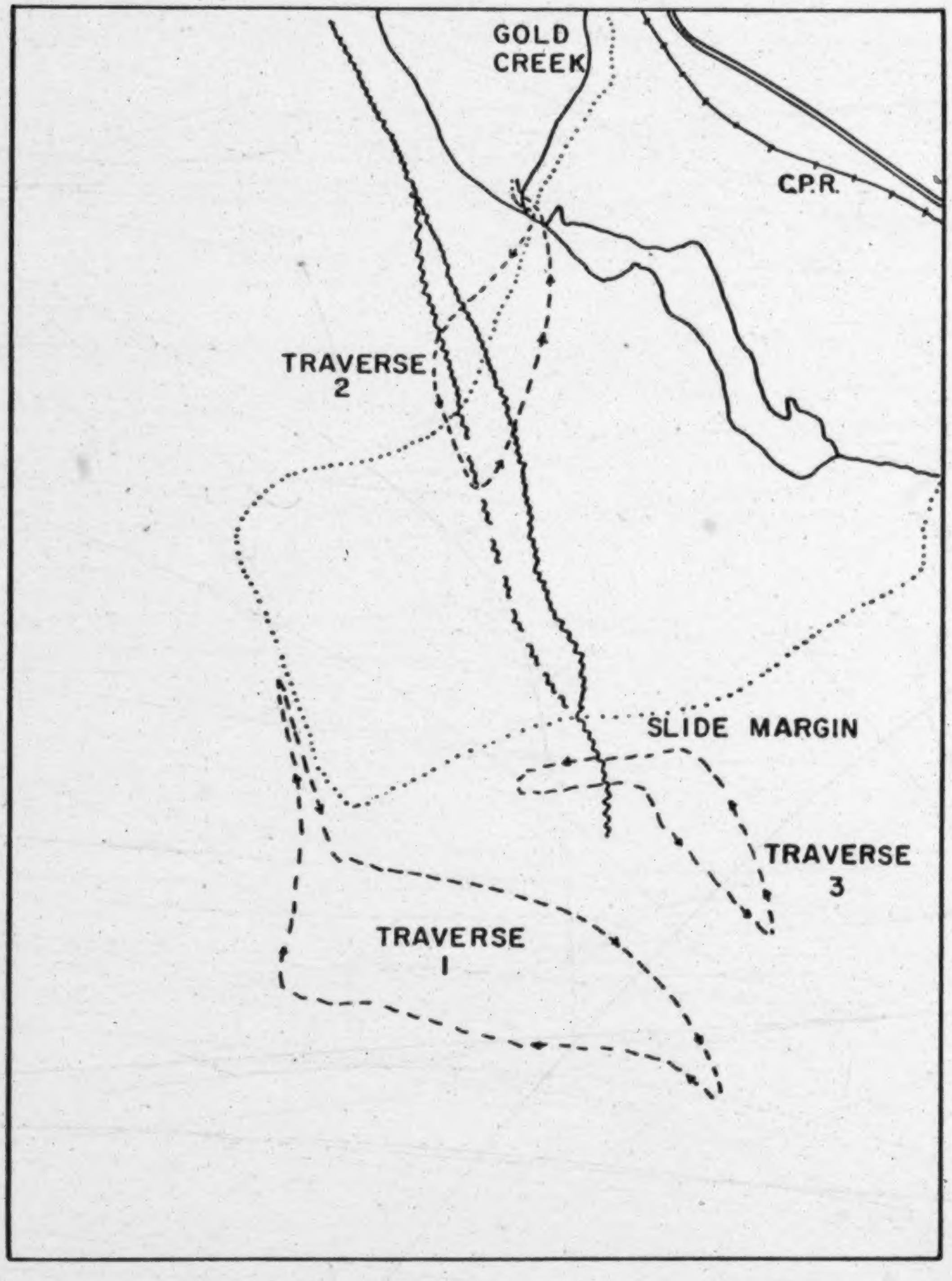
GOLD CREEK
C.P.R.
TRAVERSE 2
SLIDE MARGIN
TRAVERSE 3
TRAVERSE 1

Figure 5.7 A plan showing the general areas of the geological traverses run

Figure 5.8 View of north face of Hillcrest Mountain from Turtle Mountain showing the Turtle Mountain Anticline in profile

Figure 5.9 The crest of Turtle Mountain

Figure 5.10 The Banff Formation in the "Hoodoo" weathered area

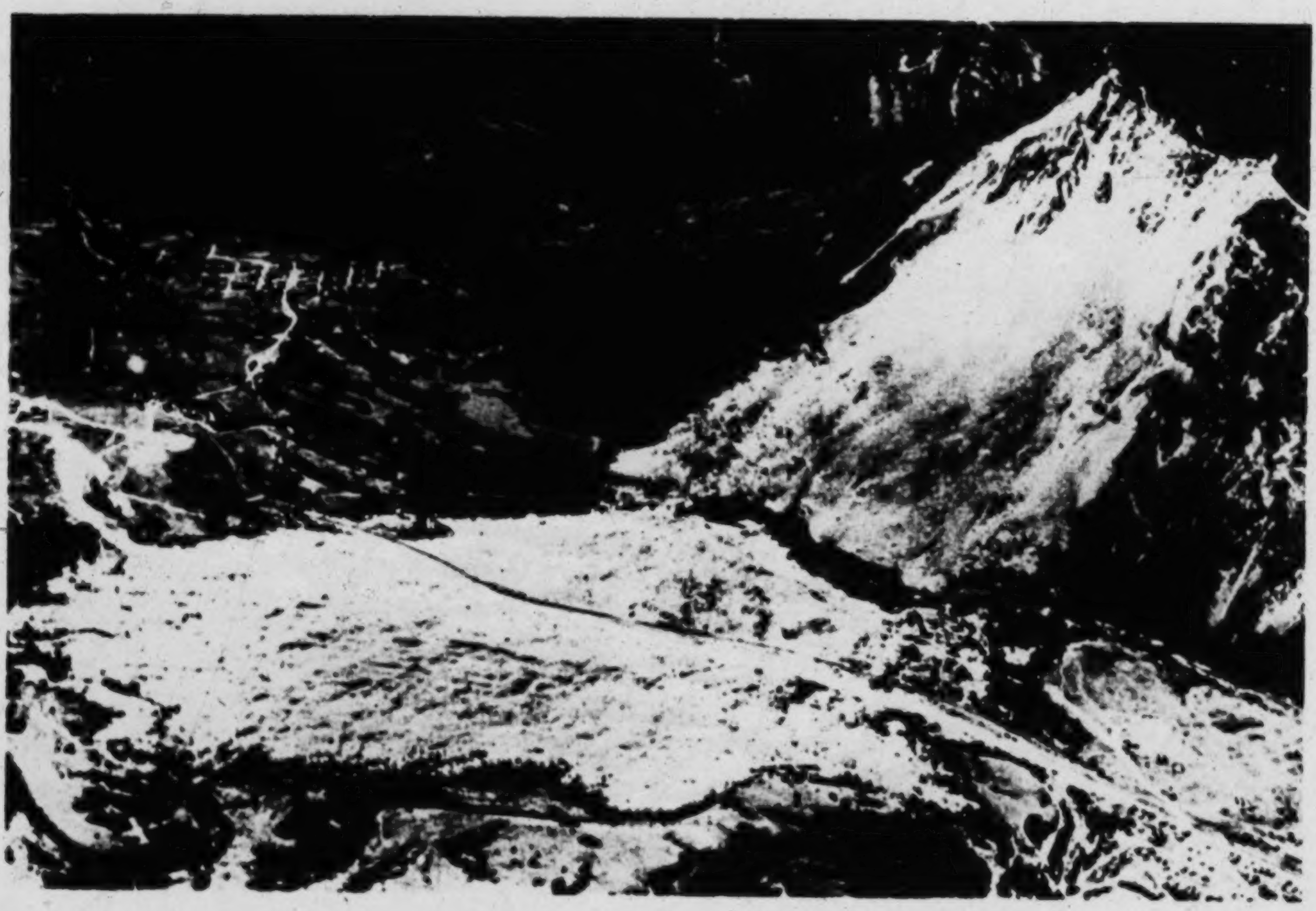

Figure 5.11 Oblique aerial view of the Frank Slide from the northeast

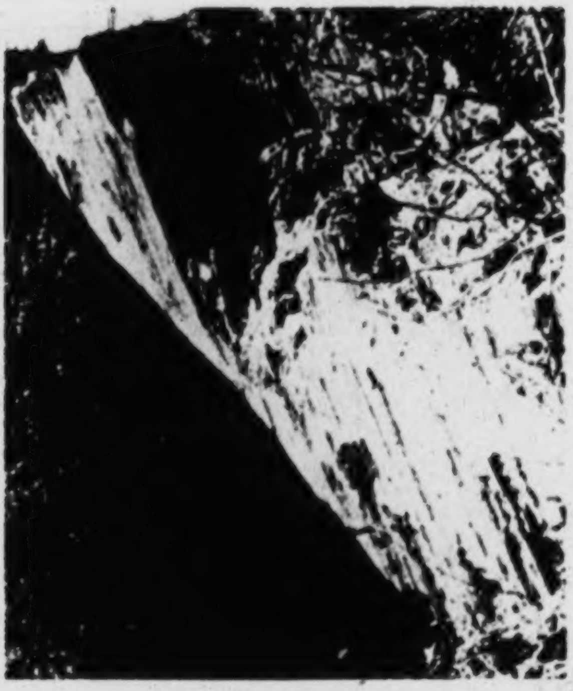

Figure 5.12 Striations on bedding surfaces in an abandoned limestone quarry at the north end of Turtle Mountain

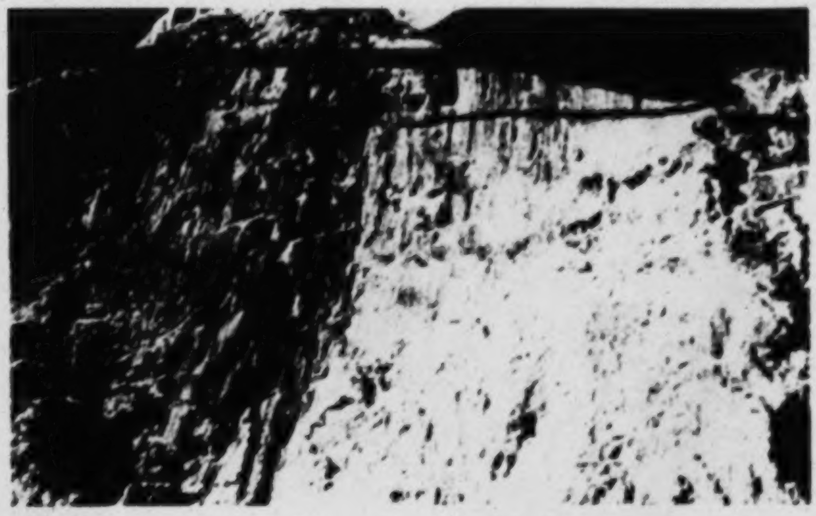

Figure 5.13 A rock within the slide debris showing a sheared surface

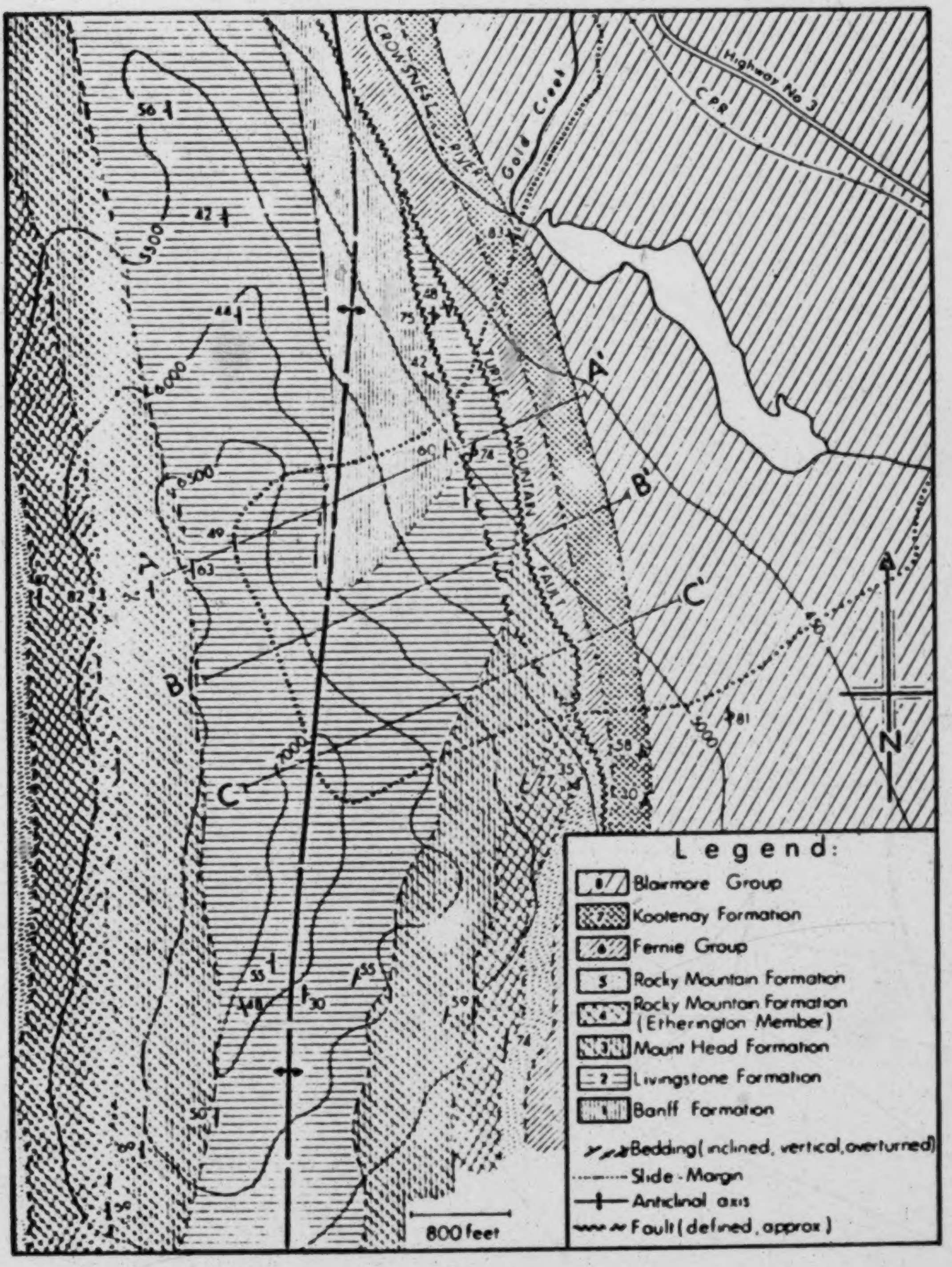
CROWSNEST RIVER
Gold Creek
Highway No 3
CPR
TURTLE MOUNTAIN FAULT
A
A'
B
B'
C
C'
N
5500
6000
6500
7000
5000
4500
56
42
44
83
48
75
42
60
74
49
63
82
58
77
35
30
81
55
48
30
55
59
74
50
69
50
800 feet
Legend:
8 Blairmore Group
7 Kootenay Formation
6 Fernie Group
5 Rocky Mountain Formation
4 Rocky Mountain Formation (Etherington Member)
3 Mount Head Formation
2 Livingstone Formation
1 Banff Formation
Bedding (inclined, vertical, overturned)
Slide-Margin
Anticlinal axis
Fault (defined, approx.)

Figure 5.14 Geological map of Turtle Mountain area

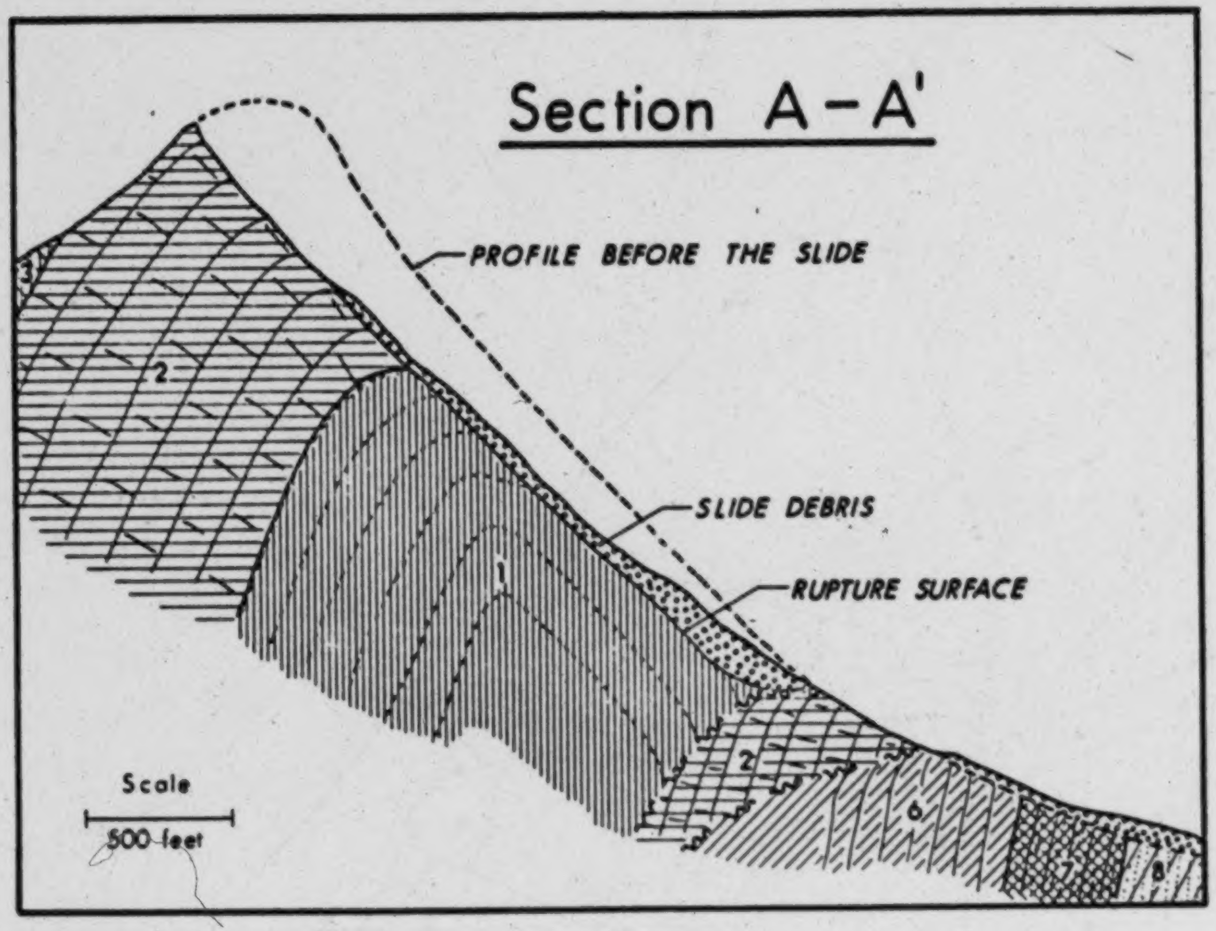
Section A-A'
PROFILE BEFORE THE SLIDE
SLIDE DEBRIS
RUPTURE SURFACE
3
2
1
2
6
7
8
Scale
500 feet

Figure 5.15 Cross-section through Turtle Mountain along line A-A'

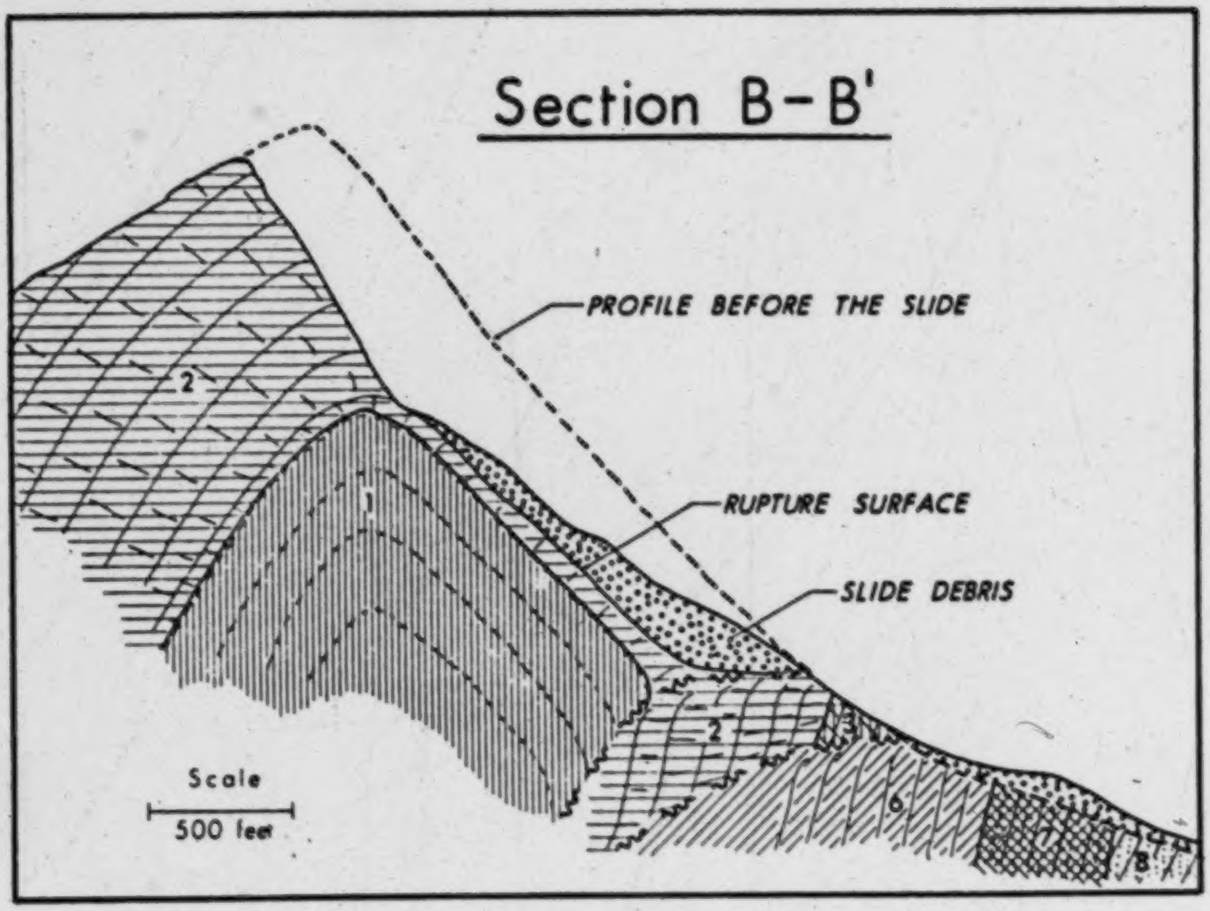
Section B-B'
PROFILE BEFORE THE SLIDE
RUPTURE SURFACE
SLIDE DEBRIS
2
1
2
3
6
7
8
Scale
500 feet

Figure 5.16 Cross-section through Turtle Mountain along line B-B'

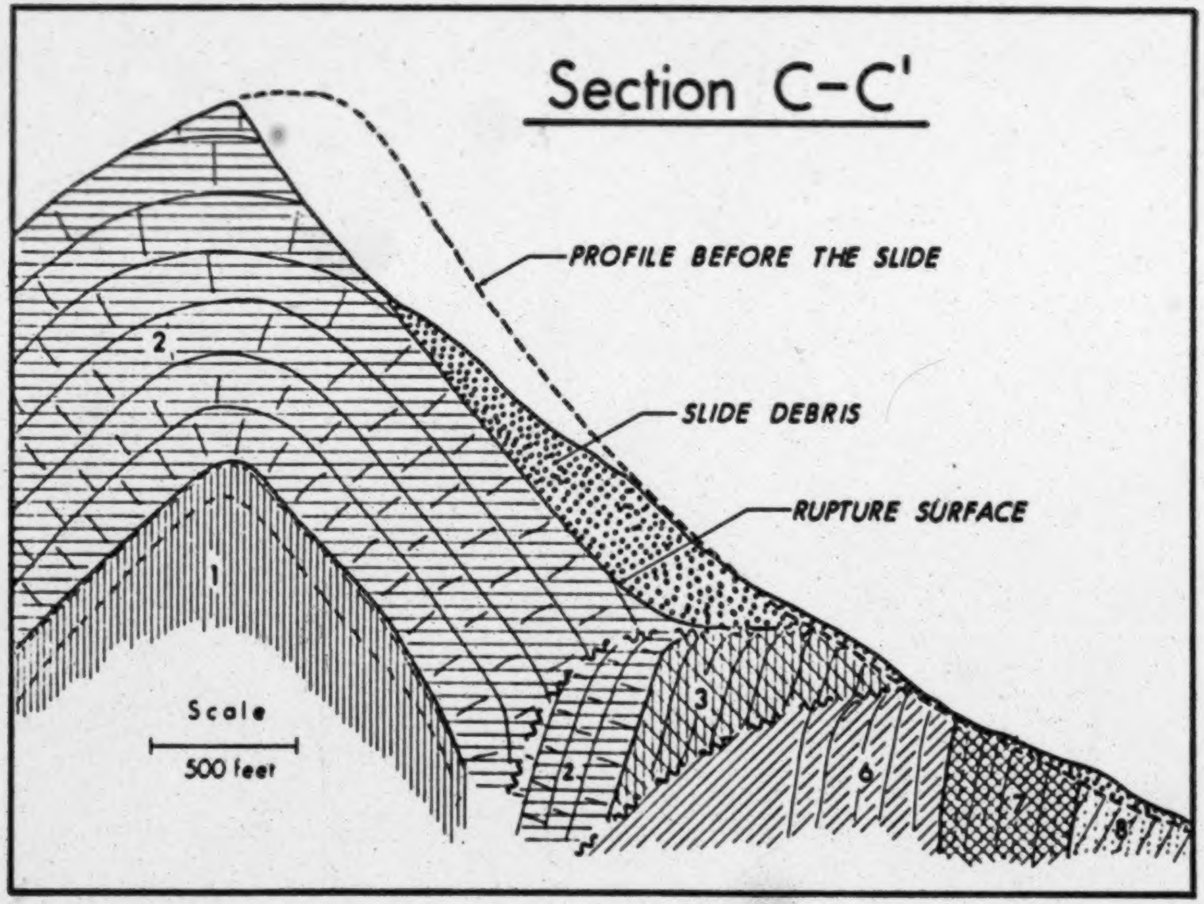
Section C-C'
PROFILE BEFORE THE SLIDE
SLIDE DEBRIS
RUPTURE SURFACE
Scale
500 feet
1
2
2
3
6
7
8

Figure 5.17 Cross-section through Turtle Mountain along line C-C'

CHAPTER VI

THE MECHANICS OF THE FRANK SLIDE

6.1 INTRODUCTION

This chapter presents the studies of two different aspects of the mechanics of the Frank Slide.

The first aspect is the stability analysis of the slide. Now that the geological setting has been correctly established and the shear strength of typical discontinuities has been measured, it is possible to perform the back-analysis.

The second aspect is the effect of the mining on the initiation of the slide. Up to now, the effect of the mining has been largely speculative. This question is considered in this chapter on a more mathematical basis by examining the change in stresses along the slip-surface which resulted from the mine opening. From the change in stresses, it was possible to determine the effect on the stability of the mountain.

6.2 THE STABILITY ANALYSIS

A limit equilibrium stability analysis was performed on the three new cross-sections, presented in the previous chapter, using the Morgenstern-Price Method (Morgenstern and Price, 1965). The analysis was done for three cases. The first was to determine the friction angle, ϕ, required for a safety factor of unity. In the second case, it was assumed that the shear strength along the entire slip surface could be represented by the peak shear strength parameters obtained on the flexural-slip surfaces. This was done because this type of discontinuity is the most prominent along the slip surface. The third case was the same as the second except that the shear strength parameters obtained on the joint surfaces were used along the failure surface where it goes across bedding. The cases were analyzed with the assumptions of a rock density of 160 pcf and zero water pressures. The zero water pressure assumption is based on field observation of no surface seepage above the major thrust fault. Since the slide occurred in April, the only possibility of any water pressure would have been from melting snow. It is doubtful, however, if there would have been enough meltwater to have a significant effect on the overall stability. Generally the conditions on top of Turtle Mountain are unfavorable for a large accumulation of snow. Since the mountain is relatively devoid of trees, the persistent west winds through the Crowsnest Pass area would prevent a large accumulation of snow. Furthermore, since the strata at the crest of the mountain dip away from the scarp, the meltwater could have accumulated only from the relatively small area between the pre-slide scarp and the present scarp. Also if there was any meltwater it would only have been active near the crest of the mountain and not in the lower regions of the failure surface where the mass obtained the majority of its resistance to sliding.

The results of the limit equilibrium analysis show that the average ϕ required for a factor of safety of 1.0 is 37.5°. For cases two and three, where the analyses are based on the shear test results, the average F.S. is 0.86. The particular results for each case and cross-section are presented in Table 6.1. The average computed F.S. of 0.86 differs by only 14% from the defined F.S. of 1.0. This is a pleasing result in the light of the discussion given in Chapter 2 where it was shown that the difference can often be several hundred percent.

Another way to inspect the agreement between the analysis and the defined F.S. of 1.0 is to calculate the average normal and shearing stresses on the failure surface and then plot them in conjunction with the shear strength envelope. If these average stresses fall above the failure envelope, the F.S. would be less than one. This was done for the Folkestone Warren Slide by Hutchinson (1969).

The foregoing procedure was used on the three new cross-sections of the Frank Slide. The average stresses were calculated at the base of each slice on the basis of knowing the weight and side forces of each slice. The side forces were taken as calculated by the Morgenstern-Price program at a F.S. of 1.0. The stresses at the base of each slice were then averaged over the whole slip surface. The results are shown in connection with the peak strength envelope in Figure 6.1. The average stresses fall just above the strength envelope indicating that the F.S. is less than 1.0. This is in agreement with the computed safety factors shown in Table 6.1.

Presenting the stability analysis this way allows the results to be viewed in conjunction with the scatter in shear test data. As can be seen in Figure 6.1, the average stresses for the Frank Slide failure surfaces fall just above the strength envelopes. They are close enough to be within the 95% confidence level of the mean of the peak flexural-slip shear test data points. Furthermore, the average stresses generally fall within the scatter of the test data. This is considered an excellent result for the analysis of rock slopes.

The assumption of zero water pressures is supported by the relatively good agreement between the F.S. obtained using the shear test results and a F.S. of 1.0. The fact that this variable is not included in the analysis is probably one of the reasons for the good agreement. Many times in a back-analysis, assumptions have to be made about the water pressures at failure. If these assumptions are incorrect, it is not possible to tell if the shear tests are representative of the field conditions. This is not to say that any small increase in the water pressure due to precipitation could not have acted as a triggering mechanism because, as has already been demonstrated, the stability of the entire mass was in a very critical state.

Generally, the F.S. in rock slope analysis is very sensitive to a change in the cohesion, C. This is not so in the analysis of the Frank Slide as shown in Figure 6.2, the reason for this being the height of the slope. For a given slope geometry and a given ϕ and water pressure condition, the F.S. will depend only on the $C/\gamma H$ ratio (Bishop and Morgenstern, 1960). H is the height of the slope and γ is the bulk density. In the case of a small H, the change in $C/\gamma H$ will be much larger for a given change in C than at a high H. Since the F.S. is a function of $C/\gamma H$, the same degree of change applies to the F.S. for a given change in C. At the Frank Slide where the height of the slope is approximately 2,000 feet, the F.S. is therefore insensitive to a change in C. This is probably another reason for the relatively good agreement between the computed F.S. and unity.

The stability analysis showed that the average ϕ required for a F.S. of 1.0, with zero cohesion, is 37.5 degrees. This is very close to the basic friction angle of 37.2° measured on the surfaces lapped with the #45/80 grit. This type of agreement has been observed on other slides as discussed in Chapter 2. On the basis of these observations, it is the writer's opinion that a fairly good first estimate of the degree of stability can be made by using the ϕ_b as measured on a flat surface which is sandblasted or lapped with a fairly coarse grit and with C equal to zero. This would provide a lower bound to the problem and be on the safe side.

It is interesting to note that ϕ required for F.S. of 1.0 is not $\phi_b + i$ but simply ϕ_b. Furthermore, the shear strength as determined on the flexural-slip surfaces has been used in the stability analysis with good success without any correction for the field roughness. This would seem to indicate that the effective i at the field scale is essentially zero. Again, to assume the i to be zero would present a lower bound solution on the safe side.

6.3 THE EFFECT OF MINING ON THE STABILITY OF TURTLE MOUNTAIN

At the time of the Frank Slide, the Canadian American Coal Company was mining a coal seam at the base of Turtle Mountain which was approximately 15 feet wide and dipped approximately 85 degrees to the west. This coal seam is identifiable in Figure 5.6 where the entrance to the mine is at the junction of the north margin of the slide and the river. On the south edge of the slide, subsidence is clearly visible marking the seam at this point. Mining had reached the south edge of the slide debris when the slide occurred.

The coal was mined in a series of chambers about 130 feet in length and and from 250 to 400 feet high. These chambers were separated by pillars 30 feet wide which contained manways and timber chutes. These large chambers had reached the south edge of the slide when the disaster occurred. In fact the edges on both sides of the slide corresponded very closely with the limits of the big chambers in the mine.

For about six months prior to the slide there had been a general squeezing in of the tunnel walls (McConnell and Brock, 1904). The coal would mine itself by breaking off the hanging wall. The miners noticed slight movements at times which were associated with shocks which felt like tremors. Gangways and manways often had to be retimbered and were even condemned due to the impossibility of keeping them timbered (Daly, et al., 1912).

Exactly how much movement occurred in the mine is difficult to determine. Daly, et al. (1912) have, from the amount of coal removed, estimated that if the entire void left by the coal was squeezed in, it would represent about four feet of movement. Although this could happen with time, it was not the case just after the slide occurred because these chambers were mined again after the slide, and witnesses also reported that the mine escaped with little damage. The testimony of the miners at the time of the disaster contains nothing that would indicate that there was a sudden movement within the mine walls just before the slide.

It is, of course, important to establish what effect the mining had on the initiation of the slide if recommendations are to be given on similar future projects. This was investigated by determining the stress changes resulting along the failure surface using the Finite Element Method.

The stress analysis was done with a Finite Element computer program based on a simple constant strain triangular element. The mountain was divided into a finite element grid as shown in Figure 6.3 (Section C-C'). The initial insitu stresses were determined using the "gravity turn on" method (Goodman and Duncan, 1968b) where K_o, the coefficient of earth pressure, was set equal to $\nu/1-\nu$ (ν = Poisson's ratio). Only the condition for K_o = 0.75 was analyzed. From the results of this analysis, the initial insitu normal and shearing stresses were calculated along the failure surface (Figure 6.4).

The mining at the base of the mountain resulted in the walls of the mine becoming a stress-free boundary. The effect of this in the stress distribution can be simulated by applying stresses to the mine boundary equal and opposite to the initial insitu stresses. With these reverse stresses applied to the mine boundary and the mass taken as weightless, the results from the analysis gives the change in stresses throughout the mass due to the mine opening. The finite element mesh with the mine open is shown in Figure 6.5. The change in stresses is shown in Figure 6.6.

The effect of these stress changes can be evaluated by defining a pseudo safety factor, SF, as the resisting forces along the failure surface divided by the shearing forces. If we assume C = 0, the resisting forces would be $\tan \phi \, \sigma_{n_o}$ ds integrated over the whole failure surface. σ_{n_o} is the normal stress over an incremental distance, ds. The shear force integrated over the failure surface would be τ_o ds. In equation form

$$SF_o = \frac{\int_a^b \tan\phi \, \sigma_{n_o} \, ds}{\int_a^b \tau_o \, ds} \quad \ldots\ldots\ldots\ldots\ldots\ldots\ldots\ldots 6.1$$

where a to b is the distance along the failure surface.

After mining, the stresses along the failure surface would be $\sigma_{n_1} = \sigma_{n_o} + \Delta\sigma_n$ and $\tau_1 = \tau_o + \Delta\tau$, where $\Delta\sigma_n$ is the change in normal stress and $\Delta\tau$ is the change in shearing stress. The safety factor after mining would be

$$SF_1 = \frac{\tan\phi \int_a^b (\sigma_{n_o} + \Delta\sigma_n) \, ds}{\int_a^b (\tau_o + \Delta\tau) \, ds} \quad \ldots\ldots\ldots\ldots\ldots 6.2$$

The change in safety factor then is

$$FS = \frac{SF_o - SF_1}{SF_o}$$

From the distribution curves (Figures 6.4 and 6.6), we can integrate using Simpson's rule. The results of these integrations are as follows:

$$\int_a^b \sigma_{n_o} \, ds = -100.2 \times 10^3 \text{ Kips/ft}$$

$$\int_a^b \tau_o \, ds = 69.9 \times 10^3 \text{ Kips/ft}$$

$$\int_a^b \Delta\sigma_n \, ds = 1.39 \times 10^3 \text{ Kips/ft}$$

$$\int_a^b \Delta\tau \, ds = -0.20 \times 10^3 \text{ Kips/ft}$$

In numerical form then

$$SF_o = \tan\phi \; \frac{100.2}{69.9}$$

$$= \tan\phi \; (1.433)$$

$$SF_1 = \tan\phi \; \frac{(-100.2 + 1.36)}{(69.9 - 0.20)}$$

$$= \tan\phi \; (1.418)$$

The percent change in SF then is

$$\frac{\tan\phi \; (1.433 - 1.418) \times 100}{\tan\phi \; (1.43)} \simeq 1\%$$

With this method of analysis, it is also possible to obtain ϕ for a factor of safety of unity. If we set SF_o equal to 1.0, we can solve for ϕ from

$$SF_o = \tan\phi \; (1.433)$$

With SF equal to 1.0

$$\phi = \tan^{-1} \left(\frac{1}{1.433} \right)$$

$$\simeq 35^\circ$$

This is in good agreement with the values obtained from the limit equilibrium stability analyses (Table 6.1).

Fortunately the stress distribution, except near the fixed boundaries, for a two-dimensional anaylsis in a homogeneous isotropic body is not affected by the magnitude of the elastic modulus, E. Thus for the above calculations of the stress changes, the results are not affected by the choice of E. To assume the entire mountain to behave as a homogeneous isotropic body is a simplification of the behaviour of the material but does allow an estimate to be made of the effect of the mining.

The deformations resulting from the mine opening, however, are directly dependent on the magnitude of E. The inward deformation at the top of the mine on the mountainside (Figure 6.7) is approximately three inches if we assume E = 1,000,000 psi. Decreasing the E value to 100,000 psi increases the deformation at the same point tenfold or to approximately 2.5 feet.

The general over-all style of deformation of the entire mountain is shown in Figure 6.8. Here we see that the top of the mountain in the region of the failure surface moved more or less as a unit. This type of movement accounts for the low change in shear and normal stresses along the failure surface.

Generally, this stress analysis does not indicate that the mining was a factor in significantly decreasing the stability of Turtle Mountain. From limit equilibrium analysis, however, it has been shown that the stability of Turtle Mountain was in a very critical state before the slide and with this in mind, the 1% decrease in stability due to the mining may have been enough to trigger the slide.

6.4 DISCUSSION

The stability analysis together with the shear strength results have shown the critically unstable state of Turtle Mountain before the slide occurred. What finally triggered the slide is difficult to say. Factors which have been cited as possible causes are the ice wedging in the cracks on top of the mountain, earthquake tremors, increased pore pressures and mining at the base of the mountain (McConnell and Brock, 1904). All these factors, although small, cannot be ruled out completely as being responsible for snapping the last bond by which the mass was held up. The primary cause, however, was undoubtedly in the form and structure of Turtle Mountain. It might be argued that this is not new since it is the same conclusion that was expressed by McConnell and Brock in 1904. What is new, though, is that now it has been substantiated by a stability analysis, and the new interpretation of the geology brings more logic to why the structure was so important. The added advantage of having shown this from a stability analysis is that the analysis can now be used with a greater degree of confidence to estimate the stability in similar situations.

One of the main items of concern throughout this thesis has been the reliability of the stability analysis of rock slopes based on shear test data. The analysis of the Frank Slide indicates that for a slope where the slip-surface follows some through-going discontinuity, where the material is a hard unweathered rock, and where the $C/\gamma H$ ratio is small, a fairly reliable estimate can be given of the F.S. on the basis of laboratory shear tests. This statement, however, assumes that the geological and geometric setting are known in detail and, furthermore, that the water pressures at the time of failure have been correctly established.

In recent years, there has been an increased interest in developing recreational facilities along the eastern slopes of the Canadian Rockies. Along these slopes, there is a possibility of encountering a geological setting similar to that of Turtle Mountain. The understanding gained about this type of situation from the Turtle Mountain investigation would be very valuable in making recommendations on areas to avoid for planned development.

TABLE 6.1

RESULTS OF STABILITY ANALYSES ON FRANK SLIDE

Section	Case 1 Ø required for F.S. equal to 1.0	Case 2 F.S. for Ø=28° C=4600 psf	Case 3 F.S. for Ø=28° C=4600 psf and Ø=32°, C=3600 psf across bedding
A-A'	39.7	0.832	0.837
B-B'	35.2	0.890	0.896
C-C'	37.4	0.853	0.863

NOTE: (1) The average for Case 1 is 37.5

(2) The average for Cases 2 and 3 is 0.86

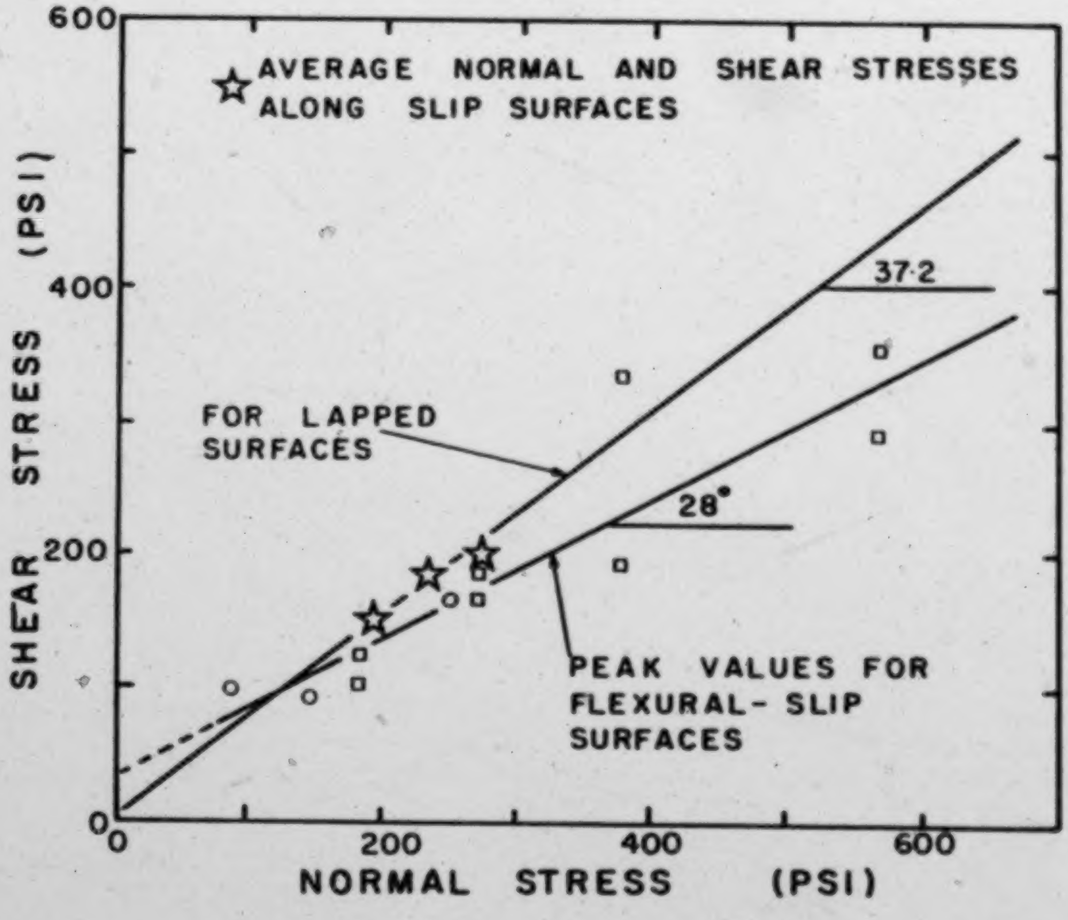

Figure 6.1 The average normal and shear stresses in relation to the failure envelopes

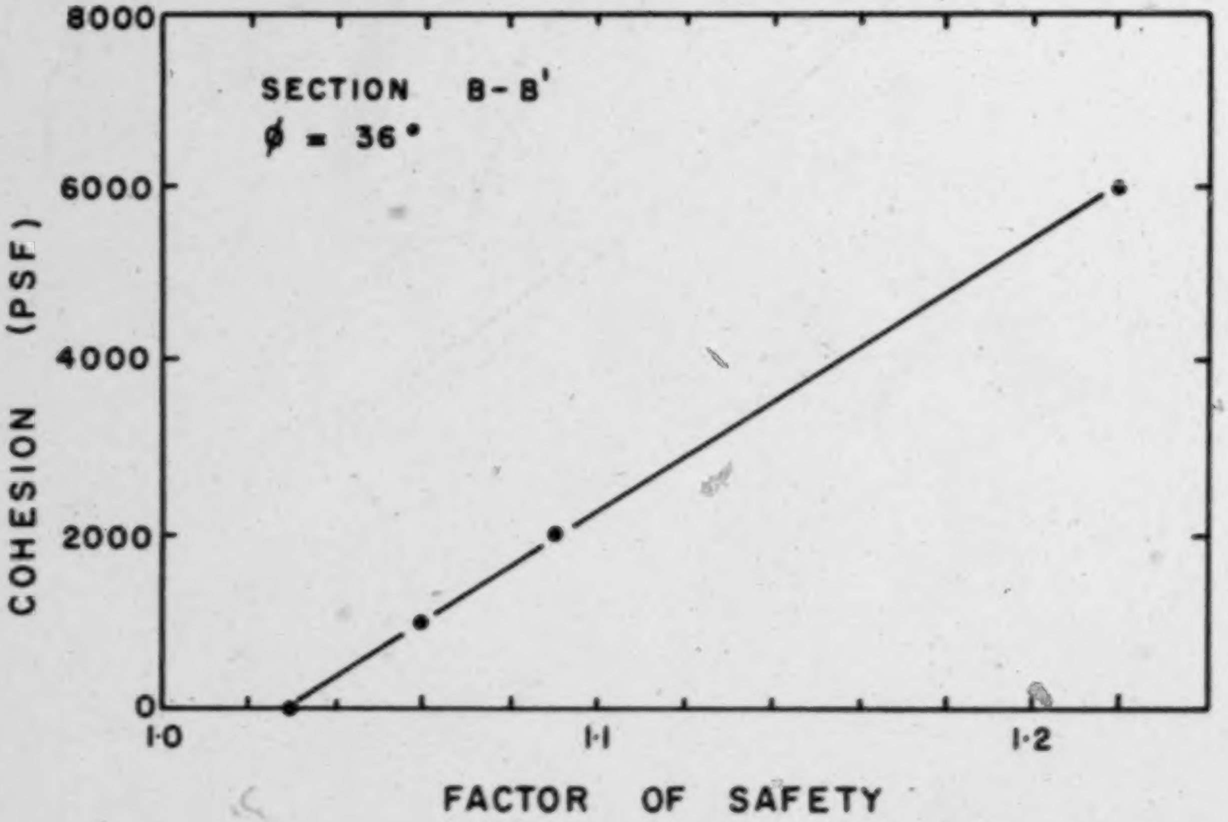

Figure 6.2 The effect of cohesion on the factor of safety for section B-B'

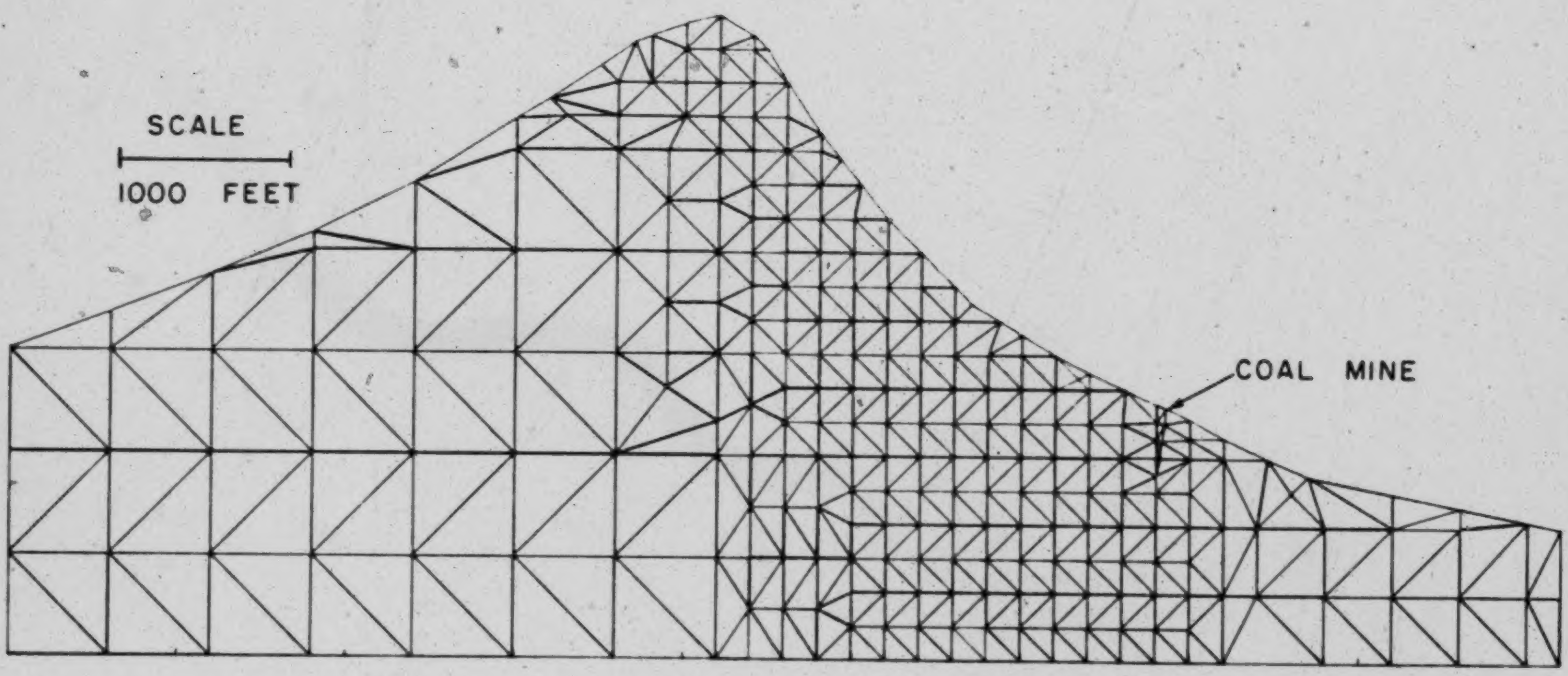
SCALE
1000 FEET
COAL MINE

Figure 6.3 The Finite Element grid for the stress analysis of Turtle Mountain

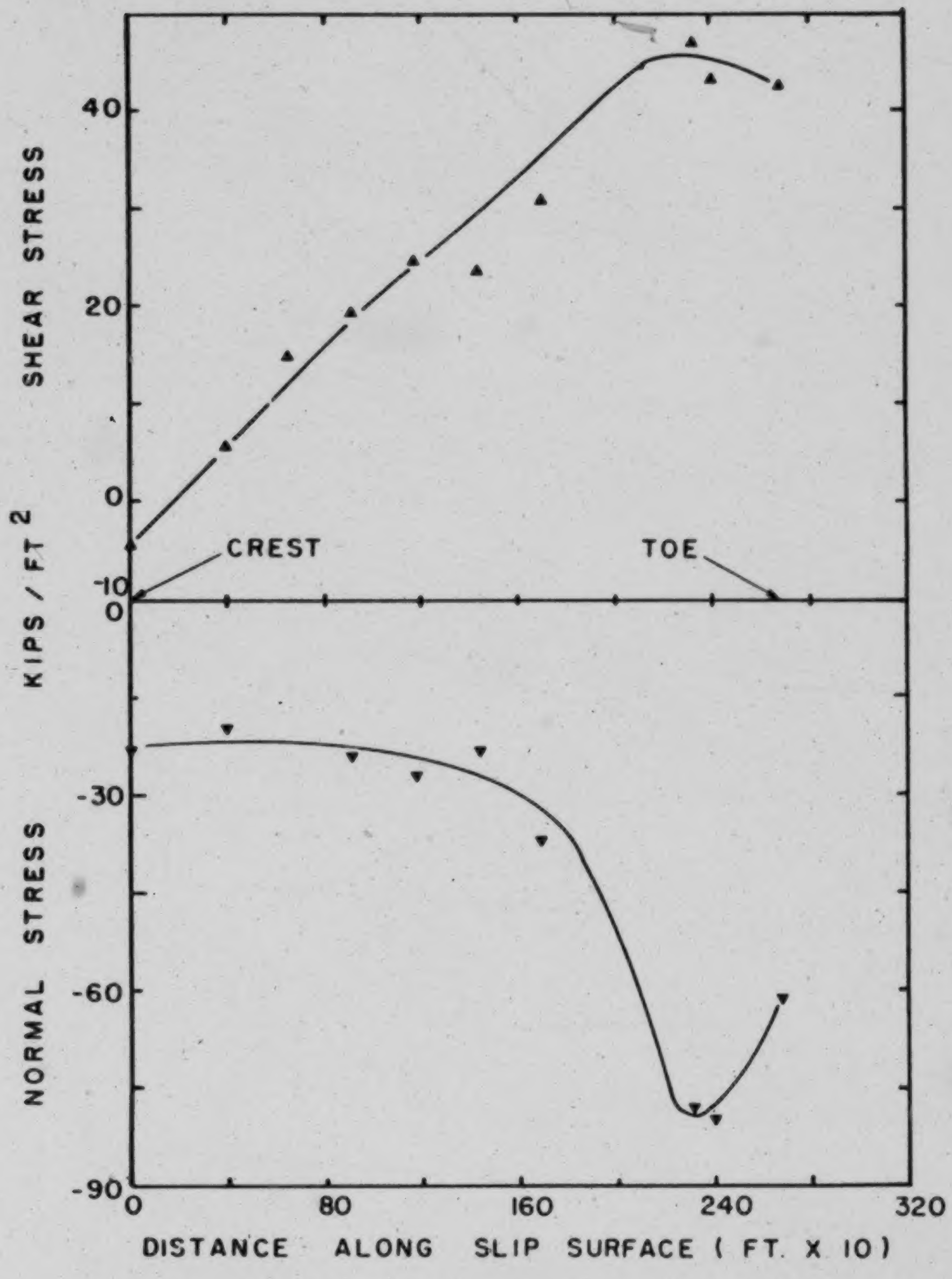

Figure 6.4 The initial stress distributions along the slip surface

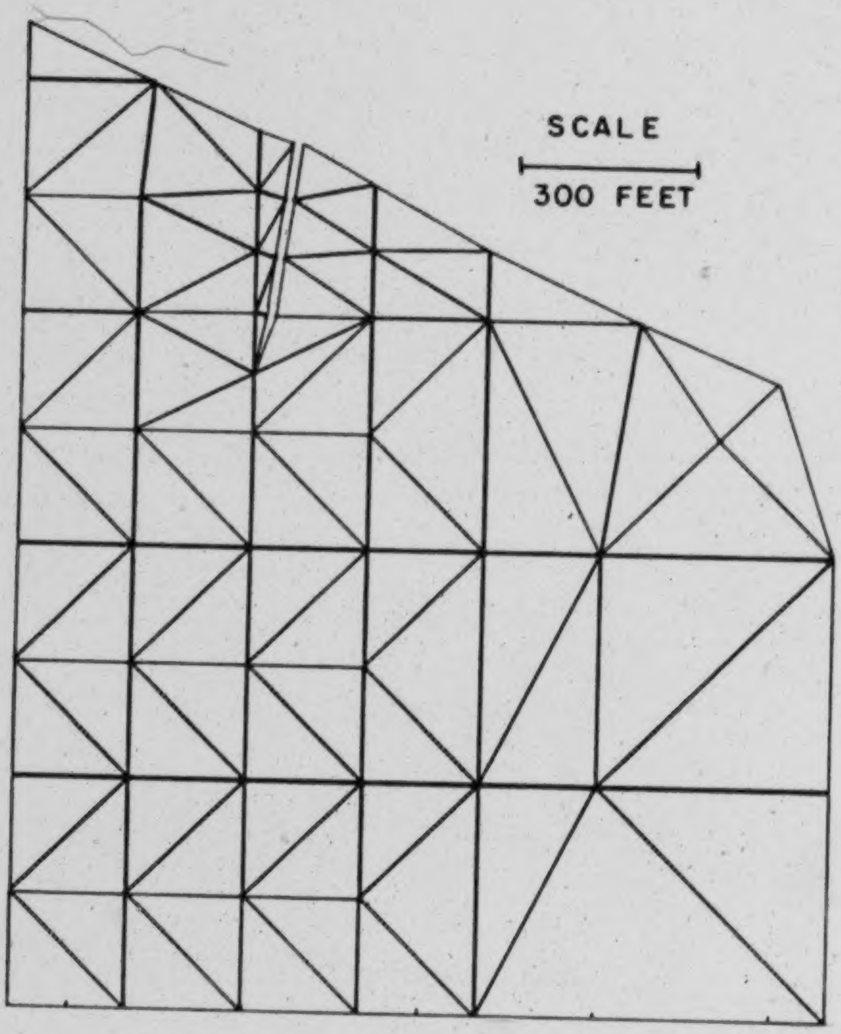
SCALE
300 FEET

Figure 6.5 The Finite Element grid around the mine area with the mine open

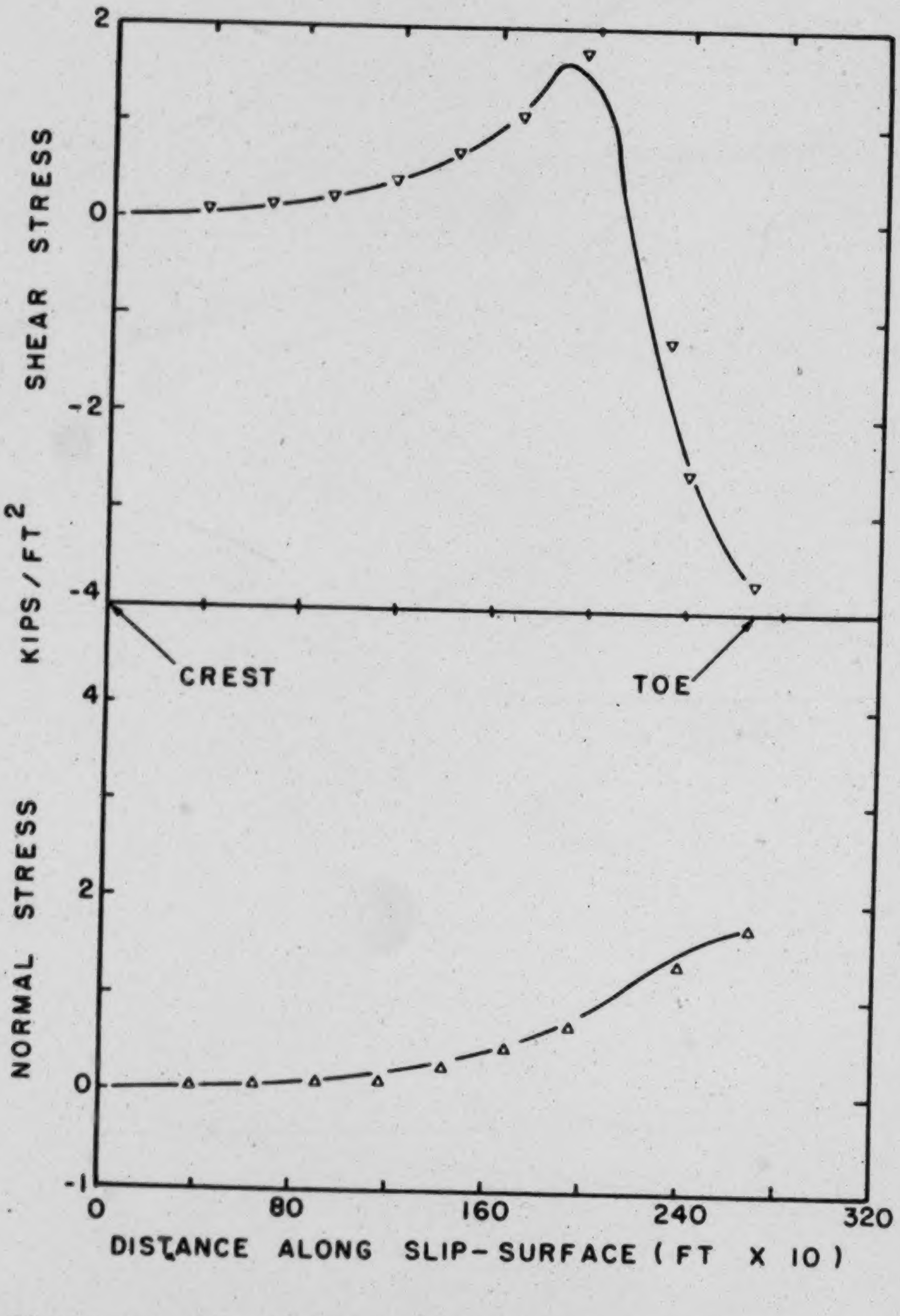

Figure 6.6 The changes in stress distributions

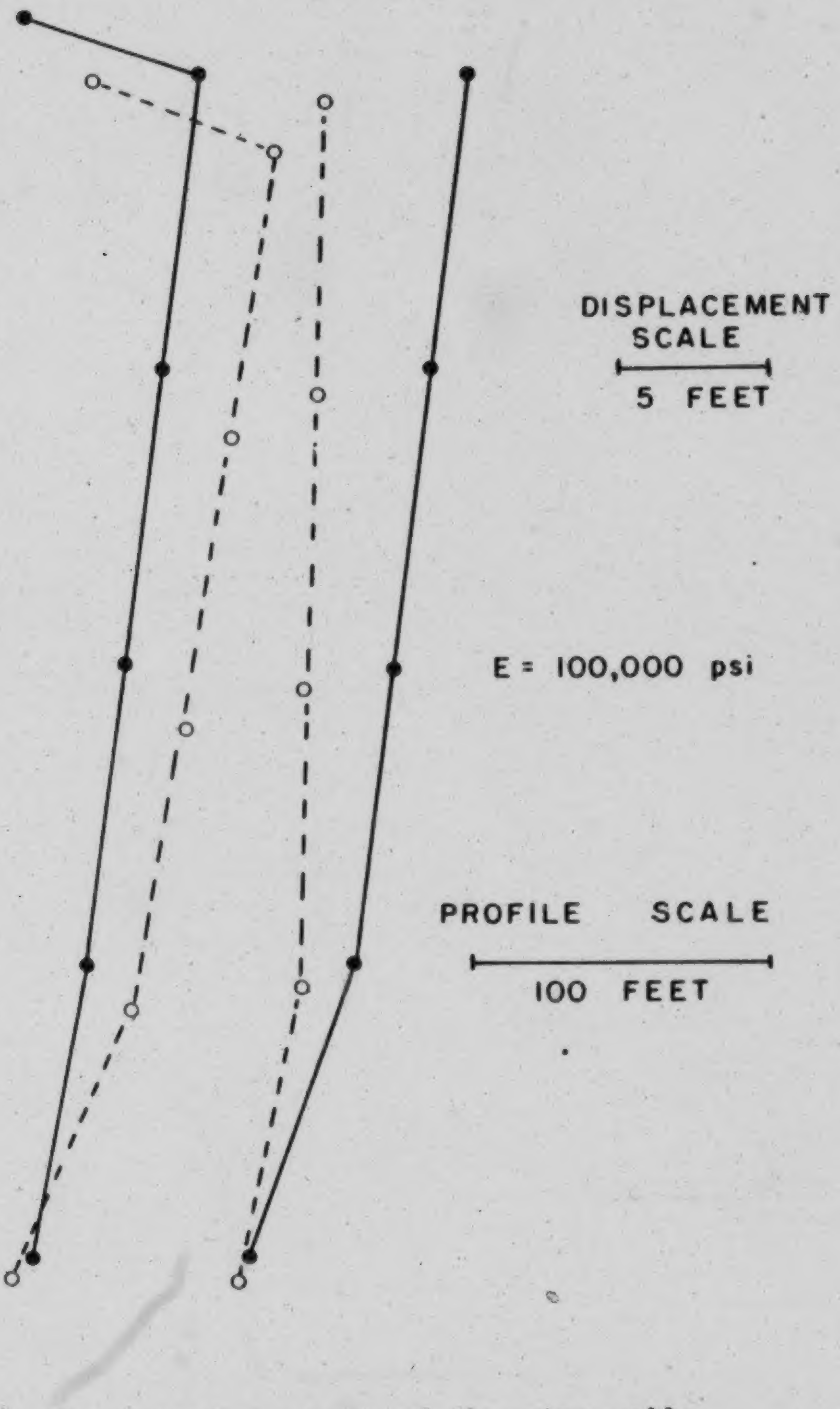

Figure 6.7 The inward movement of the mine walls

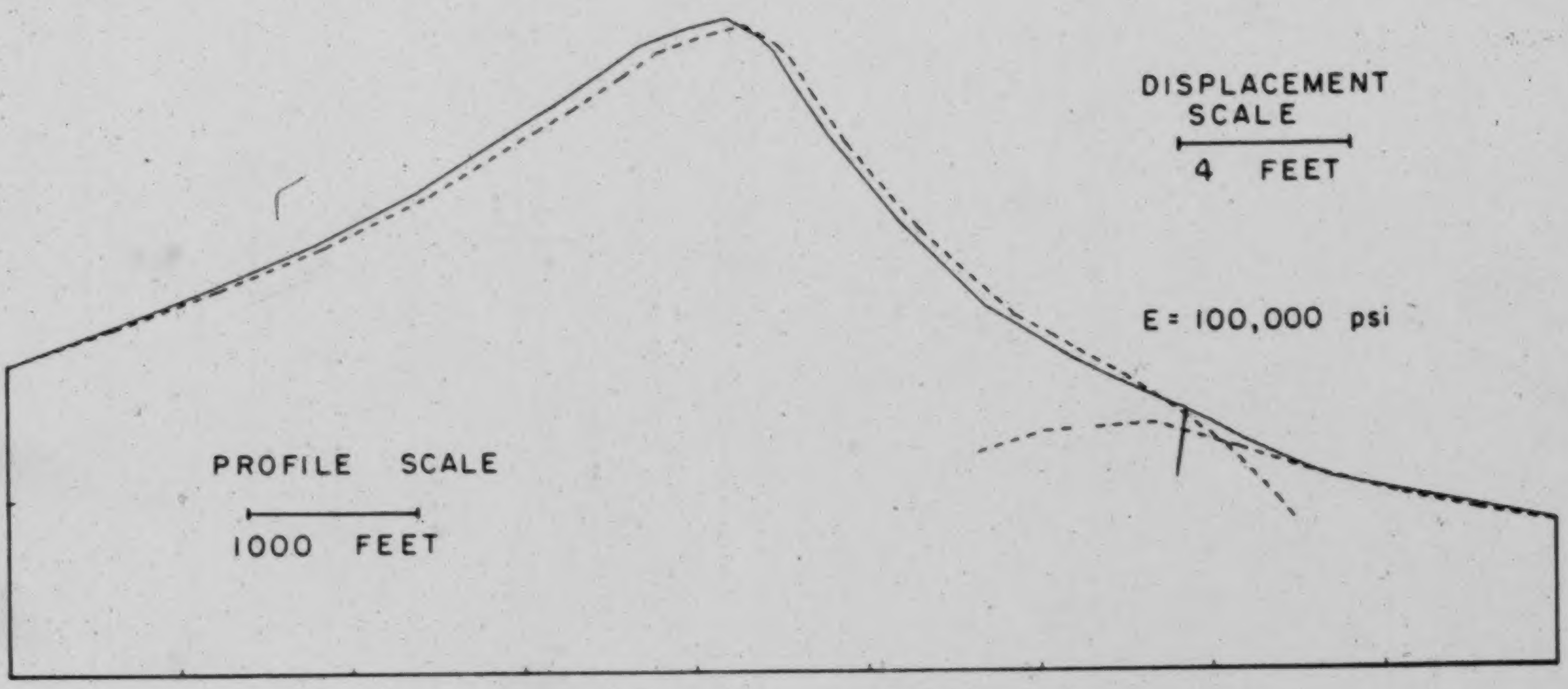
DISPLACEMENT
SCALE
4 FEET
E = 100,000 psi
PROFILE SCALE
1000 FEET

Figure 6.8 The style of deformation of Turtle Mountain due to the mining

CHAPTER VII

CONCLUDING REMARKS

In this thesis, an examination was made of the reliability of rock slope stability analysis by inspecting numerous case histories and by performing a detailed back-analysis of the Frank Slide. This study of failed rock slopes showed that in the majority of cases, the shear strength parameters required for a safety factor of 1.0 are ϕ equal to 30 ± 5 degrees and C equal to zero. Furthermore, the case histories revealed that the F.S. based on shear tests can differ from the defined safety factor of 1.0 within a range of only a small percentage to several hundred percent. For this reason, rock slopes are often designed on the basis of past experience in conjunction with a consideration of local geology and not so much on stability analysis.

In connection with the back-analysis of the Frank Slide, shear tests were performed on natural discontinuities and artificially prepared limestone surfaces. The results of these tests yield not only the necessary strength parameters for the stability analysis but also shed some new light on the shear strength behaviour of rock discontinuities.

An investigation was conducted into the possibility of mathematically characterizing the microscopic surface roughness of prepared rock surfaces and then correlating these with the friction angle. The results of this work showed that it is possible to establish this type of a correlation; however, the work involved in calculating the roughness parameter makes this an impractical method for determining ϕ. Its application to the field scale is hindered by the inability of measuring the field roughness.

The shear tests on the natural limestone discontinuities revealed that the shear strength is not affected by the size of the sample if the scale of roughness does not change with the size of the sample.

The ultimate shear strength (shear strength after larger shearing displacements) was measured on the natural discontinuities by performing a reversal shear test whereby the geometric component of the shear strength was eliminated. The results showed that the ultimate strength is greatly affected by the initial roughness of the discontinuity and the type of surface damage which occurs during the shear tests. Since the ultimate strength is a function of these conditions, it differs characteristically from the residual strength of clays.

The re-examination of the geology of Turtle Mountain proved to be most enlightening. A cross-section showing the bedding dipping into the slope and the failure surface going across bedding has appeared in many textbooks and publications. This cross-section is incorrect. The strata within Turtle Mountain are in reality folded so that on the southern margin of the slide, the bedding dips in the easterly direction out of the slope. With the strata folded in this manner, the failure surface only went across bedding at the crest of the slope. Further down it follows the flexural-slip surfaces parallel to bedding and then along a minor thrust fault at the toe.

The average safety factor of the Frank Slide as computed on the basis of the shear tests differs, on the unsafe side, by only 14% from the defined safety factor of 1.0. For rock slope analysis, this is considered to be very good. This indicates that for a potential slide in a similar geological and geometrical setting, it is possible to predict the degree of stability with considerable reliability from shear tests performed on natural discontinuities.

The study of the case histories has shown that with $C = 0$, the ϕ required for a F.S. of 1.0 is very similar to the basic friction angle, ϕ_b. This suggests that a good first estimate of the F.S. of rock slopes can be obtained by assuming $\phi = \phi_b$ and $C = 0$.

The stress analysis of Turtle Mountain demonstrated that the mining at the base of the mountain had a small effect in decreasing the stability of the rock mass. However, since the potential sliding mass was already in a critically unstable position, it is not unreasonable that the mining triggered the slide.

With regard to future research in the area of rock slope stability, there is still a need for further detailed case history studies. The reason for this is two-fold. Firstly, a back-analysis is like analyzing a large shear test and, therefore, is a means of investigating the shear strength behaviour of rock discontinuities at the field scale. For example, the study of failed slopes in this thesis seems to indicate that if there is a problem with instability, the effective i at the field scale is essentially zero. Only the analysis of failed slopes can provide this type of information. The second reason for further case studies is that they would clarify the reliability of analysis based on shear tests; i.e., they would either confirm the present position or provide more definite bounds on the reliability for various geological settings.

In the overall system of stability analysis, the problem is not so much the type of analysis as it is the establishment of the field shear strength parameters. Therefore, it is suggested that future research efforts be directed at understanding the field shear strength behaviour rather than the development of any new analytical methods.

In the design of open pit slopes, a change in even one degree in the overall slope angle can represent either a cost or saving of millions of dollars. Ideally, it would be desirable to design the slopes within this low tolerance and be certain that there would be no major failures. This, however, is an unrealistic objective, and it is not suggested that further studies of failed slopes will provide the necessary confidence in stability analyses to design at this low tolerance. The nature of the material within rock slopes is too complex in behaviour for this to be a realistic objective.

REFERENCES

Alden, W. C. (1928). "Landslide and Flood at Gros Ventre, Wyoming," *Amer Inst Mining and Metallurgical Engrs* , Tans, Vol 76, pp. 347-361.

Allan, J. A. (1933). *Report on the Stability of Turtle Mountain, Alberta* , Dept of Geology, University of Alberta, Edmonton, Alberta (unpublished).

Am. Standards Assoc. (1955). *Surface Roughness, Waviness, and Lay* , ASA B46.1.

Barney, K. R. (1960). "Madison Canyon Slide," *Civil Engineering* , Aug 1960, pp. 72-75.

Barton, N. R. (1971a). *A Model Study of the Behaviour of Steep Excavated Rock Slopes* ,Ph.D. Thesis, Imperial College, London.

Barton, N. R. (1971b). "Estimation of Insitu Shear Strength From Back Analysis of Failed Slopes," *Proc of the Inter Symp on Rock Mech* , Nancy, France, p. II-27.

Bendat, J. S. and Piersol, A. G. (1971). *Random Data: Analysis and Measurement Procedures* , Wiley-Interscience Toronto.

Billings, M. P. (1972). *Structural Geology* , Prentice-Hall, Inc., New Jersey.

Bishop, A. W. (1955). "The Use of the Slip Circle in the Stability of Slopes," *Geotechniqe* ,V5, pp. 7-17.

Bishop, A. W. and Morgenstern, N. R. (1960). "Stability Coefficients for Earth Slopes," *Geotechnique* , Vol 10, pp 129 -147.

Blackman, R. B. and Tukey, J. W. (1959). *The Measurement of Power Spectra* , Dover Publications, Inc. N.Y.

Bowden, F. P. and Tabor, D. (1956). *Friction and Lubrication*, Methuen, London (1967 ed).

Brawner, C. O. (1970). "Stability Investigations of Rock Slopes in Canadian Mining Projects," *Proc 2nd Cong Int Soc Rock Mech*, Belgrade, 3, p 7-8.

Brawner, C. O. (1971a). "Introduction", *Stability in Open Pit Mining*, Proc of the 1st Conf on Stability in Open Pit Mining, Vancouver, pp. 1-4.

Brawner, C. O. (1971b). "Case Studies of Stability on Mining Projects," *Stability in Open Pit Mining*, Proc of the 1st Conf on Stability in Open Pit Mining, Vancouver, pp. 205-226.

Brock, R. W. (1910). "Turtle Mountain," *Sum Rept Geol Surv, Canada, 1909*, p. 29.

Brock, R. W. (1911). "Turtle Mountain, Frank, Alberta," *Sum Rept Geol Surv, Canada, 1910*, p. 13.

Bugge A. (1937). "Fjellskred fra Topografisk og Geologisk Synspunkt," *Norsk Geogr Tidskr*, Vol 6, pp. 342-360.

Busk, H. G. (1929). *Earth Flexures*, Cambridge University Press, Cambridge.

Byerlee, J. D. (1967). "Theory of Friction Based on Brittle Fracture," *J of Applied Physics*, Vol 38, pp. 2928-2934.

Coates, D. F., McRorie, K. L. and Stubbins, J. B. (1963). "Analyses of Pit Slides in Some Incompetent Rocks," *Trans Am Inst Min Engs*, 226, 94-101.

Coates, D. F., Gyenge, M. and Stubbins, J. B., (1965). "Slope Stability Studies at Knob Lake," *Proc of the Canadian Rock Mech Symp*, Toronto, pp. 35-46.

Coates, D. (1967). *Rock Mechanics Principles*, Mines Branch, Ottawa, Monograph 874.

Cooley, J. W. and Tukey, J. W. (1965). "An Algorithm for the Machine Calculation of Complex Fourier Series", *Math Comp*, Vol 19.

Coulson, J. H. (1970). *The Effects of Surface Roughness on the Shear Strength of Joints in Rock*, Ph. D. Thesis, University of Illinois, Urbana.

Coulson, J. H. (1972). "Shear Strength of Flat Surfaces in Rock," *Stability of Rock Slopes* , Proc 13th Symp on Rock Mech, Urbana, Illinois, pp. 77-106.

Dahlstrom, C. D. A. (1970). "Structural Geology in the Eastern Margin of the Canadian Rocky Mountains," *Bull Can Pet Geol* , Vol 18, pp. 332-406.

Daly, R. A., Miller, W. G. and Rice, G. S. (1912). "Report of the Commission Appointed to Investigate Turtle Mountain, Frank, Alberta," *Can Geol Surv* , Mem 27.

Deere, D. U., Hendron, A. J., Patton, F. D. and Cording, E. J. (1967). "Design of Surface and Near-Surface Construction in Rock," *Failure and Breakage of Rock* , 8th Symp on Rock Mech, pp. 237 - 302.

Desai, C. S. and Abel, J. F. (1972). *Introduction to the Finite Element Method,* Van Norstrand Reinhold.

Dishaw, H. E. (1967). "Massive Landslides," *Photogrammetric Engineering* , Vol 33, pp. 603-608.

Duncan, J. M. (1972). "Finite Element Analyes of Stresses and Movements in Dams, Excavations and Slopes, State of the Art," *Applications of the Finite Element Method in Geotechnical Engineering* , Proc of Symp, Mississippi, pp. 267-326.

Fecker, E. and Rengers, N. (1971). "Measurement of large Scale Roughness of Rock Planes by Means of Profilograph and Geological Compass," *Proc of 2nd Int Symp Rock Mech,* Nancy, France, p 1-18.

Goodman, R. E. and Taylor, R. L. (1967) "Methods of Analysis for Rock Slopes and Abutments," *Failure and Breakage of Rock* , 8th Symp on Rock Mech, Minnesota, pp. 303-320.

Goodman, R. E., Taylor, R. L. and Brekke, T. (1968a). "A Model for the Mechanics of Jointed Rocks," *J Soil Mech Fdns Div* , ASCE, 94, SM3, pp. 637-659.

Goodman, R. E. and Duncan, J. M. (1968b). *Methods of Anaysis of Rock Slopes* , Report to Waterways Experiment Station, U. S. Army Corps of Engineers.

Hamel, J. V. (1972). "The Slide at Brilliant Cut," *Stability of Rock Slopes* , Proc 13th Symp on Rock Mech, Illinios, pp. 487-536.

Heim, A. (1932). "Bergsturz und Meuschenleben," Bublatt zur Vierteljahrsschrift der Naturforschenden Gesselschaft, Zurich, Vol 77, pp. 1-218.

Hendron, A. J., Cording, E. J. and Aiyer, A. K. (1971). Analytical and Graphical Methods for the Analysis of Slopes in Rock Masses, U. S. Army Corps of Engineers, Vicksburg, Mississippi, Rept No. 36.

Hobbs, D. W. (1970). "The Behaviour of Broken Rock Under Triaxial Compression," Int J Rock Mech and Min Sci, Vol 7, pp. 125-148.

Hoek, E. and Pentz, D. (1968). The Stability of Open Pit Mines, Imperial Col, Rock Mech Res Rept No. 5.

Hoek, E. (1971). "Estimating the Stability of Excavated Slopes in Open Cast Mines," Trans Inst Min Metall, Mining Industries Section 80, A72.

Hoek, E. (1971a). "Rock Slope Stability - How Far Away are Reliable Design Methods?" Proc of the 1st Australia - New Zealand Conf on Geomechanics, Melbourne, Vol 1, pp. 307-313.

Houbolt, J. C. (1961). "Runway Roughness Studies in the Aeronautical Field," J of Air Transport Div, ASCE, Vol 87, pp. 11-31.

Hutchinson, B. G. (1965). Analysis of Road Roughness Records by Power Spectral Density Techniques, Ontario Dept of Highways, Report no. 101.

Hutchinson, J. N. (1969). "A Reconsideration of the Coastal Landslides at Folkstone Warren, Kent," Geotechnique, Vol 19, pp. 6-38.

Jaeger, J. C. and Rosengren, K. J. (1969). "Friction and Sliding of Joints," Proc Aust Inst Min Metall, No. 229, pp. 93 - 104.

Jaeger, J. C. (1971). "Friction of Rock and Stability of Rock Slopes," Geotechnique, Vol 21, pp. 97-134.

Jennings, J. E. (1970). "A Mathematical Theory for the Calculation of the Stability of Slopes in Open Cast Mines," Planning Open Pit Mines, Proc of Symp, Johannesburg, pp. 87-102.

John, K. W. (1968). "Graphical Stability Analysis of Slopes in Jointed Rock," J Soil Mech Fdns Div , ASCE, 94, SM2, pp. 497-526.

Kennedy, B. A. and Niermeyer, K. E. (1970). "Slope Monitoring Systems used in the Prediction of a Major Slope Failure at the Chuquicamata Mine, Chile," Planning Open Pit Mines , Proc of Symp, Johannesburg, pp. 215-226.

Kenney, T. C. (1967). "Stability of the Vaiont-Valley Slope," Rock Mech and Eng Geology , Vol 5.

Kiersch, G. A. (1964). "Vaiont Reservoir Disaster," Civil Enginering , March 1964, pp. 32-40.

Kjaernsli, B. and Simons, N. (1962). "Stability Investigations of the North Bank of the Drammen River," Geotechnique , 12, pp. 147-167.

Krsmanovic, D. and Popovic, M. (1966). "Large Scale Field Tests of the Shear Strength of Limestone," Proc 1st Congr Int Soc Rock Mech , Lisbon, Vol 1, pp. 773 - 780.

Krsmanovic, D. (1967). "Initial and Residual Shear Strength of Hard Rocks," Geotechnique , Vol 17, pp. 145 - 160.

Ladanyi, B. and Archambault, G. (1970). "Simulation of Shear Behaviour of a Jointed Rock Mass," 11th Symp on Rock Mech , Berkeley, California, pp. 105-125.

Ladanyi, B. (1973). Testing for Field Design Properties of Rock Formations, Report for Pit Slope Project, Ecole Polytechnique, Montreal.

Lawrence, P. A., (1951). "Rock Slide in Grainger County, Tennesse," Economic Geol. , Vol 46, pp. 329 - 336.

Leggett, R. F. (1962). Geology and Engineering, McGraw-Hill, New York, N. Y.

Leggett, R. F. (1973). Cities and Geology , McGraw-Hill, New York, N. Y.

Lo, K. Y., Lee, C. F., and Gelinas, P. (1972). "Alternative Interpretation of the Vaiont Slide," Stability of Rock Slopes , Proc. 13th Symp. On Rock Mech., Urbana, Illinois, pp. 595 - 624.

Londe, P., Vigier, G., and Vormeringer, R. (1969). "Stability of Rock Slopes, A Three-Dimensional Study." *J Soil Mech Fdns Div*, ASCE, 95, SM1, pp. 235 - 262.

Londe, P., Vigier, G., and Vormeringer, R. (1970). "Stability of Rock Slopes -- Graphical Methods," *J Soil Mech Fdns Div*, ASCE, 96, SM4, pp. 1411 - 1434.

Londe, P. (1973). "The Role of Rock Mechanics in the Reconnaissance of Rock Foundations," *Q Journal of Eng Geol*, Vol 6, pp. 56 - 74.

Longwell, C. R., Flint, R. F., and Saunders, J. E. (1969). *Physical Geology*, John Wiley, New York.

Mahtab, M. A. and Goodman, R. E. (1970). "Three Dimensional Finite Element Analysis of Jointed Rock Slopes," *Proc 2nd Congr Int Soc Rock Mech*, Belgrade, 3, p. 7 - 12.

McConnell, R. G. and Brock, R. W. (1904). Report on the Great Landslide at Frank, Alberta, Canada, *Dept Interior, Ann Rept*, 1902 - 1903.

MacKay, B. R. (1932). "Geology and Coal Deposits of Crowsnest Pass Area, Alberta," *Sum Rept Geol Surv, Canada*, p. 338.

MacKenzie, J. D. (1913). "South Fork Coal Area, Oldman River, Alberta," *Sum Rept Geol Surv, Canada*, pp. 235 - 246.

Mathews, W. H. and McTaggart, K. C. (1969). "The Hope Landslide, British Columbia," *Proc of Geological Association of Canada*, Vol 20, pp. 65 - 75.

Maurer, W. C. (1966). "Shear Failure of Rock Under Axial and Hydrostatic Pressure, " *Proc 1st Int Congr Rock Mech*, Lisbon, Vol 1, pp. 337 - 343.

Mencl, V. (1966). "Mechanics of Landslides with Non-circular Surfaces with Special Reference to the Vaiont Slide," *Geotechnique*, Vol 16, pp. 329 - 337.

Morgenstern, N. R. and Price, V. E. (1965). "Analysis of the Stability of General Slip Surfaces," *Geotechnique*, Vol 15, pp. 79 - 93.

Morgenstern, N. R. (1968). "Ultimate Behaviour of Rock Structures," *Rock Mechanics in Engineering Practice*, edited by Stagg and Zienkiewicz, John Wiley, London, pp. 321 - 352.

Muller, L. (1964). "The Rock Slide in the Vaiont Valley," *Rock Mech and Eng Geology* , Vol 2, pp. 148 - 212.

Muller, L. (1968). "New Considerations on the Vaiont Slide," *Rock Mech and Engineering Geology* , Vol 6, pp. 1 - 91.

Muller, L. and Hofmann, H. (1970). "Selection, Compilation and Assessment of Geological Data for the Slope Problem," *Planning Open Pit Mines* , Proc of Symp, Johannesburg, pp. 153 - 170.

Murrell, S. A. F. (1965). "The Effect of Triaxial Stress Systems on the Strength of Rock at Atmospheric Temperatures," *Geophys J* , Vol 10, pp. 231 - 281.

Myers, N. O. (1962) "Characterization of Surface Roughness," *Wear* , pp. 182 - 189.

Newland, P. L. and Allely, B. H. (1957). "Volume Changes in Drained Triaxial Tests on Granular Materials," *Geotechnique* , Vol 7, pp. 17 - 34.

Norveiller, E. (1967). "Discussion on Mencl's Paper, 1966," *Geotechnique* , Vol 17, pp. 170 - 171.

Norris, D. K. (1955). "Blairmore, Alberta (Map)," *Can Geol Surv, Paper 55-18* .

Patton, F. D. (1966). *Multiple Modes of Shear Failure and Related Material* , Ph. D. Thesis, Urbana, Illinios.

Patton, F. D. and Deere, D. U. (1971). "Geologic Factors Controlling Slope Stability in Open Pit Mines," *Stability in Open Pit Mines* , Proc of 1st Int Conf on Stability in Open Pit Mining, Vancouver, pp. 23 - 47.

Pentz, D. L. (1971). "Methods of Analysis of Stability of Rock Slopes," *Stability in Open Pit Mines* , Proc of the 1st Int Conf on Stability in Open Pit Mining, Vancouver, pp. 119 -142.

Piteau, D, R. (1970). "Geological Factors Significant to the Stability of Slopes Cut in Rock," *Planning Open Pit Mines* , Proc of Symp, Johannesburg, pp. 33-53.

Quinn, B. E., Engja, H. and Zable, J. L. (1970). "Using a Modified Bureau of Public Roads Roughometer to Measure Pavement Roughness Spectra," *Highway Research Record* , No. 311, pp. 26 - 35.

Rengers, N. (1970). "Influence of Surface Roughness on the Friction Properties of Rock Planes," *Pro 2nd Int Congr Rock Mech* , Belgrade, Vol 1, p 1-31.

Reynolds, H. R. (1961). *Rock Mechanics* , Crosby, Lockwood, London, U. K.

Ripley, C. F. and Lee, K. L. (1961). "Sliding Friction Tests on Sedimentary Rock Specimens," *7th Congress of Large Dams* , Vol 4, pp. 657 -671.

Roberts, D. and Hoek, E. (1972). "A Study of the Stability of a Disused Limestone Quarry Face in the Mendip Hills, England," *Proc of 2nd Int Conf on Stability in Open Pit Mining* , Vancouver, pp. 239 - 256.

Robson, J. D. (1963). *Random Vibration* , Edinburgh University Press, Edinburgh.

Seegmiller, B. L. (1972). "Rock Stability Analysis at Twin Buttes," *Stability of Rock Slopes* , 13th Symp on Rock Mech, Urbana, Illinios, pp. 511 - 536.

Serafim, J. L. and Guerreiro, M. (1968). "Shear Strength of Rock Masses at Three Spanish Dam Sites," *Pro 2nd Int Symp Rock Mech* , Madrid, pp. 147 - 151.

Sevaldson, R. A. (1956). "The Slide at Lodalen," *Geotechnique* , Vol 6, pp. 167 - 182.

Sharpe, C. F. S. (1938). *Landslides and Related Phenomena* , Columbia University Press, New York, N. Y.

Skempton, A. W. and Brown, J. D. (1961). "A Landslide in Boulder Clay at Selset, Yorkshire," *Geotechnique* , Vol 11, pp. 280 - 293.

Skempton, A. W. (1966). "Bedding - Plane Slip, Residual Strength and the Vaiont Landslide," *Geotechnique* , Vol 16, pp. 82 - 84.

Stacey, T. R. (1970). "The Stresses Surrounding Open Pit Mine Slopes," *Planning Open Pit Mines* , Proc of Symp, Johannesburg, pp. 199 - 208.

Steffen, O. K. H., Holt, W. and Symons, V. R. (1970). "Optimizing Open Pit Geometry and Operational Procedure," *Planning Open Pit Mines* , Proc of Symp, Johnnesburg, pp. 9 - 31.

Stewart, R. M. and Kennedy, B. A. (1971). "The Role of Slope Stability in the Economics, Design and Operation of Open Pit Mines," *Stability in Open Pit Mining*, Proc of 1st Conf on Stability in Open Pit Mining, Vancouver, pp. 5 - 21.

Ter-Stepanian, G. (1966). "Types of Depth Creep of Slopes in Rock Masses," *Proc 1st Int Cong Rock Mech*, Lisbon, pp. 157 - 160.

Terzaghi, K. (1950). "Mechanisms of Landslides," *Berkey Volume, Geological Soc America*, pp. 83 - 123.

Wallace, G. B., Slebir, E. J. and Anderson, F. A. (1969). "Foundation Testing for Auburn Dam," *Proc 11th Symp Rock Mech*, Berkely, pp. 461 - 498.

Williamson, J. B. P. and Hunt, R. T. (1968). Res Dept No 59, Burnby Research Division, U. S. A.

Witkind, I. J., Myers, W. B., Hadley, J. B., Hamilton, W. and Fraser, G. D. (1962). "Geologic Features of the Earthquake at Hebgen Lake, Montana," *Seismol Soc Amer Bull*, Vol 52, pp. 163 - 180.

Zaruba, Q. and Mencl, V. (1969). *Landslides and Their Control*, Elsevier.

Zienkiewicz, O. C. and Cheung, Y. K. (1967). *The Finite Element Method in Structural and Continuum Mechanics*, McGraw-Hill.

Zienkiewicz, O. C., Beet, B., Dullage, C. and Stagg, K. G. (1970). "Analysis of Non-Linear Problems in Rock Mechanics with Particular Reference to Jointed Rock Systems," *Proc 2nd Congr Int Soc Rock Mech*, Belgrade, Vol 3, p 7-14.

APPENDIX A

OPTICAL ROUGHNESS PLOTTER

A.1 INTRODUCTION

At the University of Alberta hydraulics research laboratory, a device has been built for plotting the flume bed profiles under water and yet not disturb the river bed sand. A device based on the same principles as the river bed plotter was constructed for the purpose of plotting roughness profiles of rock discontinuities. This Appendix gives a description of the construction, operation and performance of the roughness plotter.

A.2 THEORY OF OPERATION

Basically, the device operates on a light source which remains a constant distance from the surface. Inside the light probe (Figure A.1), a small light bulb is located whose light is transmitted along optical fibres and projected onto the rock surface. Mixed in with the transmitting optical fibres are an equal number of fibres which carry the reflection from the rock surface to a photo resistance cell. The voltage drop across the photo cell depends on the intensity of the light directed at the cell.

The intensity of the light reflection to the fibres will depend on how close the tip of the fibres are to the rock surface. In this way the voltage drop across the photo cell is a function of the distance between the light probe and the rock surface.

Initially, a current is passed through the photo cell, and this is taken as a reference point. Then as the light probe traverses a surface and the tip moves closer or farther away from the surface, a change in potential occurs across the photo cell. This change in potential from the initial reference point activates a small D.C. electric motor which moves the probe height until it again reaches the initial distance from the surface. In this way, the electric motor lifts or lowers the probe in such a way that it is always a constant distance from the rock surface. Basically then we have a system in equilibrium designed so that if any deviations occur from the point of equilibrium, the system will automatically adjust itself to return to the equilibrium position.

A.3 CONSTRUCTION

The entire assembly of the light probe is shown by the schematic in Figure A.1. The electric motor is a 12V D.C. motor. The purpose of the bellows is to rectify any misalignment which might occur between the large pulley and the motor. The potentiometer measures the vertical displacement.

The light probe is mounted on a carriage which in turn is part of the holding frame (Figure A.2). This carriage runs along the one-inch square rails under the power of an electric motor. The potentiometer under the motor measures the horizontal displacement. The purpose of the twelve roller bearings is to allow the carriage to run along the rails regardless of the position in which the holding frame is mounted. In order to accommodate the transportation of the apparatus, the frame was constructed so that it could be taken apart and reassembled with relative ease by using slotted bolt holes and wing nuts.

The electric circuit, the power supply and the control panel are all contained in a special box. The power supply consists of six 6-volt dry cell batteries except for the light source which uses four flashlight (1.5v) batteries.

The entire apparatus is shown in a laboratory set-up in Figure A.3, and a photo of a field set-up is given in Figure A.5. The field set-up shows how it can be mounted on an overhanging rock discontinuity.

Recording the output from the potentiometers proved to be the most difficult as far as field work was concerned; mainly because no suitable analog recording device could be obtained that did not require a 110v power supply. Consideration was given to either an X-Y plotter or a magnetic tape recorder. The magnetic recorder was chosen over the plotter because it is more rugged. The recorder was a Hewlett-Packard Model 3960, 4-track, magnetic tape recorder. A small 100-watt generator with a gasoline engine was used as the power supply in the field.

After returning to the lab the signal from the tape was fed into the X-Y plotter yielding roughness profiles in graphical form.

The calibration factors for the potentiometers are as follows:

vertical;	3.02 in/V
horizontal;	8.85 in/V

A.4 OPERATING PROCEDURE

Figure A.4 gives a view of the control panel for the operation of the optical roughness plotter. The panel is divided by a dotted line and only the left side of the control panel is concerned with the operation of the optical plotter. Generally, the following steps should be observed:

(1) the button on the dividing line has a white spot on it and should be pointing to the left of the line.

(2) flip the two toggle switches side by side to the "on" position.

(3) the damping gauge should be set to approximately 80.

(4) lower the light probe manually to about half an inch from the surface by moving the "up-down" switch to

the "down" position.

(5) the gain should be set at approximately 10 to 20.

(6) the probe height should be set at approximately 80.

(7) flip the toggle switch "manual-auto" to the automatic position. With this action, the probe should move down to the equilibrium position. If the probe moves away from the surface, the probe height is set too high. If nothing happens, increase the gain very slowly. When the probe begins to chatter and vibrate, the gain has been set too high.

(8) once a stable position has been reached, the probe height can be adjusted to the desired height.

(9) when the light probe has been set, the next step is to traverse the rock surface. This is done by invoking the toggle switch, in the lower right-hand corner, to the "forward" or "reverse" position depending on where the carriage is located. There is also an adjustment with which the carriage proceeds. The carriage will continue to run along until it is stopped manually or until it hits the limit switch. To reverse the direction, place the direction switch in the opposite position and depress the "override" button until the limit switch is free.

A.5 RESULTS OF TRIAL TESTS

Figure A.6 shows the results of a traverse on an artificial surface cut from a piece of lumber. Figure A.7 shows the results of the runs made at the set-up shown by Figure A.5. These profiles show the scale of roughness which this plotter is suitable for and able to measure.

A.6 PERFORMANCE

The main advantage of the optical plotter is that the profile record is continuous as opposed to discrete readings at numerous points. Also the plotter can accommodate fairly large vertical displacements (10 in).

The accuracy of the measurements are controlled to some extent by the distance the probe tip is away from the surface. Increasing the distance results in the probe being unable to detect the reflections properly. Also the greater distance results in the light being spread over a larger area which is undesirable as the measurement is shown as an average over the area covered by the light. The accuracy depends as well on the consistency of the reflective properties of the rock surface. A change from a dark to a lighter surface will slightly change the distance between the probe tip and the surface. For this reason, the rock shown in Figure A.5 was painted white.

The most serious problem in using the optical plotter in the field is the interference of the sunlight. The reflections off the surface due to the sun simply drive the probe away. For this reason, the measurements made in the field were done late in the evening and even after dark.

Defects in the rock surface like cracks or sharp rises create real havoc with this system. As the light probe travels over a crack, it is simply driven into the crack since there is no reflection. When the probe comes upon a sharp rise in height, it will simply run up against the abutment and the rod on which it is suspended will bend.

It would appear that the only way to overcome these obstacles is to stop the horizontal movement and manually ride over them. These manoeuvers show up on the record and as such have to be noted and later corrected to obtain a true profile.

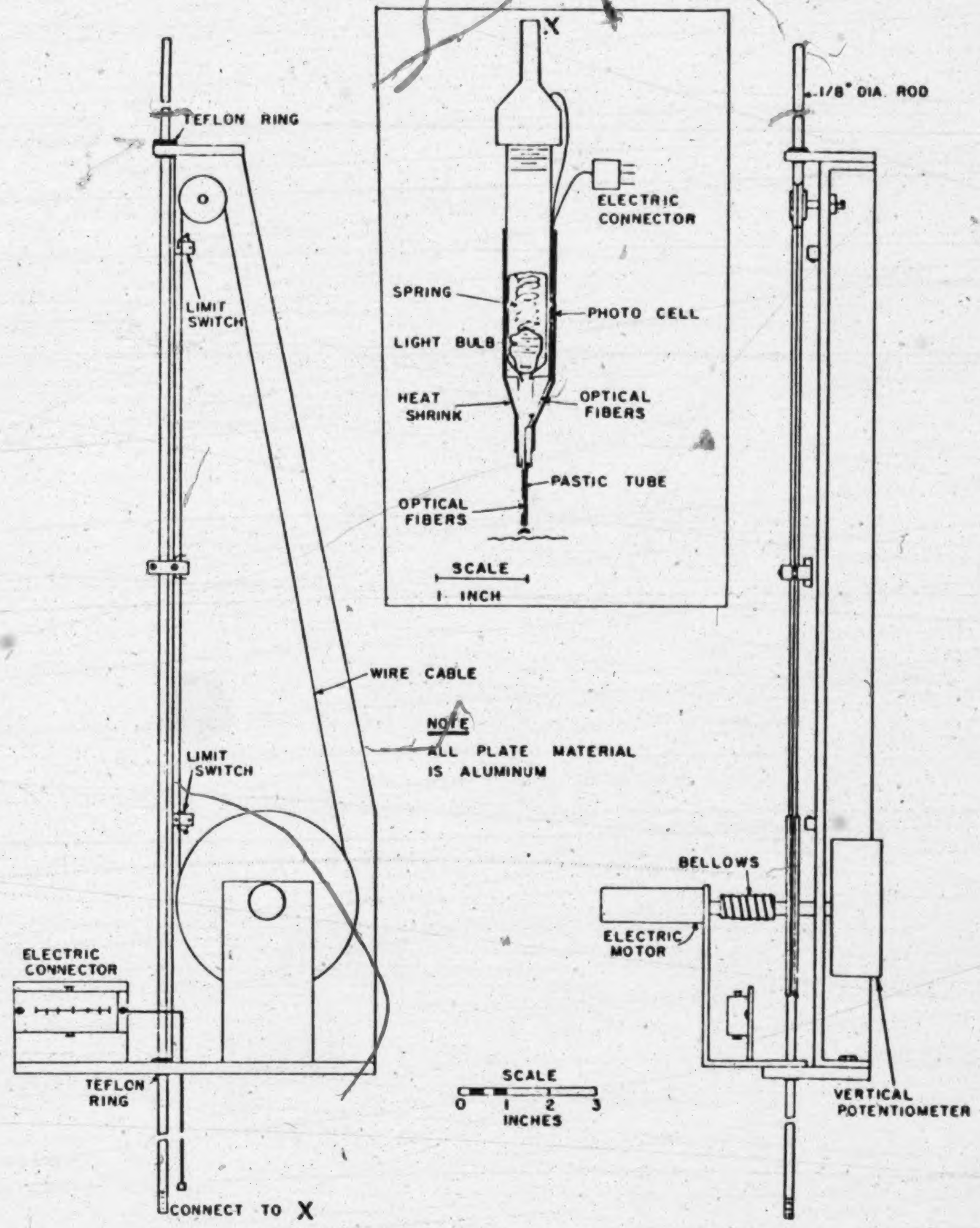
X
TEFLON RING
LIMIT SWITCH
ELECTRIC CONNECTOR
SPRING
PHOTO CELL
LIGHT BULB
HEAT SHRINK
OPTICAL FIBERS
PASTIC TUBE
OPTICAL FIBERS
SCALE
1 INCH
.1/8" DIA. ROD
WIRE CABLE
NOTE
ALL PLATE MATERIAL IS ALUMINUM
LIMIT SWITCH
BELLOWS
ELECTRIC MOTOR
ELECTRIC CONNECTOR
TEFLON RING
SCALE
0 1 2 3
INCHES
VERTICAL POTENTIOMETER
CONNECT TO X

Figure A.1 Schematic diagram of light probe for the field roughness plotter

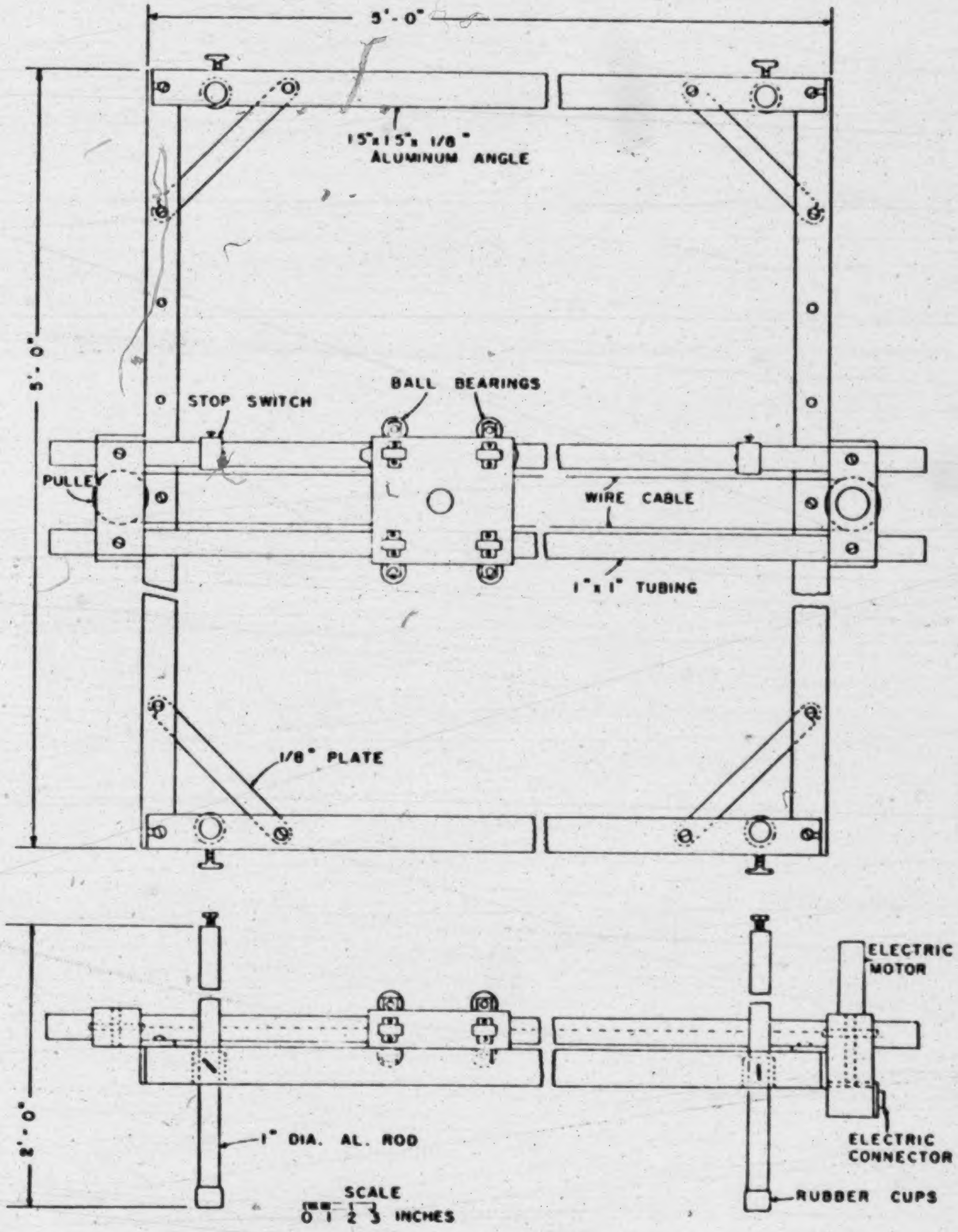
5'- 0"
1.5"x 1.5"x 1/8"
ALUMINUM ANGLE
5'- 0"
STOP SWITCH
BALL BEARINGS
PULLEY
WIRE CABLE
1"x 1" TUBING
1/8" PLATE
2'- 0"
ELECTRIC MOTOR
1" DIA. AL. ROD
ELECTRIC CONNECTOR
SCALE
0 1 2 3 INCHES
RUBBER CUPS

Figure A.2 Schematic diagram of holding frame for the field roughness plotter

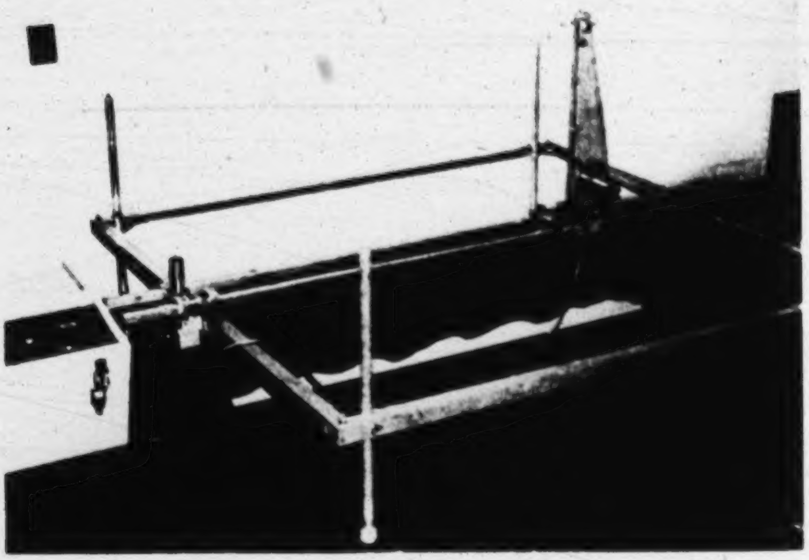

Figure A.3 The optical roughness plotter

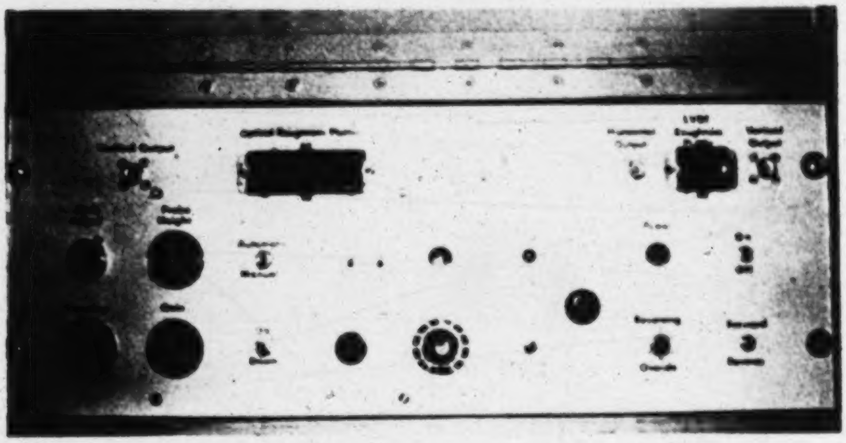

Figure A.4 Control panel for the optical roughness plotter

Figure A.5 Roughness plotter set-up in the field

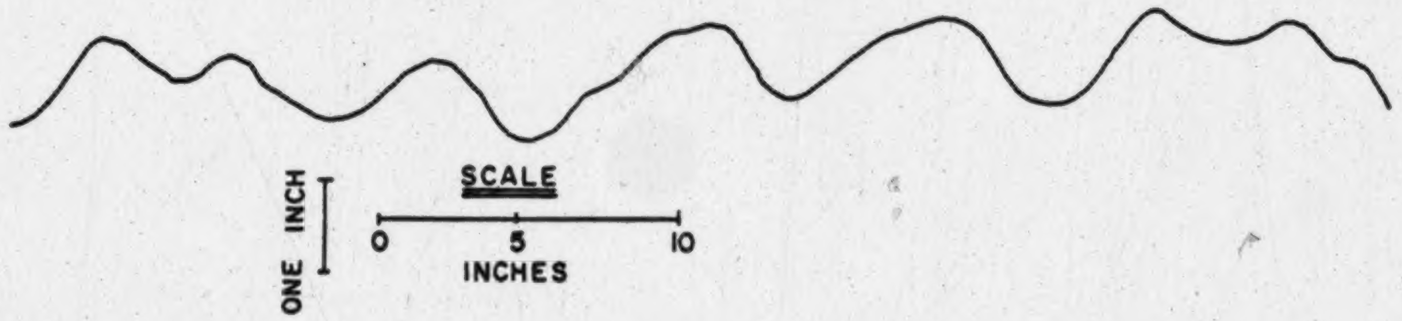
SCALE
0
5
10
INCHES
ONE INCH

Figure A.6 Profile of artificial surface shown in Figure A.3

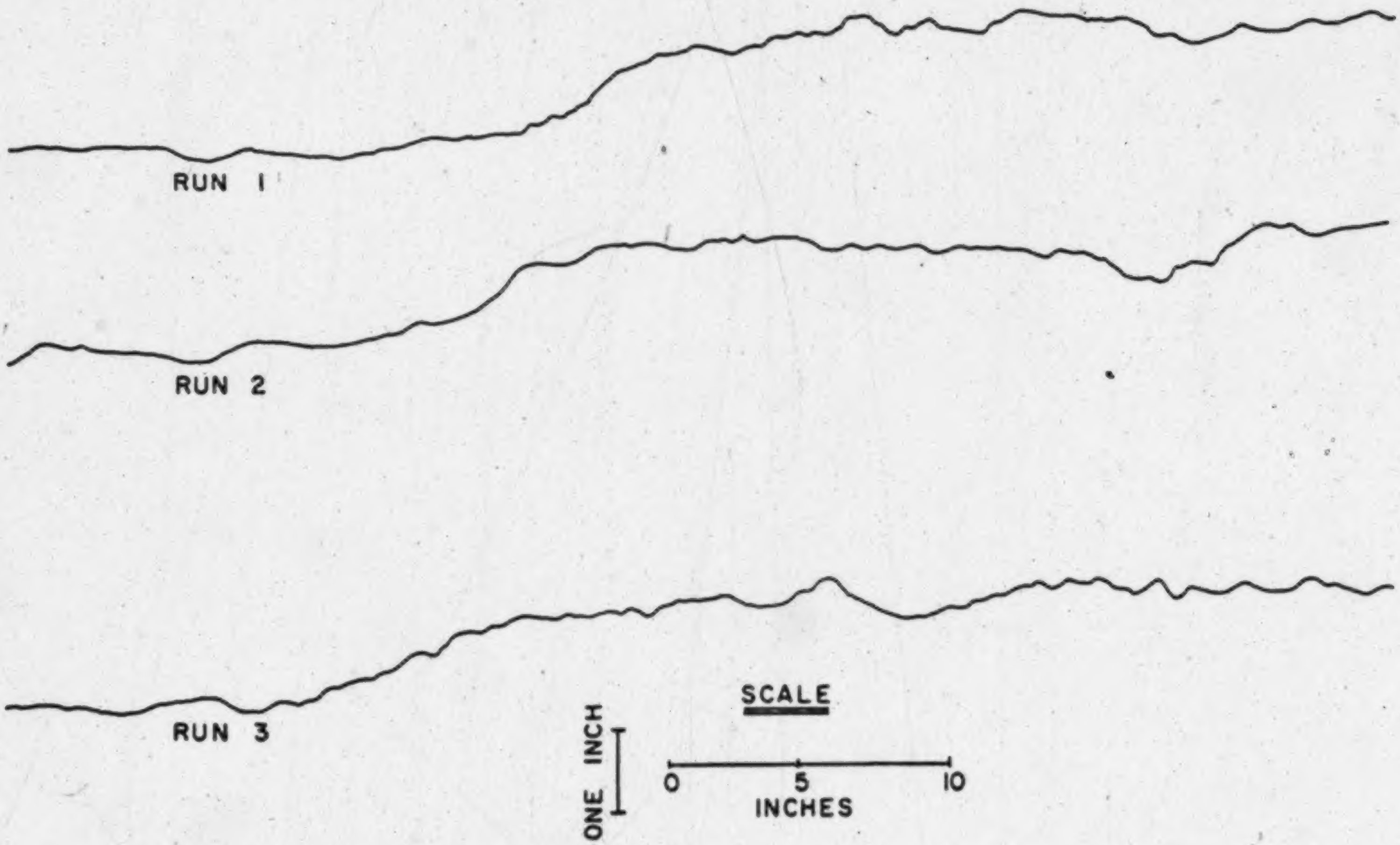

Figure A.7 Roughness profiles from the field set-up shown in Figure A.5

APPENDIX B

SHEAR TEST DATA

This Appendix presents the results of the shear tests performed in connection with the analysis of the Frank Slide as referred to in Chapter 4. Table B.1 gives the designation of each sample type, the area of each sample and the normal load at which each sample was tested. For each test performed the shear load versus deformation plot and the associated vertical deformations are presented in Figures B.1 to B.31.

TABLE B.1 SHEAR TEST DATA

SERIES	NUMBER	AREA (in sq)	NORMAL LOAD (lbs)	TYPE OF SURFACE
B	1	29.9	2,494	Bedding planes
	2	29.5	4,491	
	3	30.9	7,495	
	5	3.12	556	
	6	3.03	1,146	
	7	3.28	1,720	
	8	3.42	854	
S	1	30.5	2,695	Flexural-slip surfaces Note (5 & 5A - the same sample but run in different directions)
	2	31.4	4,693	
	3	30.6	7,694	
	4	30.2	10,695	
	5	3.03	556	
	5A	3.03	556	
	6	3.12	854	
	6A	3.12	854	
	7	3.02	1,146	
	7A	3.02	1,146	
	8	3.02	1,719	
	8A	3.02	1,719	

TABLE B.1 (continued)

SERIES	NUMBER	AREA (in sq)	NORMAL LOAD (lbs)	TYPE OF SURFACE
J	1	30.3	2,894	Joints
	2	31.1	4,892	
	3	32.1	7,893	
	4	32.7	10,880	
D	1	32.7	3,294	Diamond-cut surfaces
	2	32.7	5,294	
	3	31.8	8,297	
	4	32.2	11,292	
L	1	33.3	3,095	Lapped with #45/80 grit
	2	33.1	5,098	
	3	32.1	8,095	
	4	32.5	11,096	

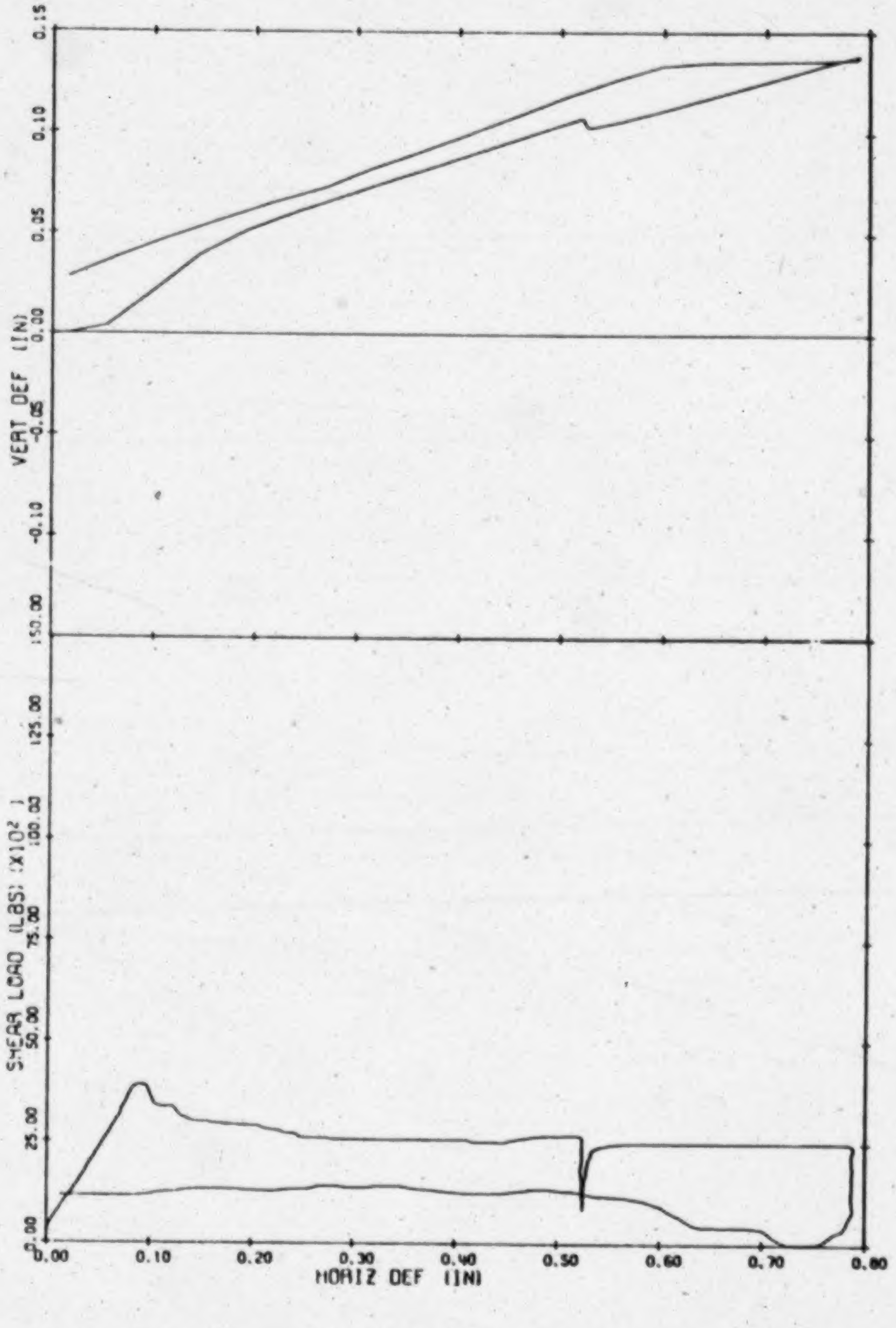

Figure B.1 Shear load and vertical deformation versus the horizontal deformation for sample B-1

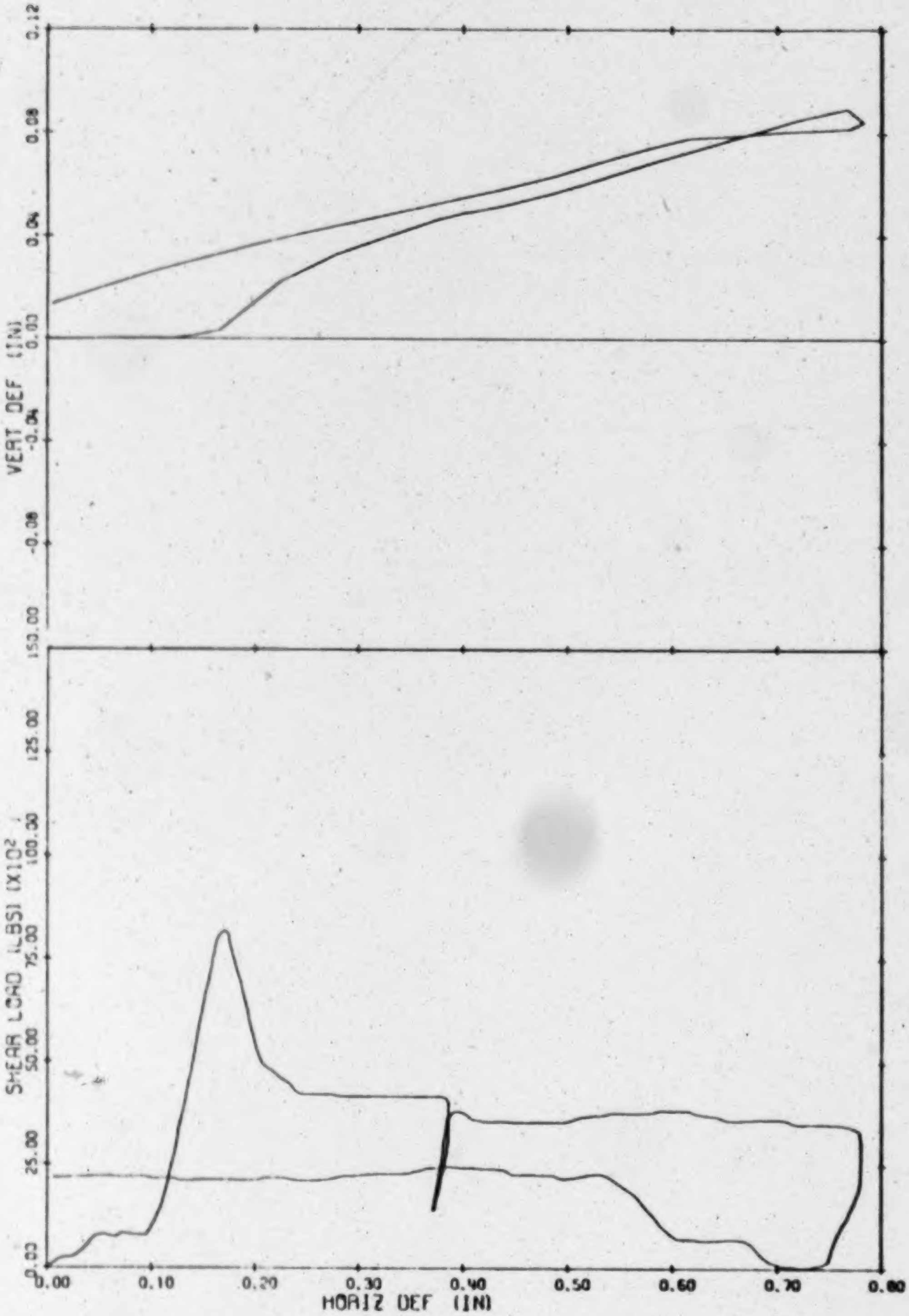

Figure B.2 Shear load and vertical deformation versus the horizontal deformation for sample B-2

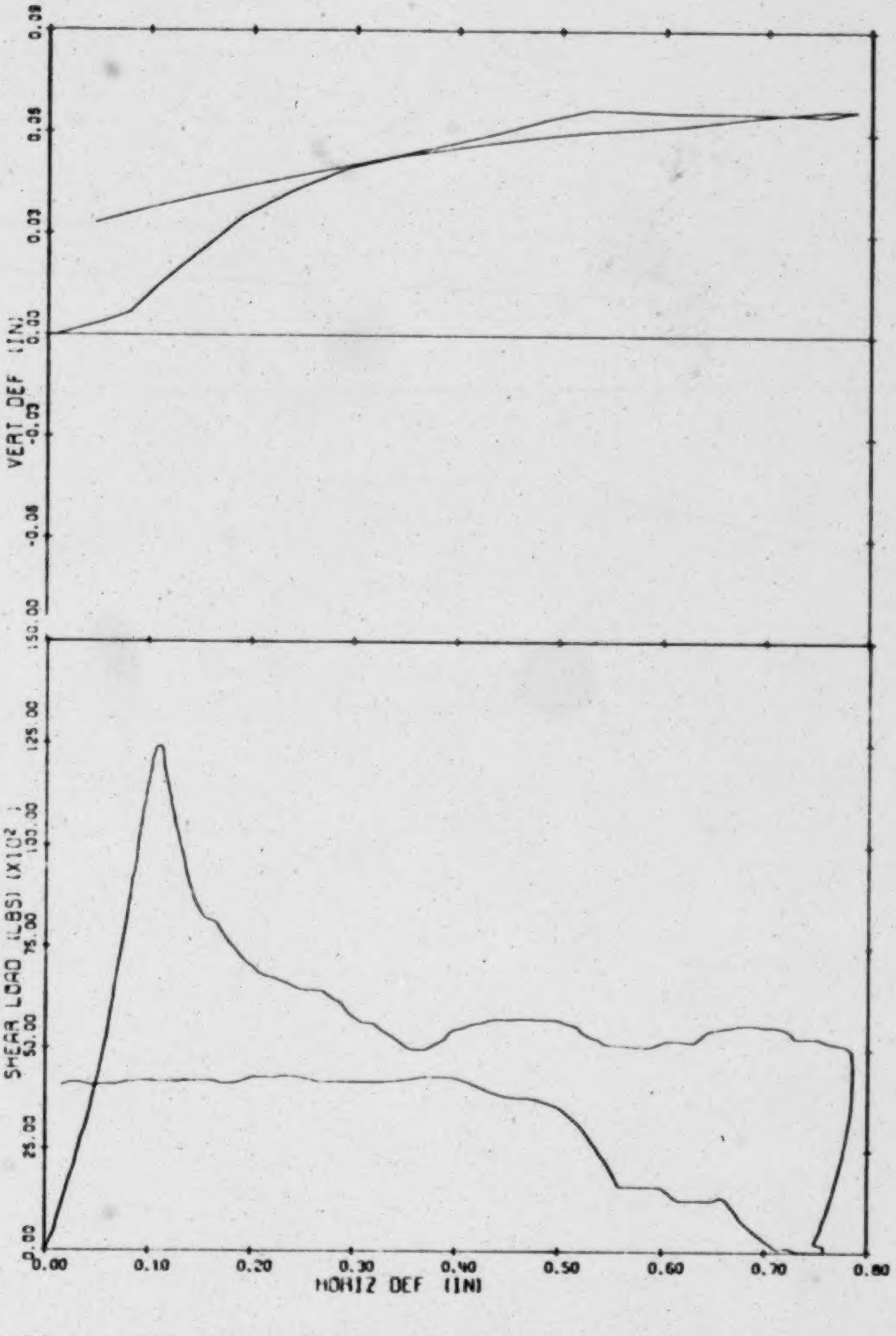

Figure B.3 Shear load and vertical deformation versus the horizontal deformation for sample B-3

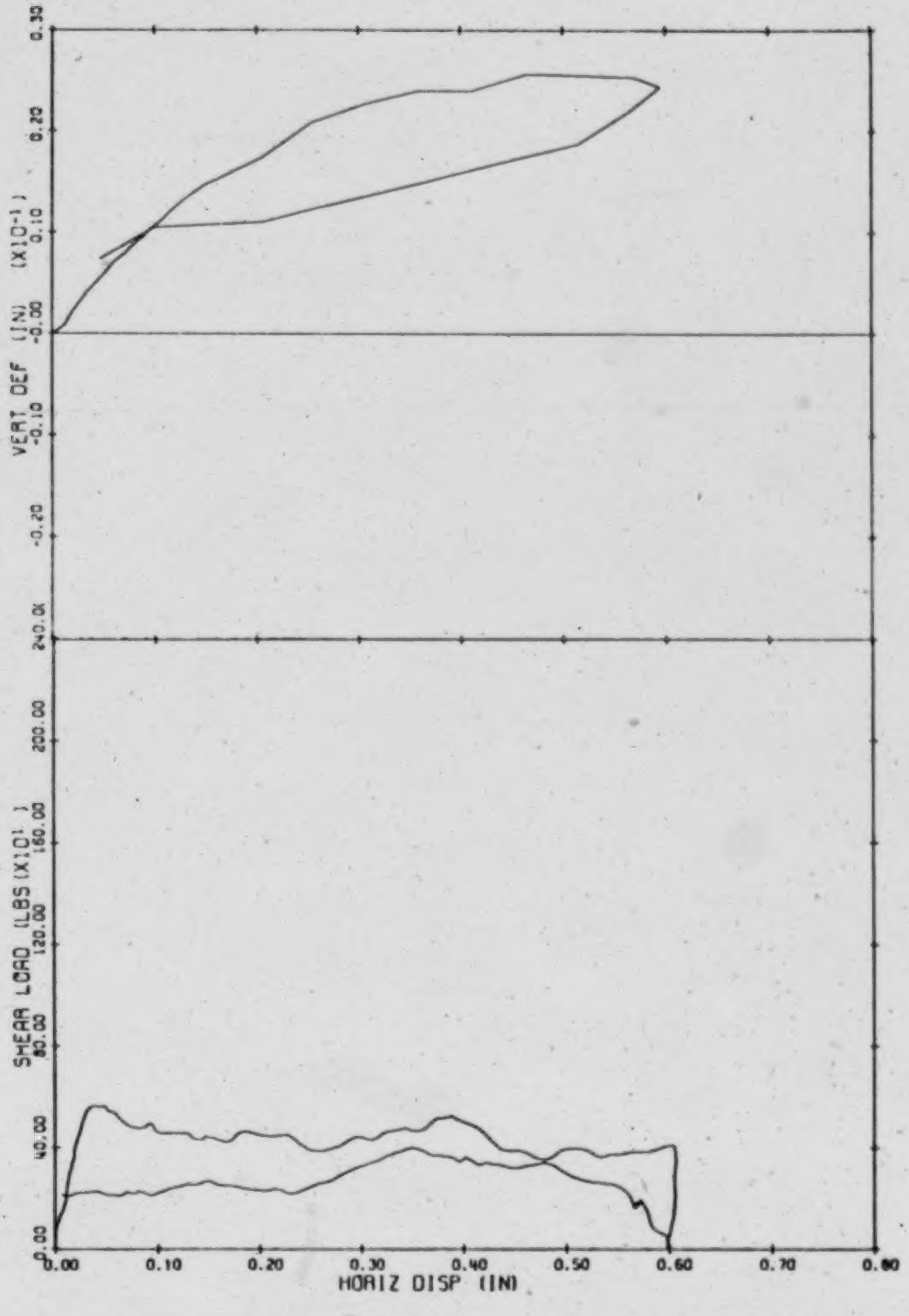

Figure B.4 Shear load and vertical deformation versus the horizontal deformation for sample B-5

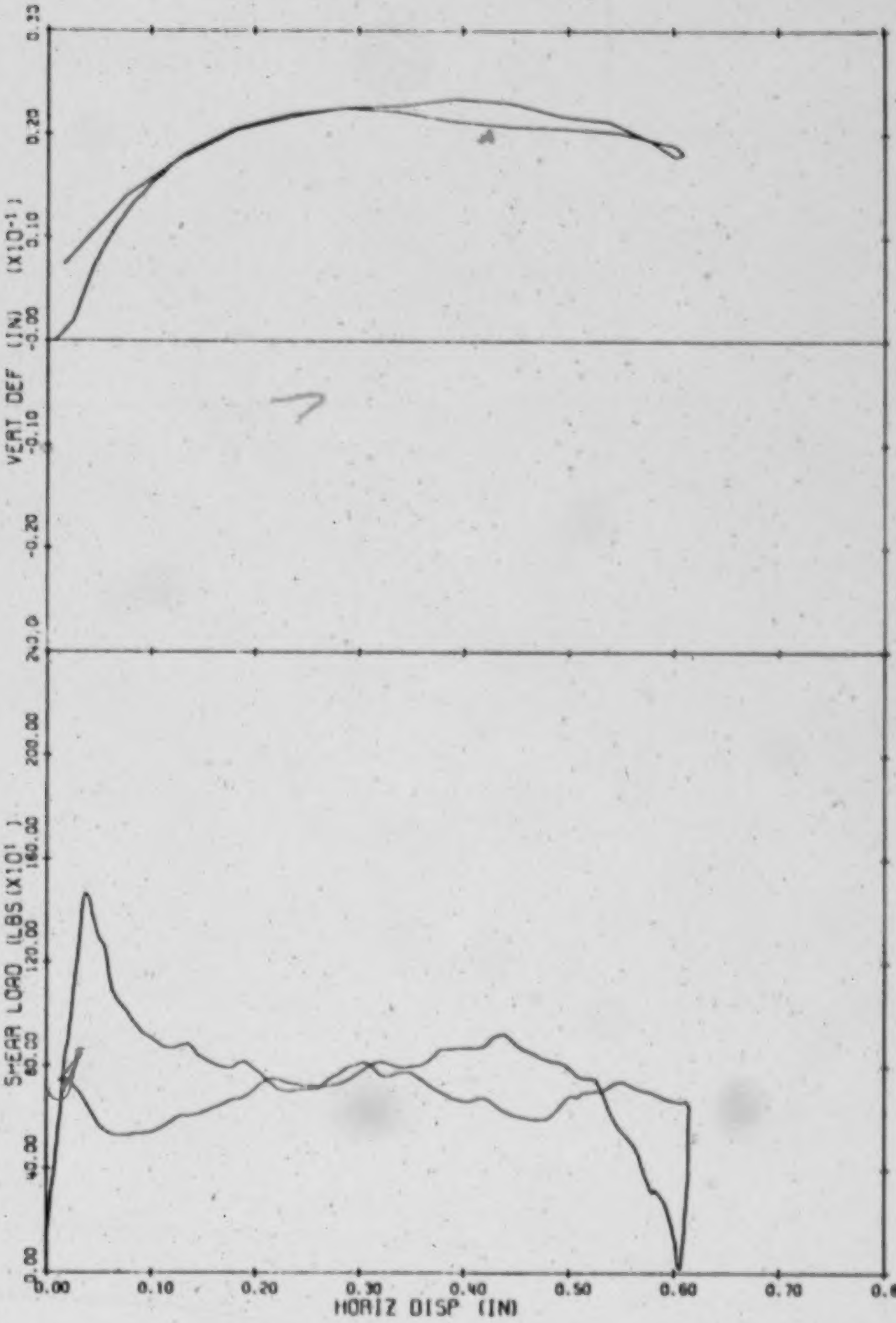

Figure B.5 Shear load and vertical deformation versus the horizontal deformation for sample B-6

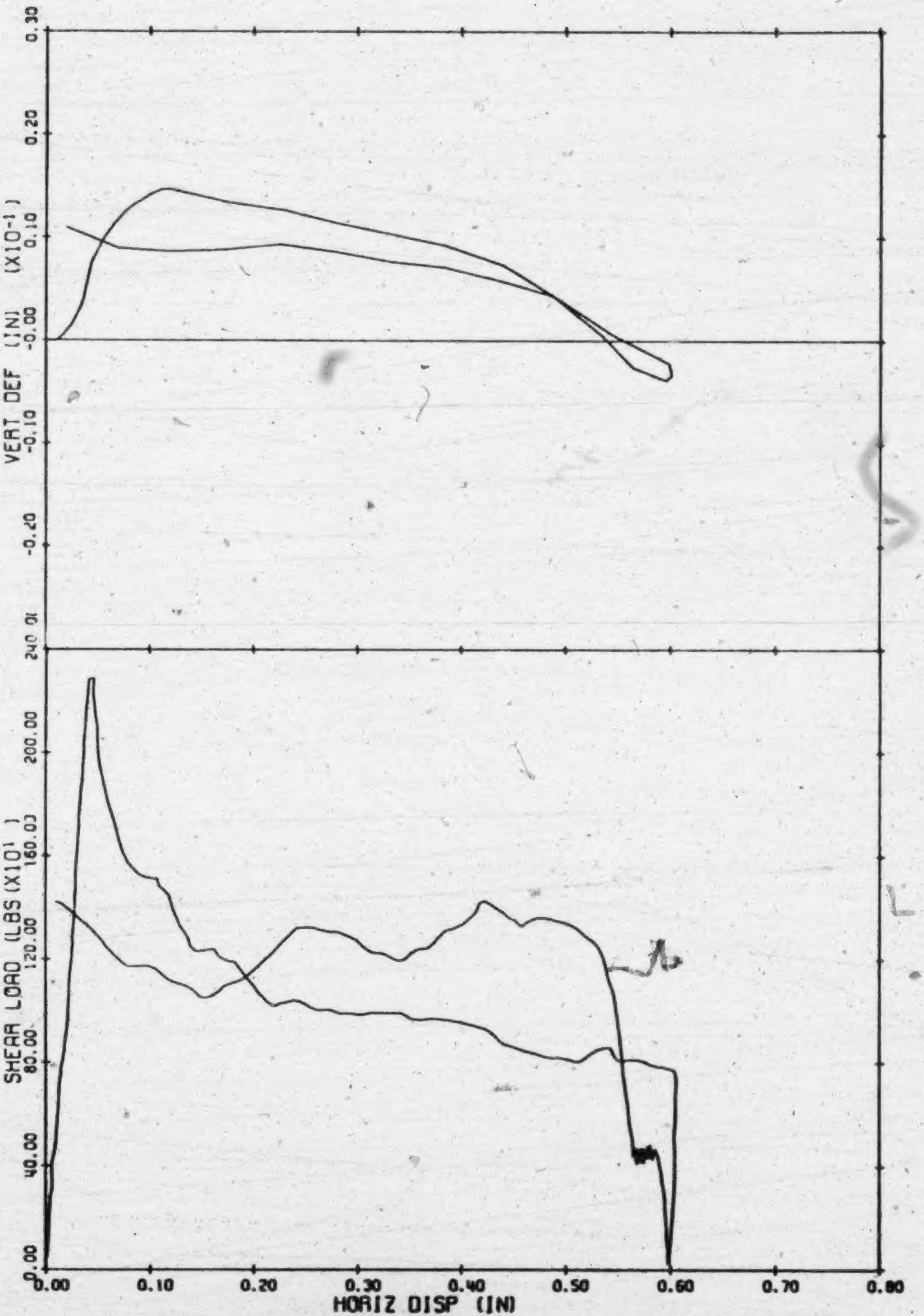

Figure B.6 Shear load and vertical deformation versus the horizontal deformation for sample B-7

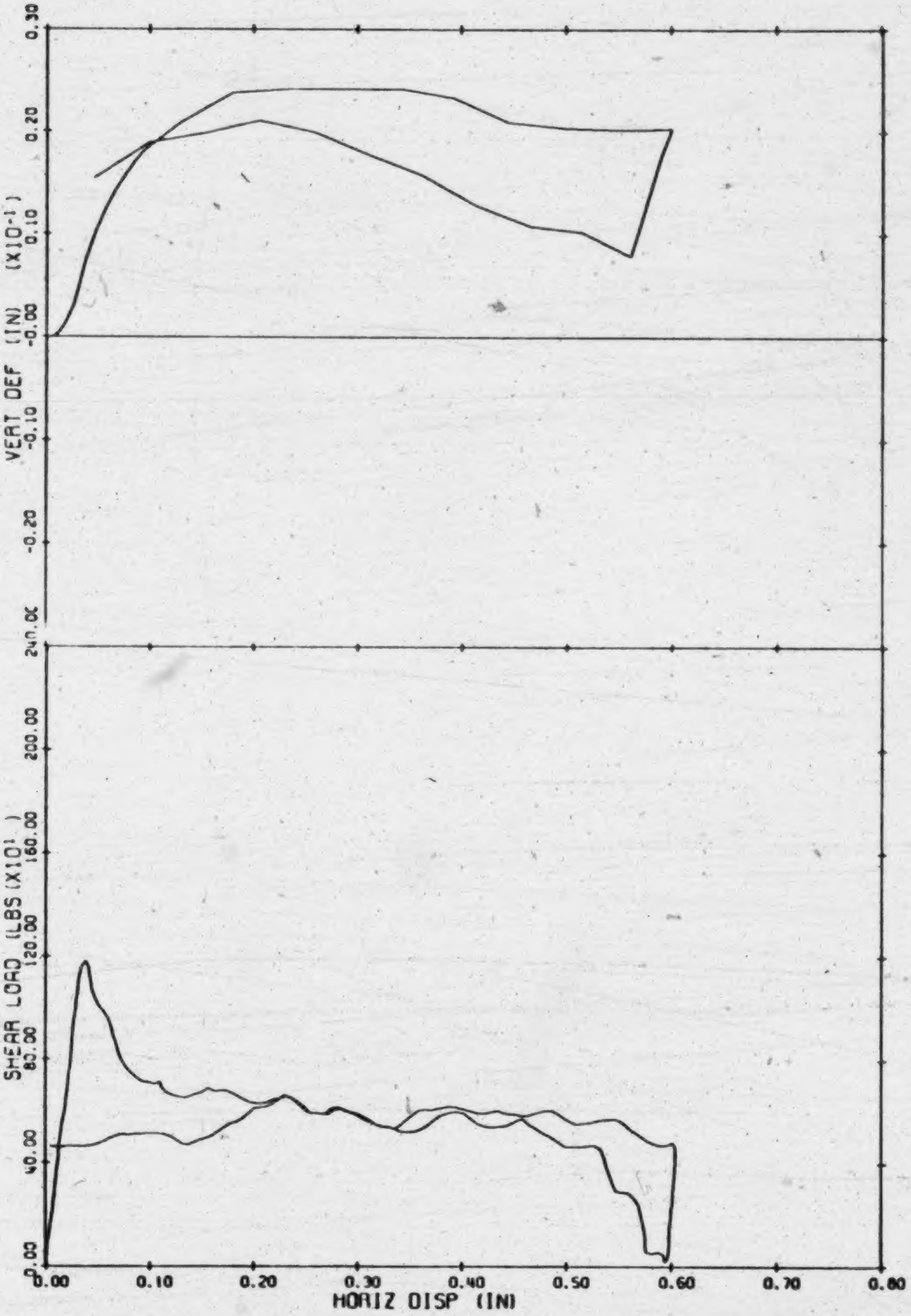

Figure B.7 Shear load and vertical deformation versus the horizontal deformation for sample B-8

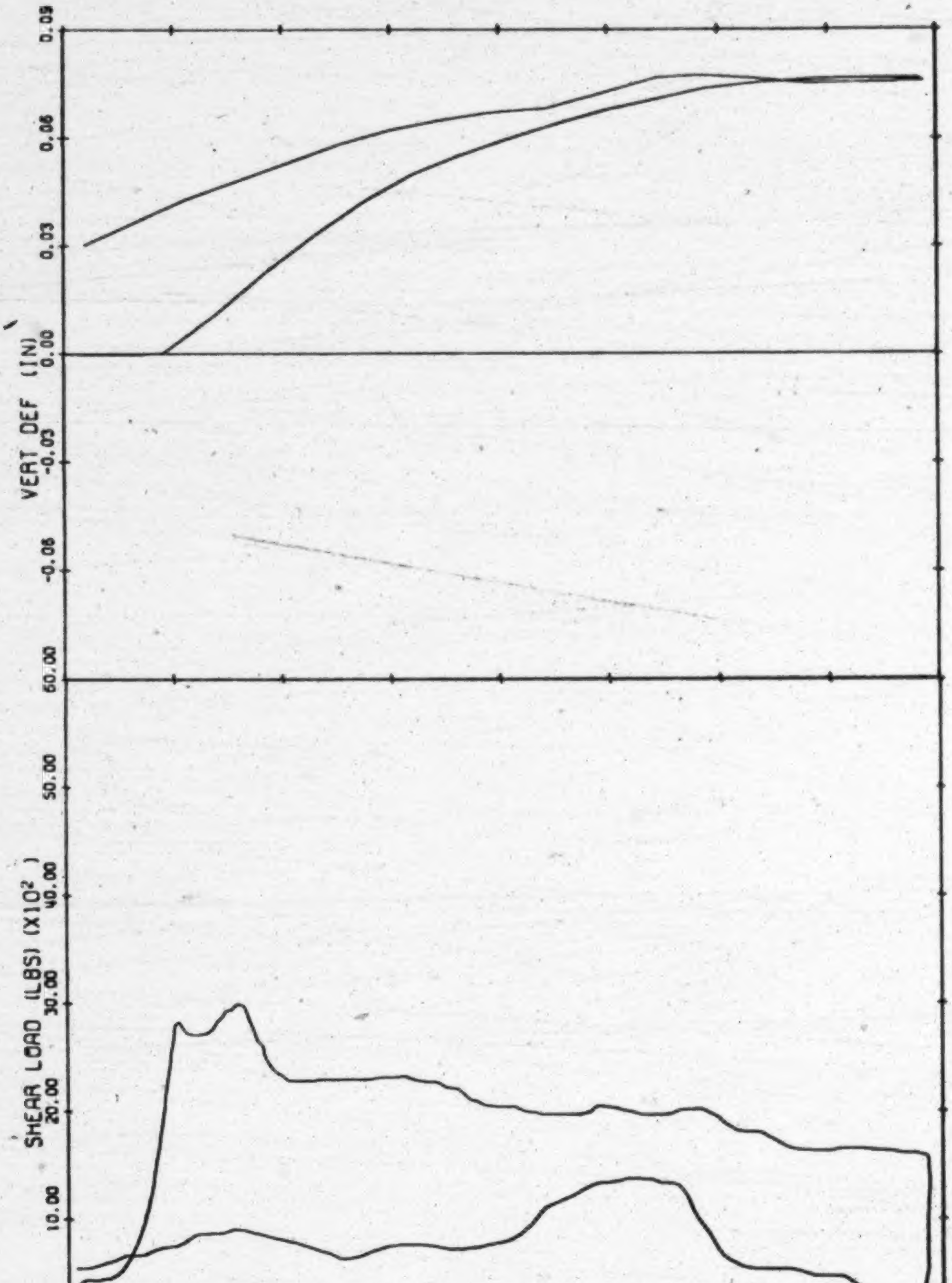

Figure B.8 Shear load and vertical deformation versus the horizontal deformation for sample S-1

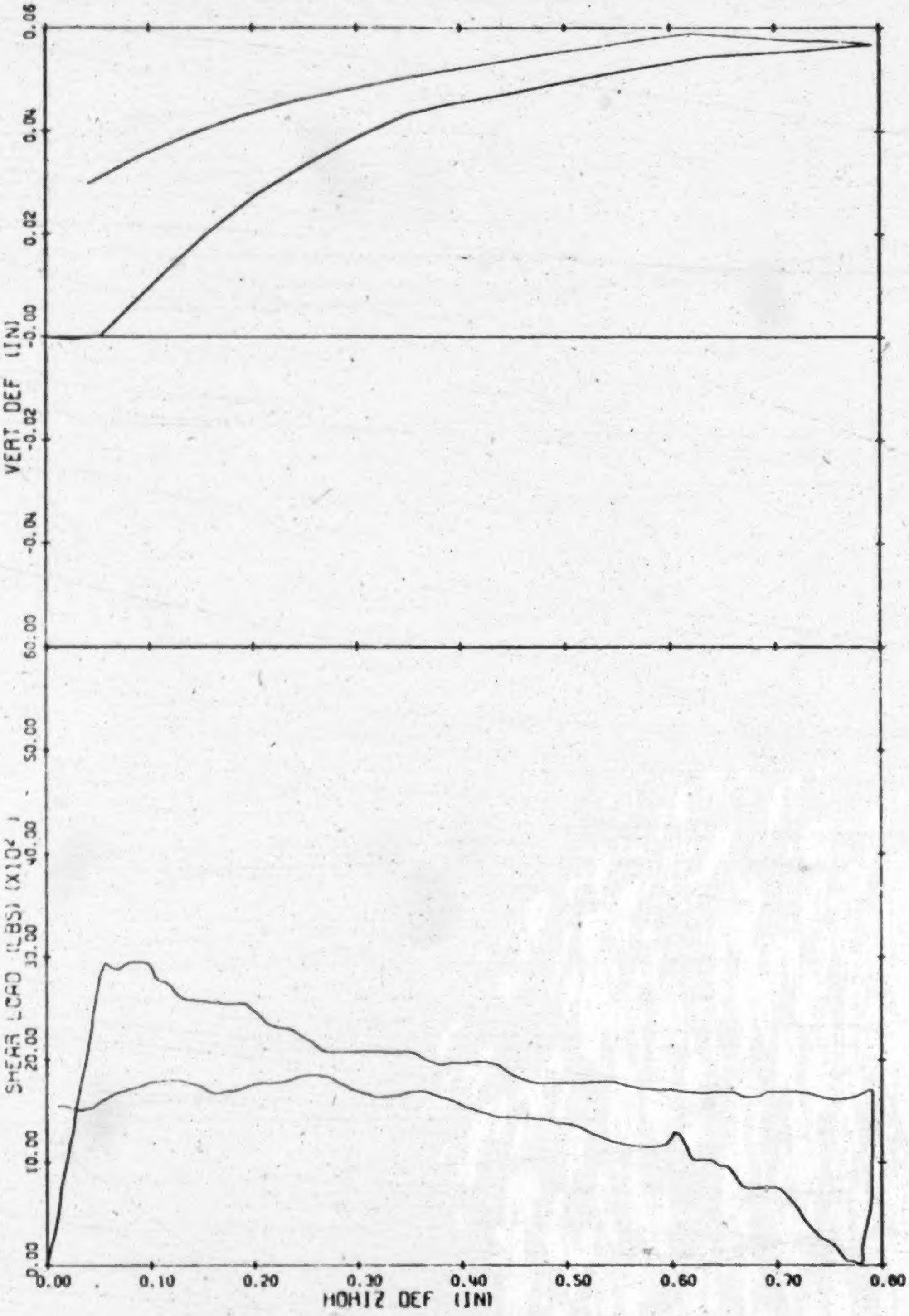

Figure B.9 Shear load and vertical deformation versus the horizontal deformation for sample S-2

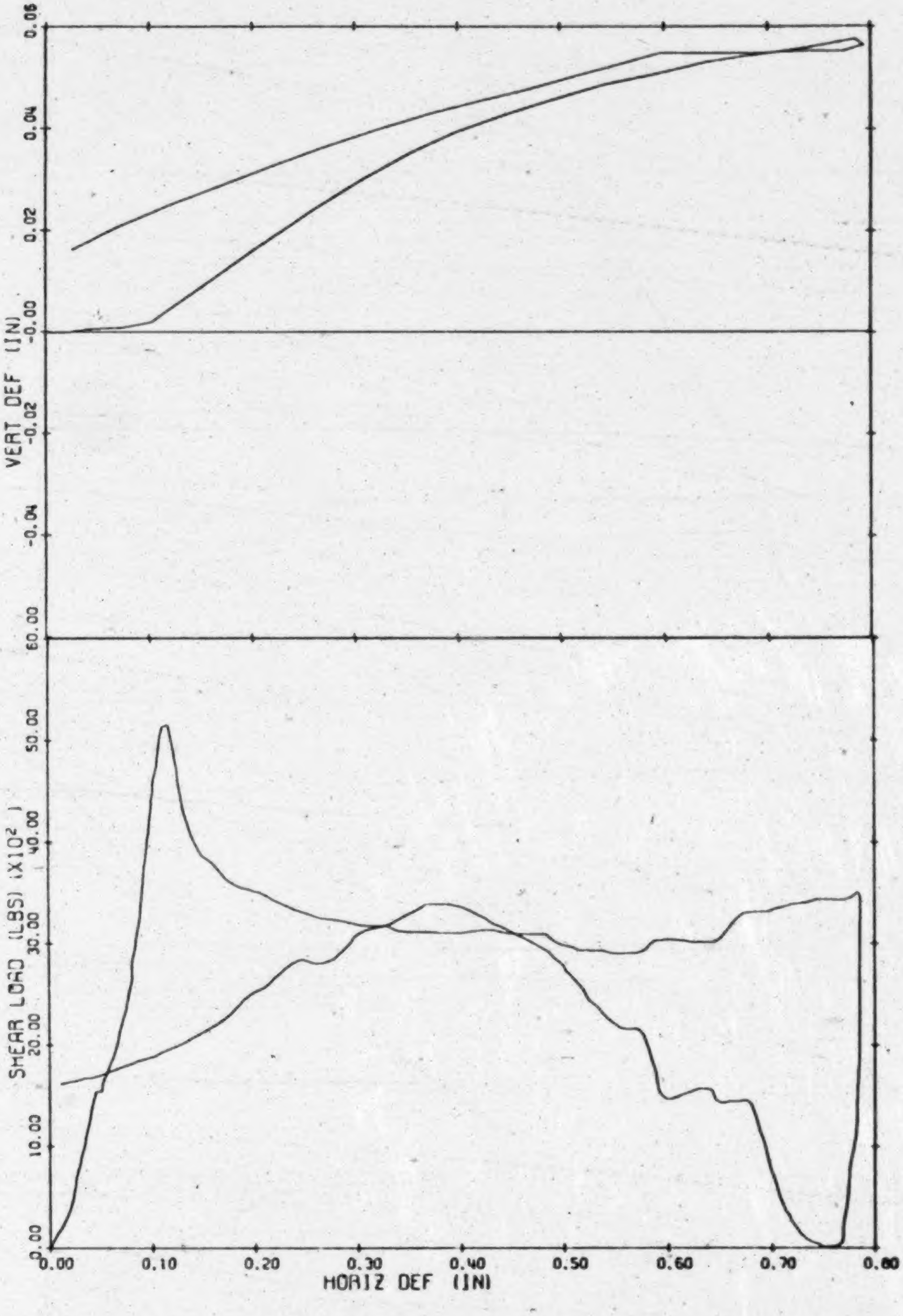

Figure B.10 Shear load and vertical deformation versus the horizontal deformation for sample S-3

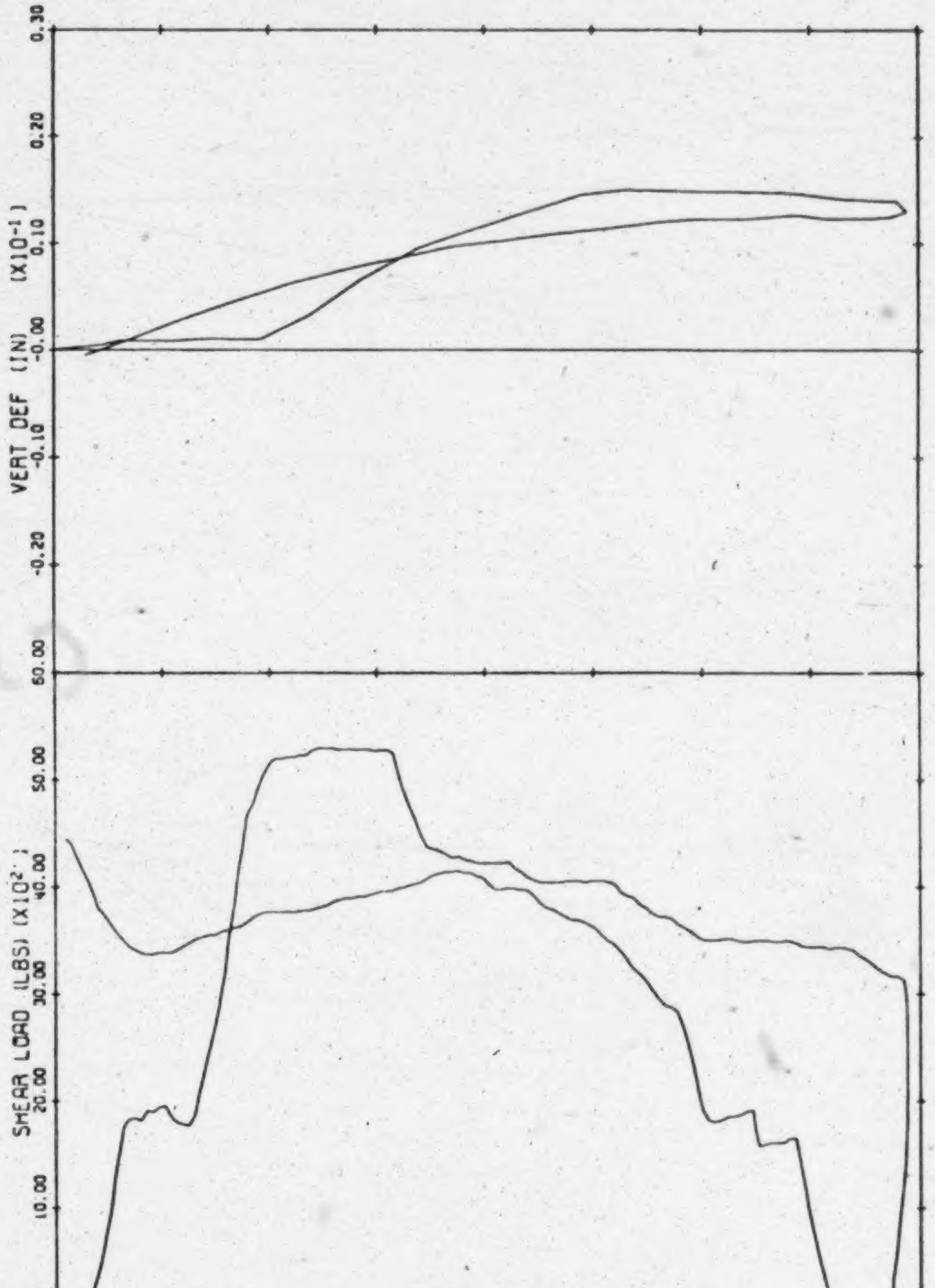

Figure B.11 Shear load and vertical deformation versus the horizontal deformation for sample S-4

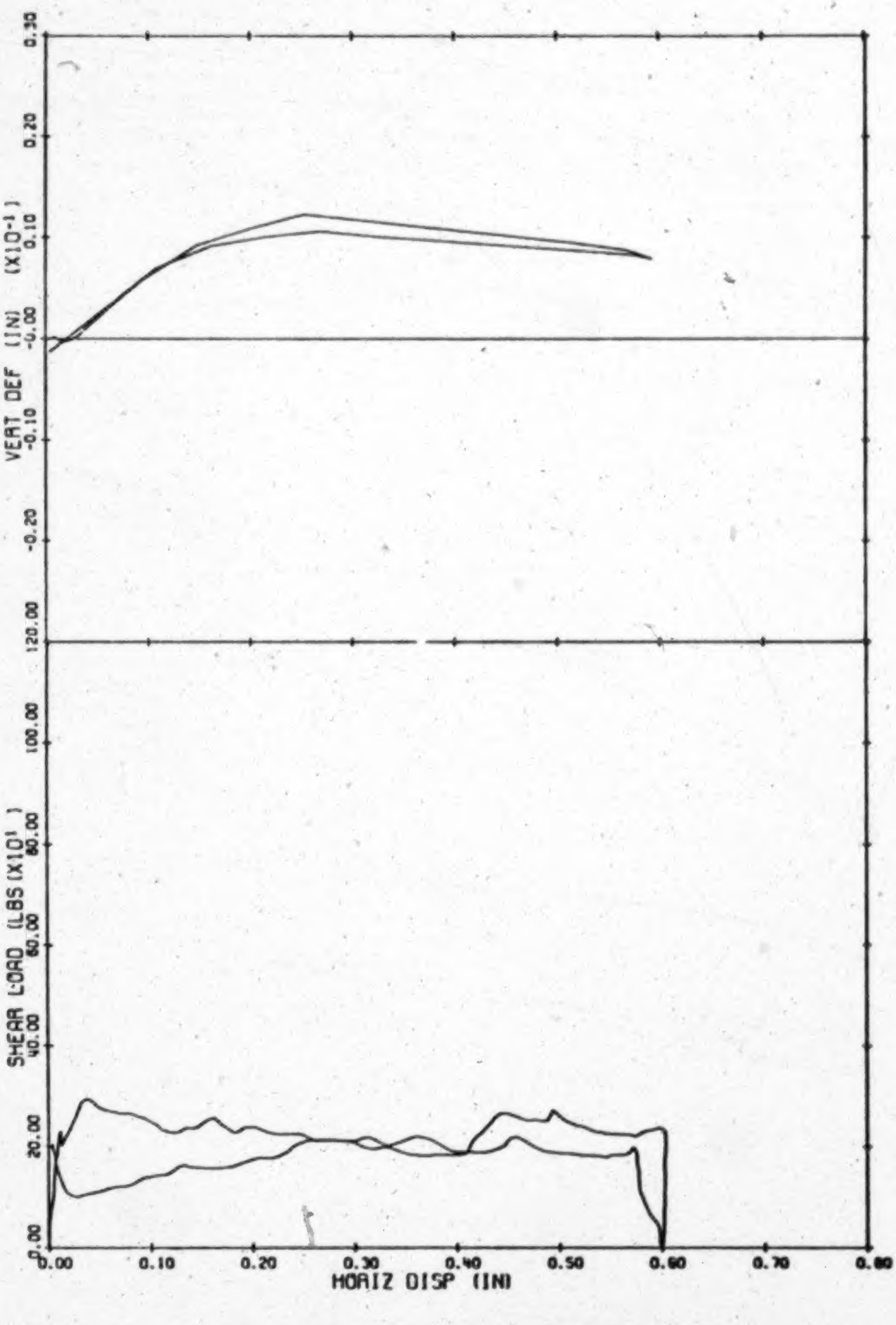

Figure B.12 Shear load and vertical deformation versus the horizontal deformation for sample S-5

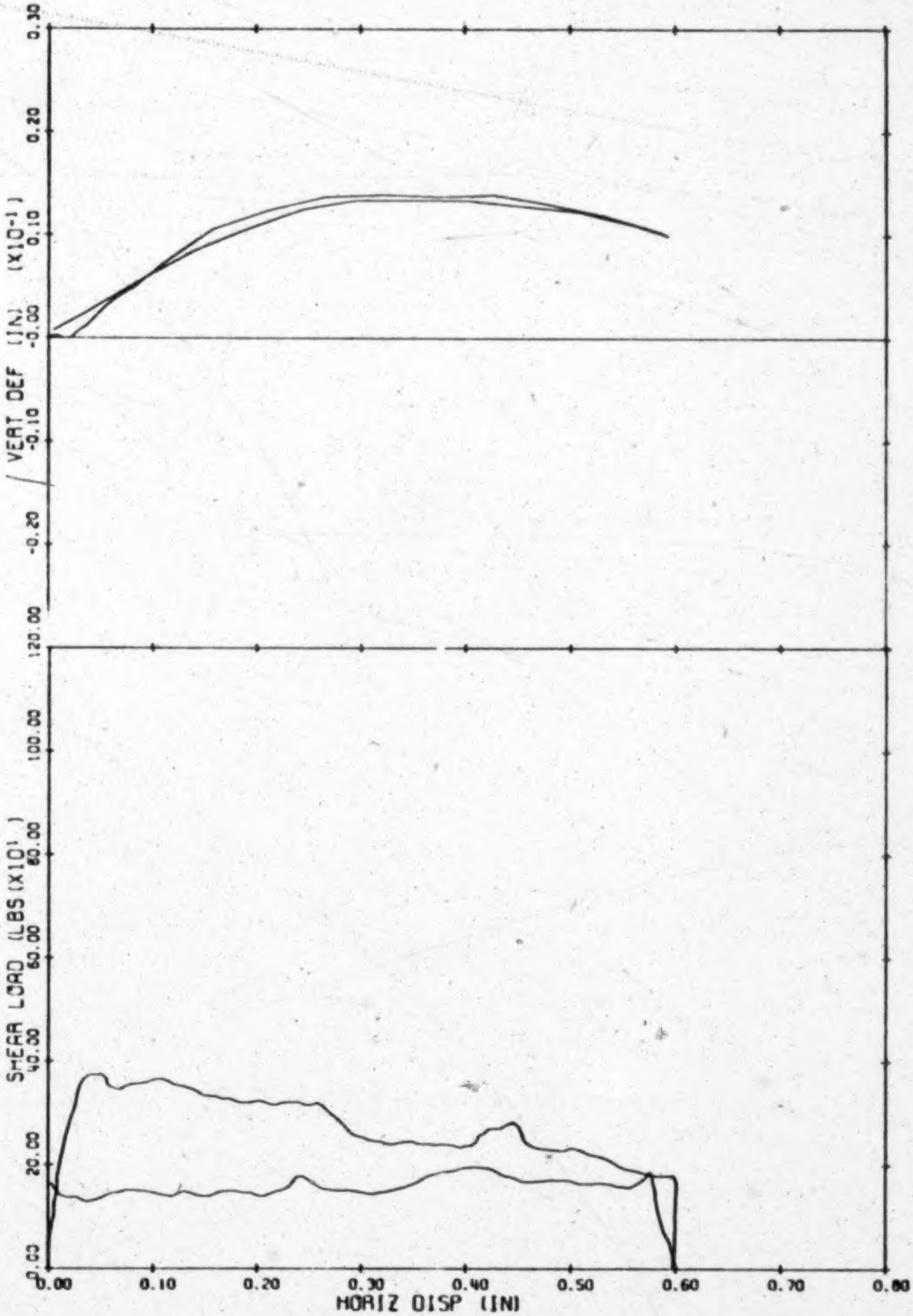

Figure B.13 Shear load and vertical deformation versus the horizontal deformation for sample S-5A

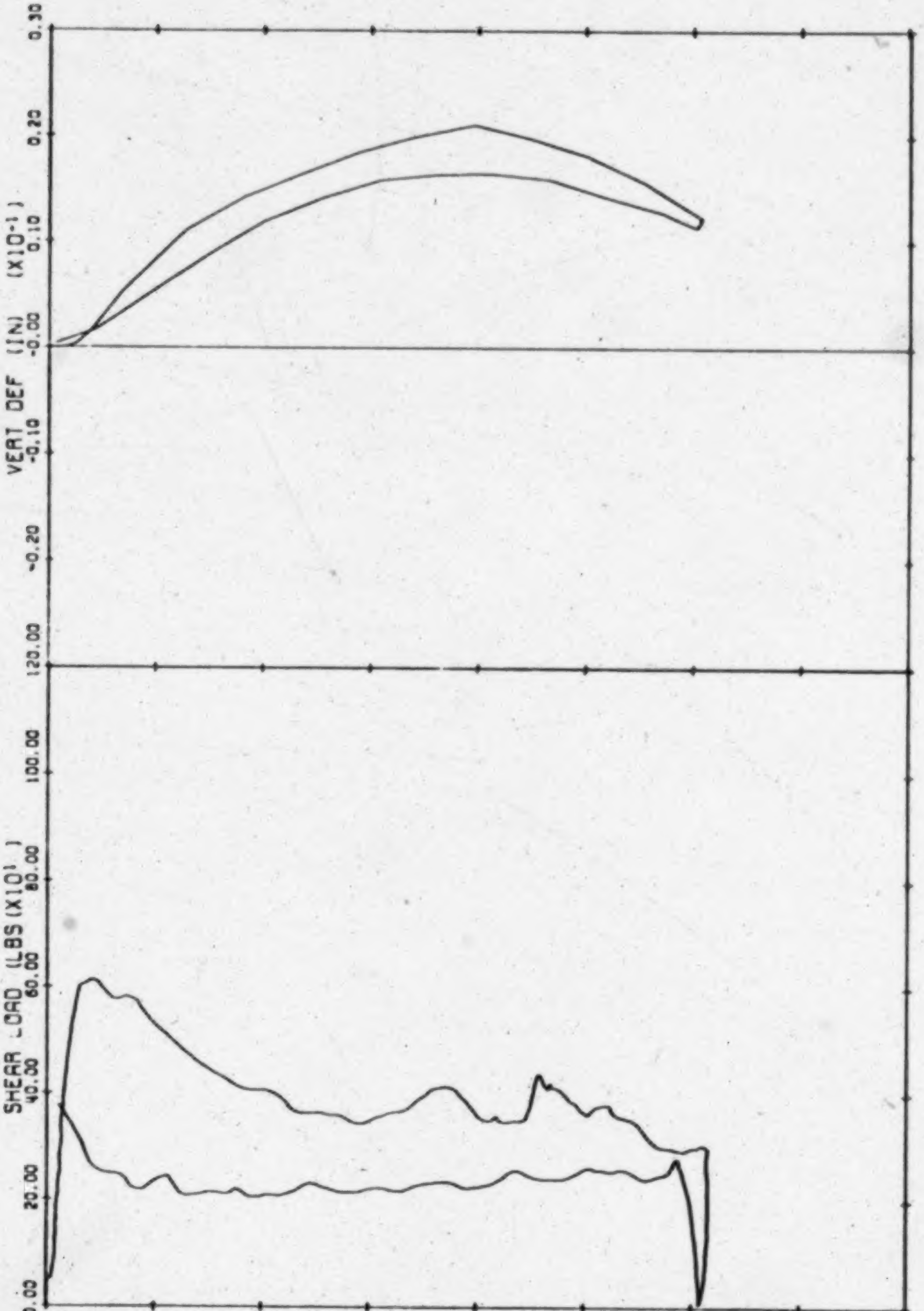

Figure B.14 Shear load and vertical deformation versus the horizontal deformation for sample S-6

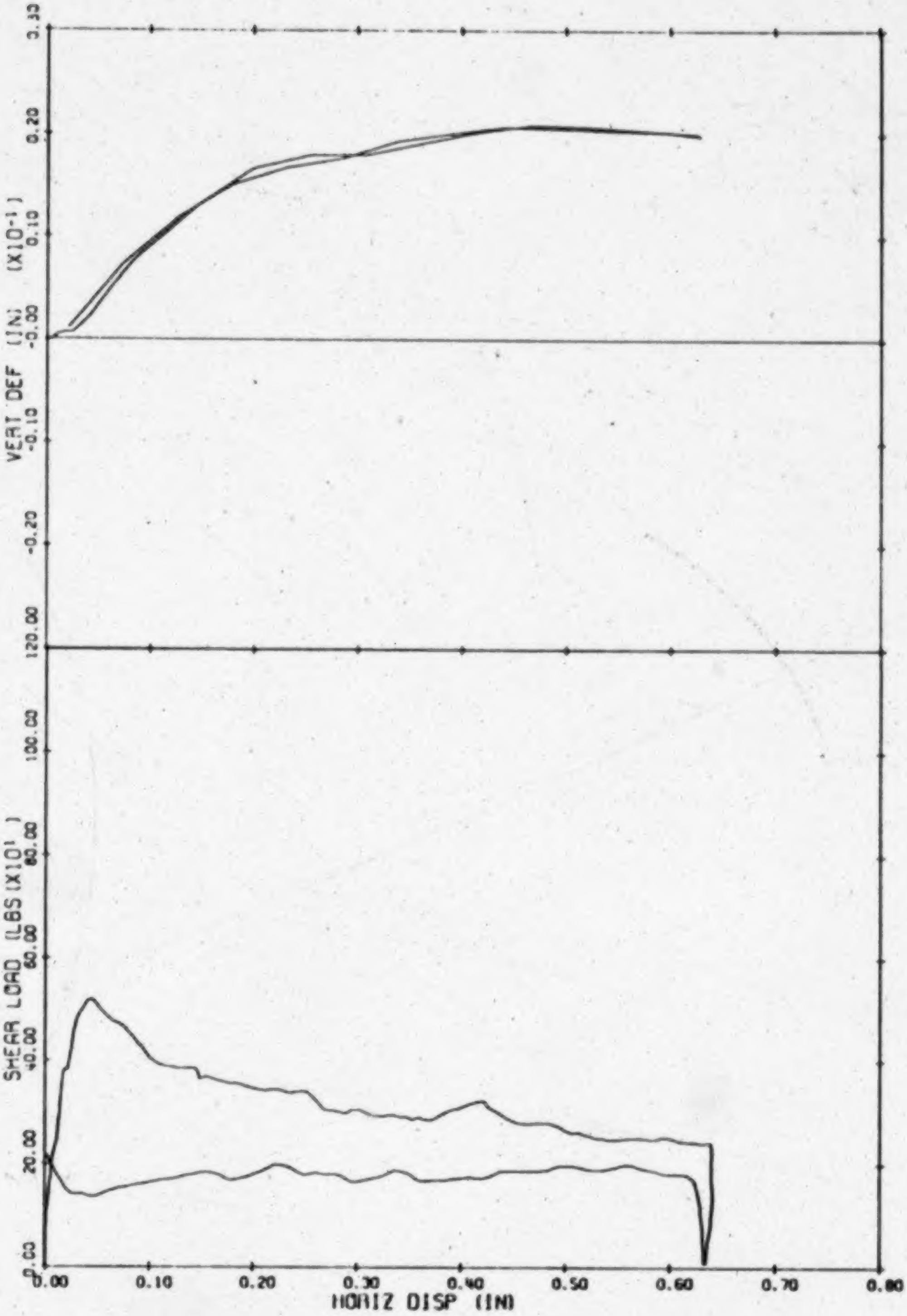

Figure B.15 Shear load and vertical deformation versus the horizontal deformation for sample S-6A

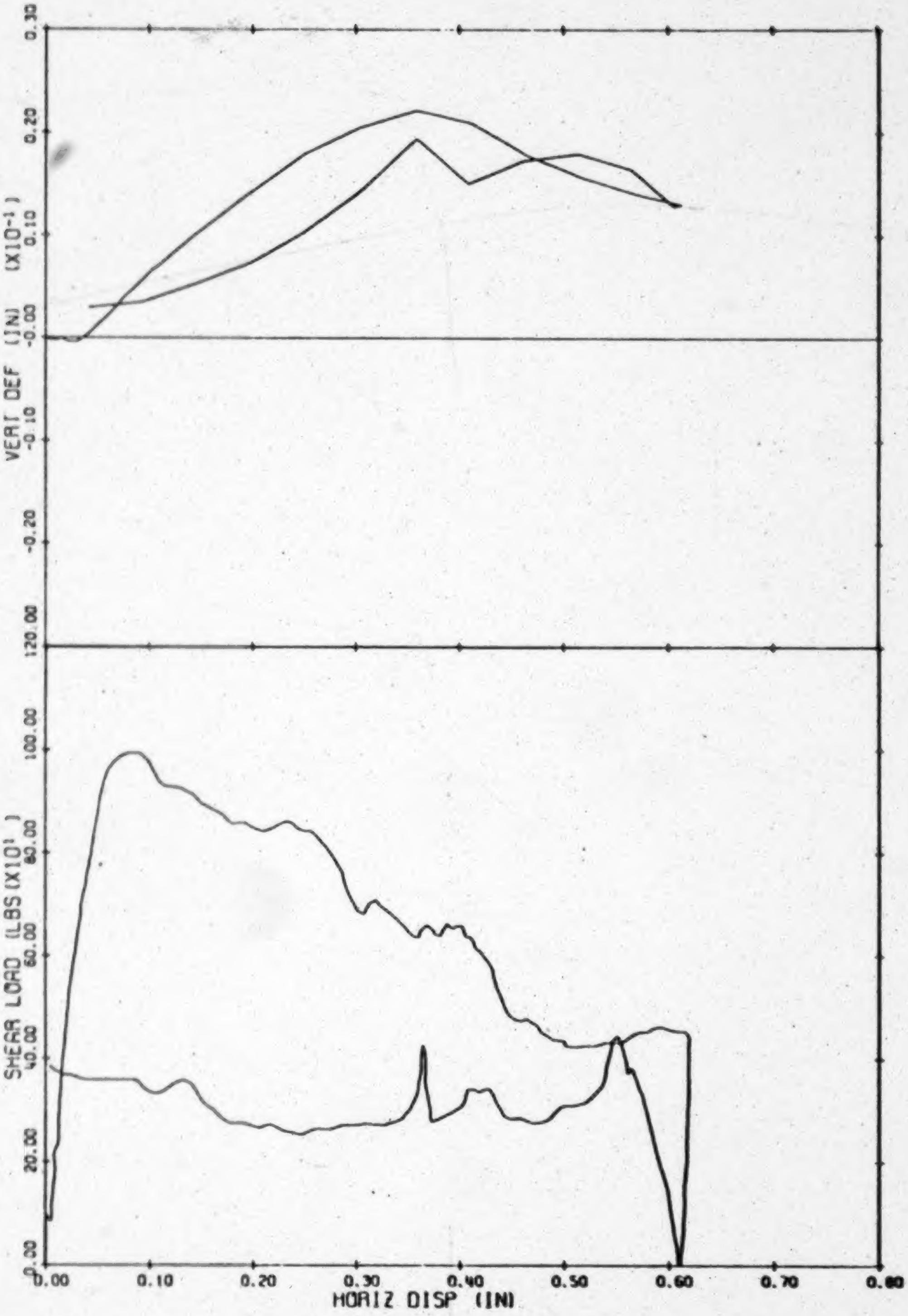

Figure B.16 Shear load and vertical deformation versus the horizontal deformation for sample S-7

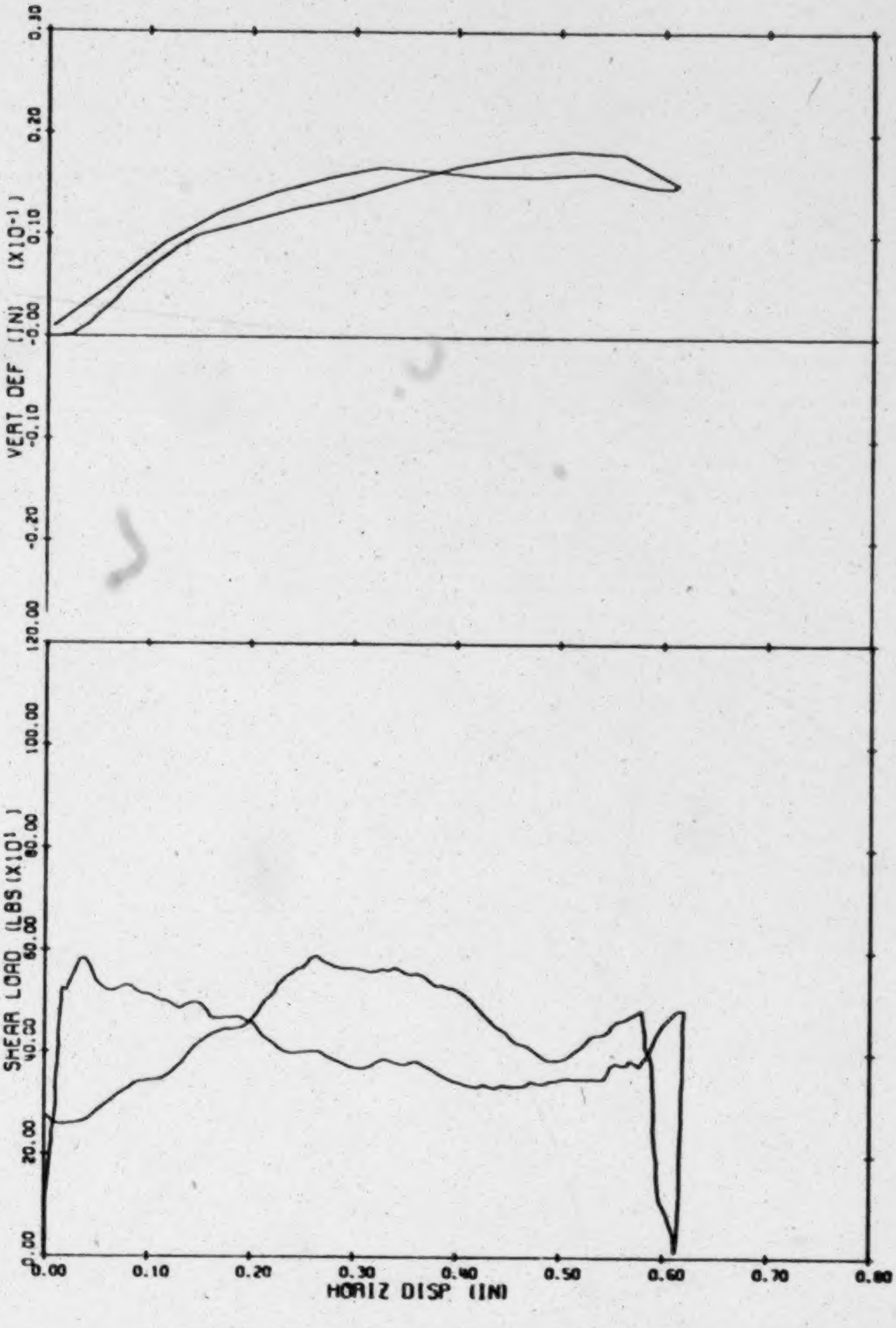

Figure B.17 Shear load and vertical deformation versus the horizontal deformation for sample S-7A

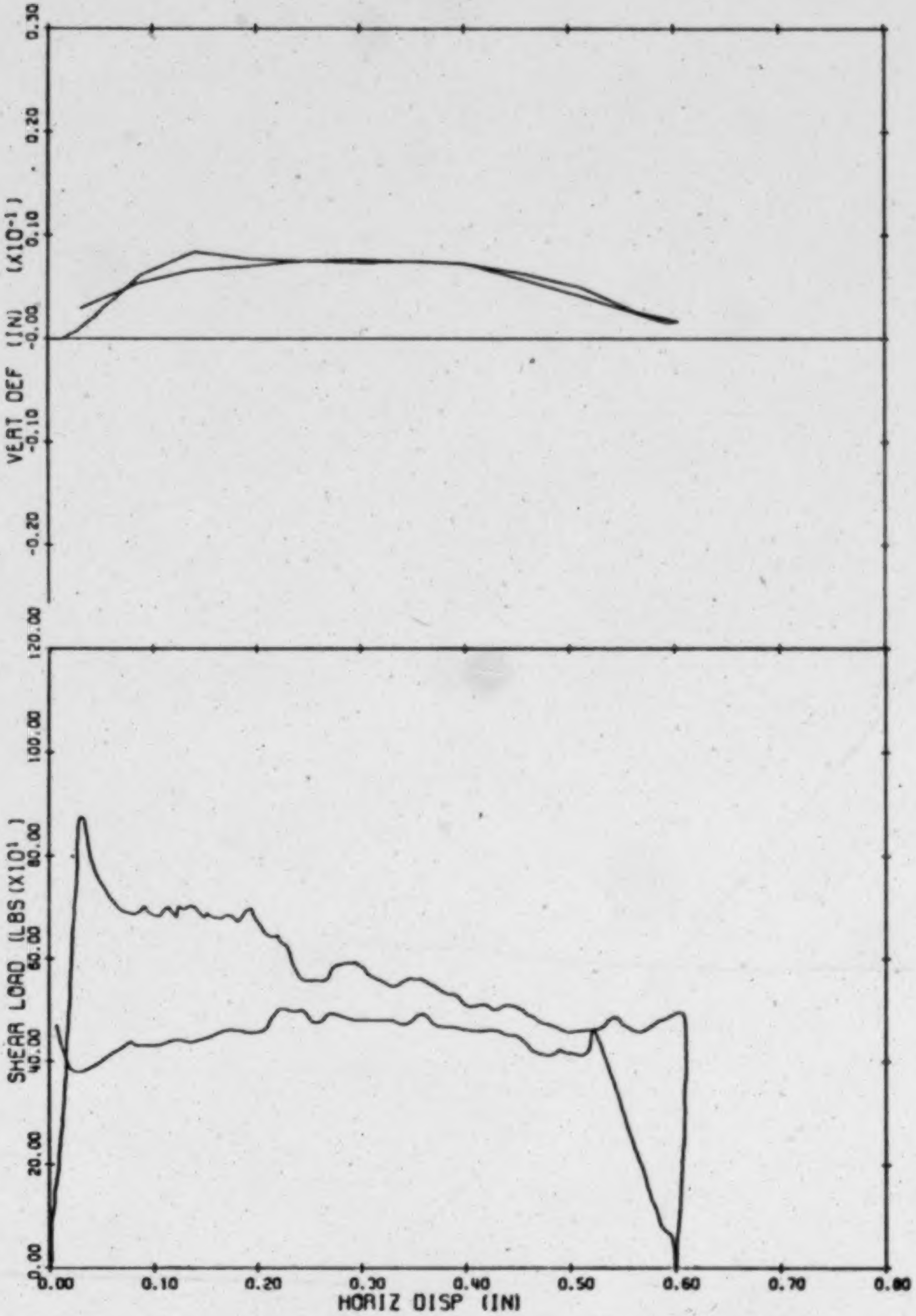

Figure B.18 Shear load and vertical deformation versus the horizontal deformation for sample S-8

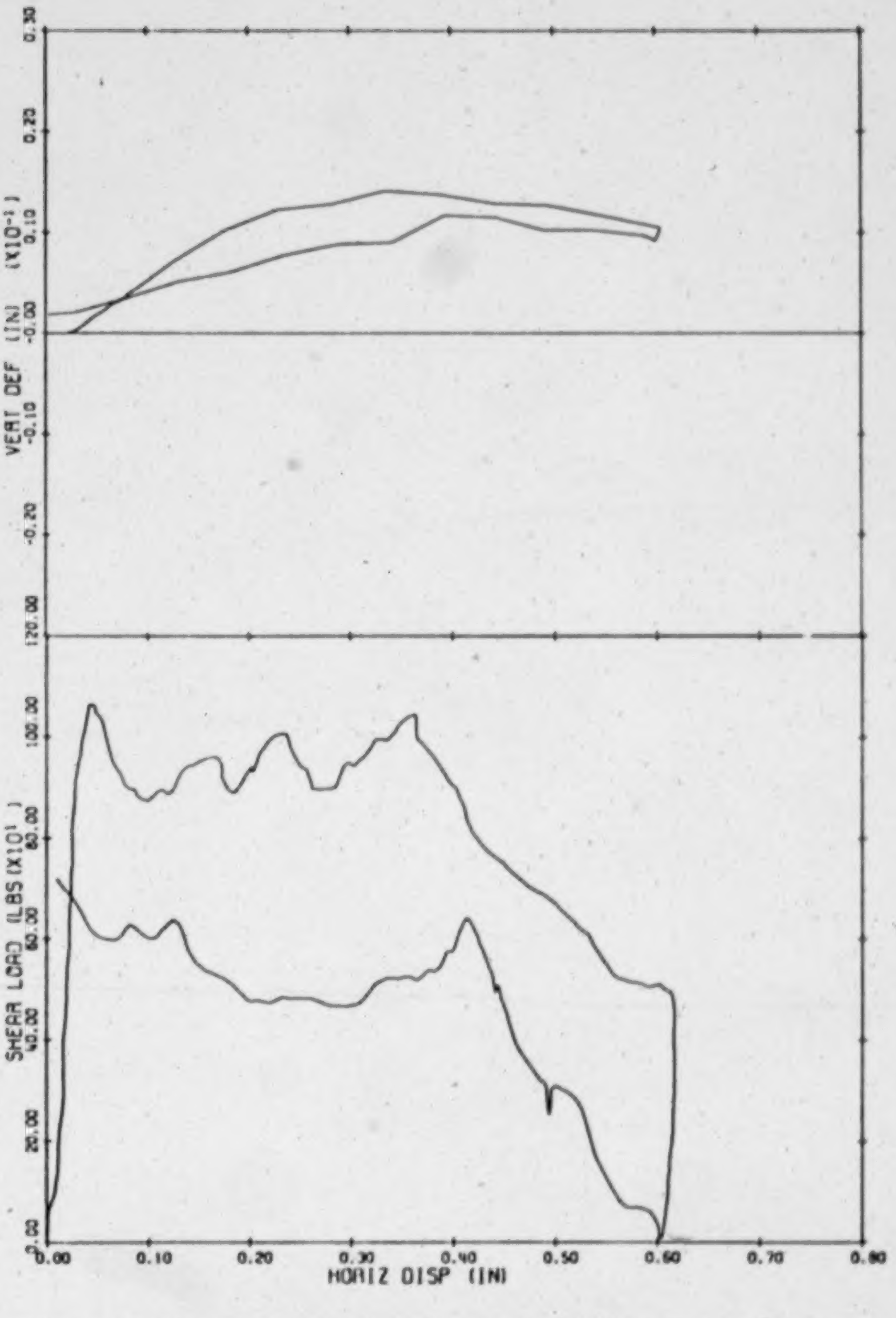

Figure B.19 Shear load and vertical deformation versus the horizontal deformation for sample S-8A

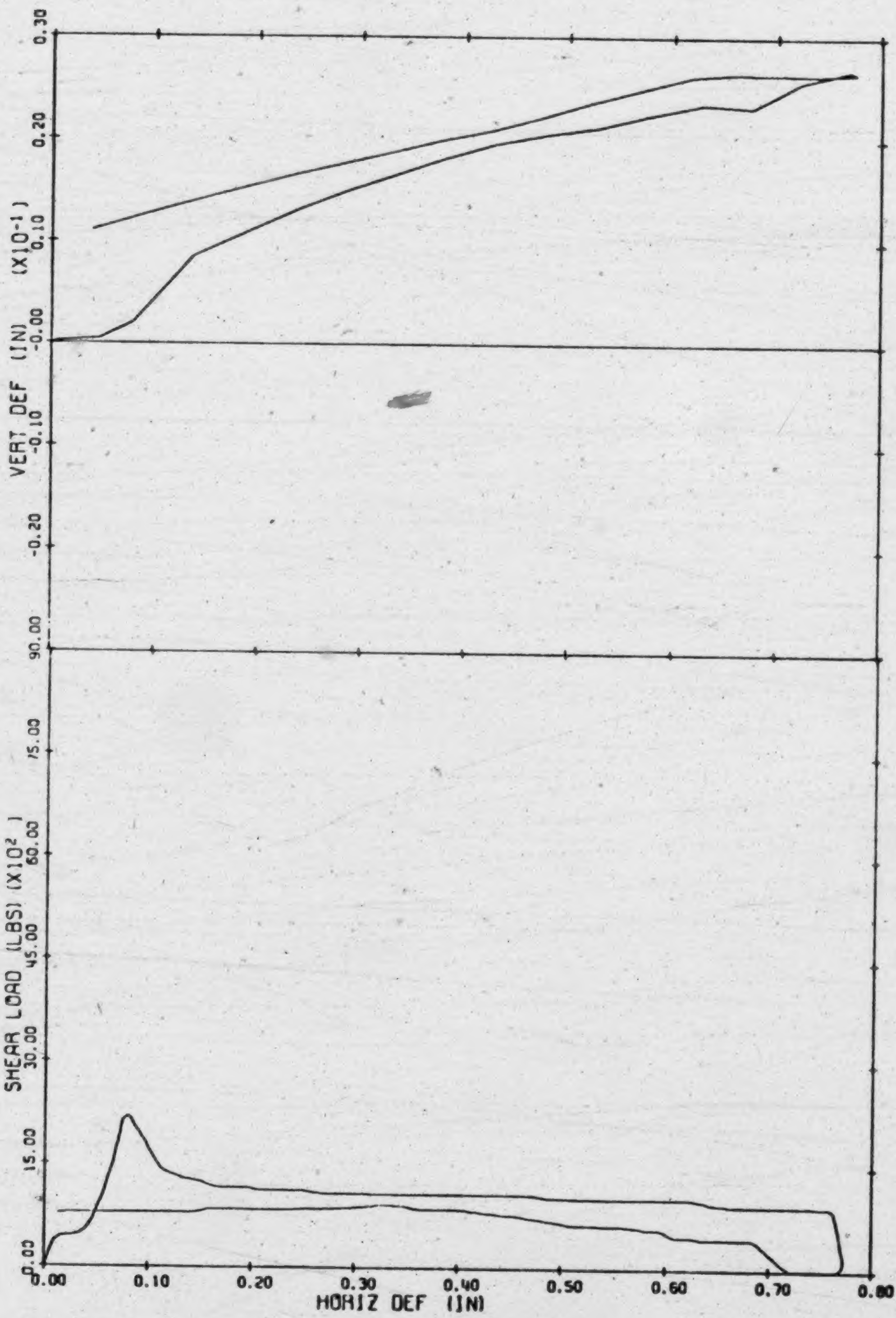

Figure B.20 Shear load and vertical deformation versus the horizontal deformation for sample J-1

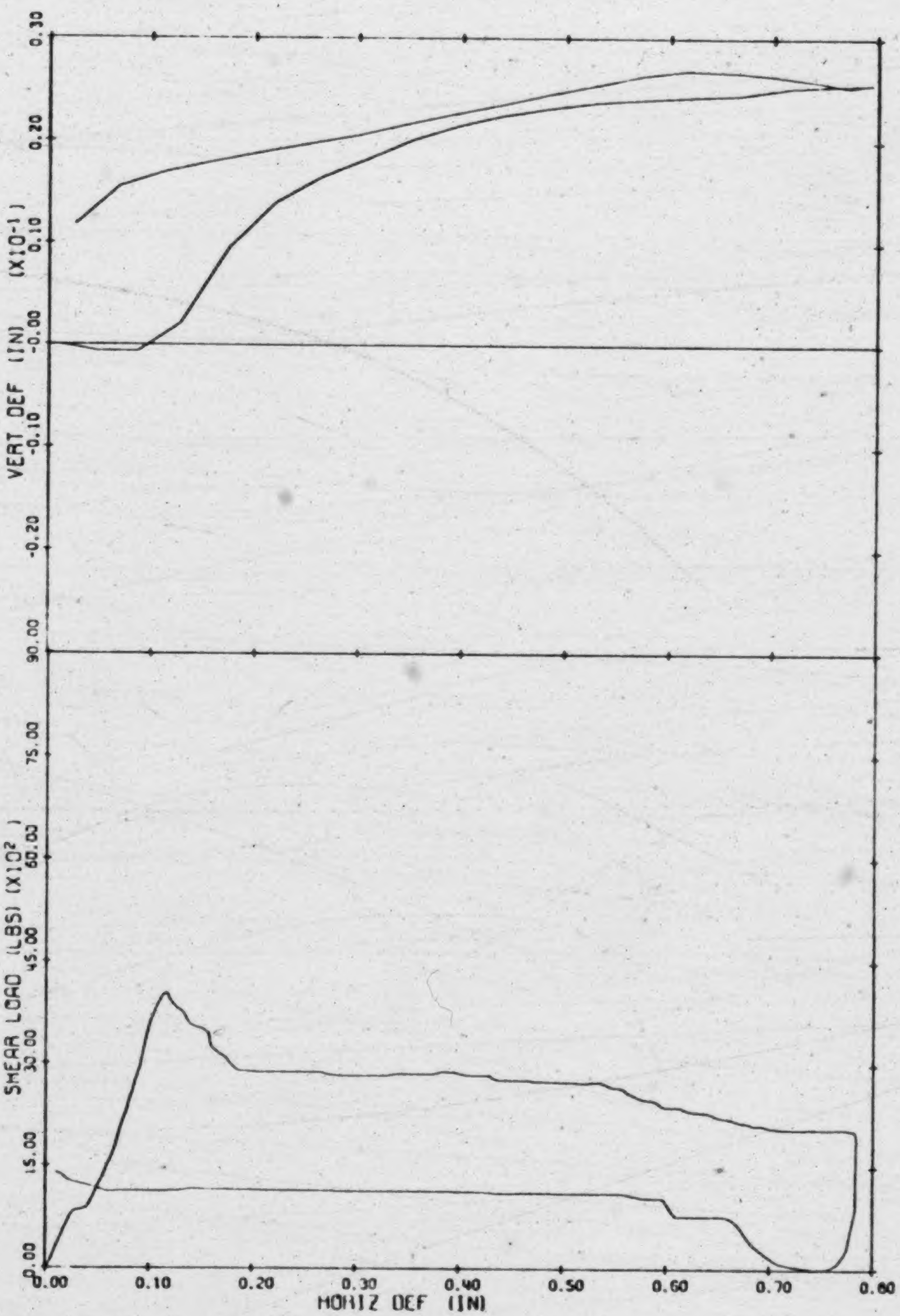

Figure B.21 Shear load and vertical deformation versus the horizontal deformation for sample J-2

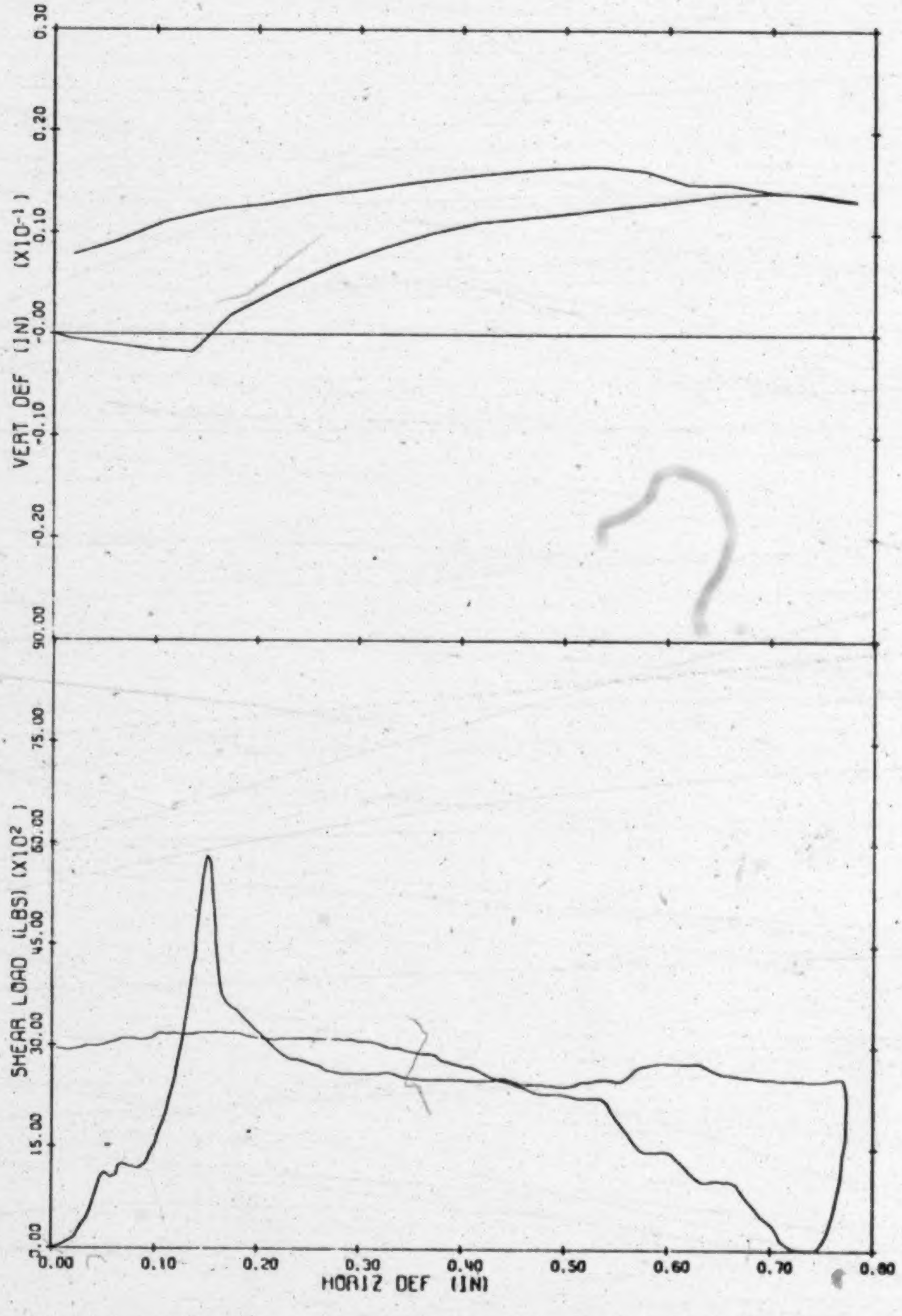

Figure B.22 Shear load and vertical deformation versus the horizontal deformation for sample J-3

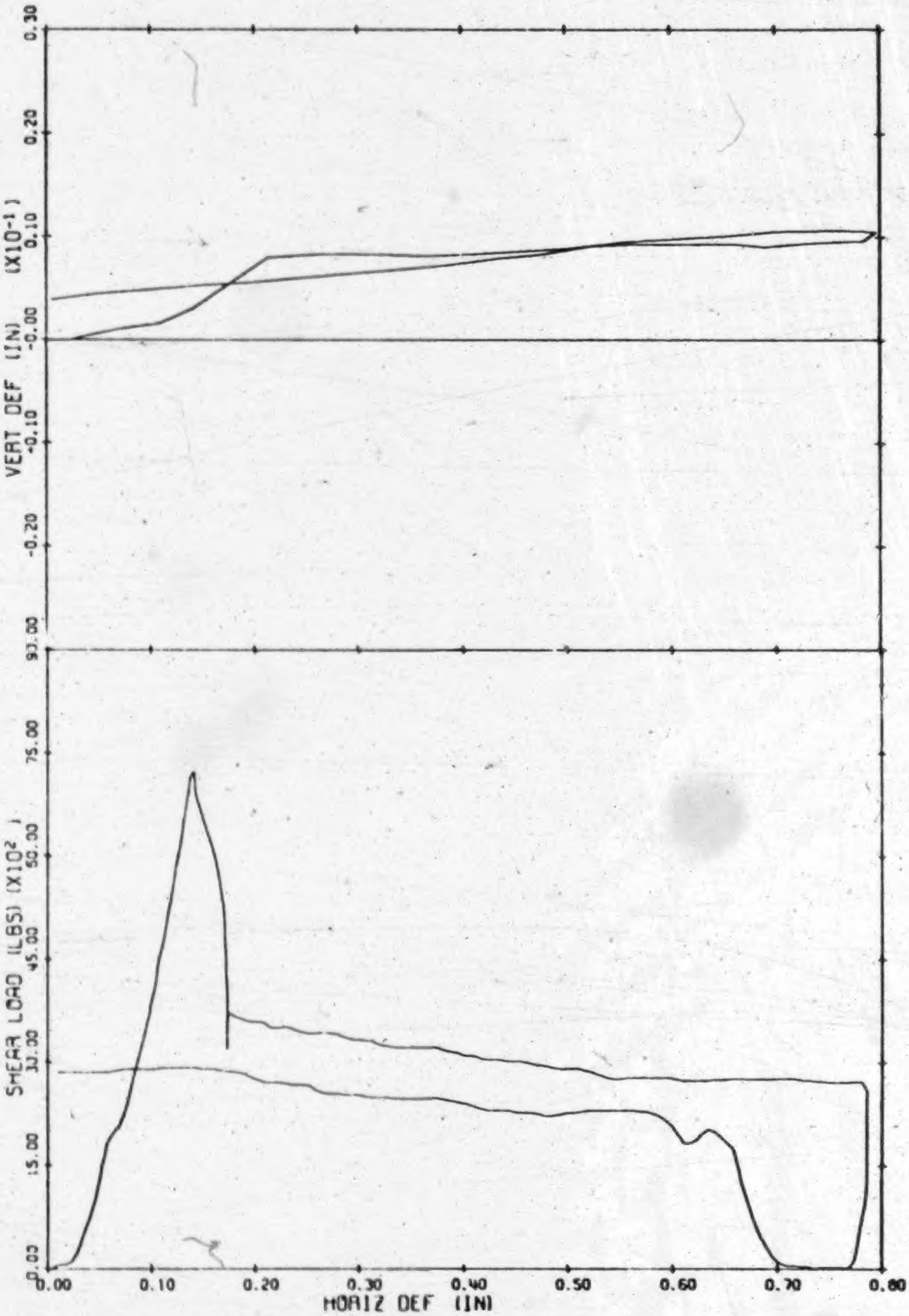

Figure B.23 Shear load and vertical deformation versus the horizontal deformation for sample J-4

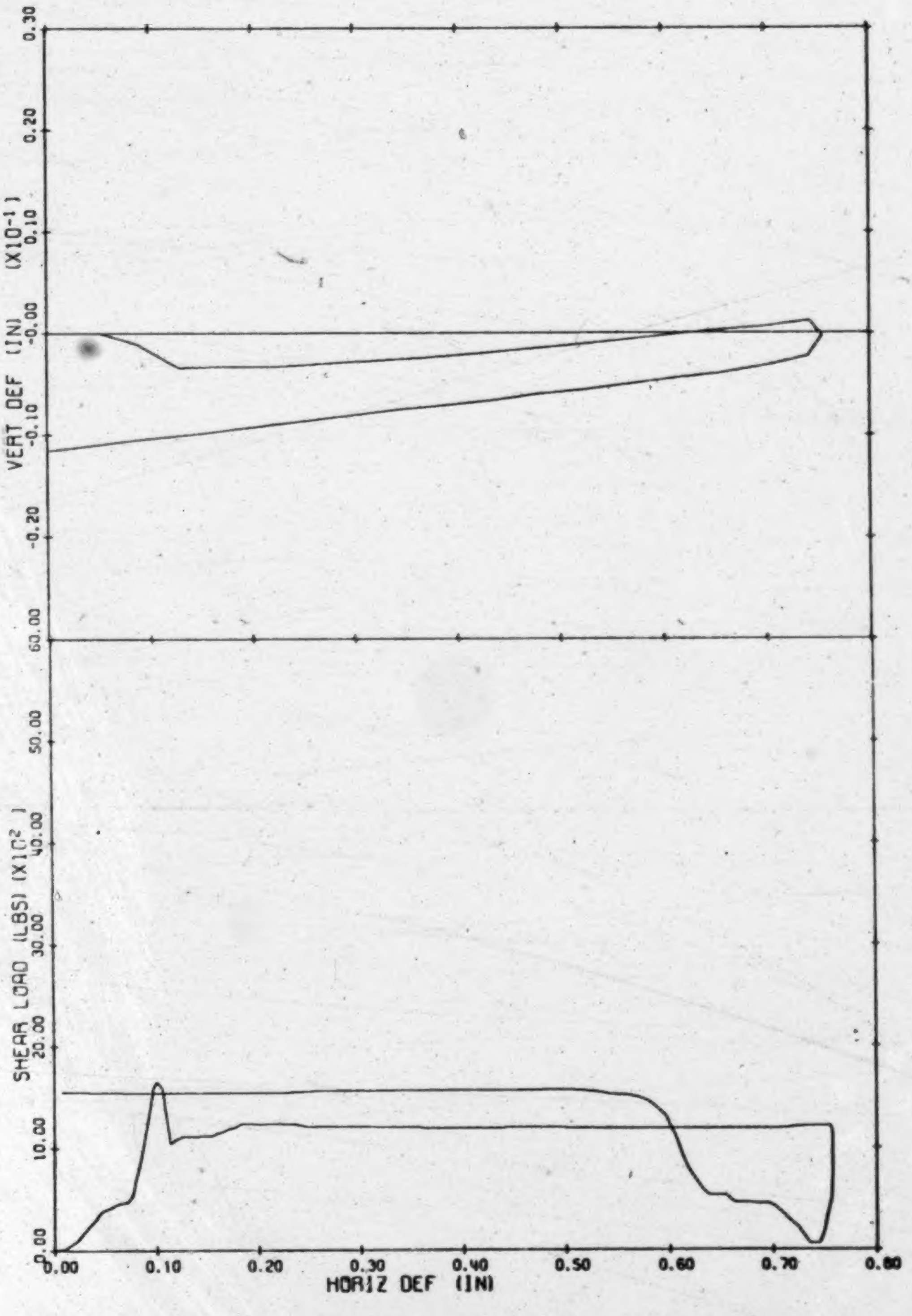

Figure B.24 Shear load and vertical deformation versus the horizontal deformation for sample D-1

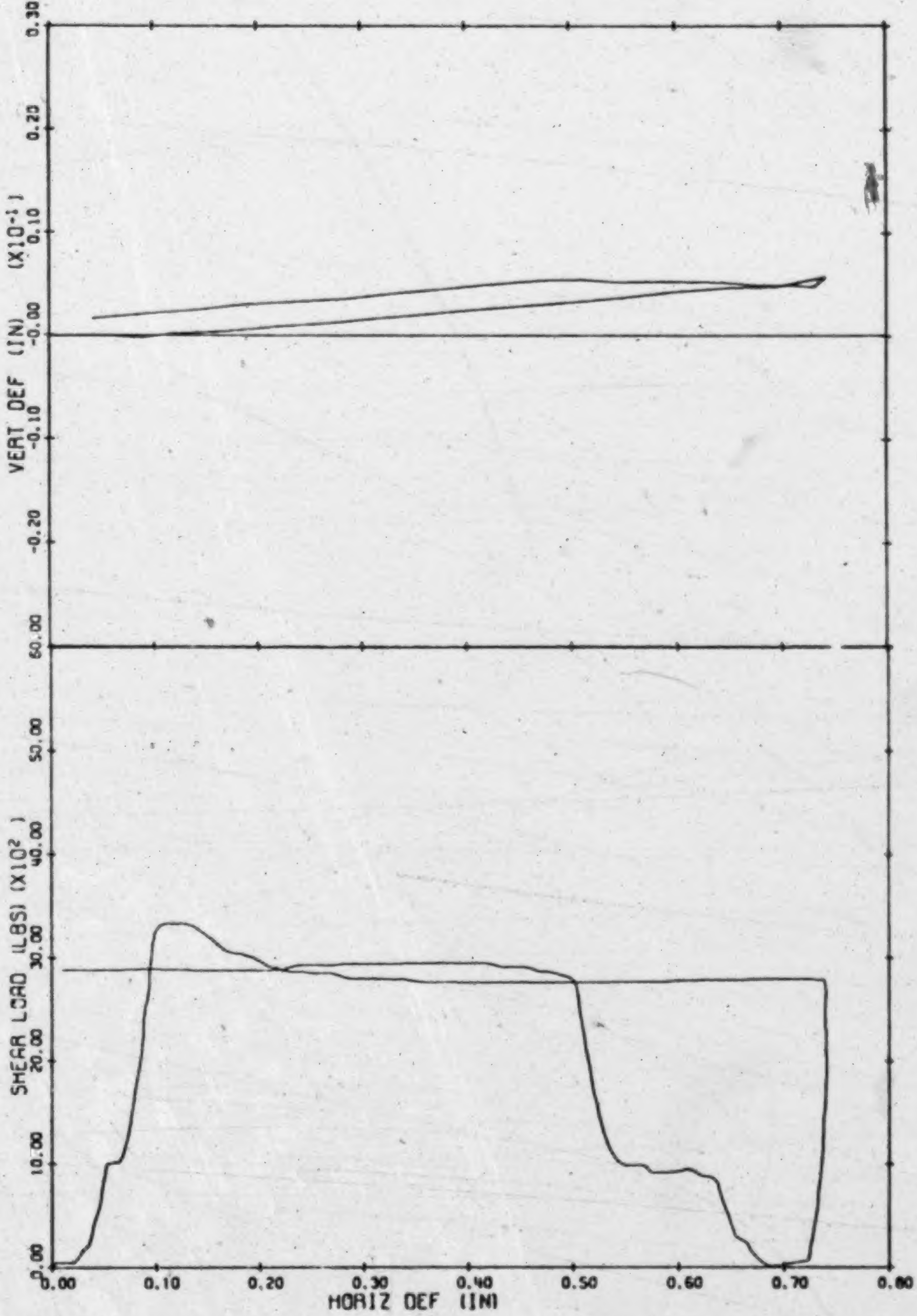

Figure B.25 Shear load and vertical deformation versus the horizontal deformation for sample D-2

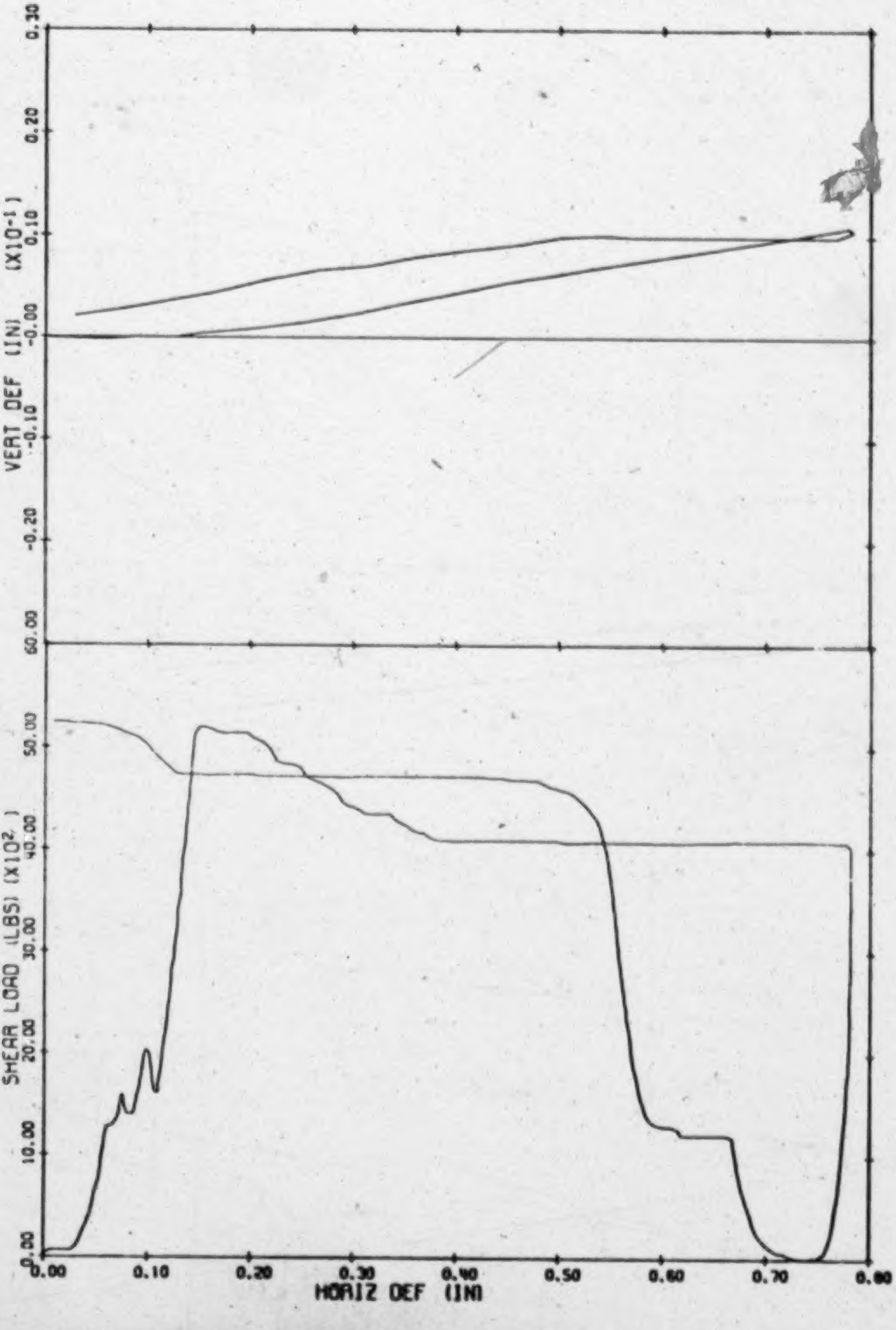

Figure B.26 Shear load and vertical deformation versus the horizontal deformation for sample D-3

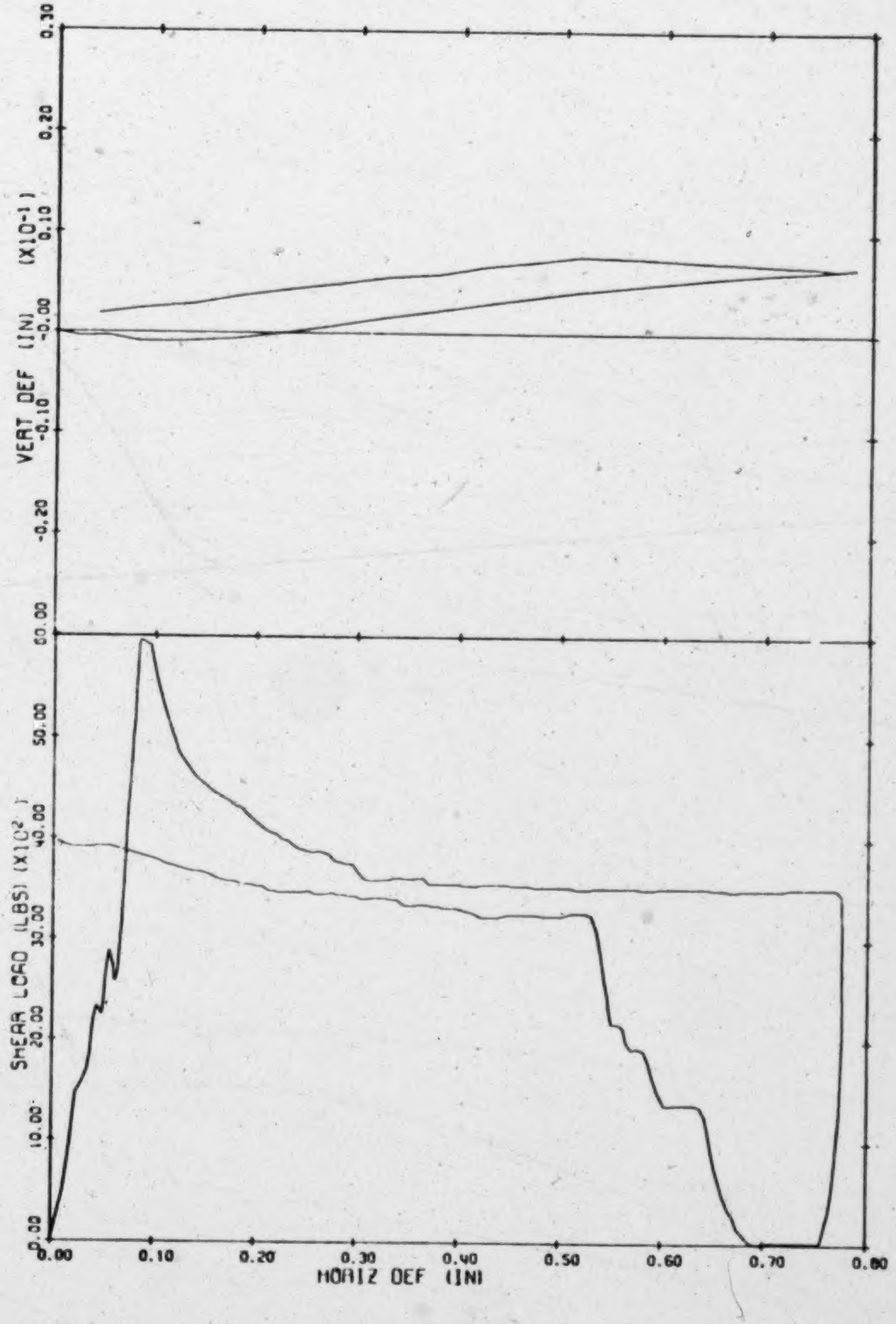

Figure B.27 Shear load and vertical deformation versus the horizontal deformation for sample D-4

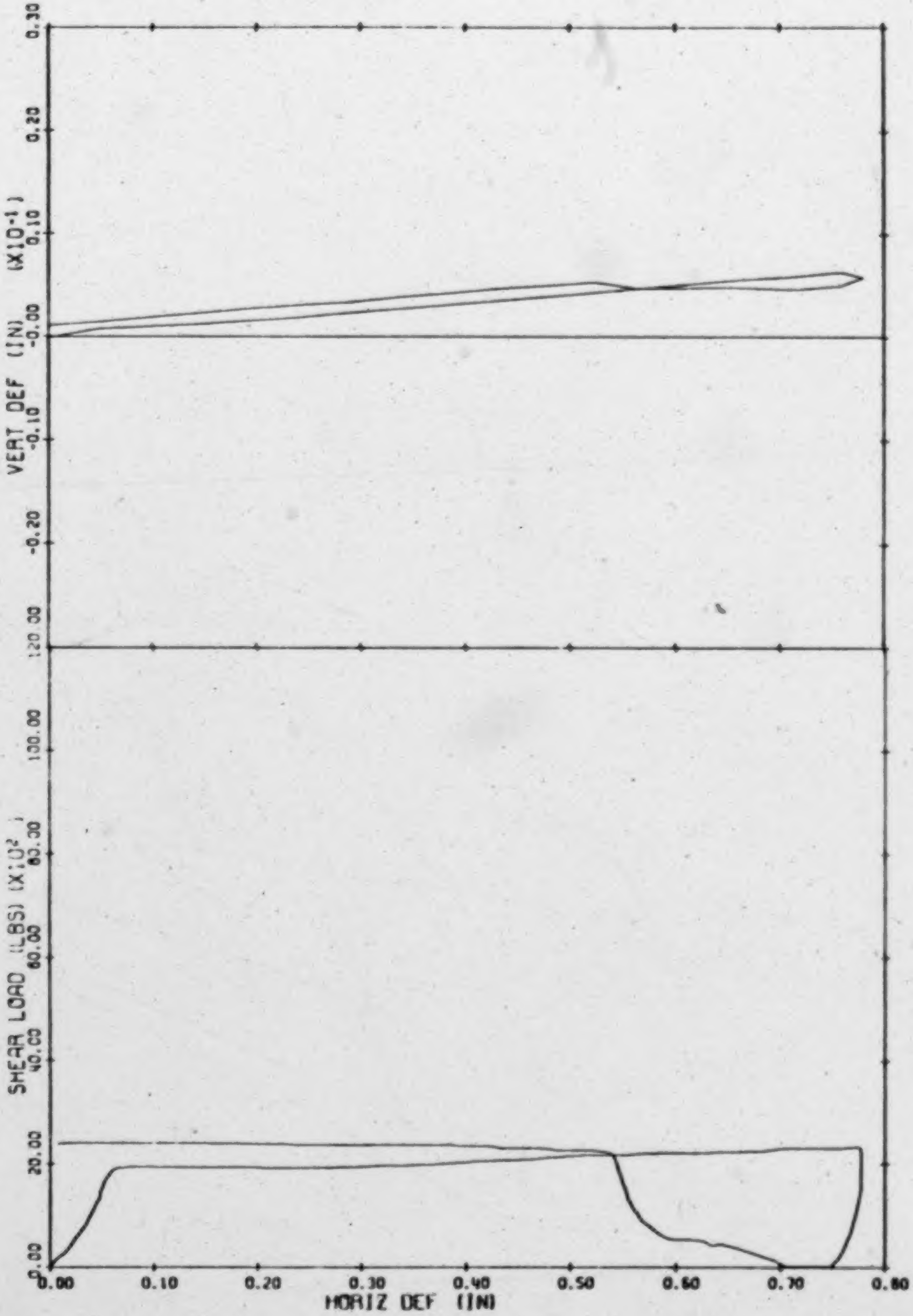

Figure B.28 Shear load and vertical deformation versus the horizontal deformation for sample L-1

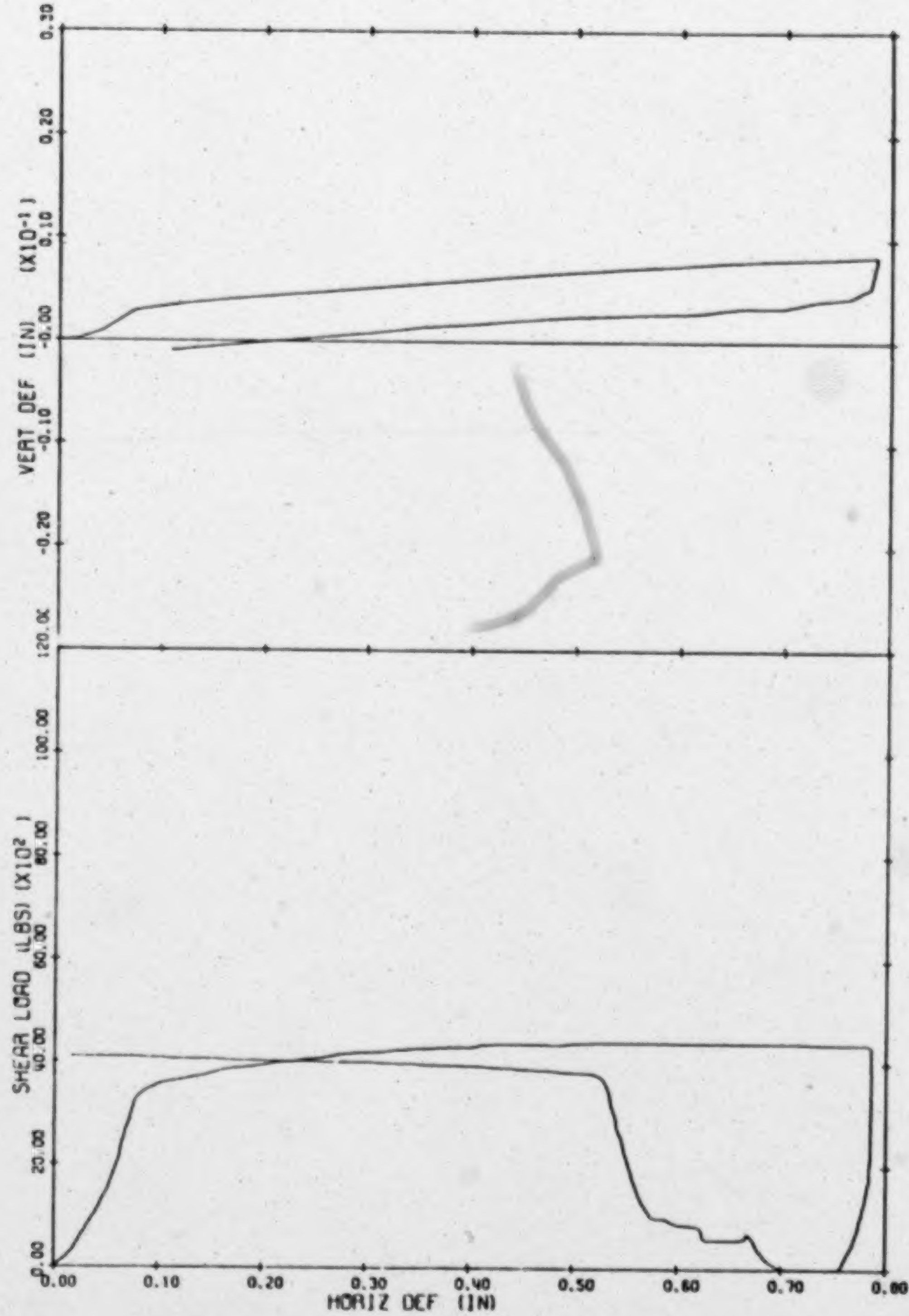

Figure B.29 Shear load and vertical deformation versus the horizontal deformation for sample L-2

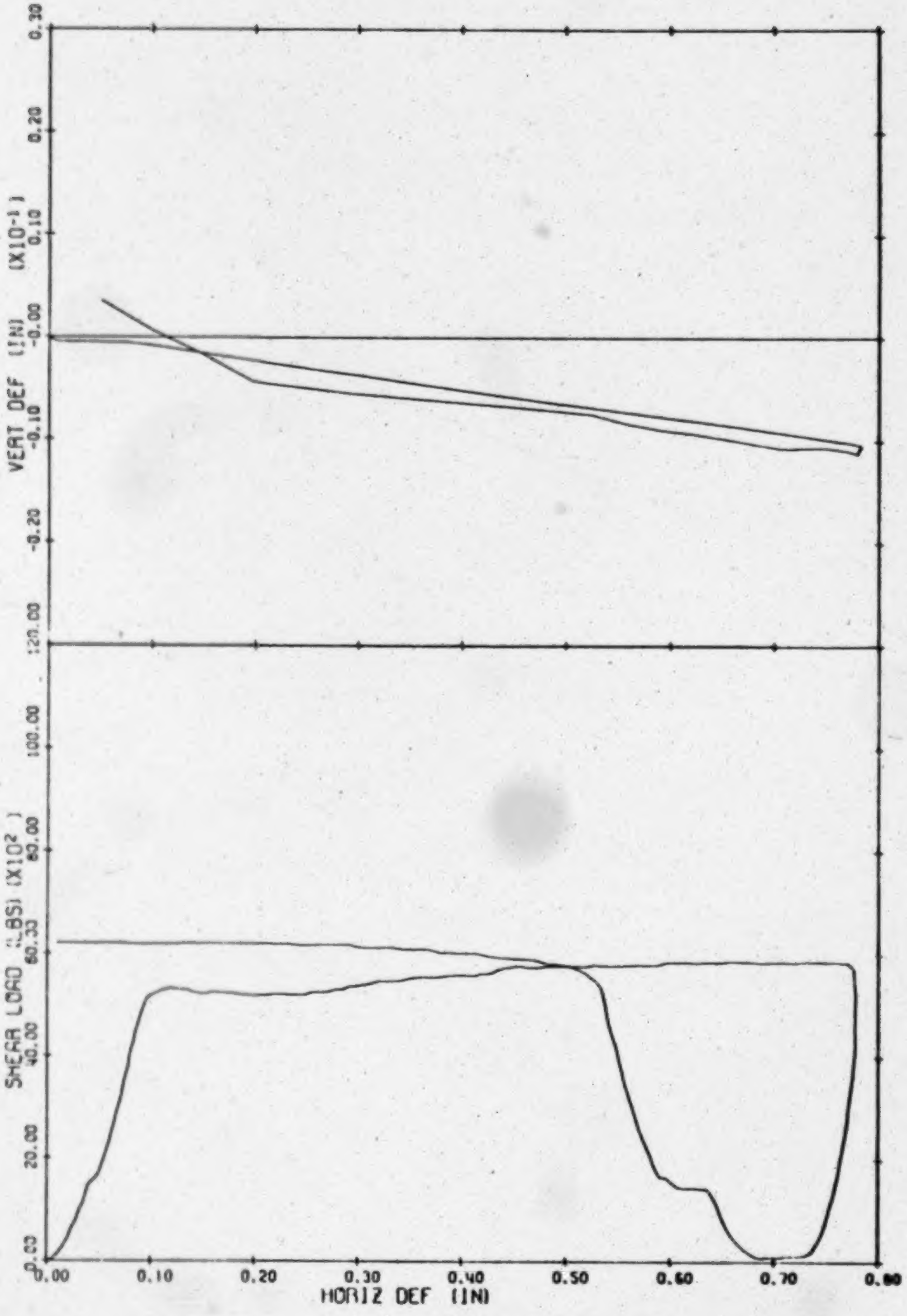

Figure B.30 Shear load and vertical deformation versus the horizontal deformation for sample L-3

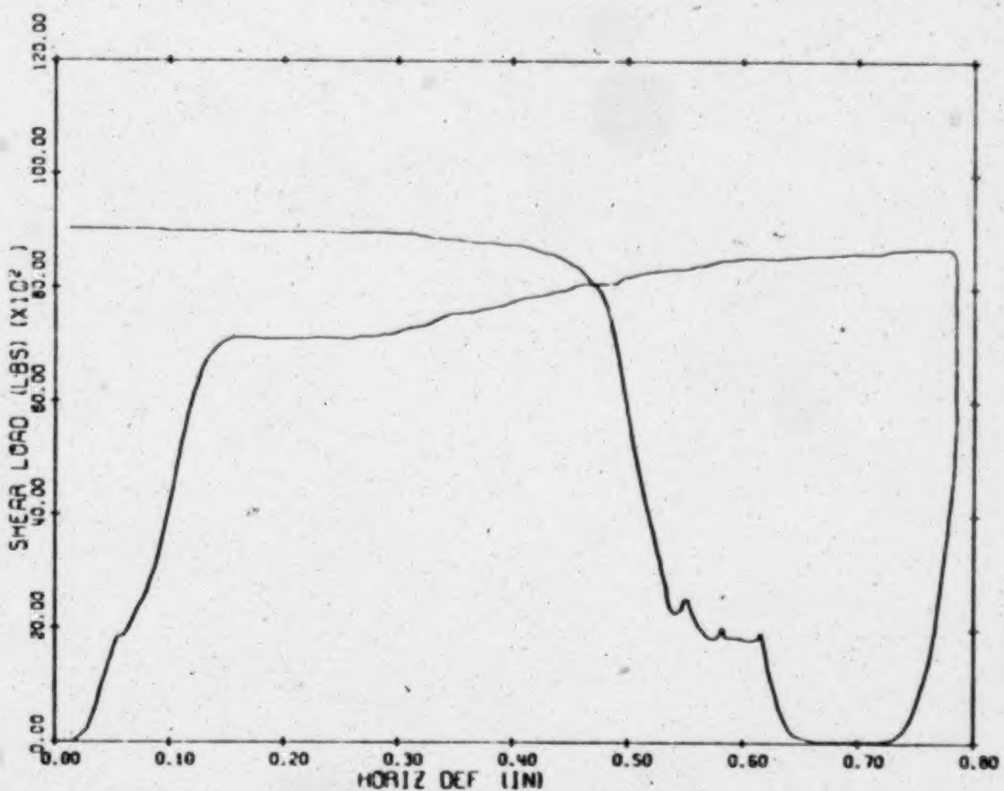

Figure B.31 Shear load and vertical deformation versus the horizontal deformation for sample L-4

APPENDIX C

SPECTRAL DENSITY COMPUTER PROGRAM

Special techniques are required for calculating the Fast Fourier Transforms (FFT) of a data sequence. To perform these complicated calculations, a computer program was obtained from the Physics Department, University of Alberta. A listing of this program is given in this Appendix.

Once the FFT are obtained, it is relatively a simple matter to calculate the spectral density estimates. The procedures for determining these estimates have been given by Bendat and Piersol (1971) and are given below in the context of the specific problem at hand.

The spectral density estimates, G_x, are defined as

$$G_x(f_k) = 2 * h/N * |X_k|^2 \ldots\ldots\ldots\ldots\ldots\ldots \quad C - 1$$

where h = the distance or time between amplitude readings

N = total number of readings

$f_k = k/Nh \qquad k = 0, 1, 2, \ldots, N-1$

X_k = the Fast Fourier Transform of the data.

The procedural steps followed in calculating the spectral density estimates are as given below:

(1) The data was truncated to a total of 2048 readings.

The FFT method requires that $N = 2^P$. When $P = 11$, $N = 2048$.

(2) The data sequence was tapered at the ends by using the cosine taper window shown in Figure C.1 (SUBROUTINE COSTAP in the computer program).

(3) The $|X_k|^2$ values were calculated by first calling SUBROUTINE ONE R FT (2048, x), which calculates the real and imaginary parts of X_k and stores them in the x array. Then, from the new x array, the $|X_k|^2$ values were computed from the following equations:

$|X_k|^2 = x_k^2$ when k=1

$|X_k|^2 = x_k^2 + x_{N+2-k}^2$ when k > 2

A total of N/2 + 1 estimates can be obtained this way.

(4) The spectral density estimates were then calculated according to equation C-1 with h = 0.0001 inches. The frequancy corresponding with each G_k estimate was calculated from

$f = k/N/h$

(5) The G_k estimates were then scaled by a factor of 1/0.875 due to the initial cosine tapering.

(6) The raw G_k estimates were smoothed by using a Trapezoidal Spectral Window. The smooth estimates are given by

$$G = [\, G_k + G_{k+1} + \cdot \quad \cdot \quad \cdot + G_{k+l-1} \,] /l$$

where l is a number dependent on the desired level of the standard error, ϵ_r. The ϵ_r is given by

$$\epsilon_r = \sqrt{1/l}$$

The effective bandwidth, B_e', then becomes

$$B_e' = l \bullet B_e = l/N/h$$

In the computer program, the frequency smoothing is done in SUBROUTINE FREQ. The final smoothed frequency curve was then plotted on the Calcomp Plotter by calling SUBROUTINE CGPL.

The input information required for the program is,

(1) the x array of amplitude readings taken from a disc file.

(2) NB, the number of sets of data.

(3) SAM, the sample number.

(4) LB, the l value.

(5) NP, the number of data points to be printed.

(6) VB, the vertical scale on the plots.

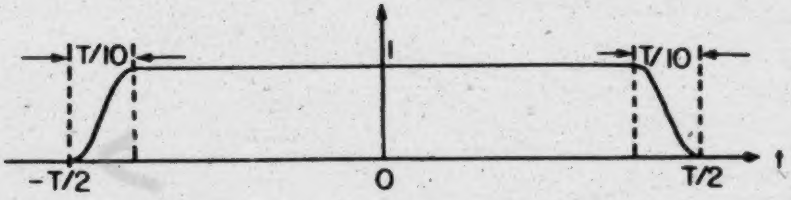
T/10
T/10
1
-T/2
0
T/2
t

Figure C.1 Cosine taper data window (after Bendat and Piersol, 1971)

```
      DIMENSION X(2048),G(1045)
      LOG2N=11
      N=2**LOG2N
      READ(5,75) N8,SAM,LB,NR,VB
   75 FORMAT(I5,1X,A4,2I5,F10.0)
      DO 100 N7=1,N8
C
C   READ DATA FROM FILE
C
      DO 10 I=1,N
   10 READ(1,1) X(I)
    1 FORMAT(F6.0)
C
      CALL COSTAP    (N,X)
C
      CALL ONE R FT(LOG2N,X)
C
C   DETERMINE THE SPECTRUM ESTIMATES G(F)
C
      N1=N/2 +1
      J=1
      G(1)=X(1)**2*2.0*0.0001/N
      DO 13 J=2,N1
      K=N+2-J
      G(J)=(X(J)**2+X(K)**2)*2.0*0.0001/N
   13 CONTINUE
C
C   SCALE DATA BY 1/0.875 DUE TO COSTAPER
C
      DO 20 I=1,J
   20 G(I)=G(I)/0.875
C
C
      CALL FREQ (N,G,J,LB,NR,SAM,N7,VB)
C
  100 CONTINUE
      CALL CGPL (X,Y,Y,N,0,1,1,1,1,HA,HB,HC,VA,VB,VC,ALPH,6)
      STOP
      END
      SUBPOUTINE COSTAP    (N,X)
C     ---------------------------
C
      REAL X(10)
      N1=N/10
      DO 10 L=1,N1
      A=3.1416/2.0/N1*L
      K=N-L+1
      X(L)=X(L)-X(L)*COS(A)
      X(K)=X(K)-X(K)*COS(A)
   10 CONTINUE
      RETURN
      END
```

1

```
      SUBROUTINE FREQ(N,G,J,L,NR,SAM,N7,VB)
C     ----------------------
C
      DIMENSION  G(J),F(50),AVE(50),ALPHA(20)
      NO=J
      H=0.0001
      NV=0
      DO 20 K=1,NO,L
      NV=NV+1
      IF(NV.GT.50) GO TO 49
      A=0.0
      LL=K+L-1
      DO 10 J=K,LL
   10 A=A+G(J)
      AVE(NV)=A/L
      ML=LL-K
      F(NV)=(FLOAT(K)+(FLOAT(ML)/2.))/FLOAT(N)/H
   20 CONTINUE
   49 WRITE(6,50) SAM,N7
   50 FORMAT('1',//,20X,'SPECTRUM ESTIMATES FOR ',A4,//,
     *20X,'RUN NUMBER ',I1,//)
      DO 60 JK=1,NR
   60 WRITE(6,55) F(JK),AVE(JK)
   55 FORMAT(15X,F7.0,F10.2)
      READ(5,65) (ALPHA(I),I=1,20)
   65 FORMAT(20A4)
      CALL CGPL(F,AVE,F,NR,1,1,1,4,1,0.0,100.,8.0,0.0,VB   ,6.0,ALPHA,6)
      RETURN
      END
      SUBROUTINE ONE R FT (LOG2N,X)
C.......................................................................
C     ONE REAL FOURIER TRANSFORM
C
      INTEGER LOG2N
      REAL X (10)
C
      INTEGER J,JN,K,KN,N,N OVER 2
      REAL ARG,C,PI,S,T,XI,XR,YI,YR
C
      PI=3.141592654
      N=2**(LOG2N-1)
      CALL P SUB B O (LOG2N,X)
      CALL R SUB B O (LOG2N-1,X(1))
      CALL R SUB B O (LOG2N-1,X(N+1))
      CALL MR 1D FT (LOG2N-1,X(1),X(N+1))
      N OVER 2=N/2+1
      DO 100 J=2,N OVER 2
      K=N+2-J
      JN=J+N
      KN=K+N
      XR=(X(J)+X(K))*.5
      XI=(X(JN)-X(KN))*.5
      YR=(X(JN)+X(KN))*.5
      YI=(X(K)-X(J))*.5
      ARG=PI*FLOAT(J-1)/FLOAT(N)
      C=COS(ARG)
      S=SIN(ARG)
      T=YR*C+YI*S
      YI=YI*C-YR*S
      YR=T
      X(J)=XR+YR
      X(K)=XR-YR
      X(KN)=XI+YI
      X(JN)=YI-XI
  100 CONTINUE
      XR=X(1)+X(N+1)
      YR=X(1)-X(N+1)
      X(1)=XR
      X(N+1)=YR
      RETURN
      END
      SUBROUTINE RECOVR (LOG2N, RE, IM)
C......................................................................
C
C      RECOVERS THE REAL AND THE IMAGINARY PARTS OF THE FOURIER
C      TRANSFORM WHICH HAS BEEN STORED IN COMPACT HERMETIAN FORM.
C
C   .  THE COMPACT STORED POIRIER TRANSFORM IS ORIGINALLY IN RE( )
C         SEE  TWO R FT  FOR DETAILS.
C
C      IN EFFECT THIS SUBROUTINE DOUBLES THE STORAGE AREA REQUIRED
C      BUT GIVES EASE IN THE MANIPULATION OF THE COEFFICIENTS WHERE
C         FTX(J) = RE(J) + IM(J)
C
      REAL  RE (10), IM (10)
      INTEGER LOG2N, N, N UPON2, MORE
C
      N = 2**LOG2N
      N UPON 2 = N/2
      MORE = N UPON 2 + 2
      IM(1) = 0.0
      DO 10 J=2,N UPON 2
         I = N-J+2
         IM(J) = RE(I)
  10     CONTINUE
      J = N UPON 2 +1
      IM(J) = 0.0
      DO 20 J=MORE,N
         I = N-J+2
         IM(J) = -RE(J)
         RE(J) = RE(I)
  20     CONTINUE
      RETURN
      END
      SUBROUTINE MR 1D FT (LOG2N,X,Y)
C.........................................................................
C     MIXED RADIX ONE DIMENSIONAL FOURIER TRANSFORM
C
      INTEGER LOG2N
      REAL X (10), Y (10)
C
      INTEGER JJ,J0,J1,J2,J3,N,M4
      REAL ARG,C1,C2,C3,I0,I1,I2,I3,R0,R1,R2,R3,S1,S2,S3,T
C
      INTEGER A,B,C,D,E,F,G,H,I,J,K,L,M,BS,CS,DS,ES,FS,GS,HS,IS,JS,KS,
     .LS,MS,AL,BL,CL,DL,EL,FL,GL,HL,IL,JL,KL,LL,ML, S (13), U (13)
      EQUIVALENCE (BS,S(2)),(CS,S(3)),(DS,S(4)),(ES,S(5)),(FS,S(6)),
     .(GS,S(7)),(HS,S(8)),(IS,S(9)),(JS,S(10)),(KS,S(11)),(LS,S(12)),
     .(MS,S(13)),(AL,U(1)),(BL,U(2)),(CL,U(3)),(DL,U(4)),(EL,U(5)),
     .(FL,U(6)),(GL,U(7)),(HL,U(8)),(IL,U(9)),(JL,U(10)),(KL,U(11)),
     .(LL,U(12)),(ML,U(13))
C
      N=2**LOG2N
      IF (LOG2N.LE.1) GO TO 500
      DO 400 K=2,LOG2N,2
      M=2**(LOG2N-K)
      M4=4*M
      DO 300 J=1,M
      ARG=6.283185307*FLOAT(J-1)/FLOAT(M4)
      C1=COS(ARG)
      S1=SIN(ARG)
      C2=C1*C1-S1*S1
      S2=C1*S1+C1*S1
      C3=C2*C1-S2*S1
      S3=C2*S1+S2*C1
      DO 200 I=M4,N,M4
      J0=I+J-M4
      J1=J0+M
      J2=J1+M
      J3=J2+M
      R0=X(J0)+X(J2)
      R1=X(J0)-X(J2)
      I0=Y(J0)+Y(J2)
      I1=Y(J0)-Y(J2)
      R2=X(J1)+X(J3)
      R3=X(J1)-X(J3)
      I2=Y(J1)+Y(J3)
      I3=Y(J1)-Y(J3)
      X(J0)=R0+R2
      Y(J0)=I0+I2
      IF (ARG.EQ.0.0) GO TO 100
      X(J2)=(R1+I3)*C1+(I1-R3)*S1
      Y(J2)=(I1-R3)*C1-(R1+I3)*S1
      X(J1)=(R0-R2)*C2+(I0-I2)*S2
      Y(J1)=(I0-I2)*C2-(R0-R2)*S2
      X(J3)=(R1-I3)*C3+(I1+R3)*S3
      Y(J3)=(I1+R3)*C3-(R1-I3)*S3
      GO TO 200
  100 CONTINUE
```

```
      X(J2)=R1+I3
      Y(J2)=I1-R3
      X(J1)=R0-R2
      Y(J1)=I0-I2
      X(J3)=R1-I3
      Y(J3)=I1+R3
  200 CONTINUE
  300 CONTINUE
  400 CONTINUE
  500 CONTINUE
      IF (LOG2N.EQ.LOG2N/2*2) GO TO 700
      DO 600 I=1,N,2
      R0=X(I)+X(I+1)
      R1=X(I)-X(I+1)
      I0=Y(I)+Y(I+1)
      I1=Y(I)-Y(I+1)
      X(I)=R0
      Y(I)=I0
      X(I+1)=R1
      Y(I+1)=I1
  600 CONTINUE
  700 CONTINUE
      MS=N/2
      ML=N
      DO 800 K=2,12
      J=14-K
      S(J)=1
      U(J)=S(J+1)
      IF (S(J+1).GT.1) S(J)=S(J+1)/2
  800 CONTINUE
      AL=BS
      JJ=0
      DO 900 A=1,AL
      DO 900 B=A,BL,BS
      DO 900 C=B,CL,CS
      DO 900 D=C,DL,DS
      DO 900 E=D,EL,ES
      DO 900 F=E,FL,FS
      DO 900 G=F,GL,GS
      DO 900 H=G,HL,HS
      DO 900 I=H,IL,IS
      DO 900 J=I,JL,JS
      DO 900 K=J,KL,KS
      DO 900 L=K,LL,LS
      DO 900 M=L,ML,MS
      JJ=JJ+1
      IF (JJ.LE.M) GO TO 900
      T=X(JJ)
      X(JJ)=X(M)
      X(M)=T
      T=Y(JJ)
      Y(JJ)=Y(M)
      Y(M)=T
  900 CONTINUE
      RETURN
      SUBROUTINE R SUB B O (LOG2N,X)
C.......................................................................
C     REVERSE SUBSCRIPT BIT ORDER
C
      INTEGER LOG2N
      REAL X (10)
C
      INTEGER JJ
      REAL T
C
      INTEGER A,B,C,D,E,F,G,H,I,J,K,L,M,N,BS,CS,DS,ES,FS,GS,HS,IS,JS,KS,
     .LS,MS,NS,AL,BL,CL,DL,EL,FL,GL,HL,IL,JL,KL,LL,ML,NL, S (14), U (14)
      EQUIVALENCE (BS,S(2)),(CS,S(3)),(DS,S(4)),(ES,S(5)),(FS,S(6)),
     .(GS,S(7)),(HS,S(8)),(IS,S(9)),(JS,S(10)),(KS,S(11)),(LS,S(12)),
     .(MS,S(13)),(NS,S(14)),(AL,U(1)),(BL,U(2)),(CL,U(3)),(DL,U(4)),
     .(EL,U(5)),(FL,U(6)),(GL,U(7)),(HL,U(8)),(IL,U(9)),(JL,U(10)),
     .(KL,U(11)),(LL,U(12)),(ML,U(13)),(NL,U(14))
C
      NS=2**(LOG2N-1)
      NL=2*NS
      DO 100 K=2,13
      J=15-K
      U(J)=S(J+1)
      S(J)=1
      IF(S(J+1).GT.1) S(J)=S(J+1)/2
  100 CONTINUE
      AL=BS
      JJ=0
      DO 200 A=1,AL
      DO 200 B=A,BL,BS
      DO 200 C=B,CL,CS
      DO 200 D=C,DL,DS
      DO 200 E=D,EL,ES
      DO 200 F=E,FL,FS
      DO 200 G=F,GL,GS
      DO 200 H=G,HL,HS
      DO 200 I=H,IL,IS
      DO 200 J=I,JL,JS
      DO 200 K=J,KL,KS
      DO 200 L=K,LL,LS
      DO 200 M=L,ML,MS
      DO 200 N=M,NL,NS
      JJ=JJ+1
      IF (JJ.LE.N) GO TO 200
      T=X(JJ)
      X(JJ)=X(N)
      X(N)=T
  200 CONTINUE
      RETURN
      END
      SUBROUTINE ONECAC (LOG2N,X)
C       ONE CYCLIC  AUTO COVARIENCE
      REAL X(10)
C      THIS ROUTINE REPLACES THE FOURIER TRANSFORM OF X(STORED IN
C        ...COMPACT HERMITIAN FORM) BY ITS CYCLIC AUTO COVARIANCE
C      THE COVARIANCE FUNCTION IS COMPUTED  BY TAKING THE  INVERSE
C      FFT OF PRODUCT OF FFT(X) AND CONJG FFT(X).
C
      N = 2**LOG2N
      X(1) = X(1) **2
      NUPON2 = N/2
C       STORE ZEROS FOR IMAGINARY PART OF THE PRODUCT.
      DO 100 J = 2,NUPON2
      K = N+2-J
      P = X(J)**2 + X(K)**2
      X(J) = P
      X(K) = 0.0
  100 CONTINUE
      K = N/2 + 1
      X(K) = X(K)**2
C
      CALL ONECFT(LOG2N,X)
C
      RETURN
      END
      SUBROUTINE ONE C FT (LOG2N,X)
C.....................................................................
C     ONE COMPLEX FOURIER TRANSFORM
C
      INTEGER LOG2N
      REAL X (10)
C
      INTEGER J,JM,K,KM,M,N OVER 2
      REAL AI,AR,ARG,BI,BR,C,PI,S,T
C
      M=2**(LOG2N-1)
      PI=3.141592654
      N OVER 2=M/2+1
      DO 100 J=2,N OVER 2
      K=M+2-J
      JM=J+M
      KM=K+M
      AR=X(J)+X(K)
      AI=X(KM)-X(JM)
      BR=X(J)-X(K)
      BI=X(JM)+X(KM)
      ARG=PI*FLOAT(J-1)/FLOAT(M)
      C=COS(ARG)
      S=SIN(ARG)
      T=BR*C+BI*S
      BI=BI*C-BR*S
      BR=T
      X(J)=AR-BI
      X(K)=AR+BI
      X(JM)=BR+AI
      X(KM)=BR-AI
  100 CONTINUE
      AR=X(1)+X(M+1)
      BR=X(1)-X(M+1)
      X(1)=AR
      X(M+1)=BR
      CALL MR 1D FT (LOG2N-1,X(1),X(M+1))
      CALL R SUB B O (LOG2N-1,X(1))
      CALL R SUB B O (LOG2N-1,X(M+1))
      CALL R SUB B O (LOG2N,X)
      RETURN
      END
      SUBROUTINE PARZEN ( M, C )
C.....................................................................
C
C      MODIFIES THE COVARIANCE FUNCTION C(T) BY THE PARZEN LAG WINDOW.
C         THE RESULTS ARE STORED IN C(T), T=1,2,3,...,M+1.
C
      REAL  C (10), D
      INTEGER M, M UPON 2, TWO M
C
      M UPON 2 = M/2
      DO 10 J=1,M UPON 2
         D = 1.0 - 6.0*( FLOAT(J)/FLOAT(M) )**2
     .             + 6.0*( FLOAT(J)/FLOAT(M) )**3
         C(J+1) = D * C(J+1)
   10    C O N T I N U E
      M UPON 2 = M UPON 2 + 1
      DO 20 J=M UPON 2,M
         D = 2.0*(1.0 - FLOAT(J)/FLOAT(M) )**3
         C(J+1) = D * C(J+1)
   20    C O N T I N U E
      R E T U R N
      E N D
```